

**Modification of the ionosphere by means of high power
radio waves**

Alan John Stocker

Being a dissertation submitted to the Faculty of Science, Leicester
University, in candidature for the degree of Philosophiae Doctor.

Department of Physics and Astronomy.
Leicester University, September 1990.

UMI Number: U038691

All rights reserved

INFORMATION TO ALL USERS

The quality of this reproduction is dependent upon the quality of the copy submitted.

In the unlikely event that the author did not send a complete manuscript and there are missing pages, these will be noted. Also, if material had to be removed, a note will indicate the deletion.



UMI U038691

Published by ProQuest LLC 2015. Copyright in the Dissertation held by the Author.
Microform Edition © ProQuest LLC.

All rights reserved. This work is protected against
unauthorized copying under Title 17, United States Code.



ProQuest LLC
789 East Eisenhower Parkway
P.O. Box 1346
Ann Arbor, MI 48106-1346



7500733789

X-75-174986-8

Modification of the ionosphere by means of high power radio waves

A. J. Stocker

Abstract

Experiments have been performed at Tromsø, Norway and Arecibo, Puerto Rico to investigate the effects produced by high power radio waves (heating) on the high and low latitude ionospheres, respectively. The modifications induced in the F-region have been observed with both incoherent scatter radars and low power HF diagnostic radio waves. These observations provide information on both heater-induced large scale changes, and small scale density structures.

The spatial and temporal development of the perturbation in electron temperature caused by heating, measured at Tromsø for the first time, compares well with theory. Observations of thermal striations, which may be the result of the thermal self-focussing of the heater wave, are also presented.

The large-scale heater-induced changes in the electron density measured by EISCAT have been compared with those derived from measurements of the phase of reflected HF diagnostic signals. Both methods yield consistent results with regard to whether the electron density is enhanced or depleted but there are, however, differences in the magnitudes of the measured changes. The sign of the perturbation can reveal aeronomical information on the chemical and diffusion characteristics of the unheated ionosphere.

The first observations of low latitude heating by means of low power HF diagnostic waves are presented. The anomalous absorption measured at low latitudes is less than that at high latitudes, in agreement with theory. The scale length and amplitude of the associated small-scale density structures are comparable at both high and low latitudes.

A detailed comparison has been undertaken of the effect of heating at high and low latitudes and the results compared with current theoretical models. The two independent diagnostic techniques (incoherent scatter and low power HF waves) provide a consistent picture of the ionospheric perturbation induced by both heating facilities

I dedicate this thesis :

to my parents, who encouraged the beginning but who missed the end...

and to Lyn, who missed the beginning but who encouraged the end...

Acknowledgements

I am indebted to Professor Tudor Jones for allowing me the opportunity to work in the Ionospheric physics group at the University of Leicester. I would also like to thank Farideh and Terry for the many fruitful discussions on various aspects of the work contained in this thesis.

Many thanks are also due to,

The Royal Aerospace Establishment, Farnborough for their financial support in the first 3 years of this project, and SERC for the last 2 years.

The staff of the Arecibo Observatory, the Ramey Solar observatory and the Sabana Seca Naval base who gave their expertise and support during the experiments in Puerto Rico. Of these, Mike Sulzer and Roger Burnside of Arecibo observatory deserve a special mention for running the 430 MHz radar and providing the software with which to analyse the data, respectively. The Arecibo Observatory is part of the National Astronomy and Ionosphere Centre, which is operated by Cornell University under contract with the National Science Foundation.

Ian and Nigel for all things EISCAT.

The remaining members of the Leicester ionospheric physics group for providing the right *atmosphere*.

and finally, LUAFC "Lemmings" for keeping me sane!

Contents

Contents

	Page
1.0 Introduction.	
1.1 The Upper Atmosphere.	1
1.2 Ionospheric Modification.	4
1.3 Aim of present investigation.	6
1.4 Concluding Remarks.	7
2.0 Review of Previous work.	
2.1 Introduction.	8
2.2 Ionospheric Modification Facilities.	10
2.3 Collisional Absorption.	13
2.4 Anomalous Absorption.	15
2.5 Observations of large scale changes to the electron and ion temperatures.	17
2.6 Heater induced changes in the electron density.	20
2.7 Ion line overshoot.	24
2.8 Concluding Remarks.	25
3.0 Theoretical modelling.	
3.1 Introduction.	26
3.2 Large scale temperature and density changes.	27
3.3 Calculation of anomalous absorption.	32
3.4 Concluding remarks.	36
4.0 Equipment.	
4.1 Introduction.	38
4.2 The Tromsø heater.	39
4.3 EISCAT.	41

Contents

	Page
4.4 Leicester HF diagnostics.	43
4.5 Ionosonde and Dynasonde.	45
4.6 Derivation of temperatures from EISCAT observations.	46
4.7 Derivation of electron density from power profile observations.	49
4.8 The Arecibo Experiment.	50
4.9 Concluding remarks.	54
5.0 Electron and Ion temperature effects.	
5.1 Introduction.	56
5.2 General characteristics of temperature observations.	56
5.3 The experiments of 23 March 1985 and 26 February 1987 at Tromsø.	60
5.4 Temporal evolution of the enhancement in electron temperature.	61
5.5 Thermal Striations.	66
5.6 Spatial structure of the electron temperature enhancement.	67
5.7 Power dependence of $\Delta T_e/T_e$.	70
5.8 Electron temperature measurements at Arecibo.	72
5.9 Chapter summary.	74
6.0 Electron Density effects.	
6.1 Introduction.	76
6.2 General characteristics of incoherent scatter measurements.	76
6.3 General characteristics of test wave phase and Doppler measurements.	80
6.4 Spatial structure of heater-induced change in electron density.	82
6.5 Temporal development of heater-induced change in electron density.	90
6.6 Dependence of phase change on $\Delta T_e/T_e$.	93
6.7 Concluding remarks.	94

Contents

	Page
7.0 HF diagnostic observations at Arecibo	
7.1 Introduction.	95
7.2 General Characteristics of the diagnostic signals.	96
7.3 Measurement of diagnostic signal absorption.	99
7.4 Possible causes of reduction in diagnostic signal level.	101
7.5 Calculation of FAI scale lengths.	103
7.6 Response times.	105
7.7 Concluding remarks.	109
8.0 Conclusions.	
8.1 Introduction.	110
8.2 Summary of principal observations.	110
8.3 Future work.	112
References.	114

Chapter 1 Introduction

1.1 The Upper Atmosphere

The earth's atmosphere can be characterised in terms of parameters such as temperature, pressure, density, composition and the degree of ionisation all of which vary considerably with altitude. At heights above about 60 km solar ionising radiation, and at high latitudes the solar wind, produce free electrons in sufficient quantities to significantly affect the propagation of radio waves. This region, which has an upper boundary at approximately 1000 km, is known as the ionosphere.

The atmosphere has, conventionally, been divided into a number of regions, based upon the altitude variation of the various characterising parameters. The name of these regions is appended with -sphere, and the upper boundary of each region is known as the -pause. The average temperature of the neutral atmosphere, as a function of height, is indicated in Figure 1.1. Four regions may be identified, the Troposphere (0 - 11 km) where the composition is roughly uniform and the temperature decreases with increasing height, the Stratosphere (11 - 50 km) where the temperature is roughly constant at a value of approximately 220 K, the Mesosphere (50 - 85 km) at the top of which the temperature reaches the lowest value found in the atmosphere (180 K) and finally, the Thermosphere (> 85 km) where the temperature gradually increases until it reaches a constant value of between 1500 - 2000 K. The temperature structure of the thermosphere is strongly dependent upon the absorption of short wavelength UV radiation and therefore exhibits marked diurnal and solar cycle variations.

At an altitude of close to 100 km, the turbopause marks the boundary between the turbulent mixing and diffusive separation of the atmospheric constituents. Below 100 km, the relative abundances of the atmospheric constituents may be assumed to be roughly

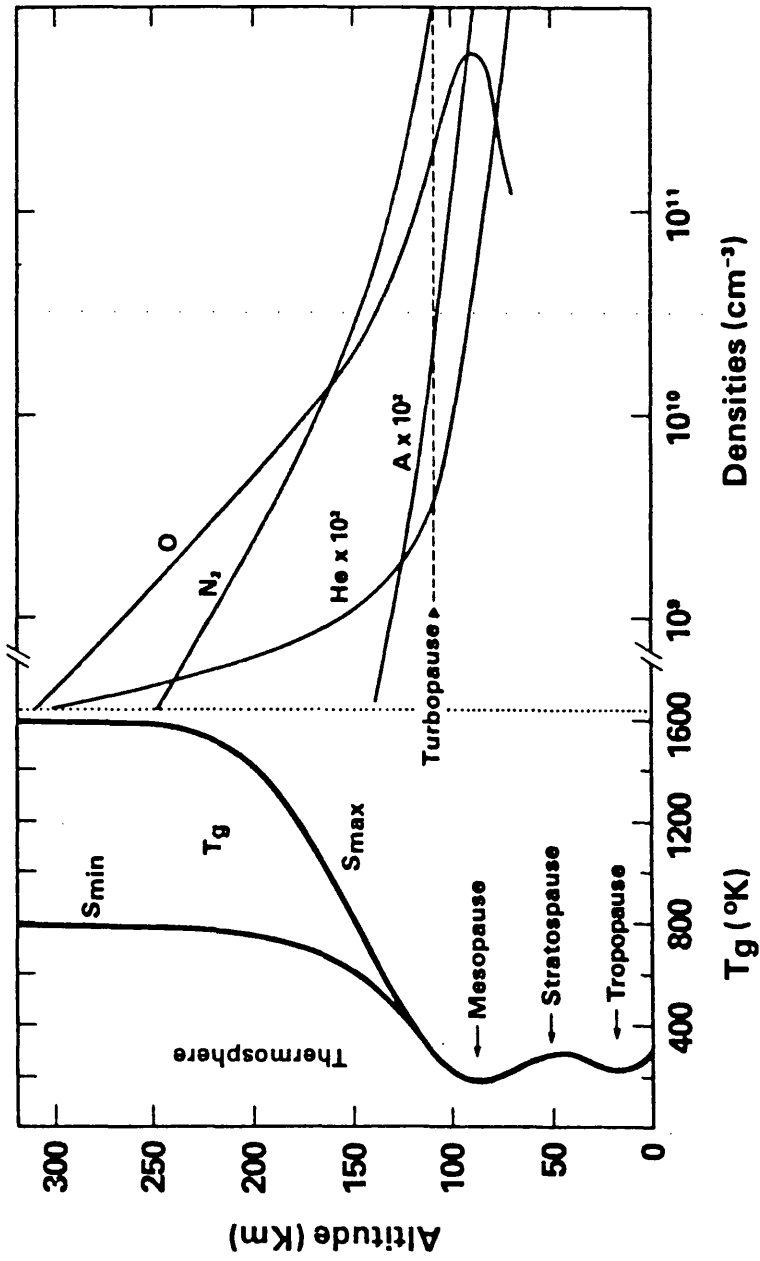


Figure 1.1 Average neutral temperature and density distributions. S_{min} and S_{max} refer to conditions of minimum and maximum solar activity, respectively (after Mayr and Harris 1980).

Chapter 1 Introduction

independent of height, while above this height the vertical distribution of each neutral gas depends on its molecular weight. However, the distribution will be distorted by chemical activity (eg ionisation and dissociation).

The influx of solar radiation in the UV band has the effect of ionising a small (<1%) fraction of the neutral atmosphere. A dynamic equilibrium between this production mechanism and the various loss processes, eg recombination, gives rise to a population of free electrons. A schematic of the electron concentration (otherwise known as the electron or number density) height profile is illustrated in Figure 1.2. The degree of ionisation is dependent upon the time of day, geomagnetic latitude and solar activity.

Following the notation devised by Appleton, the three principal layers distinguishable in Figure 1.2 are referred to as the D-, E-, and F-layers (or regions). Although the location of the boundaries between the layers are variable, the D-region may be taken to lie between 60 - 90 km, the E-region between 90 - 150 km and the F-region above 150 km. Under certain daytime conditions it is possible to observe two sub-layers within the F-region, the lower of which is known as the F₁ layer, while the upper is called the F₂ layer. The ionosphere above the peak in electron density located in the F-region is known as the "topside" ionosphere. It should be noted that the topside electron density distribution is an effect of diffusion rather than a balance between photoionisation and recombination.

The magnetoionic theory (eg Budden 1961) indicates that the plasma angular frequency, ω_N is related to the electron density, N by the following expression,

$$\omega_N^2 = (2\pi f_N)^2 = N e^2 / m \epsilon_0 \quad (1.1)$$

where, m and -e are the electron mass and charge, ϵ_0 is the electric permittivity of free space and f_N represents the corresponding radio wave frequency. The Appleton-Hartree

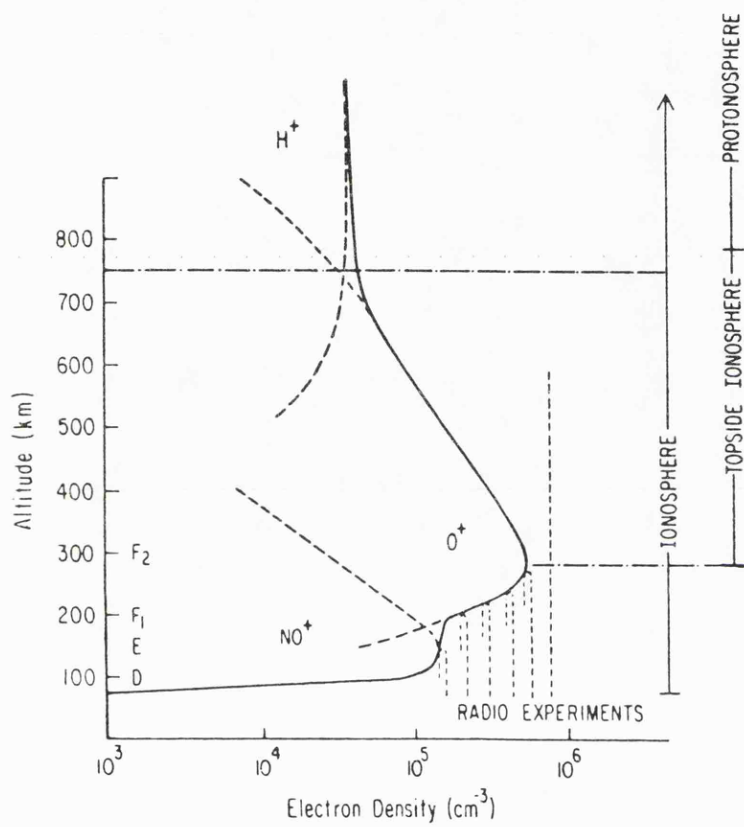


Figure 1.2 Schematic illustration of the ionosphere showing the various layers; D, E, F₁ and F₂ (after Schunk 1983).

Chapter 1 Introduction

expression (Appleton 1932, see also Equation 3.15) for the refractive index reveals that “ordinary” polarised waves reflect at a height where the wave frequency equals the plasma frequency. Hence, by inserting the appropriate numerical values into Equation 1.1 it is found that for N in electrons per cubic meter,

$$f_N \approx (80.6 N)^{1/2} \quad [\text{Hz}] \quad (1.2)$$

This relationship between radio wave frequency and plasma electron density is the principle which governs the sounding of the ionosphere by means of vertical ionosondes (eg Rishbeth and Garriott 1969).

At low altitudes (E-region and below) there are sufficient collisions to maintain thermal equilibrium between the neutrals, ions and electrons. At F-region heights no such equilibrium exists, and therefore the electron temperature exceeds the ion and neutral temperatures during both day and night (Figure 1.3). During the day, the higher electron temperatures are a consequence of the energy of the photoionising UV radiation being greater than the energy required for ionisation, with most of the excess energy removed by photoelectrons. As the time taken for these fast photoelectrons to recombine is, typically, shorter than the time taken in losing the excess energy to the neutral gas, then the average electron energy, and therefore temperature, exceeds that of the other particles. At night, the topside thermal structure is largely maintained by a flow of heat from the magnetosphere.

The magnetosphere lies above the ionosphere at an altitude of about 1000 km. In this region the dynamics of the atmosphere (ie the charged particles) are controlled by the geomagnetic field. The boundary between the ionosphere and the magnetosphere is difficult to fix with any precision because, to a large extent, the movement of ionised particles can be controlled by the geomagnetic field at heights as low as 150 km. The edge of the earth's atmosphere (ie where the earth ceases to have significant effect on the medium) may be taken

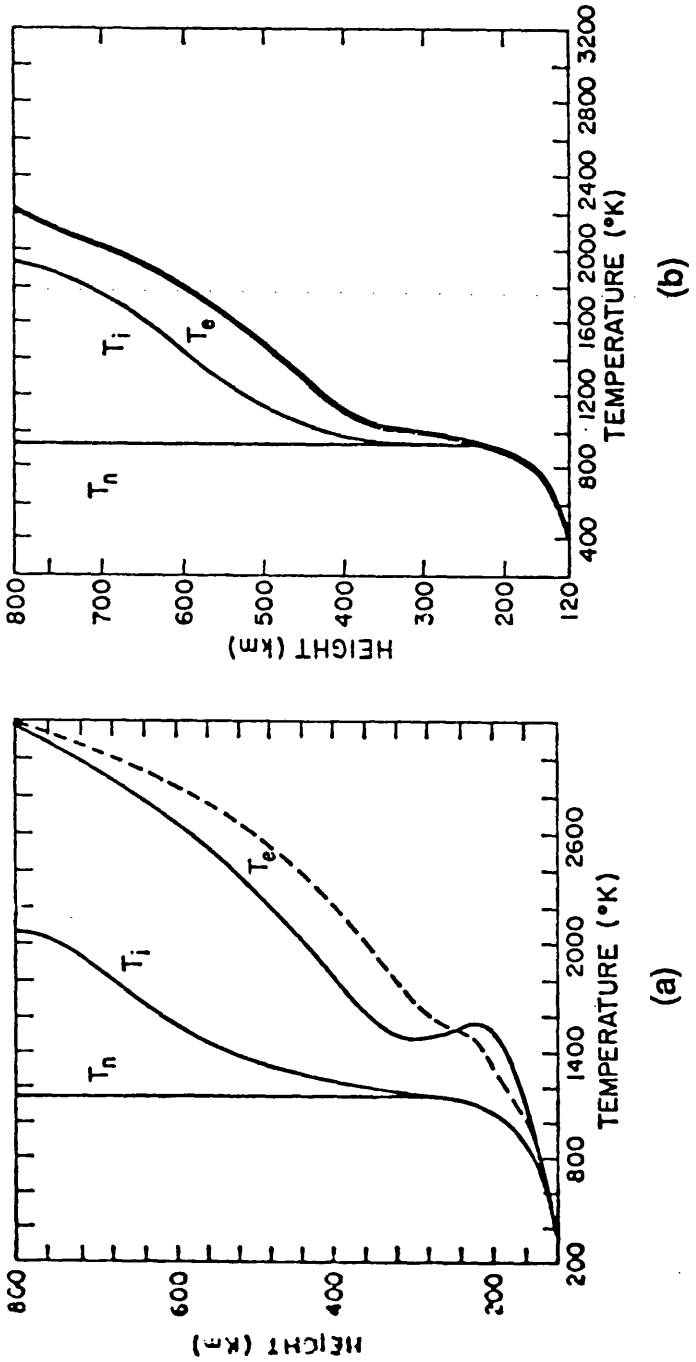


Figure 1.3 Calculated electron, ion and neutral temperature profiles over Millstone Hill during a) daytime and b) nighttime (after Roble 1975).

Chapter 1 Introduction

to coincide with the upper boundary of the magnetosphere (magnetopause) which extends to approximately 10 earth radii on the sunward side, and considerably further on the night side.

A schematic of the near earth environment and magnetic field is presented in Figure 1.4. The geomagnetic field may be approximated by a central dipole with the poles displaced from the geographic poles by about 11° . This offset implies that any given point on the surface of the earth, in general, possesses different geomagnetic and geographic coordinates. The dip angle, which is the angle between the magnetic field and a plane perpendicular to the earth's surface, is a function of latitude.

The solar wind is a stream of ionised particles which are continuously emitted by the sun. The pressure from the solar wind distorts the geomagnetic field from a simple dipole shape at distances greater than a few earth radii (R_E). On the sunward side the geomagnetic field is compressed, while on the night side it is extended to form the magnetotail. The magnetotail extends to well beyond the orbit of the moon ($60 R_E$).

At high geomagnetic latitudes the earth's magnetic field lines either extend far into the magnetosphere, or within the polar cap boundaries they open directly onto the interplanetary medium via the polar cusp. These 'open' field lines allow the interchange of both particles and energy between the ionosphere and magnetosphere. The precipitation of the so-called "auroral particles" which lie outside the stable trapping regions of the radiation belts leads to the well known optical phenomena of the aurorae (Northern and Southern Lights).

1.2 Ionospheric Modification

Artificial ionospheric modification experiments may be defined as those in which any of the ionospheric plasma parameters are deliberately altered. Principally, this means changes to the

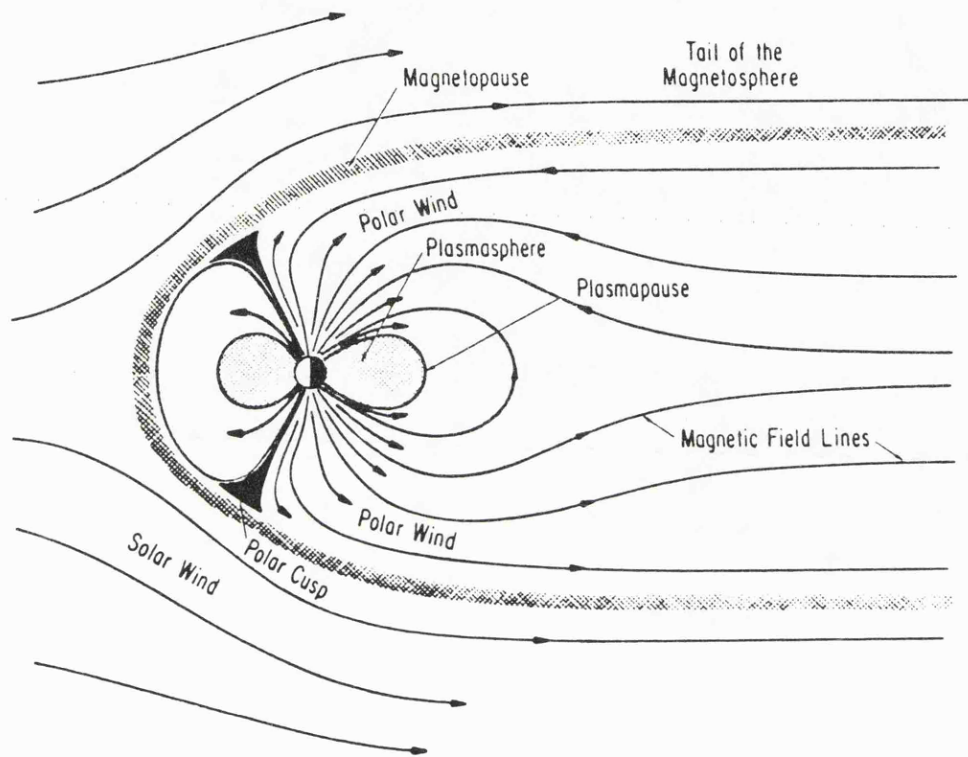


Figure 1.4 Schematic view of the near earth environment (after Banks and Kockharts 1973).

Chapter 1 Introduction

electron density, electron temperature and ion temperature, but may also include changes to the chemical processes or the formation of field-aligned density structures. The ionosphere has been modified by means of man's activities in a number of ways, for example by atmospheric nuclear detonations (eg magnetospheric effects, Helliwell and Carpenter 1963), ground detonations (eg Barry *et al* 1966), rocket exhausts (eg Zinn *et al* 1982), chemical releases from rockets (eg Mendillo 1981) and illumination of the ionosphere by high power radio waves (heating). Only experiments which have employed high power HF radio waves as a source of ionospheric modification are discussed in this thesis. High frequency waves in the range 3 - 15 MHz have been employed during most radio experiments because, at vertical incidence, the strongest interactions occur when the wave frequency is close to the plasma frequency.

As an example of a naturally occurring plasma the ionosphere is of interest from the perspective of plasma physics as well as geophysics. A number of scientific and engineering goals may be served by modifying the ionosphere with high power radio waves, for instance:

(a) *To investigate the properties of the natural ionosphere.* The electron temperature may be changed in a quantifiable way by the incident radio waves. Observation of the response of the ionosphere to this change can reveal the rate coefficients of several aeronomically important processes such as particle diffusion and recombination.

(b) *To perform controlled plasma experiments in a natural plasma laboratory.* For many plasma phenomena, the characteristic scale length is much smaller than the ionospheric scale length. This means that, compared to conventional laboratory plasmas, the ionospheric plasma is far more homogeneous. This property results in the ionosphere being suitable for the investigation of the nonlinear interactions of the various types of wave which can propagate in plasmas and which have relatively large scale sizes (~ kms).

Chapter 1 Introduction

(c) *To study the effects of modification on radio wave propagation.* Since 1901, when Marconi successfully transmitted radio signals across the Atlantic, the ability of the ionosphere to reflect radio waves has been utilised in long distance radio communication. Even in recent years which have seen the development of satellite systems, communication at HF frequencies and below still remains important. However, the unpredictability of the ionosphere can render this method of communication unreliable. Thus, if the properties of the ionospheric plasma within the confines of a high power radio beam can be controlled, then the performance of a communication channel propagating through the modified region might be enhanced.

In a long series of heating experiments conducted since the early 1970's, these three goals have been pursued at a number of low-, mid- and high-latitude sites. Much of this experimental effort has been concentrated on the effect of heating at F-region heights.

1.3 Aim of the present investigation

Since the beginning of the 1980's the Ionospheric Physics Group of the University of Leicester have collaborated with the Max Planck Institut für Aeronomie in a joint study of the ionospheric modification effects excited by the heating facility located at Ramfjordmoen, near Tromsø, Norway. More recently, the Leicester group has been invited to participate in a similar series of experiments at low-latitudes at Arecibo, Puerto Rico in association with Cornell University, USA. These latter experiments were designed to make the first direct measurements of anomalous absorption at low latitudes. The aim of this experiment corresponds to objective b, described in the previous section.

The experimental program at Tromsø involved the use of the EISCAT (European Incoherent SCATter) radar to investigate the effect of heating on the ionospheric plasma parameters, eg electron temperature and electron density, which corresponds to objective a. In addition to the EISCAT observations, the phase and amplitude of several low power

Chapter 1 Introduction

diagnostic HF radio waves which propagated through the heated volume were also measured. From these observations it is possible to deduce several characteristics of the modified ionospheric plasma. Finally, the experiments were supported by the measurement of the F-region critical frequency by a vertical incidence ionosonde and of the reflected heater signal.

A similar experimental configuration was adopted during the heating experiments at Arecibo. These experiments were primarily involved with obtaining amplitude measurements of the HF diagnostic signals. The background ionospheric parameters were measured by the 430 MHz incoherent scatter facility and ionosonde located at the Arecibo Observatory.

1.4 Concluding Remarks

In this thesis the spatial and temporal characteristics of the heater-induced changes to the electron temperature and density are investigated for experiments at high latitudes. These experimental observations are then compared with those reported from previous experiments and with theory.

The first direct observations of the anomalous absorption of low power test waves at low-latitudes are also reported. These results are then interpreted in terms of current theory and compared with the results obtained at high latitudes. The data have been interpreted in terms of the non-linear theory of ionospheric modification which provides an adequate representation of the experimental observations at both high and low latitudes.

Chapter 2 Review of previous work

2.1 Introduction

The first example of a change (modification) of the ionospheric parameters produced by high power radio waves was discovered in the early 1930's when the Radio Luxembourg transmitter became operational (Tellegen 1933; Bailey and Martyn 1934a,b). Tellegen found that the programme broadcast by the high power Luxembourg transmitter was audible on a weaker station propagating through the region illuminated by the Luxembourg transmitter. It is now well known that this effect (the "Luxembourg effect") is due to the modulation of the collisional absorption (see Section 2.3) by the amplitude modulated high power wave. Cross-modulation of this type has been employed since 1955 (Fejer 1955,1970; Jones *et al* 1972; Gurevich 1978) to gain information about D-region electron densities and collision frequencies. More recently, F-region cross-modulation has been observed (Stubbe *et al* 1982a; Robinson 1983, 1989), although this arises from anomalous absorption processes, and provides a method of determining the time constants associated with the instabilities which cause such absorption.

Intentional modification of the ionospheric F-region has taken place since the early 1970's at a range of latitudes, eg low-, at Arecibo, Puerto Rico; mid-, at Platteville, Colorado and high-, Murmansk, Soviet Union. A further modification facility was built by the Max Planck Institut für Aeronomie (MPAe) and the University of Tromsø at Ramfjordmoen, near Tromsø, Norway (high latitude) and has been operational since 1980. The large effective radiated power (ERP) of up to 360 MW and the considerable number of diagnostic installations located close to the Tromsø site has resulted in the production and observation of a wealth of modification phenomena. An overview of some of the wide range of heating effects which have been observed worldwide is presented below.

Chapter 2. Review of previous work

The large scale temperature changes which were expected by the early workers (eg Thomson 1970) have been observed at all latitudes (eg Meltz *et al* 1974; Mantas *et al* 1981; Holt 1985; Jones *et al* 1986; Djuth *et al* 1987b; Robinson 1989; and see Chapter 5) by a variety of diagnostic techniques. The corresponding changes in the electron concentration have been described theoretically and observed at some sites (Gurevich 1978; Jones *et al* 1982; Gurevich and Migulin 1982; Shoucri *et al* 1984; Djuth *et al* 1987b; Robinson 1989; and see Chapters 3 and 6). The reflection coefficient of the ionosphere in the region illuminated by high power radio waves has been modified. This is due in part to anomalous (or wideband) absorption which is caused by the excitation of small scale density irregularities (eg Cohen and Whitehead 1970; Fialer 1974; Utlaut and Violette 1974; Stubbe *et al* 1982a,b, 1985; Jones *et al* 1984; Coster *et al* 1985 and Chapter 3) and in part to collisional (deviative or ohmic) absorption (Thomson 1970; Meltz and Lelevier 1970; Gurevich 1978). Modification of the ion-line and plasma-line spectra measured by incoherent scatter radars have been observed at all latitudes (Carlson *et al* 1972, 1982; Hagfors *et al* 1983; Duncan 1985; Jones *et al* 1986). Other phenomena which have been observed during high power radio wave heating of the ionosphere include airglow at the oxygen red and green lines (Haslett and Megill 1974; Utlaut 1975; Carlson *et al* 1982; Stubbe *et al* 1982a; Gurevich *et al* 1985; Bernhardt *et al* 1989), stimulated electromagnetic emissions (Thidé *et al* 1983; Stubbe *et al* 1984, 1985; Fejer *et al* 1985; Derblom *et al* 1989), and the production of ELF/VLF radiation via modulation of ionospheric currents both deliberately (Willis and Davies 1973; Ferraro *et al* 1982; Stubbe *et al* 1982c,1985; Barr *et al* 1985, 1986; Rietveld *et al* 1989) and by commercial radio stations (Cannon 1982; Cannon *et al* 1982).

A full discussion of all of the phenomena mentioned above is beyond the remit of this review. However, there are many excellent review papers in the literature which consider the full range of modification effects (eg Utlaut 1975; Carlson and Duncan 1977; Stubbe *et al* 1985; Fejer *et al* 1985; Migulin and Gurevich 1985; Robinson 1989). In addition to these papers there have been a number of "special issues" of the geophysics and radio science

Chapter 2. Review of previous work

journals which have been devoted to ionospheric modification, eg *Journal of Geophysical Research* (Vol. 75, Nov. 1970), *Radio Science* (Vol. 9, Nov. 1974, and Vol. 18, Nov. 1983), and *Journal of Atmospheric and Terrestrial Physics* (Vol. 44, Dec. 1982, and Vol. 47, Dec. 1985).

The work presented in this thesis includes a) the large scale changes in the electron and ion temperatures, b) the resultant changes to the electron concentration during experiments at Tromsø and Arecibo, and c) the first direct observations of anomalous absorption at low-geomagnetic latitudes (Arecibo). The previous work pertaining to these subjects will be reviewed in detail in the following sections while some of the relevant theory is discussed in Chapter 3. However, before this discussion, the characteristics of the modification facilities, worldwide, are summarised.

2.2 Ionospheric Modification facilities

There are a number of purpose built high power radio wave ionospheric modification facilities ("heaters" or "pumps") located at various magnetic latitudes. These include installations at Platteville, Boulder, Colorado (Carroll *et al* 1974), Arecibo, Puerto Rico (Gordon and Carlson 1974; Duncan and Gordon 1982), Ramfjordmoen, Tromsø, Norway (Stubbe and Kopka 1979; Stubbe *et al* 1982a), Fairbanks, Alaska (Wong *et al* 1983; Brandt 1990) and at various sites within the Soviet Union (Gurevich and Migulin 1982; Duncan 1990). The Tromsø and Arecibo heaters and the diagnostic equipment employed in the experiments discussed in this thesis are described in detail in Chapter 4. All of these heating facilities radiate in the HF band so that the wave frequency can match the plasma frequencies typically observed in the F-region (about 3-12 MHz). The operating characteristics of a selection of these facilities are summarised in Table 2.1. The effectiveness of a heater in performing modification experiments and the diversity of those experiments depends in large measure on the operating characteristics of the transmitter, eg power, frequency range, polarisation etc. The

LOCATION	LATITUDE	FREQUENCY (MHZ)	ERP (MW)
USA			
ARECIBO	18°	3 - 11	256 (80) ¹
FAIRBANKS	64°	4.905 (3 - 5) ²	106 ³ (80) ²
PLATTEVILLE	40°	5 - 10	200
USSR			
DUSHANBE	39°	4 - 5	80
GORKI	54°	4 - 6	20
	56°	5 - 10	400
MOSCOW	55°	4 - 5	80
MURMANSK	68°	3.3 (15) ⁴	10
NORWAY			
TROMSØ	70°	4 - 8	360 (1000) ⁴

(1) After about 1980. (2) After 1987. (3) For 1 ms pulses. (4) Proposed

Table 2.1 Operating parameters of ionospheric modification facilities including upgrades where appropriate.

Chapter 2. Review of previous work

principal operating parameters and their effect on the type of experiments which may be performed are described in the following paragraphs. A comparison is made between the Tromsø heater and those located elsewhere.

The effective radiated power (ERP) of a heater is equal to the transmitted power multiplied by the antenna gain (eg Walker 1979) and is a measure of the energy which is directed into the ionosphere. For experiments where the heater reflection height (ie the height at which the heater frequency matches the plasma frequency) is in the F-region or where the heater wave penetrates the ionosphere, then the amount of energy deposited in the interaction region will be dependent on the level of D-region (collisional) absorption which can vary considerably with local conditions and time of day. If the D-region absorption is ignored (a good approximation for nighttime experiments) then the electric field strength is given by (Gurevich 1978),

$$E_0 = 300 (\text{ERP})^{0.5} / Z \quad (2.1)$$

where, ERP is in kW, Z is the altitude in km and E_0 is in mV m^{-1} .

If the effects of refraction are ignored, then for the Tromsø heater the electric field strength at full power is approximately 0.7 V m^{-1} at 100 km. However, as the wave approaches the reflection height the electric field will be subject to amplitude “swelling” (eg Lundborg and Thidé 1985,1986) due to an increase in the energy density as the group velocity decreases. With the field swelling included the electric-field generated in the F-region by the Tromsø heater becomes 3 V m^{-1} or more.

The pump electric fields required to excite a selection of plasma instabilities (some of these are described in Chapter 3) are given in Table 2.2. The thresholds presented in Table 2.2 have been derived for conditions at Tromsø from the expressions presented by Stubbe and Kopka

INSTABILITY	THRESHOLD (Vm^{-1})
Parametric Decay	0.3
Oscillating Two stream	0.4
Brillouin Scattering	0.2
Raman Scattering	1.0
Stimulated Diffusion	0.25

Table 2.2 The electric field required to excite various instabilities for a 5 MHz heating wave at Tromsø. The Tromsø heater has an electric field of approximately 3 Vm^{-1} in the F-region neglecting D-region absorption. Calculated from Fejer (1979) and Stubbe and Kopka (1980).

Chapter 2. Review of previous work

(1980) and Fejer (1979). Examination of this table reveals that the Tromsø heater is capable of exciting a wide range of plasma instabilities and, hence, given the appropriate conditions the wave energy may be transferred to the plasma. It should be noted that the thresholds of many of the instabilities may well be exceeded even in conditions when heater powers considerably less than full power penetrate to the F-region (eg during intervals with significant D-region absorption). Lower power facilities (eg Moscow) may equally be capable of exciting at least some of the instabilities (eg parametric decay, oscillating two stream etc.).

Based on classical thermal balance assumptions, Gurevich (1978) has defined the plasma electric field, E_p (Equation 2.3) which is required to cause perturbations to the plasma electron temperature which are larger than the ambient value. In the F-region, E_p is typically about 1 Vm^{-1} and therefore comparable to the electric field strength of the Tromsø heater. This implies that the Tromsø heater is capable of causing strong electron temperature perturbations and some observations of this phenomenon are reported in Chapter 5.

In order to vary the height of reflection and to perform underdense experiments (ie where the radio wave frequency is higher than the peak of the F-region plasma frequency) or overdense experiments (ie where the radio wave frequency is below the peak of the F-region plasma frequency), the heating facility must have the ability to transmit waves over a range of frequencies. The Soviet transmitter at Murmansk and the original American station at Fairbanks are only able to transmit on a single fixed frequency (3.3 MHz and 4.905 MHz respectively) and are therefore limited to a single reflection height for a given set of ionospheric conditions. Recently, the Fairbanks transmitter has been upgraded and can now operate between 2.8 and 5 MHz (Brandt 1990). Of course, the height of the F-region peak and critical plasma frequency change diurnally and with sunspot cycle and therefore this results in some variation in the heater reflection height. The Tromsø heater is currently capable of transmitting over a continuous range of frequencies between 4 and 8 MHz, although licensing regulations restrict it to a number of discrete frequencies within this range (see Chapter 4). At solar minimum this

Chapter 2. Review of previous work

can present problems if overdense heating is required, because at auroral latitudes the peak F-region plasma frequency can remain lower than 4 MHz throughout the day. During solar maximum the critical frequency may be well above the maximum heater frequency thereby preventing underdense experiments from being performed.

In order to excite instabilities with long growth times the heater must be capable of transmitting in a continuous wave (CW) mode. The HIPAS facility at Fairbanks, Alaska could initially only operate in a pulsed mode with a maximum pulse length at full power of about 0.1 ms (Wong *et al* 1983), whereas the Tromsø heater is capable of not only CW operation but also a variety of modulation schemes. However, recent upgrades to the heater at Fairbanks (Brandt 1990) have given it a CW capability. CW operation also enables large scale changes to the ionospheric plasma (eg changes to the electron temperature and electron concentration) to be sustained. The changes in electron temperature which have been observed at Arecibo (eg Gordon and Carlson 1974) and in preliminary experiments at Tromsø (Jones *et al* 1986; Robinson 1989) are described in detail in the Section 2.5 (see also Chapter 5).

The processes, collisional (ohmic or deviative) absorption and anomalous (or wideband) absorption, by which large scale changes in the electron and ion temperatures and electron concentration may be induced by high power radio waves will be discussed in the following sections. In the D-region an additional process, cyclotron resonance (Clavier 1961), may also occur, but this will not be discussed further.

2.3 Collisional Absorption

Theoretical work by Ginzberg and Gurevich (1960), Farley (1963), Meltz and LeLevier (1970), Stubbe and Kopka (1977), Gurevich (1978), Perkins and Roble (1978), and Shoucri *et al* (1984) has suggested that plasma heating by ohmic dissipation should produce large-scale changes in the electron temperature and hence in the electron density (see Section 2.6)

Chapter 2. Review of previous work

and other parameters. Ohmic heating occurs because the electric field of the incident radiowave (or pump wave) accelerates the electrons in the ionospheric plasma resulting in an increase in the electron temperature. Collisions retard the electrons and therefore energy is extracted from the wave. In the F-region, only a small fraction of the excess energy is transferred to the ion or neutral mass because of the low electron-ion collision frequency ($\leq 10^3 \text{ s}^{-1}$) and fractional energy loss per collision ($\leq 10^{-4}$) (Farley 1963) which results in a time constant for the energy loss to the ions of about 10 s. This low loss rate, therefore, allows considerable heating of the electrons to occur. However, in the E-region the electron-neutral collision frequency is $\sim 2 \times 10^5 \text{ s}^{-1}$ and the fractional loss per collision is 5×10^{-3} resulting in a time constant for the energy loss $\sim 1 \text{ ms}$ which enables significant ion heating to occur. For steady state conditions and following Walker (1979), the electron temperature perturbation due to collisional absorption is given by,

$$\Delta T = (E_0 / E_p)^2 T \quad (2.2)$$

where, E_0 is the pump electric field, T is the temperature of the collision species and E_p is the plasma electric field defined by Gurevich (1978) and given by,

$$E_p^2 = (3Tm\delta / e^2) (\nu^2 + \omega^2) \quad (2.3)$$

where m and e are the electron mass and charge respectively, δ is the fractional energy loss per collision, ν is the effective collision frequency and ω is the pump frequency. It should be noted that, because ν is a function of temperature, for large changes in temperature ΔT will not be linearly proportional to ERP (ie E_0^2).

For $\omega \gg \nu$, E_p varies from $3 \times 10^{-4} f \text{ (mVm}^{-1}\text{)}$ in the D and E regions to about $10^{-4} f \text{ (mVm}^{-1}\text{)}$ in the F-region (Walker 1979), where $f = \omega / 2\pi$. At Tromsø for typical heater frequencies (~ 6

Chapter 2. Review of previous work

MHz) and F-region heights (~ 200 km) E_0 exceeds E_p at effective radiated powers greater than about 150 MW (Equation 2.1). Collisional heating is largest where the pump frequency is close to the ionospheric penetration frequency (Thomson 1970; Utlaut and Cohen 1971). The ion temperature will be largely unaffected because of the high ion-neutral collision frequency and the considerable quantity of neutrals which leads to the dissipation of the energy in the neutral ionosphere.

2.4 Anomalous Absorption

Anomalous self absorption of the incident heating wave is a consequence of the excitation of various types of plasma instabilities such as the parametric decay instability (Perkins *et al* 1974; Fejer 1979) and the generation of field-aligned density striations. A more detailed account of how anomalous absorption arises may be found in Chapter 3. The anomalous absorption of low power diagnostic waves propagating through the heated region occurs when they are scattered into Langmuir waves by the pump-generated field-aligned irregularities. Anomalous absorption of low power test waves has been observed at Platteville (Cohen and Whitehead 1970), Tromsø (Stubbe *et al* 1982b; Jones *et al* 1984, 1986; Robinson 1989) and more recently at Arecibo (Stocker *et al* 1990; see Chapter 7). The self-absorption of the heater wave was first observed at Tromsø (Jones *et al* 1983; Robinson 1983, 1985, 1989; Wilkinson 1988) and later at Arecibo (Djuth *et al* 1986; Fejer *et al* 1989). These experiments have confirmed a number of theoretical predictions and are discussed below.

Jones *et al* (1982) presented evidence (see Figure 2.1) which suggested that O-mode heating causes significantly more absorption, typically 10-15 dB, of a low power HF diagnostic signal traversing the heated volume than X-mode heating, which typically causes less than 1 dB. This is consistent with the absorption being a consequence of anomalous processes (eg Robinson 1989) and also implies that the diagnostic signal absorption is not caused by D-region heating where O- and X- mode heating would lead to similar levels of signal attenuation.

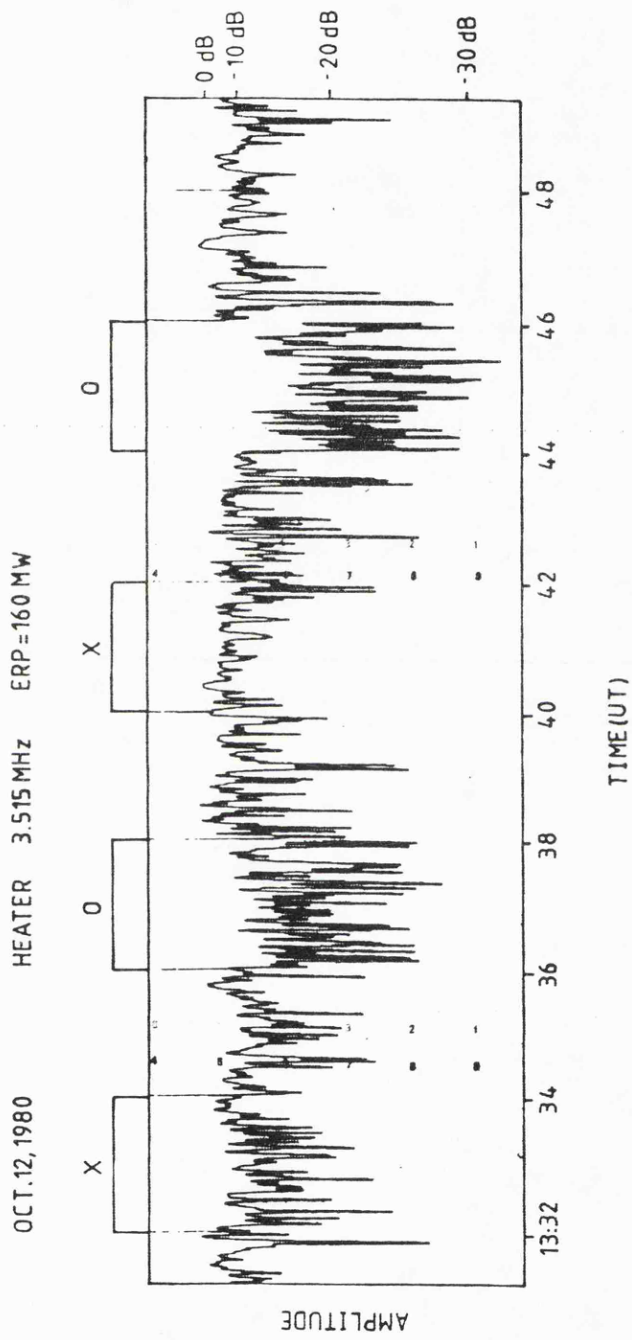


Figure 2.1 3.778 MHz diagnostic field strength versus time, October 12, 1980, 1332-1348 UT. Heater operated at 3.515 MHz, alternate X, O mode, ERP=160 MW. The heater on times are indicated by bars (from Jones *et al* 1982).

Chapter 2. Review of previous work

The onset time of anomalous absorption during heating experiments at Tromsø has been observed by Wilkinson (1988) to lie in the range 2 to 14 seconds depending upon the pump power (the signal decay time decreases with increasing power) which is consistent with theory (Stubbe *et al* 1982b; Robinson 1989). Robinson (1989) has also presented data obtained during heating experiments at Tromsø which suggest that the growth time of the absorption can be less than 0.5 s. Large scale density perturbations resulting from electron heating which can lead to defocussing, exhibit rise times of more than 20 s (Sections 2.4 and 2.5) and are, therefore, unlikely to be the cause of the observed signal attenuation. During intervals at Tromsø where fast amplitude fading is observed, the diagnostic absorption is weakly dependent upon pump ERP. With a slowly varying ionosphere this correlation is no longer observed for heater powers above the threshold of the instability growth (Stubbe *et al* 1982b; Robinson 1989).

Theory predicts (Robinson 1989; Chapter 3) that the level of anomalous absorption should decrease as the angle between the pump wave and the earth's magnetic field increases (Figure 2.2) which implies that it should increase with increasing magnetic latitude. Experiments at Arecibo (low latitude) and Tromsø (high latitude) provide evidence which supports this prediction (Robinson 1989; Stocker *et al* 1990; Chapter 7). In contrast, for given conditions, the level of collisional absorption is independent of latitude.

From measurements at Arecibo, Mantas *et al* (1981) found that the contribution of anomalous heating to the F-region electron temperature and density changes slightly exceeded that of deviative heating. In contrast, experiments at Tromsø indicate that the anomalous absorption processes dominate (Jones *et al* 1982; Wilkinson 1988; Robinson 1989). Jones *et al* (1982) measured the phase change of a low power diagnostic wave traversing the heated volume and these authors reported that the phase changes were well correlated with the anomalous absorption (Figure 2.3). They concluded that as the change in phase was likely to have been caused by perturbations in the electron density and hence the

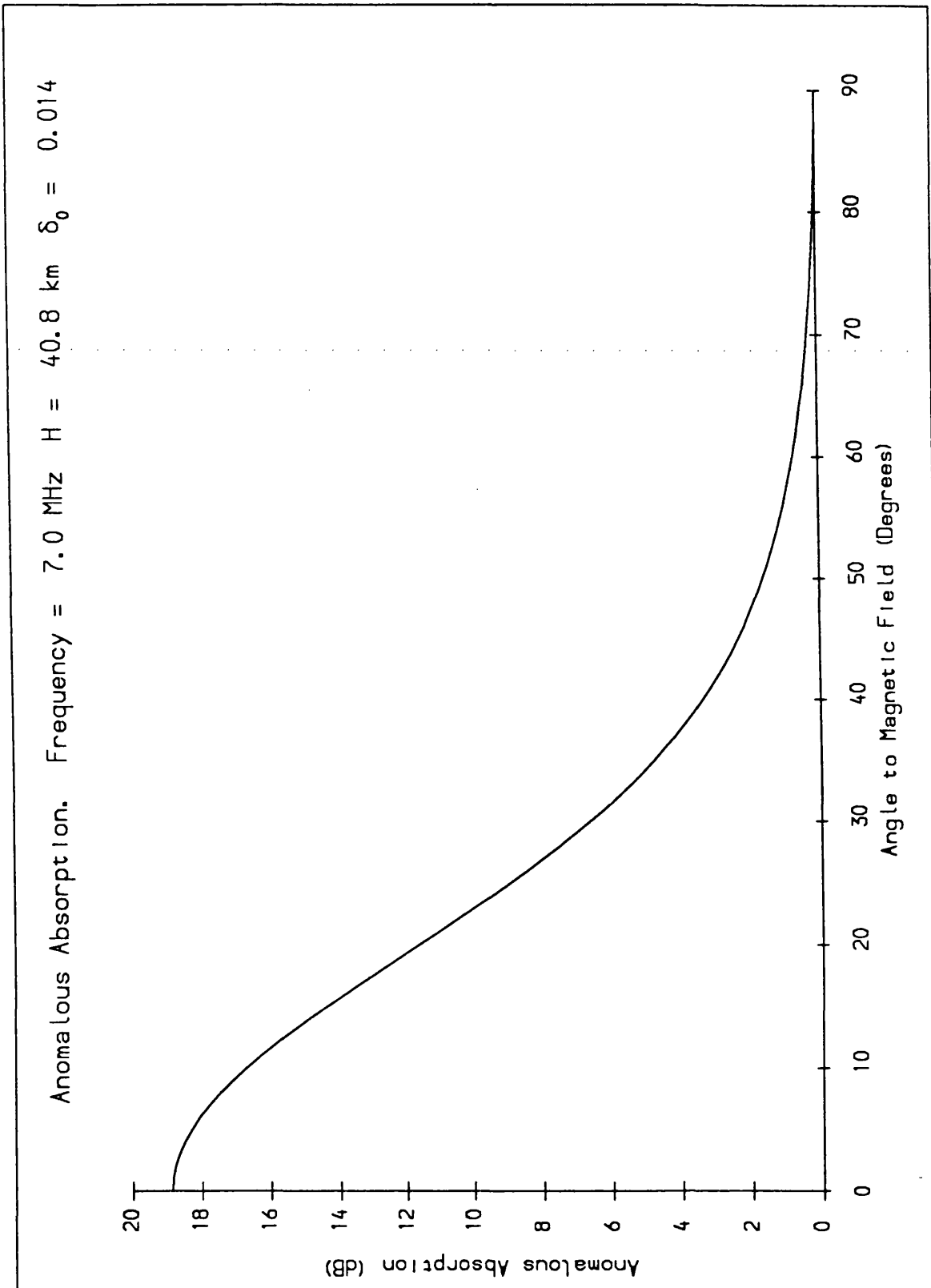


Figure 2.2 Graph of anomalous absorption versus angle of inclination of the geomagnetic field to the vertical (after Robinson 1989).

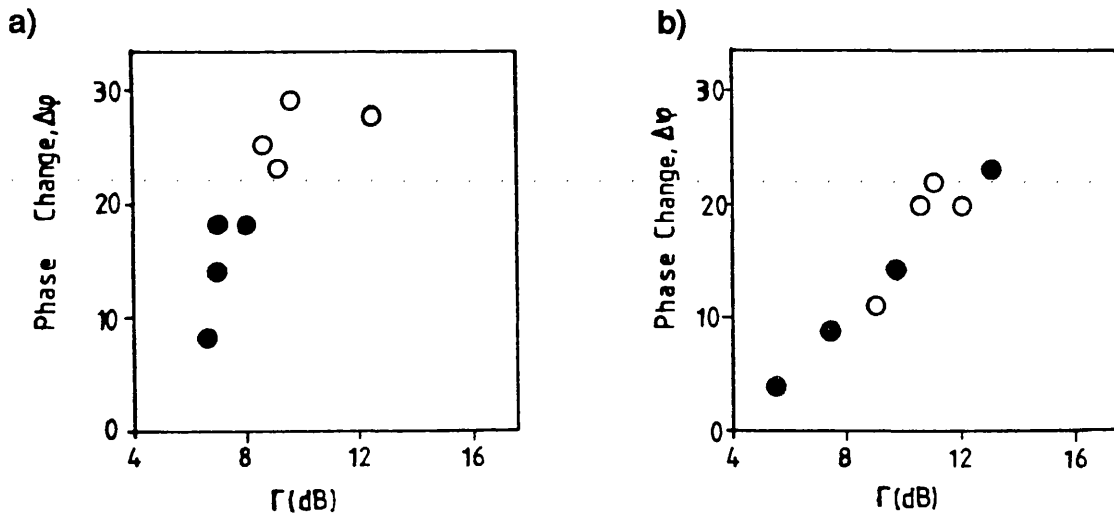


Figure 2.3 Graph showing diagnostic phase change versus wideband absorption on a) October 8, 1980 and b) October 12, 1980. Each data set comprises two cycles of 4 successively reduced ERP levels. Open circle is first cycle, solid dot is second cycle (after Jones *et al* 1982).

electron temperature (Section 2.6) then it followed that electron heating was largely controlled by the anomalous processes. This is consistent with EISCAT observations of the heater-induced electron temperature enhancement (Wilkinson 1988), which were found to be well correlated with the level of diagnostic anomalous absorption (Figure 2.4).

A number of authors (Robinson 1983, 1989; Jones *et al* 1984; Wilkinson 1988) have suggested that the strength of the diagnostic signal absorption observed on a given frequency should depend to some extent on the altitude separation between the reflection height of the diagnostic wave and that of the pump wave (see Chapters 3 and 7). This relationship is illustrated in Figure 2.5, where it may be observed that an increase of 8 km in the separation results in a reduction of 6 dB in the level of absorption.

2.5 Observations of large scale changes to the electron and ion temperature

Since high power radio wave transmitters which are colocated with incoherent scatter radars have become available, it has been possible to measure the heater induced changes in electron and ion temperatures directly to good accuracy and high spatial and temporal resolution. The first experiments of this type were performed at the Arecibo observatory (Gordon *et al* 1971; Gordon and Carlson 1974). The heater-induced spatial and temporal variation of electron temperature (T_e) for a nighttime experiment at Arecibo is illustrated in Figure 2.6. In this example the heater has been on continuously for the 30 minutes prior to the start time of the data interval depicted in the figure. The electron temperature is increased by some 100-200 K (10-20% of ambient) with the peak enhancement situated at about 10-20 km below the heater reflection height. Gordon and Carlson (1974) describe a similar experiment in which high time resolution is achieved by superimposing the data from ten heater on/off cycles (Figure 2.7). There have been many attempts (Meltz *et al* 1974; Showen and Behnke 1978; Gurevich 1978; Mantas *et al* 1981) to fit response curves to data of this type (Figure 2.8).

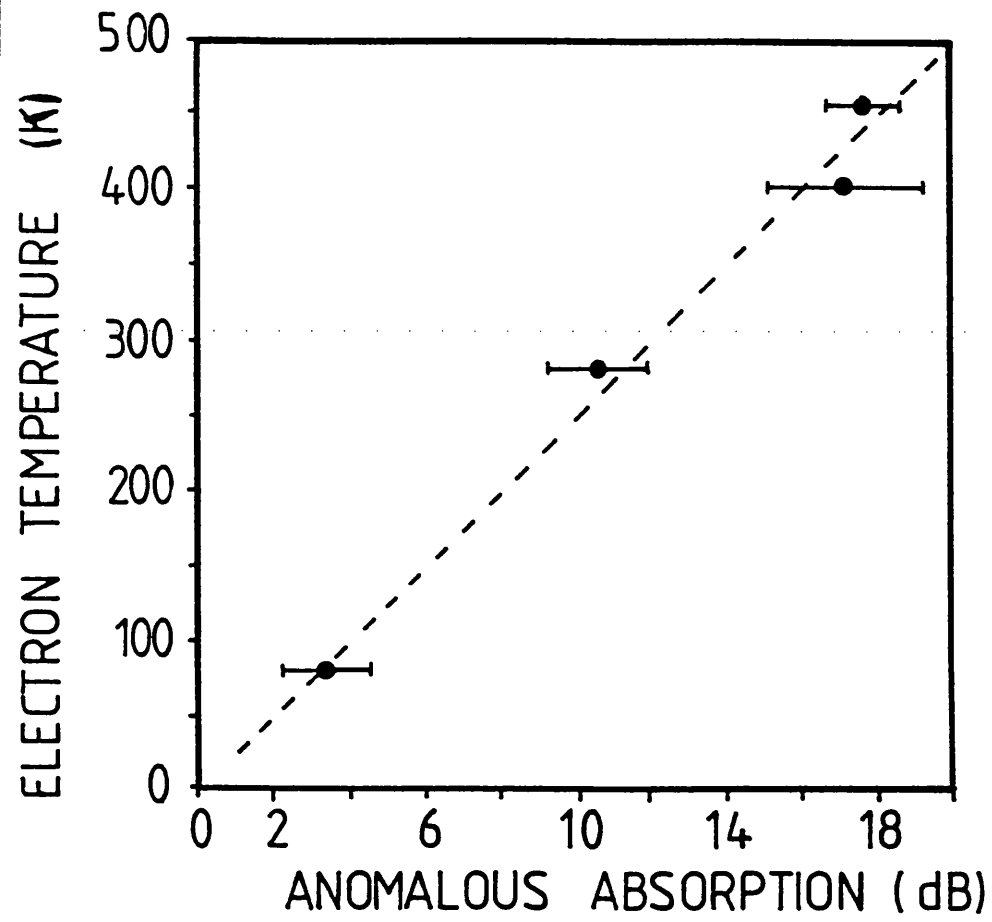


Figure 2.4 A graph of electron temperature enhancement against anomalous absorption from data obtained at Tromsø on several days in March 1985 (from Wilkinson 1988).

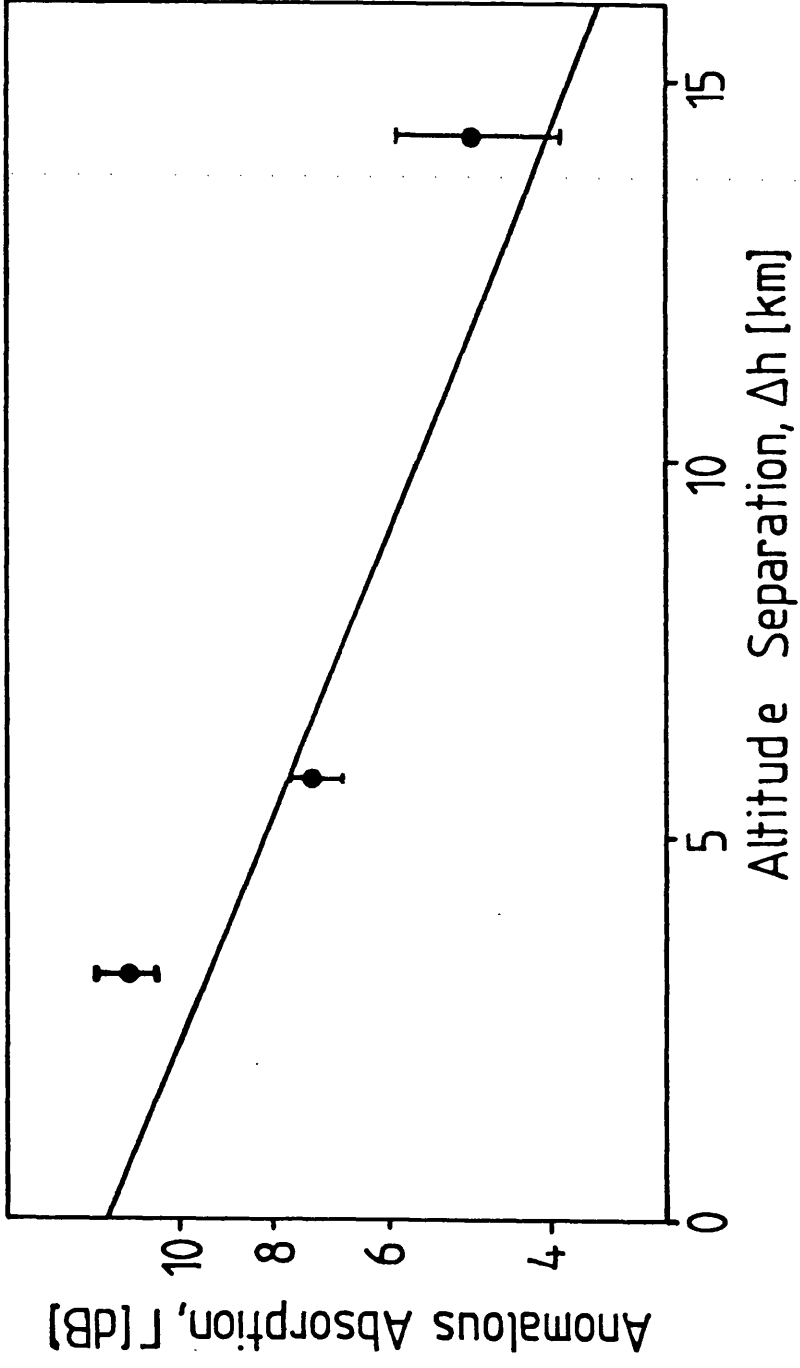


Figure 2.5 A graph of measured diagnostic absorption versus reflection height separation, Δh , for data from September 8, 1981 (from Robinson 1989).

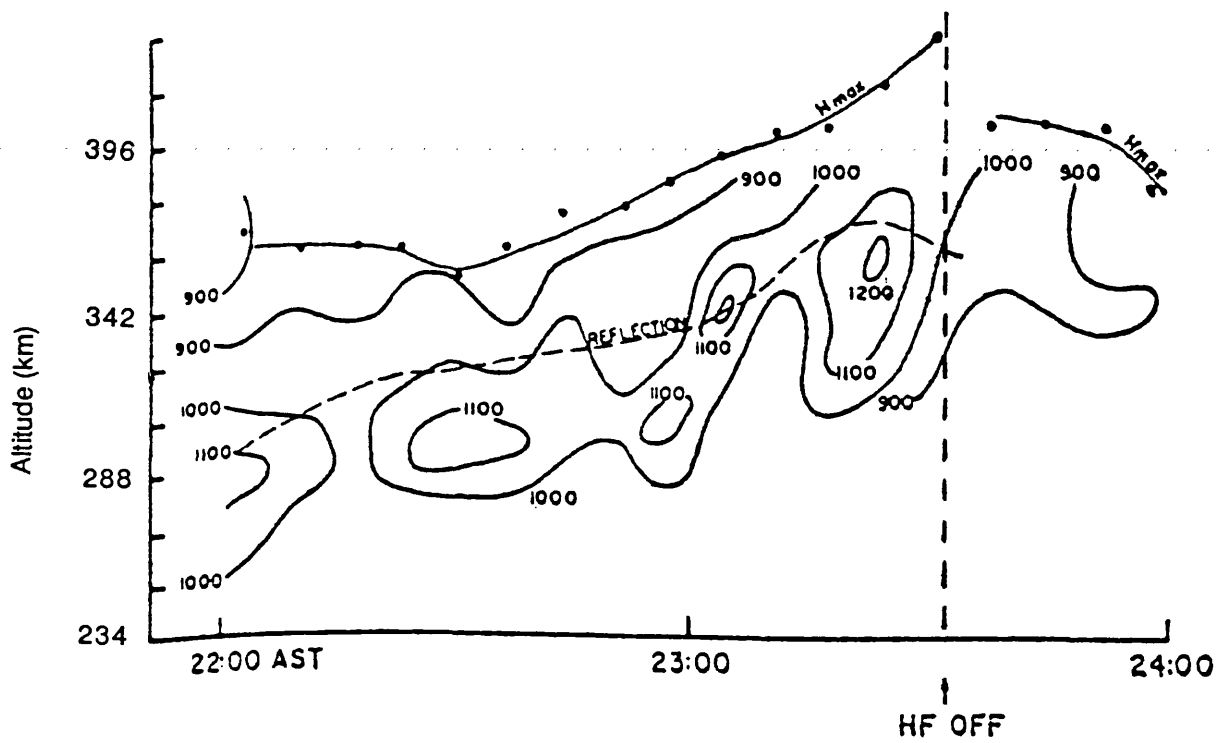


Figure 2.6 Electron temperature distribution : contours in degrees Kelvin, on time height coordinates (19 July 1971) showing heating near height of reflection of HF wave and relaxation to ambient conditions after turn off of the HF transmitter. Heater frequency is 5.1 MHz, transmitter power is 100 kW (from Gordon and Carlson 1974).

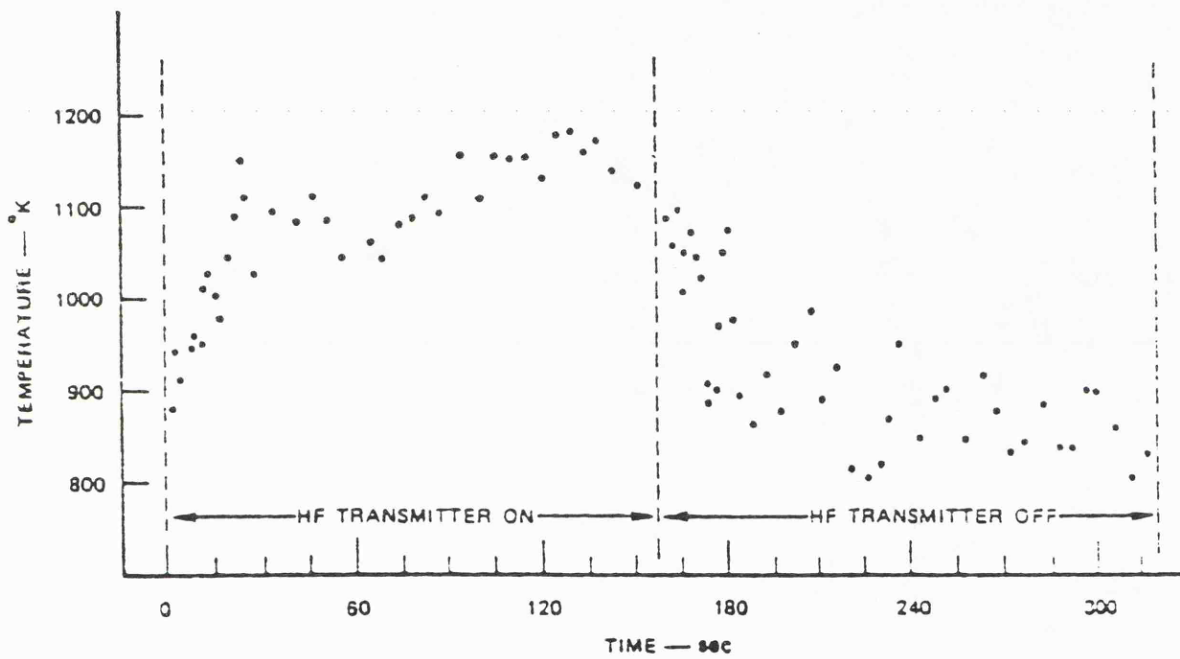
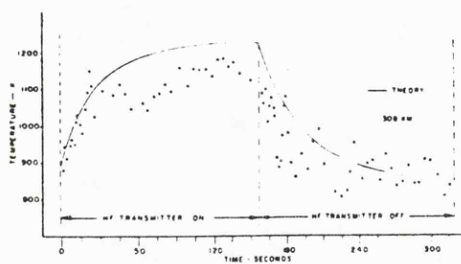
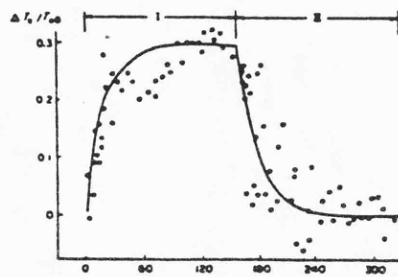


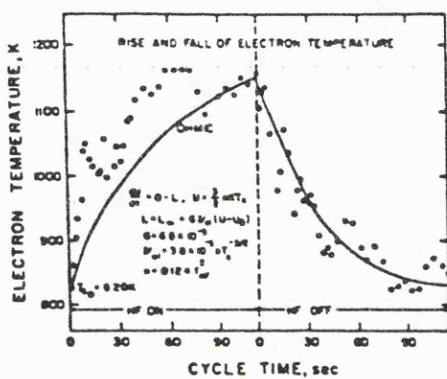
Figure 2.7 Electron temperature versus time : a superposition of 10 on-off cycles of the HF transmitter to show transient response (from Gordon and Carlson 1974).



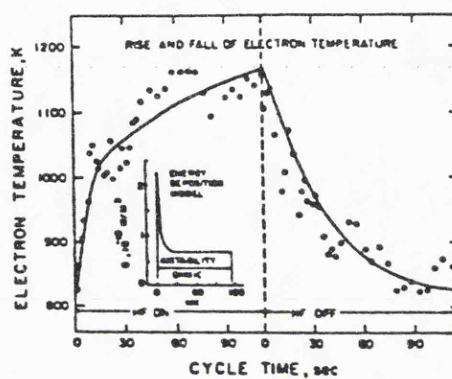
a



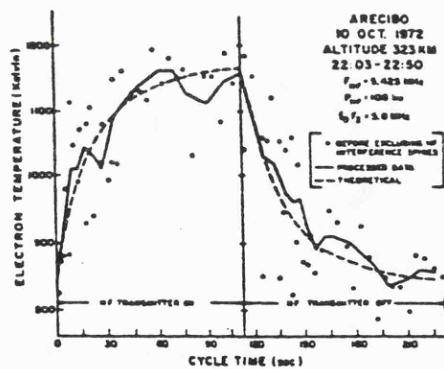
b



c



d



e

Figure 2.8 Theoretical curve fitting to electron temperature data from Arecibo. a) Meltz *et al* 1977, b) Gurevich 1978, c),d) Showen and Behnke 1978, e) Mantas *et al* 1981.

Chapter 2. Review of previous work

Meltz *et al* (1974) assumed that both deviative and anomalous absorption contributed to the temperature enhancement and obtained time constants for both heating and cooling which were in reasonable agreement with the data (Figure 2.8a). However, they predicted an equilibrium level which is higher than that exhibited by the data. Gurevich (1978) has fitted a curve with a single time constant to these data and obtained a response time ~ 20 s for both growth and decay (Figure 2.8b). Showen and Behnke (1978) maintained that ohmic heating alone was insufficient to explain the sharp initial rise in electron temperature. They invoked both ohmic heating and overshooting instability sources (ie anomalous heating due to the excitation of plasma instabilities) as the cause of the electron temperature enhancement (Figure 2.8c,d). The temperature growth and decay are satisfactorily modelled by this theory. Finally, Mantas *et al* (1981) argued that there was no requirement for the rapidly varying heat source described by Showen and Behnke as they maintained that some of the "spikes" present in the data were caused by equipment problems. Therefore, these authors employed a constant heating rate and obtained the response curve illustrated in Figure 2.8e. The theoretical curve has been derived from numerical solutions of the coupled time-dependent heat conduction equations for the electron and composite ion gases and produced a reasonable fit to the data.

Wilkinson (1988) deduced the time constants for the decay of the enhanced electron temperature after heater switch off during modification experiments at Tromsø from high time resolution data obtained by the EISCAT radar (Figure 2.9). The electron temperature was found to saturate about 20-30 s after heater switch on which is similar to the observations at Arecibo. The decay time at Tromsø varies with height (Table 2.3) with larger decay times being observed at greater altitudes. A theoretical model which attempts to calculate the electron temperature perturbation during heating is discussed in Chapter 3.

The spatial development of the electron temperature perturbation during heating at Arecibo has also been investigated theoretically (Mantas *et al* 1981) and compared with the

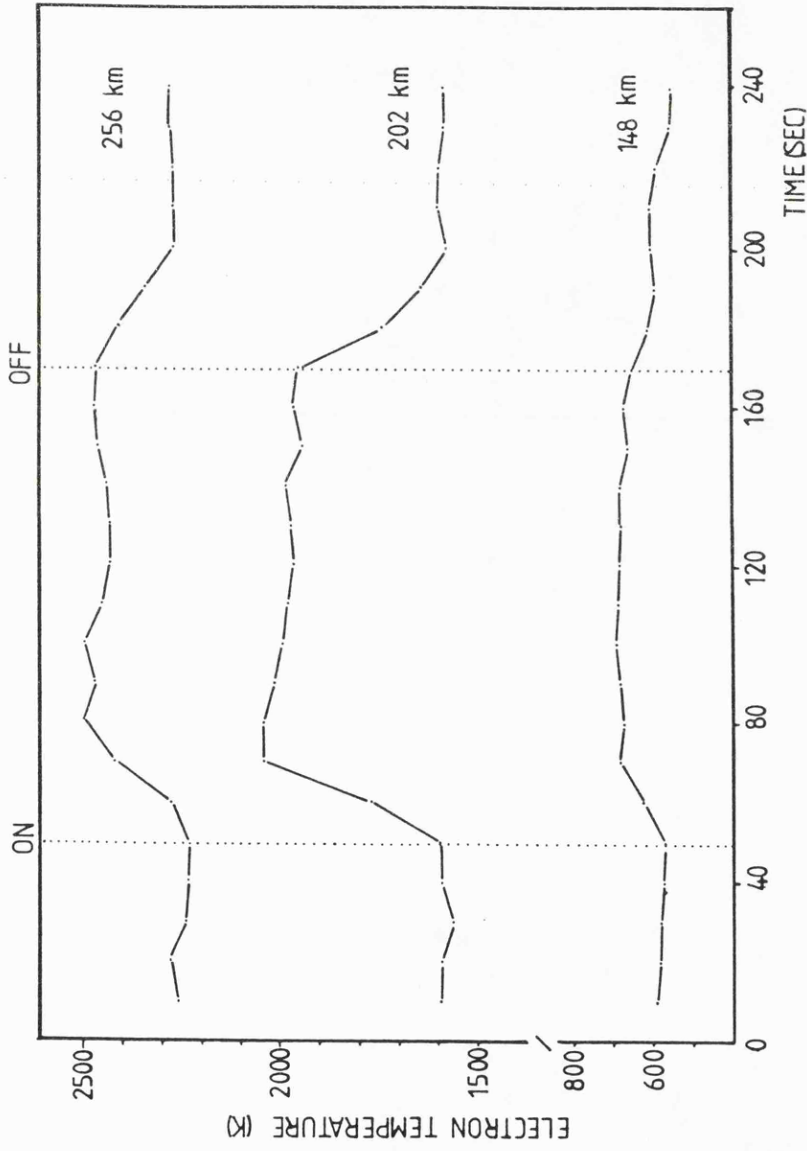


Figure 2.9 Characteristic response of electron temperature to heater switch on and off at Tromsø. The data represents an average over 10 heater cycles on 17 March 1985. The heater was reflected at a height close to 202 km (after Wilkinson 1988).

Date	Height (km)	Time Constant (s)
14/03/85	148	-
	202	34 ± 5
	256	63 ± 5
17/03/85	148	-
	202	38 ± 4
	256	48 ± 4

Table 2.3 Electron temperature decay constants obtained by simple exponential curve fitting to EISCAT data. No values were obtained at 148 km because the heater induced electron temperature enhancement was too small for accurate fitting (after Wilkinson 1988).

Chapter 2. Review of previous work

steady state experimental results (Figure 2.10). In the initial stage of heating (0 - 10 s after switch on) the electron temperature remains essentially unaffected outside of the region of heat input (Q_0), subsequently heat conduction ensures that the electron temperature is enhanced over a large height range. At steady state conditions, the theory agrees very well with experimental results at altitudes close to the height of heat input. However, the theory overestimates the temperature above and below these heights. The peak enhancement is close to 40% of the pre-heated equilibrium value, which is similar to the peak values obtained during daytime heating at Tromsø (Robinson 1989; Chapter 5). Large increases in the nighttime electron temperature at Arecibo of 150% above the equilibrium level (Figure 2.11) have been observed by Djuth *et al* (1987b). These observations have been ascribed to rather low cooling rates rather than exceptionally high heating rates (Newman *et al* 1988).

Although the incoherent scatter technique remains a powerful method of probing the heater induced changes of the electron temperature, other diagnostics have also been employed with some success. Biondi *et al* (1970) measured the intensity of the 6300 Å airglow during experiments at Boulder and inferred electron temperature changes of up to 30% of the pre-heated equilibrium level. The authors argued that the results were consistent with the airglow intensity being dependent on the electron- O_2^+ dissociative recombination, the rate of which is inversely related to the electron temperature.

In *situ* measurements of the heated ionosphere above Tromsø have been performed by rocket instrumentation (Rose *et al* 1985). Observations which were obtained in the vicinity of the heater reflection height (252-256 km) are presented in Figure 2.12. These observations reveal electron temperature enhancements of ~ 800 K (40% ambient) during some of the periods when the heater is on. This magnitude is consistent with EISCAT measurements of electron temperature changes at Tromsø (Jones *et al* 1986; Wilkinson 1988; see also Chapter 5). However, the rate at which the temperature is enhanced as measured by the rocket experiments, 40% of ambient in a few seconds, is considerably faster than that observed by

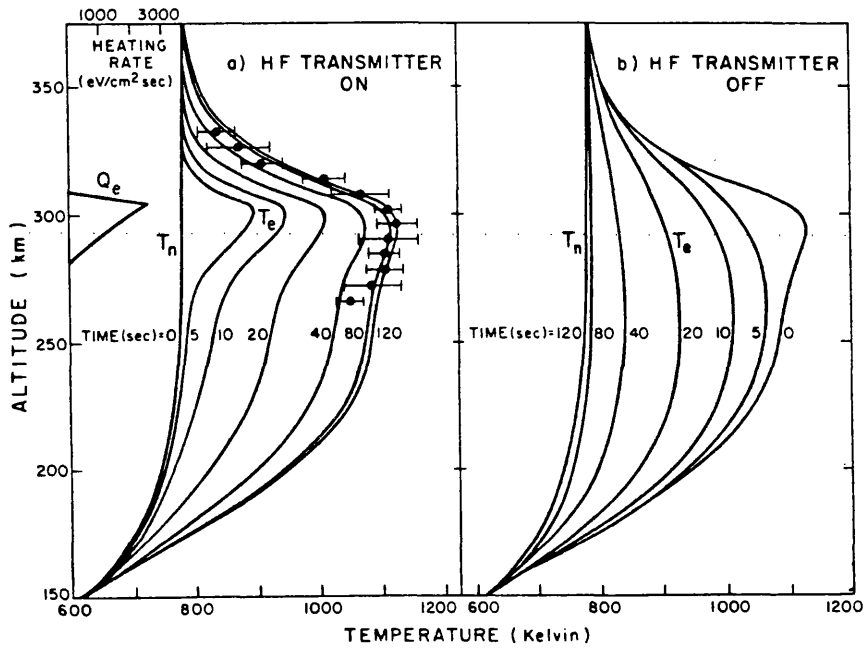


Figure 2.10 Comparison of the observed and calculated electron temperature profiles at Arecibo. The points represent the averaged observations between 80 and 120 s after heater switch on (steady state). The curves represent the calculated profiles using the heating rate, Q_e given in Figure 2.10a (from Mantas *et al* 1981).

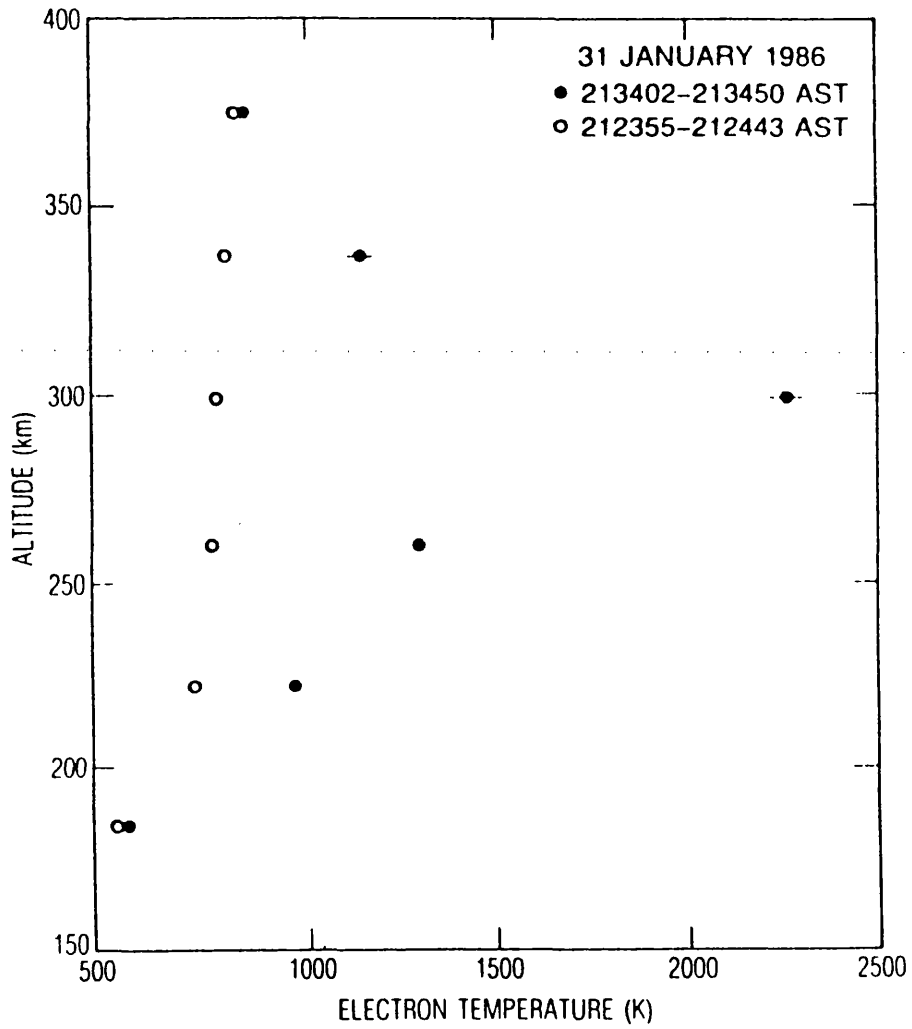


Figure 2.11 Electron temperature profile measured at Arecibo 8 minutes after heater switch on (solid dots) and the ambient profile (open circles) (from Djuth *et al* 1987).

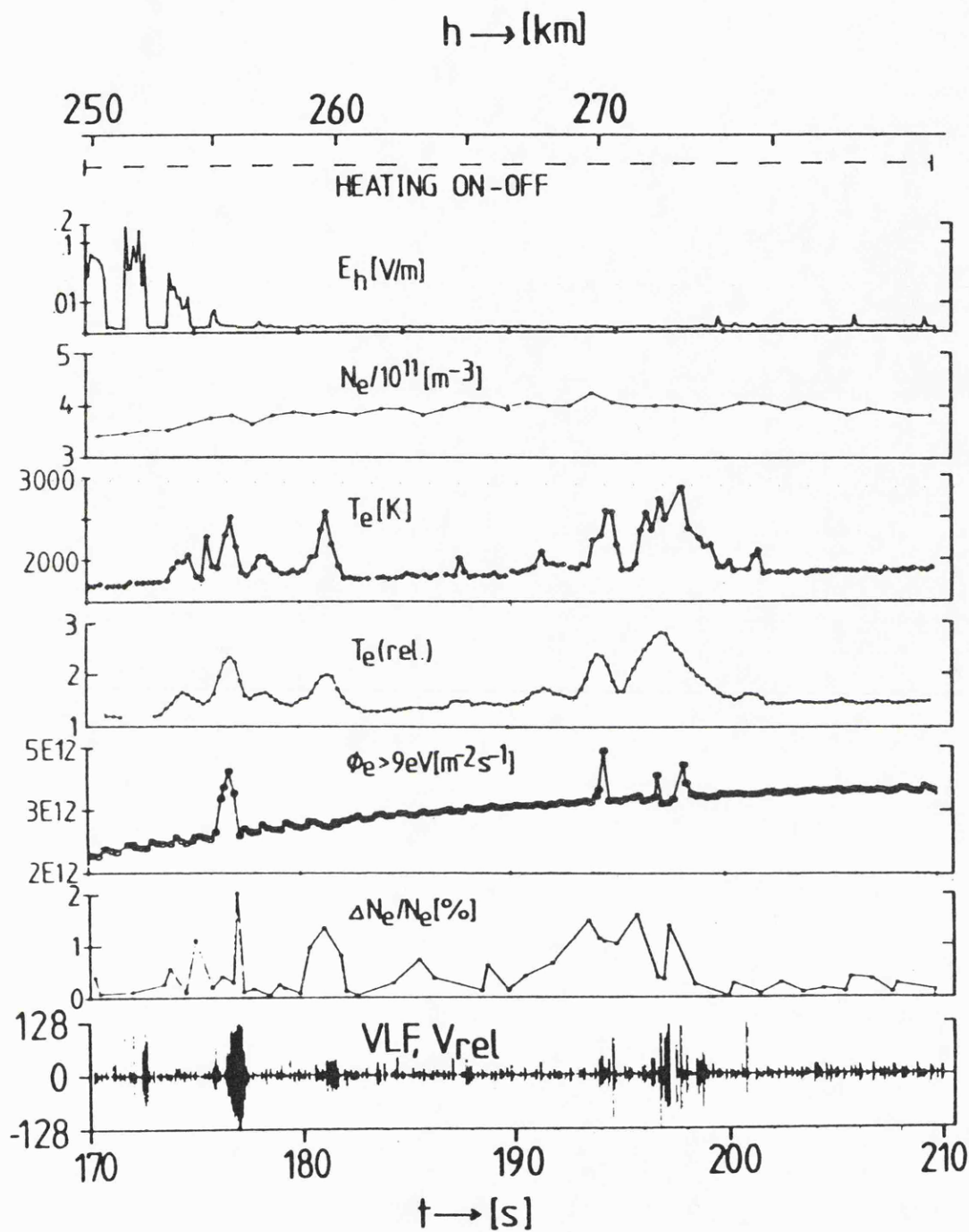


Figure 2.12 Survey of rocket measurements near and above the modified region over Tromsø on October 23, 1982, 0617 UT. Time is in seconds after launch. E_h is the heater field strength, N_e the electron density, T_e the electron temperature, ϕ_e the electron flux, and $\Delta N_e / N_e$ the change in electron density (from Rose *et al* 1985).

EISCAT. As the initial growth of the electron temperature perturbation occurs over a relatively narrow height range (Mantas *et al* 1981), then this discrepancy may be due to the relatively low altitude resolution of the EISCAT observations which suffer from “altitude smearing” (eg Lejuene and Lathuillere 1986).

The heater induced changes in the ion temperature are much smaller than those of the electron temperature due to the high ion-neutral collision frequency and large concentration of neutrals (Meltz *et al* 1974). Early measurements (Gordon and Carlson 1974) suggested that the ion temperatures were unchanged within the accuracy of the observations (~ tens of degrees Kelvin). However, theoretical results for conditions pertaining to Arecibo (Mantas *et al* 1981) predict a rise of 50 K (~ 6% above the pre-heated equilibrium values). Observations by Djuth *et al* (1987b) have revealed increases in the ion temperature of 50 - 300 K (Figure 2.13) which have been ascribed to the low cooling rates prevailing at that time (Newman *et al* 1988). Measurements of the ion temperature during heating at Tromsø indicate no systematic changes in this parameter (see Chapter 5).

2.6 Heater induced changes in the electron density

The previous sections have described how illumination of the ionosphere by a high power HF radiowave can, through the action of collisional and anomalous heating, raise the electron and ion temperatures. Many of the chemical reaction and recombination rates within the ionosphere are controlled by the prevailing electron temperature. If diffusion processes are neglected (valid in the E- or lower F-region) then the change in the electron density, N_e is determined by the temperature dependence of the electron loss rate (Jones *et al* 1982),

$$\frac{dN_e}{dt} = q_p - q_L = q_p - \alpha N_e^2 \quad (2.4)$$

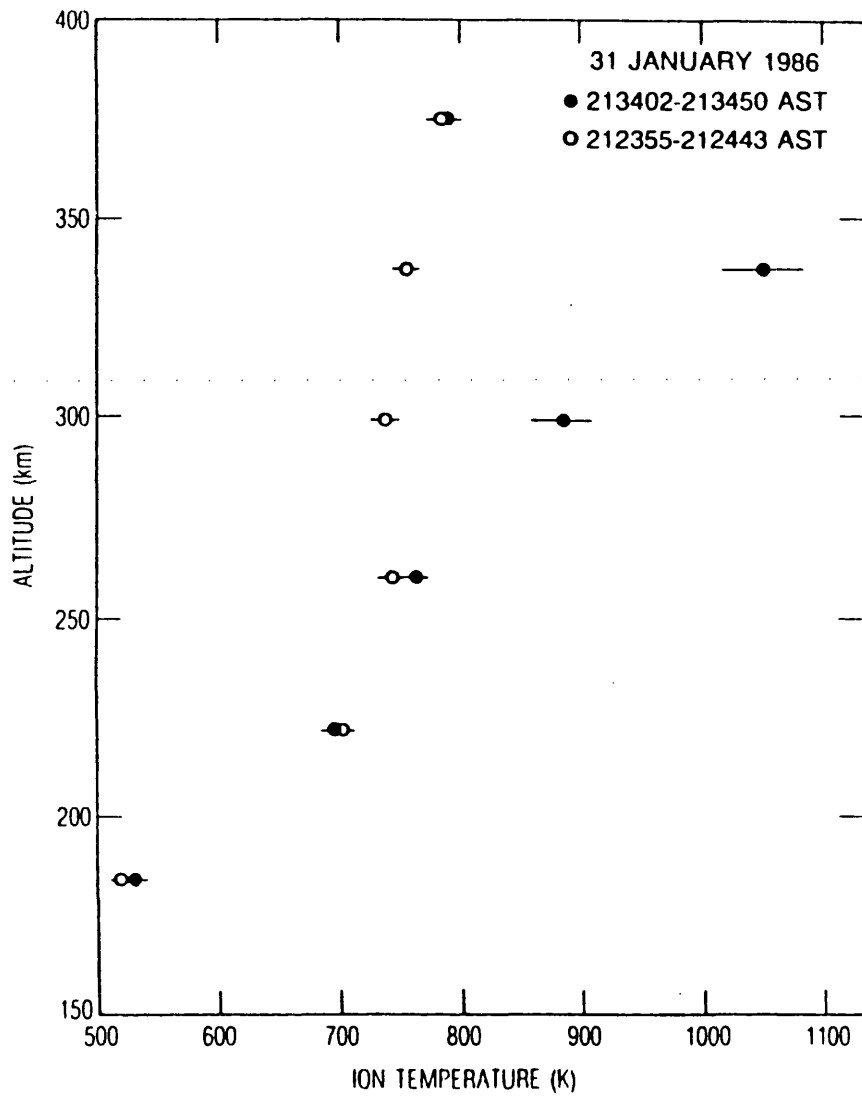


Figure 2.13 As for Figure 2.11, except ion temperature measurements (from Djuth *et al* 1987).

Chapter 2. Review of previous work

where, q_p and q_L are the total electron production and loss rates, respectively, and α is the effective recombination coefficient. The value of α decreases with increasing electron temperature (Holway and Meltz 1973; Gurevich 1978) and therefore N_e increases. However, in the upper F-region the situation is more complicated because transport (diffusion) processes tend to limit the growth of N_e and this simple model is insufficient to describe the electron density response to heating. In general, transport begins to dominate above about 200 km with recombination dominating below this height (Gurevich 1978). A model which invokes both recombination and transport processes has been discussed by Robinson (1989) and is presented in some detail in Chapter 3. The modelled results are compared with observations of the change in electron density derived from EISCAT and HF phase measurements in Chapter 6.

Some of the theoretical descriptions of the modified density which have appeared in the literature will now be discussed briefly. Meltz *et al* (1974) solved the continuity and momentum equations in order to determine the effect of heating on the electron density. The results for nighttime heating at Arecibo and Platteville are illustrated in Figure 2.14a. After about 2 minutes of heating the model predicts a density depletion of about 3%. Gurevich (1978) also predicted a depletion of a few percent (Figure 2.14b) by considering the stationary solutions of a perturbation analysis of the transport processes. Bernhardt and Duncan (1982) developed a numerical model to simulate the effects of underdense heating. The modified electron density structure predicted by this model is reproduced in Figure 2.14c. In all these cases the theories predict small depletions in the electron density at heights close to the heater reflection height (or F-region peak in the case of underdense heating simulated by the model of Bernhardt and Duncan).

Measurements of the heater induced changes in the electron density have been reported for many different ionospheric conditions, time of day, and interaction heights and are marked by a considerable variation in results. Density enhancements have been observed by Vas'kov

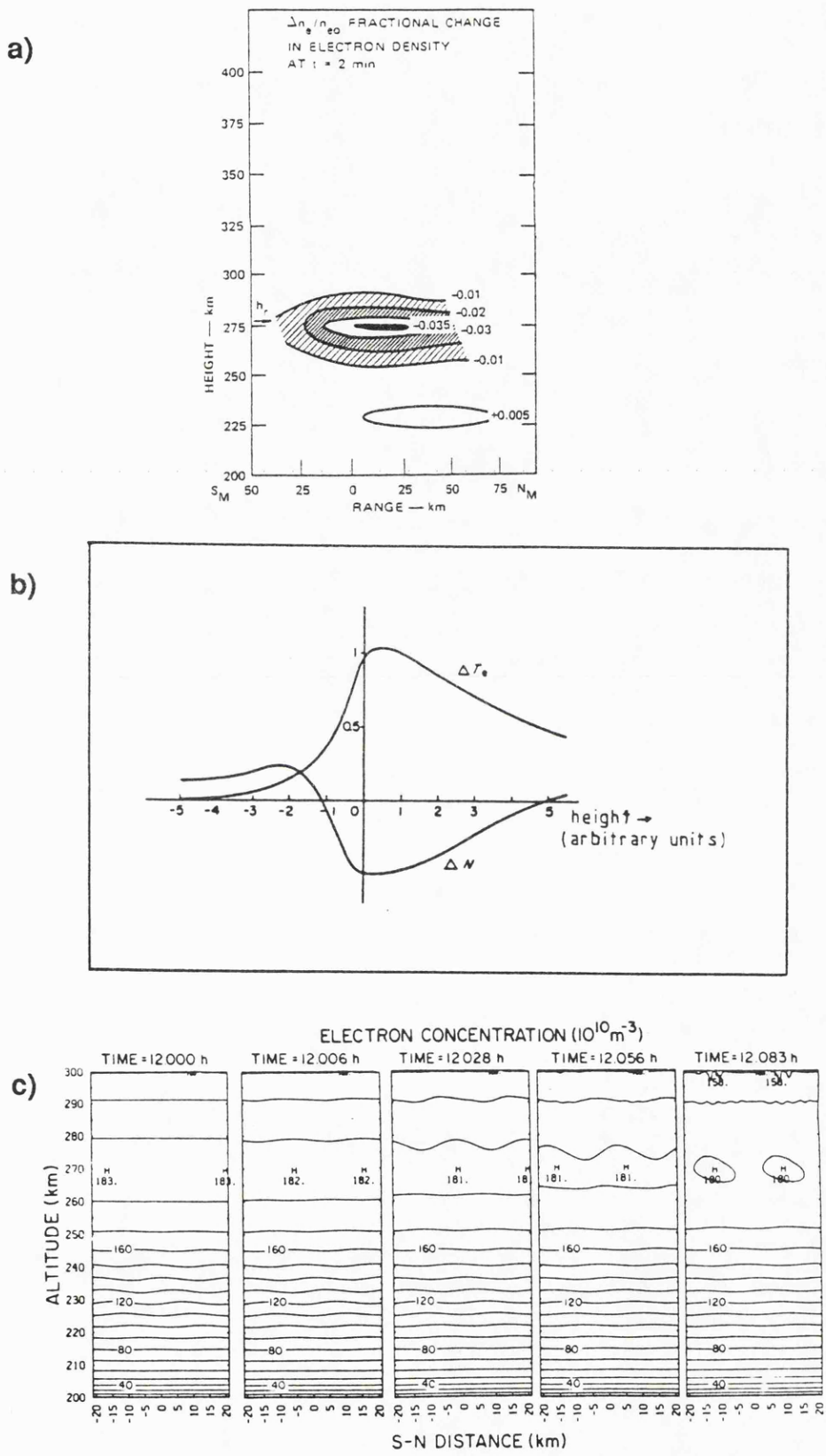


Figure 2.14 Theoretical calculations of heater-induced electron density perturbations
 a) Meltz *et al* 1974, b) Gurevich 1978, c) Bernhardt and Duncan 1982.

Chapter 2. Review of previous work

et al (1981), Jones *et al* (1982) and Robinson (1989) and density depletions have been reported by Utlaut and Violette (1972), Birkmayer *et al* (1986), Wong *et al* (1987), Djuth *et al* (1987b), Wright *et al* (1988b) and Duncan *et al* (1988). These experiments are each described below and the results summarised in Table 2.4.

At Platteville, examination of ionograms recorded during nighttime heating experiments has revealed an electron density depletion of about 7% of ambient after a few minutes heating (Utlaut and Violette 1972). These authors also described a possible increase in the density during daytime heating, although the magnitude of this enhancement was not established. RMS density deviations of typically 1-2%, and below 4%, have been inferred from measurements of VHF/UHF radar backscatter coefficients (Minkoff 1974) although these are consistent with scattering from small scale field aligned irregularities rather than large scale changes. Biondi *et al* (1970) have conducted measurements of the 6300 Å airglow and inferred a density change via the change in the electron- O_2^+ recombination rate, but they have not determined the sign or magnitude of the perturbation.

The first studies of large scale heating at Tromsø were conducted by Jones *et al* (1982). These authors measured the phase changes (Figure 2.15) of a low power HF diagnostic wave propagating through the heated volume. The resultant positive phase change was attributed to an increase in the electron density as the phase path of a wave is reduced by a decrease in the plasma refractive index (eg Davies 1969). The growth and decay time of the density perturbation is approximately 38 s, but the authors were unable to ascertain the magnitude of the electron density enhancement. Preliminary investigations of the heater induced change in the EISCAT power profile (Robinson 1989) have revealed an enhancement in the electron density of a few tens of percent. These results will be discussed in more detail in Chapter 6. Recent observations by the dynasonde (Wright *et al* 1988b) have recorded an electron density depletion ~ 15% in the heated ionosphere above Tromsø.

Location	Time of Day	Altitude	Observation Technique	Ne change	Authors
Platteville	Nighttime		Ionograms	7% depletion	Utlaut & Violette (1972)
	Daytime		VHF/UHF backscatter	Enhancements	
	?		Airglow	1-2% deviations	Minkoff (1974)
Tromsø	Nighttime			Altered N_e	Biondi <i>et al</i> (1970)
	Daytime	F1	HF phase path	Enhancement	Jones <i>et al</i> (1982)
	Daytime	F1 - F2	Incoherent Scatter	10-20% increase	Robinson (1988)
Arecibo	Daytime	F2	Dynasonde	15% depletion	Wright <i>et al</i> (1988b)
	Daytime	F	Chirped Inc. Scatter	3-5% depletion	Birkmayer <i>et al</i> (1986)
	Daytime	F	Plasma lines	7% depletion	Wong <i>et al</i> (1987)
	Nighttime	F	Incoherent Scatter	10-15% depletion	Djuth <i>et al</i> (1987)
	Nighttime	F	Incoherent Scatter	50 % + depletion	Duncan <i>et al</i> (1988)
Moscow	Sunlit Unlit	F	HF Doppler shift	2-10% increase Usually depletion	Vas'kov <i>et al</i> (1981)

Table 2.4 Summary of experimental observations of heater induced electron density perturbations

OCT. 12, 1980 14:12-14:28 UT HEATER 3.515 MHz O-MODE ERP = p. 160 MW

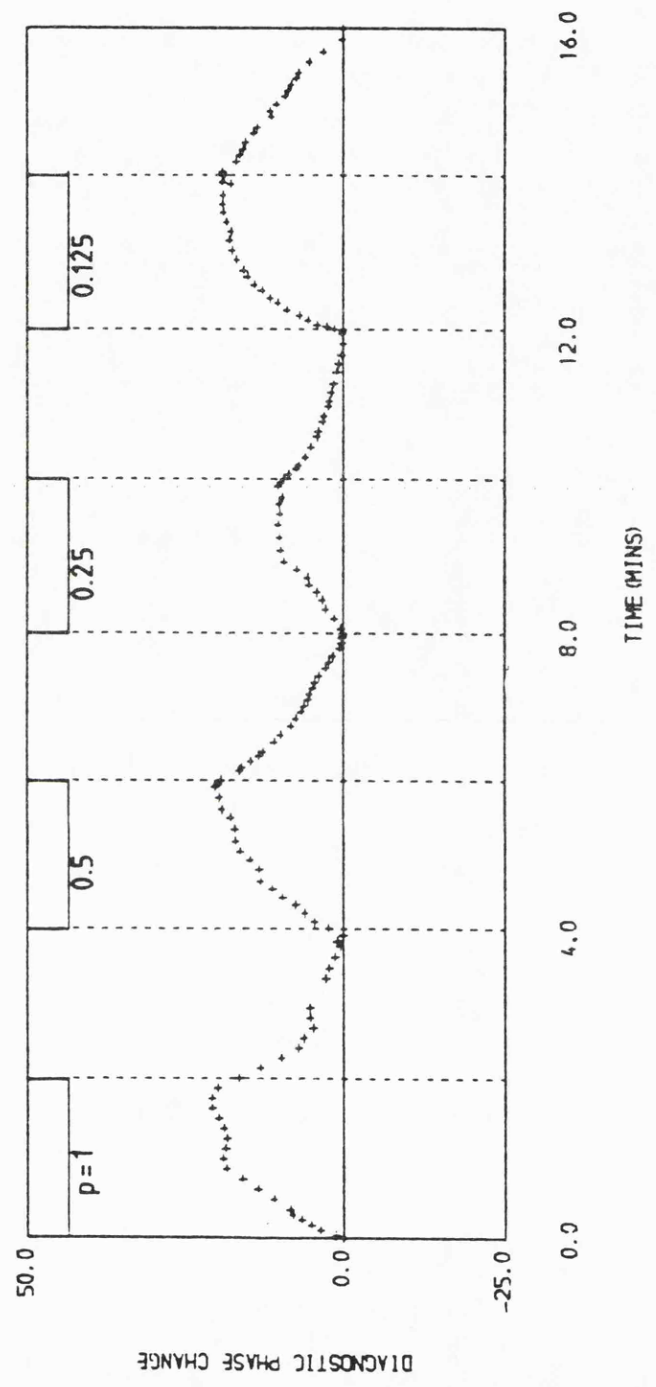


Figure 2.15 Phase of 3.778 MHz diagnostic wave in units of 2π versus time, October 12, 1980, 1412-1428 UT. The heater operated at 3.515 MHz, O-mode, ERP = p. 160 MW. The heater on times are indicated by bars (from Jones *et al* 1982).

Chapter 2. Review of previous work

Measurements of electron density at Arecibo during F-region heating have predominantly revealed depletions of a few percent. Birkmayer *et al* (1986) employed the 430 MHz incoherent scatter radar in a chirped frequency mode which afforded excellent height and time resolution and provided evidence for a depletion of between 3 and 5%, at a height close to, but below, the reflection height. Wong *et al* (1987) utilised a time of flight radar technique and observed a depletion of ~ 7% in a narrow region (~ 5 km) below the reflection height (Figure 2.16a). Djuth *et al* (1987b) observed changes in the 430 MHz radar power profile and discovered a depletion of 10-15% (Figure 2.16b). During experiments in winter and after local sunset, Duncan *et al* (1988) measured electron density depletions of over 50 % (Figure 2.16c) which persisted for at least 30 minutes after heater switch off. These large depletions have been explained in terms of the non-linear refraction of the heater wave (Hansen *et al* 1990).

In the Soviet Union the Doppler shifts and phase of diagnostic waves which propagate through the heated volume have been recorded at several different frequencies (Vas'kov *et al* 1981; Gurevich and Migulin 1982; Migulin and Gurevich 1985; Belikovich *et al* 1989; Zyuzin *et al* 1989). An example of the frequency change observed during these heating experiments is presented in Figure 2.17a. A Doppler shift of approximately 1 Hz is evident on all of the probe frequencies, which implies an initial velocity of ~ 50-100 ms⁻¹. The steady-state is attained after about 60 s following a total ionospheric displacement of 3-6 km which corresponds to a density enhancement of between 2 and 10 %. Vas'kov *et al* report that in the sunlit ionosphere the change in electron density was always positive, but in the unlit ionosphere the change was usually negative (eg Figure 2.17b). This behaviour has been ascribed to an enhancement in the ionising effectiveness of photoelectrons in the sunlit ionosphere.

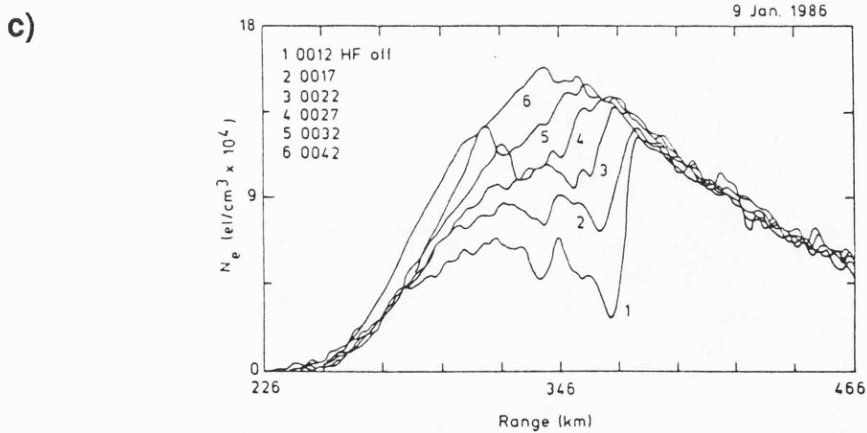
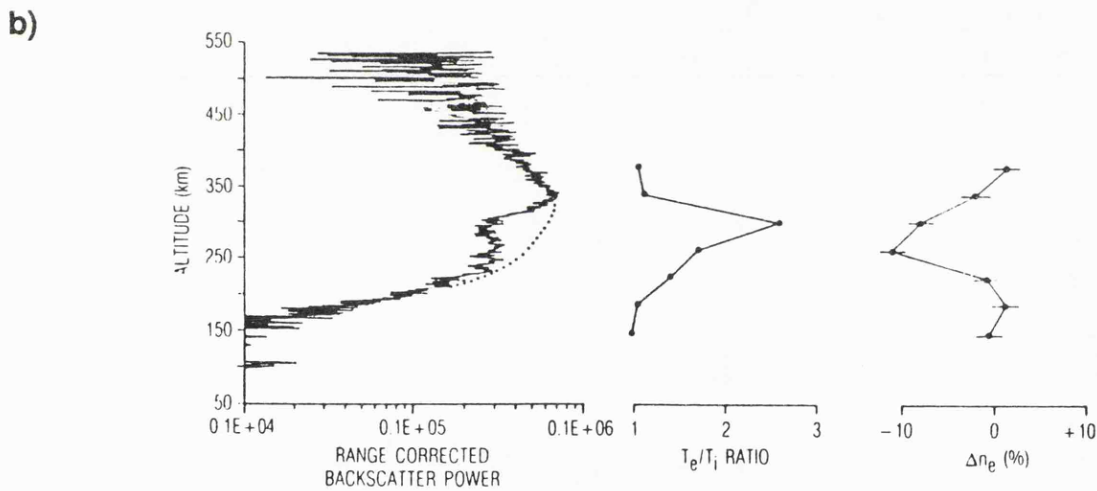
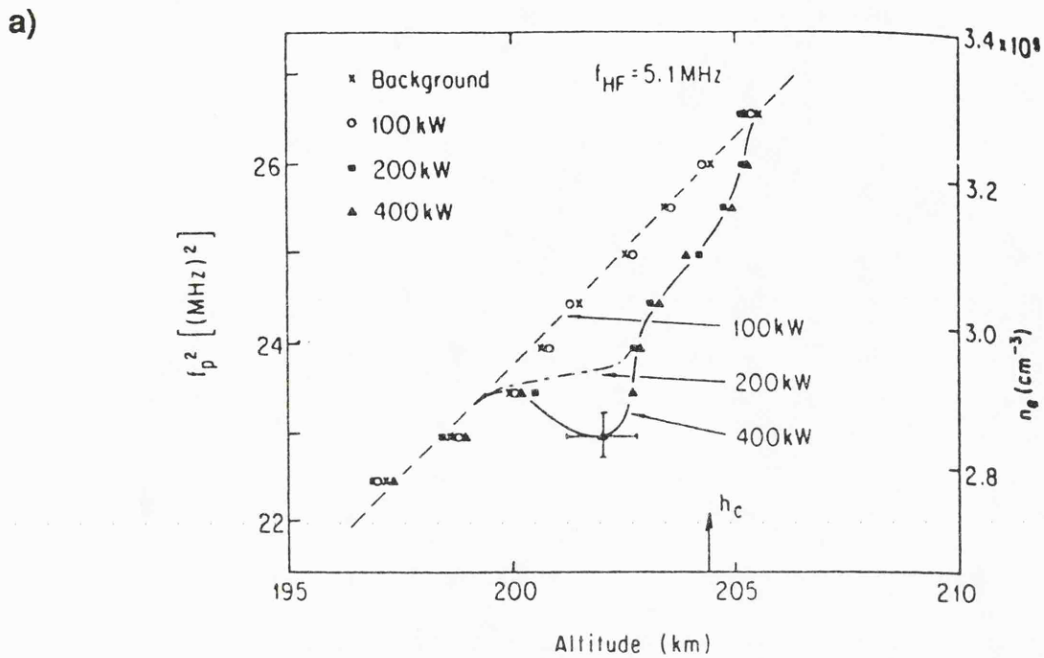


Figure 2.16 Height profiles of the heater induced Ne perturbation measured by the 430 MHz radar at Arecibo. a) calculated from time of flight measurements (from Wong *et al* 1987), b) power profile (left), T_e/T_i profile (centre), and Ne perturbation deduced from the temperature corrected power profile (right) (from Djuth *et al* 1987), c) recovery of Ne after heater switch off (from Duncan *et al* 1988).

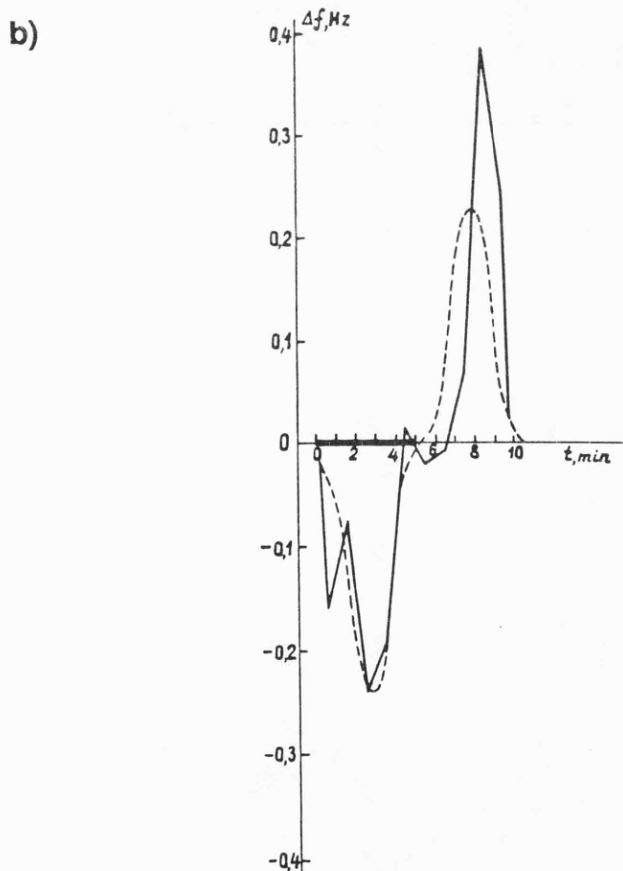
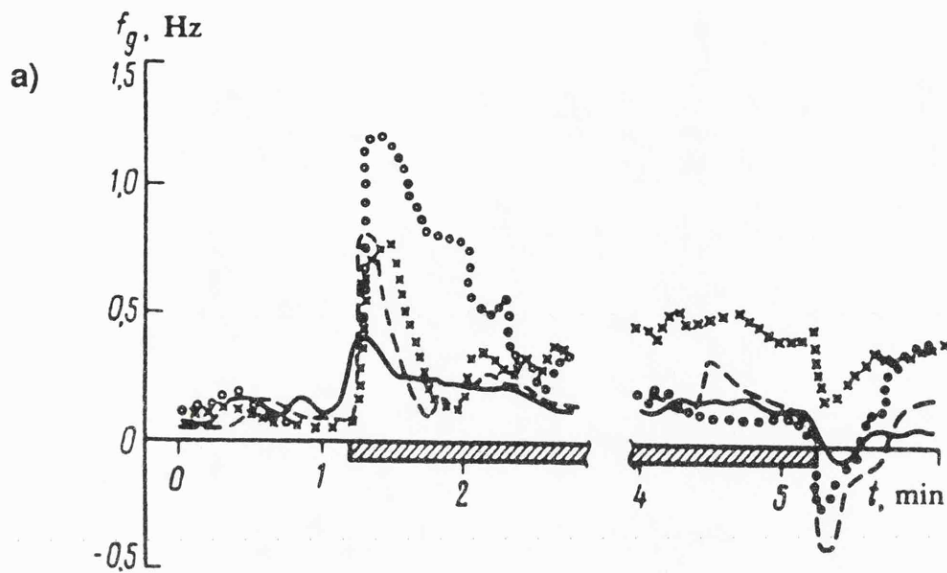


Figure 2.17 Doppler shift of low power HF signals reflected from a modified ionosphere. a) Daytime, the hatching shows the time over which the pump transmitter operated. Solid curve $f_1 = 3.4$ MHz; dashed curve $f_2 = 4.6$ MHz; xxx, $f_3 = 4.7$ MHz; ..., $f_4 = 4.9$ MHz. Heater 4.8 MHz (from Vas'kov *et al* 1981), b) Nighttime, dashed line is theoretical prediction (from Gurevich and Migulin 1982).

2.7 Ion line Overshoot

The type of backscatter spectrum observed by an incoherent scatter radar depends upon the ratio of the Debye length to the radar wavelength. For typical daytime conditions at Tromsø and for the UHF EISCAT system the "ion-line" spectrum is observed at heights above 80 km and below 1500 km (Rishbeth and Williams 1985). The ion-line spectrum is characterised by a double-hump which corresponds to upward and downward going ion-acoustic waves. Scattering also occurs from electron-acoustic (Langmuir) waves which appear in the spectrum as the so-called "plasma" lines, Doppler shifted upwards and downwards from the radar frequency by the local plasma frequency.

When the F-region is illuminated by a powerful HF radio wave polarised in the O-mode, Langmuir waves are parametrically excited (eg Robinson 1989) leading to increased power in the plasma lines. Examples of enhanced plasma lines during heating experiments have been observed at both Arecibo (eg Carlson *et al* 1972; Showen and Kim 1978; Wong *et al* 1983; Djuth 1984; Duncan and Sheerin 1985; Djuth *et al* 1986, 1987a; Fejer and Sulzer 1987; Sulzer *et al* 1989) and Tromsø (eg Kohl *et al* 1983; Hagfors *et al* 1983; Stubbe *et al* 1985).

There have been fewer examples of the ion-line (or power profile) enhancement reported in the literature. The first recorded incidence of the ion-line overshoot was reported by Carlson *et al* (1972) for an experiment performed at Arecibo. Observations at Tromsø indicate that the overshoot has growth times of a few tens of milliseconds (Stubbe *et al* 1985) with decay times less than 5 s (Kohl *et al* 1983). It has also been noted that, for heating at Tromsø, in the majority of cases the overshoot is quenched regardless of whether the heater remains on or not (Jones *et al* 1986). Furthermore, where this is the case the overshoot does not reoccur until the heater is switched off and then switched back on. The overshoot occurs close to the heater reflection height, and therefore can indicate where the heater was initially reflected. This property has been employed in scaling power profile data (see Chapters 4 and 6).

2.8 Concluding Remarks

This review highlights the effects on the bulk properties of the ionospheric plasma during artificial modification experiments. The incident wave energy is absorbed by the plasma which results in electron heating via two processes, anomalous and collisional absorption. The enhanced temperature then leads to a change in the chemistry and hence the electron number density. These properties have been extensively studied at low latitudes, but theory suggests that the response at high latitudes will be different. In this thesis observations of large scale effects obtained during experiments at Tromsø are presented (Chapters 5 and 6).

The anomalous absorption of low power HF diagnostics has been reviewed briefly in this chapter. The processes which result in anomalous absorption will be reviewed in more detail in the next chapter and the first direct observations of the anomalous absorption of low power test waves during heating experiments at Arecibo presented in Chapter 7.

Chapter 3 Theoretical Modelling

3.1 Introduction

The electric field of a radio wave propagating through a plasma gives rise to a sympathetic motion of the charged constituents (ie ions and electrons) of the plasma. If the electrons or ions undergo collisions, then energy will be transferred from the electromagnetic (EM) wave to the neutral gas and dissipated in the form of heat. The transfer of energy from the wave to the plasma results in the collisional (or deviative) absorption of the incident wave. The increased energy of the ions, electrons and neutrals represents an increase in their respective temperatures. These collisional effects occur for all wave amplitudes and are linear phenomena except insofar as the collisional frequencies themselves depend on temperature. Other absorption effects which occur only for high amplitude waves and are non-linear, are now known to play a major role in ionospheric modification experiments.

The most important of these non-linear phenomena are the wave-wave interactions, eg the oscillating two stream instability (OTSI) and the thermal oscillating two stream instability (TOTSI), which can lead to the generation of field aligned density striations (Grach *et al* 1977, 1979; Das and Fejer 1979; Inhester *et al* 1981; Stubbe *et al* 1982a, b; Kuo and Lee 1982; Dysthe *et al* 1983; Robinson 1989). These striations are responsible for the anomalous absorption (Vas'kov and Gurevich 1975, 1977; Graham and Fejer 1976; Jones *et al* 1984; Mjølhus 1985; Robinson 1989) of the incident wave. A high power radio wave excites other wave modes (eg Langmuir waves) and thereby loses energy, ie undergoes absorption. Langmuir waves have much lower group velocities than the radio wave and therefore undergo more collisional absorption which results in greatly enhanced large-scale effects. The large-scale effects of anomalous absorption are in addition to any caused by collisional absorption.

Chapter 3. Theoretical Modelling

In this chapter two separate models are discussed. These models address the large scale response of the electron temperature and density to heating and the calculation of the coefficient of anomalous absorption as a function of wave frequency and magnetic latitude. The results of these models are employed in Chapters 5 and 6, and Chapter 7 respectively where they are compared with experimental results.

3.2 Large Scale Temperature and Density Changes

Features in the ionospheric plasma which occur on spatial scales of 10 km or more perpendicular to the magnetic field are, in the context of heating experiments, termed large-scale. These features are, in general, non-periodic in contrast to small-scale features such as field-aligned irregularities. During artificial modification experiments the energy of the incident electromagnetic wave is absorbed by the plasma via collisional or anomalous heating processes which results in increases in the electron and ion temperatures. The enhanced temperatures in turn lead to a change in the electron density through the action of diffusion and changes in the chemical reaction rates. Robinson *et al* (1988) have determined the magnitude of the electron density and temperature changes due to heating by a high power radio wave by solving the one-dimensional linearised heat conduction and diffusion equations (Equations 3.1 and 3.2 respectively, derived by Gurevich 1978),

$$\frac{d \Delta T_e}{d t} - K_e \frac{d^2 \Delta T_e}{d x^2} = -\frac{\Delta T_e}{\tau_T} + Q \quad (3.1)$$

$$\frac{d \Delta N}{d t} - D_a \frac{d^2 \Delta N}{d x^2} - D_{Tea} \frac{N_0}{T_{e0}} \frac{d^2 \Delta T_e}{d x^2} = -\frac{\Delta N}{\tau_n} - \frac{N_0}{T_{e0}} \gamma_1 \frac{\Delta T_e}{\tau_n} \quad (3.2)$$

where ΔT_e and ΔN are the change in electron temperature and density respectively, t is time, x is altitude, $K_e = T_e / m_e (v_{en} + v_{ei})$, $D_a = (T_e + T_i) / m_i v_{in}$, $D_{Tea} = T_e / m_i v_{in}$, T_i and T_e are

Chapter 3. Theoretical Modelling

the ion and electron temperatures, m_i and m_e are the ion and electron masses, v_{in} and v_{en} are the ion- and electron- neutral collision frequencies, v_{ei} is the electron-ion collision frequency, Q is the heat input per unit volume from the EM wave, and γ_1 is the ionisation-equilibrium shift coefficient.

Following the non-stationary perturbation approach (ie $\Delta N \ll N_0$ and $\Delta T_e \ll T_{e0}$) of Vas'kov and Gurevich (1975) the solutions to Equations (3.1) and (3.2) are as follows,

$$\Delta T_e(x, t) = T_{e0} \int_{-\infty}^{\infty} \frac{dx'}{L_T} \int_{-\infty}^t \frac{dt' Q(x', t')}{\sqrt{4\pi\tau_T(t-t')}} \exp \left[-\frac{t-t'}{\tau_T} - \frac{(x-x')^2}{4K_e(t-t')} \right] \quad (3.3)$$

and

$$\Delta N(x, t) = N_0 \int_{-\infty}^t \frac{dt''}{\tau_T} \int_{-\infty}^{\infty} \frac{dx''}{L_T} G(x-x'', t-t'') Q(x'', t'') \quad (3.4)$$

where $G(x, t-t'')$ is a Green function given by,

$$G(x, t-t'') = \int_{t''}^t \frac{dt'}{\tau_n} \frac{L_T}{\sqrt{\pi b}} \left[\gamma_1 + \frac{4L_N^2 K_T}{b} \left(\frac{x^2}{b} - \frac{1}{2} \right) \right] \cdot \exp \left[-\frac{t-t'}{\tau_n} - \frac{t-t''}{\tau_T} - \frac{x^2}{b} \right] \quad (3.5)$$

and $b = 4D_a(t-t') + 4K_e(t-t'')$, $L_N = (D_a \tau_n)^{1/2}$, $L_T = (K_e / \delta v_{en})^{1/2}$, and δ is the fractional energy loss per collision. L_N and L_T are characteristic lengths which determine the role of the density and temperature inhomogeneities respectively, D_a is the coefficient of ambipolar diffusion, K_T the thermal diffusion ratio and K_e is the electron thermal conductivity.

Equations 3.3, 3.4 and 3.5 have been solved numerically which allows the initial conditions to be closely matched to those encountered during experiments. The numerical modelling results presented in Chapters 5 and 6 employed the ambient electron and ion temperatures

Chapter 3. Theoretical Modelling

and electron density height profiles measured by EISCAT prior to the heater switch on, the neutral atmosphere parameters from MSIS (Hedin 1983), the ion-composition from the UCL-Sheffield model (Quegan *et al* 1982; Quegan private communication) and the electron loss rates from expressions in Schunk and Nagy (1978). The pre-heated parameters adopted in modelling the conditions observed during the heating experiments held at Tromsø in 1987 are reproduced in Table 3.1. It should be noted that the height resolution of these data is only 10 km, while the height resolution of the computer model was 5 km and therefore a linear interpolation technique was adopted. The results from the model are obviously dependent upon the input parameters, and the effect of changing some of these parameters is investigated below.

For heating at high latitudes it is well established (eg Robinson 1989) that anomalous heating, due to field aligned irregularity (FAI) generation in a narrow region close to the upper-hybrid height (see Section 3.3), dominates over collisional heating at the reflection height. Robinson *et al* (1988) therefore assumed that the energy deposition during heating at high latitudes occurs over a narrow region and that the heat input may be defined by a delta function in height at the upper-hybrid height such that,

$$Q(x, t) = Q_0 \delta(x - x_0) \quad (3.6)$$

In the model the heater interaction height, x_0 was allowed to vary self-consistently as changes in the electron density altered the height where the heater wave frequency matched the upper-hybrid resonance condition. The value of Q_0 was chosen such that the peak value of $\Delta T_e/T_{e0}$ produced by the model was consistent with that observed by EISCAT (or the 430 MHz radar in the case of experiments at Arecibo) during modification experiments. Calculations of the energy flux of the heater at Tromsø (Robinson 1989) result in values of Q_0 which are consistent with those chosen in the manner described above.

Height (km)	Te (K)	Ti (K)	Ne (10^{10} m^{-3})	γ	M (amu)
150	800	792	6.10	0.41	30.05
160	840	787	7.17	0.408	29.55
170	1000	784	8.60	0.397	28.38
180	1210	782	10.7	0.370	28.07
190	1420	780	13.2	0.302	25.05
200	1550	799	18.1	0.215	21.73
210	1640	799	21.5	0.141	19.53
220	1710	780	22.4	0.0876	18.03
230	1770	784	22.0	0.0543	17.14
240	1820	785	21.2	0.0347	16.60
250	1850	788	20.4	0.0228	16.32
260	1880	790	18.8	0.0162	16.32
270	1920	795	17.2	0.0114	16.17
280	1960	798	14.5	0.00817	16.10
290	2000	800	12.2	0.00597	16.08
300	2010	806	10.5	0.00444	16.09
310	2050	809	9.50	0.00322	16.04
320	2090	818	8.60	0.00239	16.01

Table 3.1 Background parameters adopted for modelling the 1987 heating experiments.

Chapter 3. Theoretical Modelling

The sensitivity of the model results has been investigated by arbitrarily changing some of the input parameters. In addition, two different models of the thermal conductivity, K_e (Gurevich 1978; Schunk and Nagy 1978, models 1 and 2, respectively) have been employed. The value of K_e determined from these two models has then been changed, and also the number density of N_2 has been adjusted from the result obtained from the MSIS model.

The ionospheric response of the electron temperature and density after 60 s of heating for both of the thermal conductivity models is depicted in Figure 3.1. A height resolution of 5 km, a heater reflection height of 200 km, and the background conditions pertaining to 12 UT on 26 February 1987 have been employed. The value of Q_0 has been chosen to give a peak equilibrium value of $\Delta T_e/T_e$ of 50%. Above the reflection height the two thermal conductivity models give very similar results in both T_e and N_e , with $\Delta T_e/T_e$ falling from the peak value with a scale length of a few ten's of km. With model 1, the peak in $\Delta T_e/T_e$ is fairly narrow (~ 5 km), with a much faster fall-off below the peak than above, while with model 2 the peak is much wider (~ 20 km) than for model 1, but the characteristic length of the fall-off is much the same.

Thermal conductivity model 2 results in a higher peak in $\Delta N_e/N_e$ (~ 13%) compared to model 1 (~ 10%), although in both cases the peak is located approximately 15 km below the heater reflection height. Above 210 km the value of $\Delta N_e/N_e$ is roughly the same for both models. The small "notch" in the density which is visible at the original reflection height for model 1, may be observed as an inflection in model 2. At heights below the peak, the fall-off is similar for both models.

In Figure 3.2 the effect of changing the value of the thermal conductivity for each model on the electron temperature is illustrated. The thermal conductivity has been multiplied by a factor which is constant at all heights, the factors chosen being 50% and 150%. Changing the thermal conductivity in this way has an effect on the value of L_T , the thermal scale length, by about 20-30%, a value similar to the accuracy claimed for model 2 by Schunk and Nagy. The

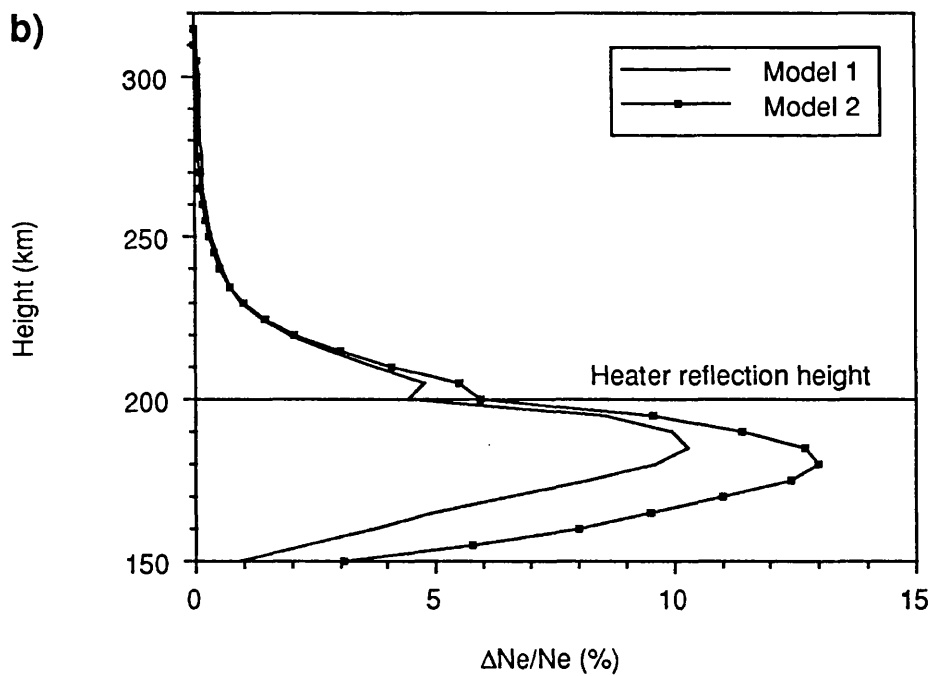
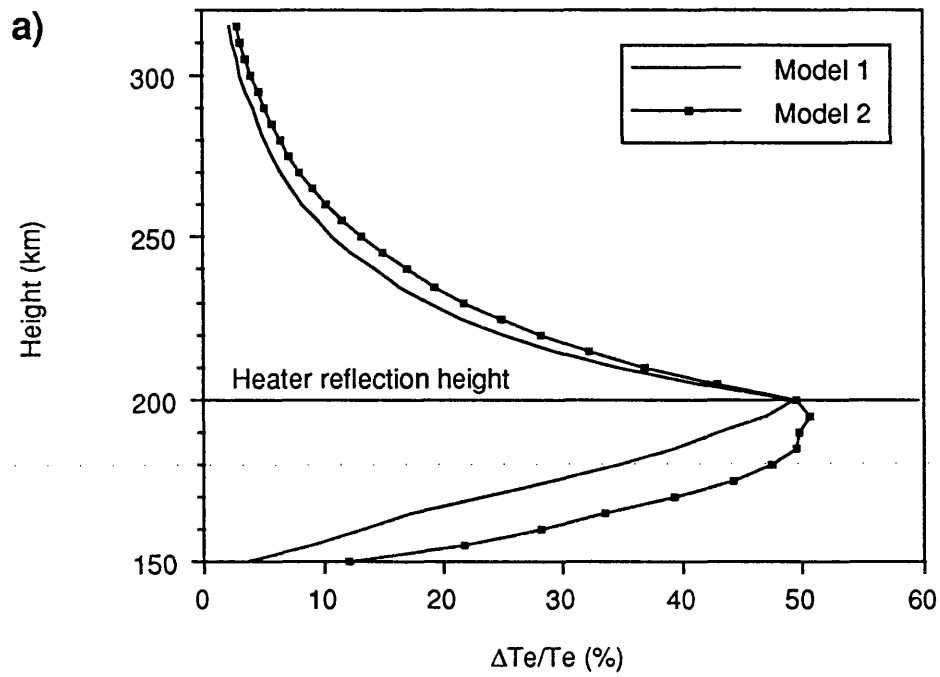


Figure 3.1 Modelled changes in a) electron temperature and b) electron density after 60 s of heating for two different thermal conductivity models.

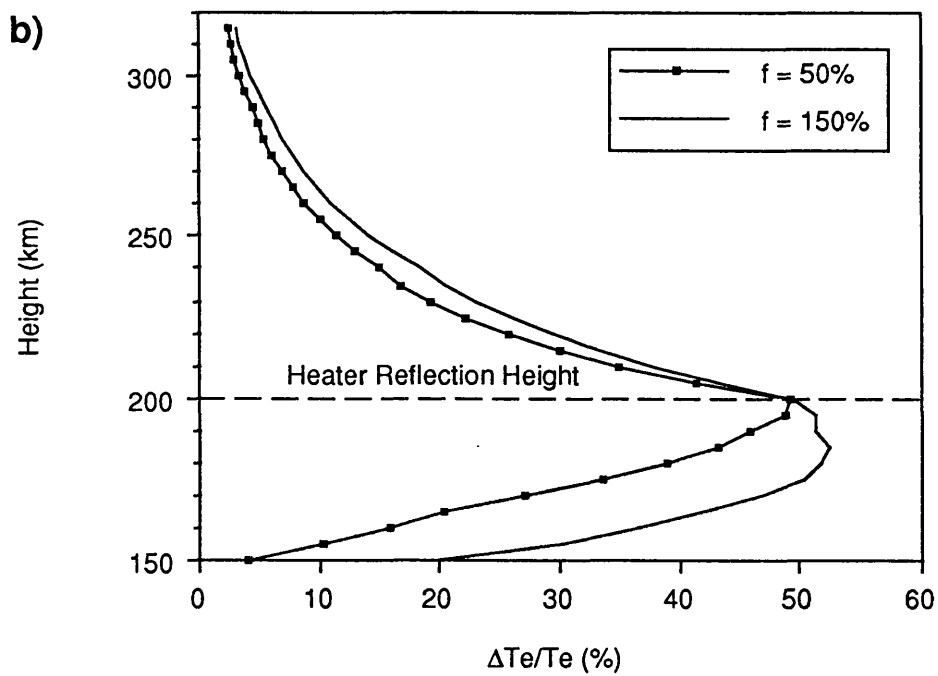
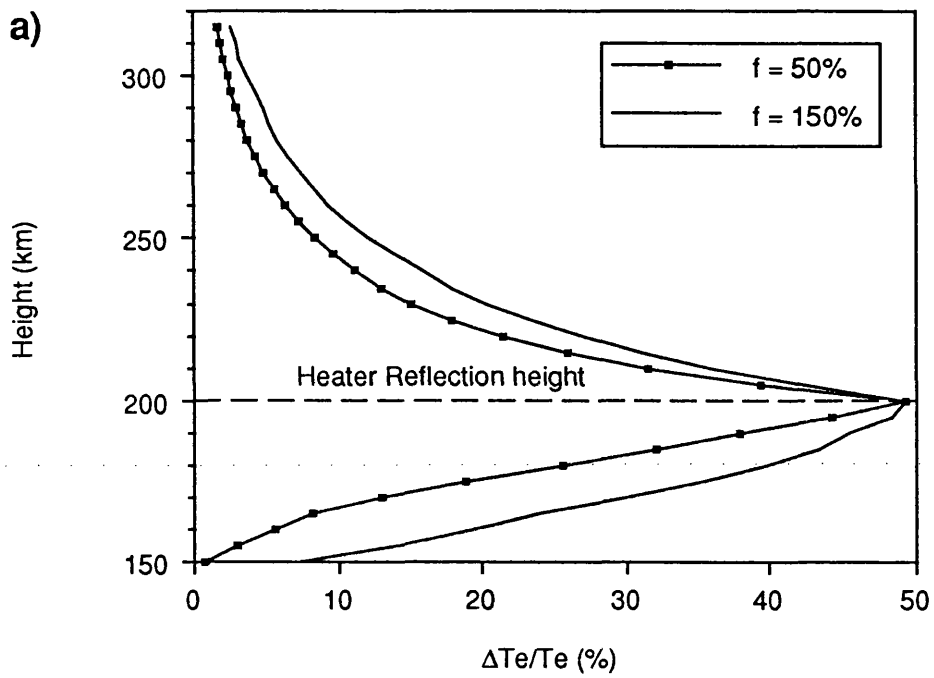


Figure 3.2 Modelled changes in electron temperature for different thermal conductivity models, a) Gurevich and b) Schunk and Nagy. The standard values of the thermal conductivity have been multiplied by a factor, f .

Chapter 3. Theoretical Modelling

change in L_T may be observed in Figure 3.2 where, with both of the thermal conductivity models, increasing the thermal conductivity broadens the peak in $\Delta T_e/T_e$. The effect of changing the thermal conductivity on the $\Delta T_e/T_e$ profile is more pronounced at heights below about 200 km for both models. At altitudes above 200 km, $\Delta T_e/T_e$ exhibits a greater change with model 1 than with model 2. At heights well away from the interaction region (above ~ 300 km), changing the thermal conductivity has little effect on the value of $\Delta T_e/T_e$.

The effect of changing the neutral density of N_2 on $\Delta T_e/T_e$ and $\Delta N_e/N_e$ for the Schunk and Nagy model of thermal conductivity is depicted in Figure 3.3. For both $\Delta T_e/T_e$ and $\Delta N_e/N_e$, decreasing the value of $[N_2]$ broadens the peak below the initial heater reflection height, but has little effect above this height.

Taking the stationary solution of Equation (3.1) and assuming that the heat source is a time invariant delta function (Equation 3.6), then the field-aligned spatial variation of the temperature perturbation is given by (Robinson 1989),

$$\frac{\Delta T_e}{T_{e0}} = \left(\frac{\Delta T_e}{T_{e0}} \right)_0 \exp\left(-\frac{|x - x_0|}{L_T}\right); \quad \left(\frac{\Delta T_e}{T_{e0}} \right)_0 = \frac{Q_0}{6 N_{e0} T_{e0}^{3/2}} \sqrt{\frac{m_e v}{R}} \Big|_{x=x_0} \quad (3.7a, b)$$

where R is the heat loss per electron to the background particle species.

A curve of the form of Equation 3.7a which has been derived from typical conditions found during F-region heating at Tromsø is illustrated in Figure 3.4. A heater interaction height of 200 km and a peak value of $\Delta T_e/T_e$ of 40% have been chosen. The thermal conductivity model of Gurevich has been employed in calculating the value of L_T (=33 km) at 200 km.

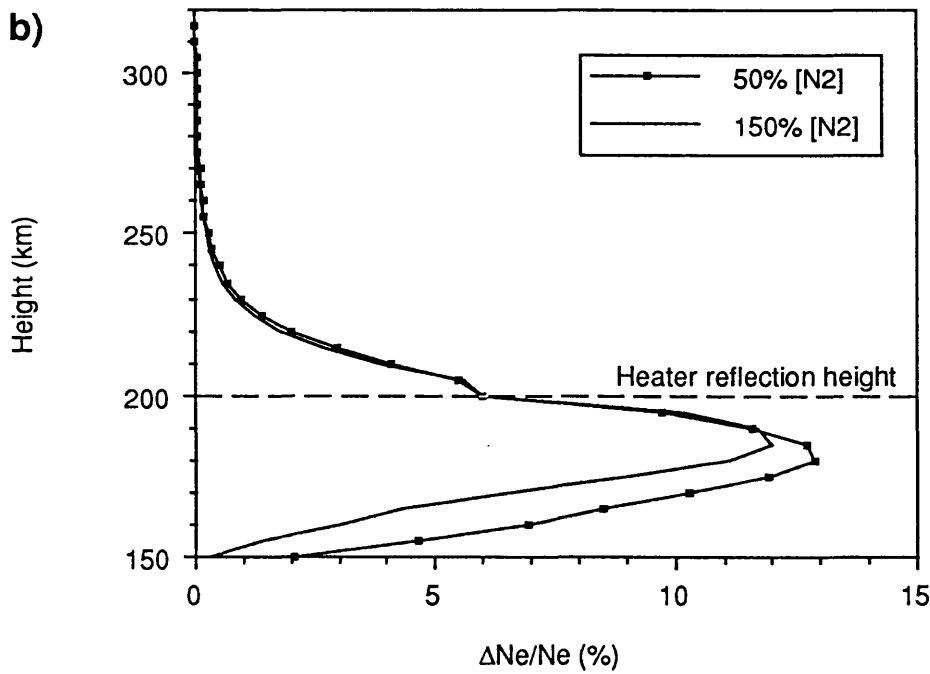
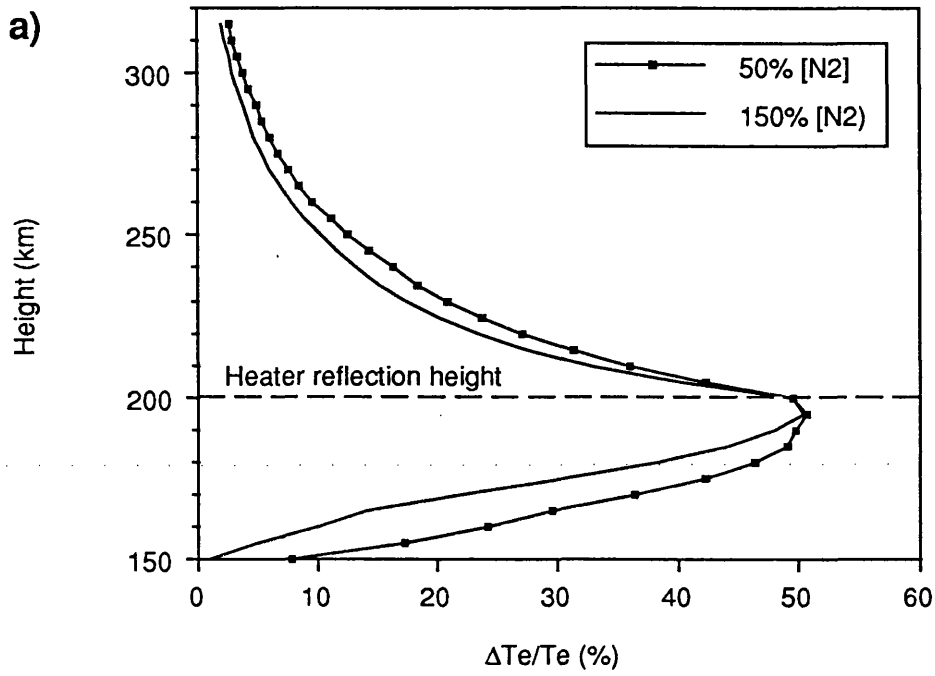


Figure 3.3 Modelled changes in a) electron temperature and b) electron density as a function of the density of molecular Nitrogen (as a percentage of the value given by the MSIS model).

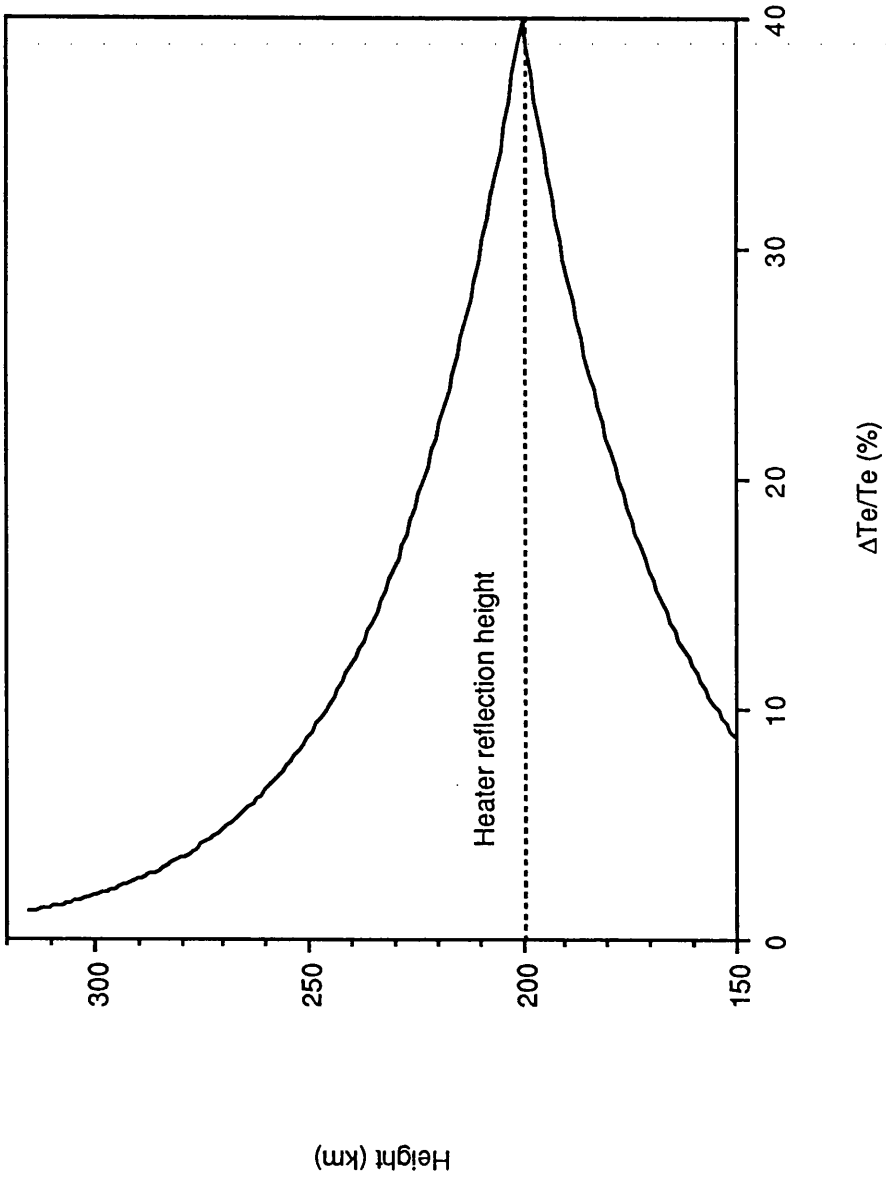


Figure 3.4 Equilibrium profile of $\Delta T_e / T_e$.

3.3 Calculation of Anomalous Absorption

Small-scale field-aligned irregularities (FAI) with dimensions of a few metres across the geomagnetic field and several kilometres parallel to it have been observed during artificial modification experiments at Platteville by UHF and VHF radars (Fialer 1974; Minkoff *et al* 1974; Thome and Blood 1974). These experiments revealed that the FAIs were only generated by high power electromagnetic (EM) waves polarised in the O-mode (Graham and Fejer 1976) with frequencies below the F-region critical frequency. The former observation is reminiscent of the conditions required for the observation of anomalous absorption and this prompted a number of theoretical studies into this relationship (eg Graham and Fejer 1976; Mjølhus 1985; Robinson 1989). An expression for the anomalous absorption coefficient in terms of the amplitude of the FAIs is presented below (Equation 3.8). Low power EM waves also undergo anomalous absorption in the presence of FAIs already excited by a high power EM wave. This is caused by the scattering of EM waves into electron acoustic (Langmuir) waves and to a lesser extent into EM waves.

A number of theoretical models have been proposed to explain the generation of FAIs during F-region heating and these will now be discussed in brief (more extensive reviews may be found in Fejer 1979; Stubbe and Kopka 1980; Robinson 1989). The earliest models have been reviewed by Fejer (1979) and involve three wave interactions, where a strong wave (the heating wave in ionospheric modification experiments) with angular frequency ω_0 and wave vector \mathbf{k}_0 excites weak waves with parameters ω_1, \mathbf{k}_1 and ω_2, \mathbf{k}_2 . The wave parameters must satisfy the following conditions,

$$\omega_0 = \omega_1 + \omega_2, \quad \mathbf{k}_0 = \mathbf{k}_1 + \mathbf{k}_2 \quad (3.8a, b)$$

Chapter 3. Theoretical Modelling

Three mechanisms have been suggested as the means by which FAIs are excited by high power radio waves. The mechanisms include the oscillating two stream instability (OTSI) where waves 1 and 2 are Langmuir and zero-frequency ion-acoustic waves, respectively, linear mode conversion (LMC) where small scale inhomogeneities present in the F-region plasma cause linear mode coupling between EM waves and Langmuir waves and the thermal parametric instability (TPI) where waves 1 and 2 are a Langmuir wave and a zero-frequency spatially periodic structure, respectively. In the OTSI case the waves are coupled via the nonlinear ponderomotive (electrostatic) force (Landau and Lifshitz 1960).

Although the OTSI is readily excited by the Tromsø heater (see Table 2.2), it has been eliminated as a direct source of FAIs as the PDI growth time (10^{-3} s) is short compared with the growth time of the FAIs (0.1 - 10 s). The LMC theory predicts that for an inhomogeneous plasma such as is found in the F-region, the mode conversion occurs at a height where the heater frequency is close to the local upper-hybrid frequency. X-mode waves transmitted from the ground reflect below, and O-mode waves above, the upper-hybrid resonance height and therefore only O-mode EM waves can undergo mode conversion. This result is consistent with the generation of FAIs only by O-mode heating. The growth of the FAIs during intense heating of the ionosphere by a high power radio wave (pump) have been attributed to two mechanisms. Type I processes require no initial instabilities but do exhibit a pump power threshold. The threshold of type II instabilities depends on the product of the pump power and the striation amplitude. Once this threshold is exceeded the striation growth is explosive. These mechanisms have been successfully employed in explaining the observations of the hysteresis effect of pump anomalous absorption (Kopka *et al* 1982; Jones *et al* 1983; Robinson 1988, 1989) and the so-called heater overshoot (Robinson 1985, 1989; Jones *et al* 1986; Wilkinson 1988).

In order to calculate the anomalous absorption Jones *et al* (1984) have modified the theories of Dawson and Oberman (1963) and Graham and Fejer (1976) by including the effects

Chapter 3. Theoretical Modelling

of the geomagnetic field on the HF conductivity. During the development of the theory it was assumed that the scale length of the field-aligned irregularities (FAI) perpendicular to the magnetic field is small compared to both the parallel scale length and the wavelength of the vertically propagating EM wave. If it is also assumed that a significant contribution to the anomalous absorption occurs only at an altitude, h_1 where the diagnostic frequency is close to the local upper-hybrid frequency then the coefficient of anomalous absorption, Γ is given by,

$$\Gamma = R(h_1) (e^4 / 8\pi \epsilon_0^2 m^2 c^4) \langle |\Delta n|^2 \rangle \quad (3.9)$$

where Γ is defined by Graham and Fejer (1976) as

$$P_R = P_I e^{-\Gamma} \quad (3.10)$$

where m and e are the electron mass and charge respectively, c is the speed of light, ϵ_0 is the permittivity constant, $\langle |\Delta n|^2 \rangle$ is the mean square amplitude of the FAI and P_R and P_I are the reflected and incident power of a vertically propagating EM wave. $R(h_1)$ is given by,

$$R(h_1) = \left| \frac{8\pi^2 \omega_p^2 c^3 (1 + |\alpha|^2) \{ [(1+u) - 4\sqrt{u}|\alpha|(1+|\alpha|^2)^{-1}](1-u)^{-2} \}}{\omega_0^3 (d\omega_p^2/dh) \mu (|\alpha|^2 + |\beta|^2 \sin^2 \theta + \cos^2 \theta - 2|\beta| |\sin \theta \cos \theta)} \right|_{h=h_1} \quad (3.11)$$

where, $\alpha = E_y / E_x$, $\beta = E_z / E_x$, θ is the angle between the EM wave vector and the magnetic field, μ is the refractive index, $u = \omega_H^2 / \omega_0^2$ and ω_H is the electron gyrofrequency. E_x , E_y and E_z are the electric field components of the radio wave, with the geomagnetic field in the z direction and the EM wave propagation vector in the x, z plane.

The electric polarisation relations may be written as follows,

$$\alpha = -iD / (\mu^2 - S), \quad \beta = \mu^2 \cos \theta \sin \theta / (\mu^2 \sin^2 \theta - P) \quad (3.12 a, b)$$

Chapter 3. Theoretical Modelling

At the upper-hybrid resonance height the plasma frequency, ω_e is given by,

$$\omega_e^2 = \omega_o^2 (1 - u) \quad (3.13)$$

and neglecting the effect of ions,

$$D = u^{1/2}, \quad S = 0, \quad P = u \quad (3.14 \text{ a, b, c})$$

If collisions are ignored, then the Appleton-Hartree formula for the refractive index (Appleton 1932) at the upper-hybrid height becomes,

$$\mu_{h1}^2 = 1 - \frac{1 - u}{1 - \frac{1}{2} \sin^2 \theta \pm \left[\frac{1}{4} \sin^4 \theta + u \cos^2 \theta \right]^{1/2}} \quad (3.15)$$

The plus and minus signs in Equation 3.14 correspond to the ordinary (O) and extraordinary (X) polarisation modes, respectively.

A mean square FAI amplitude relative to a reference plasma density may be defined as follows,

$$\delta_0^2 = \langle |\Delta n|^2 \rangle / N_0^2 \quad (3.16)$$

where N_0 is chosen such that the equivalent angular frequency, ω_R , given by $\omega_R \approx (81N_0)^{1/2}$, lies within the frequency range of interest, ie near to the diagnostic frequencies employed during the experiments.

It should be emphasised that Equation (3.8) assumes vertically propagating EM waves. During the experiments described in Chapter 7 the diagnostic waves propagated at an angle of

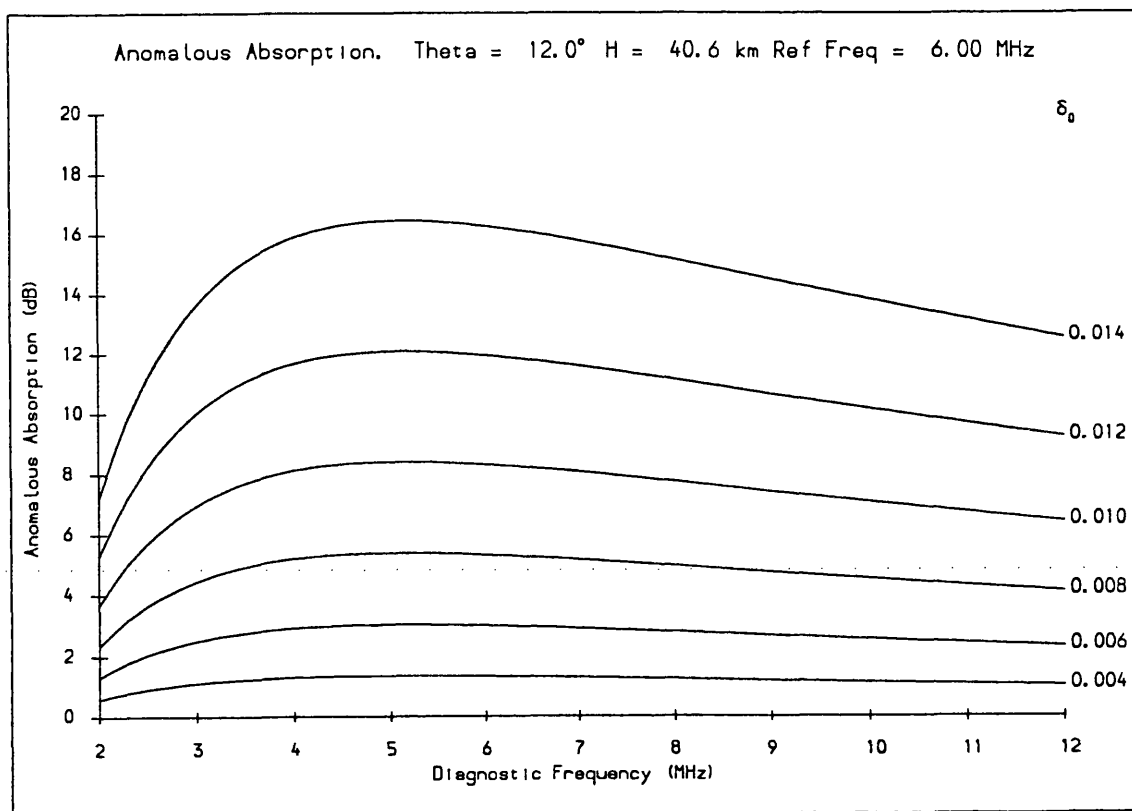
about 12° to the vertical. Jones *et al* (1984) suggested that this assumption results in a discrepancy between theory and experiment of the order of 10%.

The latitudinal (ie θ) dependence of Γ for a given diagnostic frequency and value of δ_0 has been studied by Robinson (1989) by means of Equation 3.8. For a fixed set of ionospheric conditions it was found that Γ decreases with decreasing latitude (see Figure 2.2). It follows from the theory that the frequency dependence of Γ also varies with latitude. In Figure 3.5, contours of constant δ_0 have been plotted against diagnostic frequency for two values of θ , corresponding to the dip angles ($90^\circ - \theta$) at Tromsø ($\theta = 12^\circ$) and Arecibo ($\theta = 40^\circ$). A reference frequency of $2\pi \cdot 6$ MHz (corresponding to $N_0 = 4.5 \times 10^{11} \text{ m}^{-3}$) and a scale height (at the height corresponding to the reference density) of 41 km have been adopted. For Tromsø (Figure 3.5a) the value of Γ is virtually independent of ω_0 for $\omega_0/2\pi \geq 3$ MHz. However, for Arecibo (Figure 3.5b) Γ peaks at $\omega_0/2\pi \sim 3$ MHz. Above the peak, Γ falls off rapidly with increasing frequency until at $\omega_0/2\pi \sim 12$ MHz it is approximately 25% of the value at the peak. The differing frequency response is a result of the different magnetic field geometry. Because Γ is not independent of frequency at Arecibo, the FAI scale length must be calculated by a slightly different technique from that of Jones *et al* (1984). The differences between these methods are discussed in more detail in Chapter 7.

3.4 Concluding Remarks

The theory (eg Robinson 1989) which addresses the ionospheric response to a narrow heat source has been reviewed. The effect of changing the input parameters on the model results has been investigated and important differences noted. A high power radio wave may provide the heat source via the processes of collisional and anomalous absorption although at high latitudes the contribution to heating of the collisional absorption is significantly lower than that of anomalous absorption. A comparison between the results of the theory and experiments carried out at Tromsø is presented in Chapters 5 and 6.

a)



b)

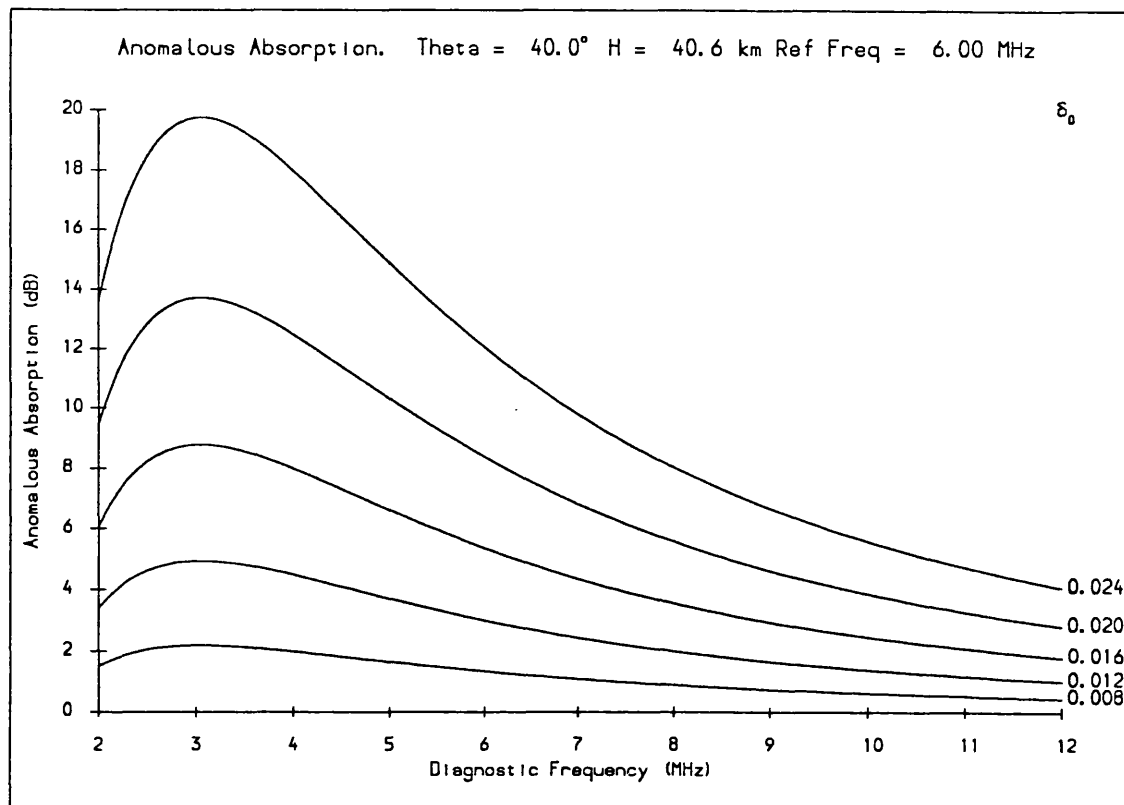


Figure 3.5 Theoretical contours of constant δ_0 for anomalous absorption as a function of ω_0 at geomagnetic latitudes corresponding to a) Tromsø and b) Arecibo.

Chapter 3. Theoretical Modelling

The theory for calculating the coefficient of anomalous absorption is reviewed and the dependence of this parameter on magnetic latitude is considered. By means of these theoretical results the scale length of the FAIs generated during heating experiments at Arecibo are determined (see Chapter 7).

Chapter 4 Equipment and Experimental Procedure

4.1 Introduction

High power HF radio waves are capable of producing large scale effects in the ionosphere, including changes to the electron density, electron temperature, and ion temperature and possibly composition. Some of these effects have been investigated in a series of experiments conducted at the ionospheric modification facility at Ramfjordmoen, Tromsø, Norway during the last 10 years (see Chapter 2; Stubbe *et al* 1982a,1985). This facility is operated jointly by the Max-Planck Institut für Aeronomie (MPAe), Lindau, West Germany and the University of Tromsø. The principal diagnostic probe which has been employed during the current investigation is the EISCAT incoherent scatter radar which is co-located with the heater and is described in more detail below.

In addition to the large-scale heating effects the action of powerful HF radio waves on the ionosphere can also produce field aligned density irregularities (see Chapters 2 and 3). The formation of these irregularities may lead to the anomalous absorption of the heater wave and also a reduction in the signal strength of HF diagnostic waves propagating through the heated volume. The anomalous absorption of low power HF diagnostic waves during heating has been extensively investigated during modification experiments at Tromsø (eg Robinson 1989) and more recently in a heating campaign at Arecibo, Puerto Rico (Stocker *et al* 1990).

The observations presented in this thesis were obtained during two experimental campaigns conducted at Tromsø in March 1985 and February 1987 and during a further campaign at Arecibo in May 1989. In this chapter the experimental equipment and techniques employed during these campaigns are discussed.

4.2 The Tromsø heater

The Tromsø high power HF radio wave transmitter (or heater) was built between 1979 and 1980 by the MPAe and the University of Tromsø. Testing at low powers commenced in August 1979 and full operation in September 1980. The Ramfjordmoen site is located at geographic coordinates 69.6° N, 19.2° E (67.1° geomagnetic north) with a magnetic dip angle of approximately 78° and an L-shell of 6.2. The principal operating characteristics of the heater are summarised in Table 4.1. Early in 1986 the low frequency antenna array (2.5 to 4 MHz) was disabled by storm damage and has not been repaired since. This has resulted in a reduced frequency range of 3.8 to 8 MHz. Unfortunately, the damage occurred at a time which coincided with sunspot minimum and in consequence the range of frequencies available for overdense heating (ie where the heater frequency is below the peak plasma frequency) during the 1987 campaign was severely curtailed.

A large number of ionospheric diagnostic facilities are located in Northern Scandinavia and some of these sites are illustrated in Figure 4.1. Only a few of the available diagnostics have been employed during the experiments discussed in this thesis and these are described in more detail in the following sections.

The Ramfjordmoen high power transmitter is capable of producing a continuous power of 1.5 MW derived from 12 independent 125 kW transmitters. The power is then fed into one of three (two since early 1986) antenna arrays. These arrays were designed to optimise the transmission on several frequency ranges, 2.5 to 4 MHz, 3.85 to 5.65 MHz and 5.5 to 8 MHz. Due to licensing restrictions only the following discrete frequencies may be employed 2.759, 3.324, 3.515, 4.04, 4.544, 4.9128, 5.423, 6.770, 6.960, 7.1 and 7.953 MHz. Each array consists of six rows of six crossed full wavelength dipoles. Each transmitter drives a row of dipoles and hence the requirement for 12 transmitters, one for each orientation. The arrays are positioned such that the antenna rows lie in the East-West direction and therefore the beam

NUMBER OF TRANSMITTERS	12
POWER OF EACH TRANSMITTER	125 kW
TOTAL TRANSMITTER POWER	1.5 MW
ANTENNA GAIN	24 dBi
BEAMWIDTH	14.5°
MAXIMUM RADIATED POWER	360 MW
SIGNAL RISE TIME	< 5 μ s
FREQUENCY SWEEP RATE	100 kHz s ⁻¹
MAXIMUM SWEEP RANGE	7 %
FREQUENCY RANGE	3.8 - 8 MHz
DISCRETE FREQUENCY CHANGE TIME	10-25 sec / MHz

Table 4.1 Principal operating characteristics of the Ramfjordmoen modification Facility.



Figure 4.1 Sketch map of EISCAT. The UHF transmitter is at Tromsø, the receivers are at Tromsø, Kiruna and Sodankylä. The dynasonde, an ionosonde, the partial reflection experiment (PRE), optical and magnetic instrumentation are also at Tromsø. The dashed line shows the southern boundary of the auroral oval under quiet geomagnetic conditions at 00h UT (after Rishbeth and Williams 1985).

Chapter 4. Equipment and Experimental Procedure

may be steered in the North-South meridian by beam-phasing. The transmitted signal may be circularly polarised (ie O- or X- mode) or linearly polarised. The gain of the antenna arrays is 24 ± 1 dBi, varying slightly with transmitter frequency. This results in a beamwidth of approximately 14.5° . The effective radiated power (ERP) is given by,

$$\text{ERP} = \text{gain} \times \text{transmitted power} \quad (4.1)$$

It follows from Equation 4.1 that the maximum ERP obtainable by the Tromsø heater is approximately 360 MW. Recent campaigns have employed less power than this for two reasons, firstly to avoid damage to the equipment, and secondly because the power required to excite a whole range of ionospheric plasma instabilities is considerably less than the maximum (Fejer 1979; Stubbe and Kopka 1980; Jones *et al* 1988; Chapter 2). If it is assumed that little D-region absorption occurs and the effects of amplitude swelling are included, then at full power an energy flux of 0.3 mWm^{-2} and an electric field of 3 Vm^{-1} can be achieved at a height of 300 km (Walker 1979).

The heater power, frequency, polarisation, beam direction, modulation frequency, modulation depth and pulse sequence are all computer controlled which results in a great flexibility and enables a wide range of experiments to be performed. This may be contrasted with the largely manually operated heater at Arecibo which is described in Section 4.8

A period of approximately three minutes is required to prepare the heater for transmission from a state of complete power off, due to the complicated tuning and beam forming operation that this entails. Therefore, during the experiments described in this thesis "heater off" implies a state whereby the heater radiates HF power approximately 37.5 dB below that employed during "heater on". The heater can be switched on from this stand-by state in approximately 5 μs .

4.3 EISCAT

The European Incoherent Scatter (EISCAT) radar has been employed as the principal diagnostic during the experiments at Tromsø described in this thesis. The incoherent scatter technique has been discussed in detail elsewhere (eg Evans 1969; Beynon and Williams 1978). It is an extremely powerful method of determining many of the parameters which characterise the ionospheric plasma. The plasma parameters which are potentially measurable by EISCAT are summarised in Table 4.2. However, for the purposes of the current investigation only the electron density, electron temperature and ion temperature have been examined in any great detail.

The EISCAT system consists of two components, a tristatic UHF (933 MHz) radar and a monostatic VHF (224 MHz) radar. Only the UHF system will be discussed in the following section as the VHF radar was not employed during any of the experiments described. The EISCAT transmitter and one receiver are co-located with the MPAe heater at Ramfjordmoen and therefore this provides an excellent opportunity to undertake coordinated heater-EISCAT experiments. Two UHF remote site receiver systems are located at Kiruna, Sweden and Sodankyla, Finland (see Figure 4.1). All three UHF antennas are 32 m diameter paraboloids which are fully steerable at a rate of up to $80^\circ \text{ min}^{-1}$ with an RMS error in pointing direction which can be less than 0.02° . A peak power of 2 MW may be transmitted but the duty cycle is limited to 12.5% resulting in an maximum average power of 0.25 MW. EISCAT may transmit signals on up to 16 different frequencies in the range 929.5 to 937 MHz separated by 0.5 MHz intervals. The transmitted frequency may be changed in about $1 \mu\text{s}$. The ability to change frequency rapidly enables several pulse schemes to be transmitted by the radar during one pulse repetition period. During the experiments conducted in March 1985 and February 1987, EISCAT employed only 2 pulse schemes, firstly a long pulse which enabled the ion-line spectrum and hence T_e/T_i and T_i/m_i (see Table 4.2) to be derived (Section 4.6), and secondly

(i) *Directly Measured*

Electron concentration, N

Electron temperature, T_e

Ion temperature, T_i

Ion composition

Ion drift velocity, V_i

Ion-neutral collision frequency, ν_{in}

Photoelectron flux

(ii) *Derived Indirectly*

Neutral particle density, ρ

Neutral gas temperature, T

Neutral air velocity, U

Pedersen and Hall conductivity, Σ_p, Σ_H

Electric current

Heat flux

Table 4.2 Parameters measured by incoherent scatter (after Rishbeth and Williams 1985).

Chapter 4. Equipment and Experimental Procedure

a short pulse which enabled the, so-called, "power profile" and hence electron density profile to be obtained (Section 4.7). After the signal has been received it is sampled at either 500 kHz or 10 MHz (depending on channel number) by one of eight analogue-to-digital converters (ADC). The PROG7 (Ho 1981) correlator programs were employed during the 1985 campaign and the GEN correlator programs (Turenen 1986) during the 1987 campaign. The GEN programs provide a major improvement in the determination of the ionospheric parameters. During the 1985 campaign a 30 μ s pulse, 33 gate power profile was transmitted on two frequencies, and a 360 μ s, 3 gate long-pulse on four frequencies. For the 1987 campaign the pulse lengths remained the same but 6 long-pulse gates were employed and 40 power profile gates. In the 1987 campaign each pulse scheme was transmitted on four frequencies. Transmitting the same pulse scheme on more than one frequency enables the data to be averaged which leads to a reduction in the variance of the received signal strength. It should be noted that, in general, the long-pulse range gates are overlapped in altitude which means that measurements in adjacent range gates are not independent.

The remote site receivers at Kiruna and Sodankyla were employed during the 1985 and 1987 campaigns although the method of deployment was different in each case. During 1985 experiments the Kiruna beam was directed to intersect the Tromsø beam at an altitude close to the heater reflection height, and the Sodankyla beam at a height 10 to 15 km below this. The heater interaction height was determined from the altitude at which the overshoot in the EISCAT power profile (eg Jones *et al* 1986) occurred. During the 1987 campaign the remote site antenna were oriented such that the beams scanned the Tromsø beam from altitudes above the heater reflection height to heights below the reflection height (Figure 4.2) in order to obtain good height resolution within the interaction region. The heights at which the Kiruna and Sodankyla beams intersected the Tromsø beam were, for the most part, separated by 5 km. A common dwell position close to the heater reflection height was the exception to this. On heater switch on the remote site beams from Kiruna and Sodankyla were directed to heights K_1 and S_1 respectively (see Figure 4.2). After the appropriate dwell time the beams

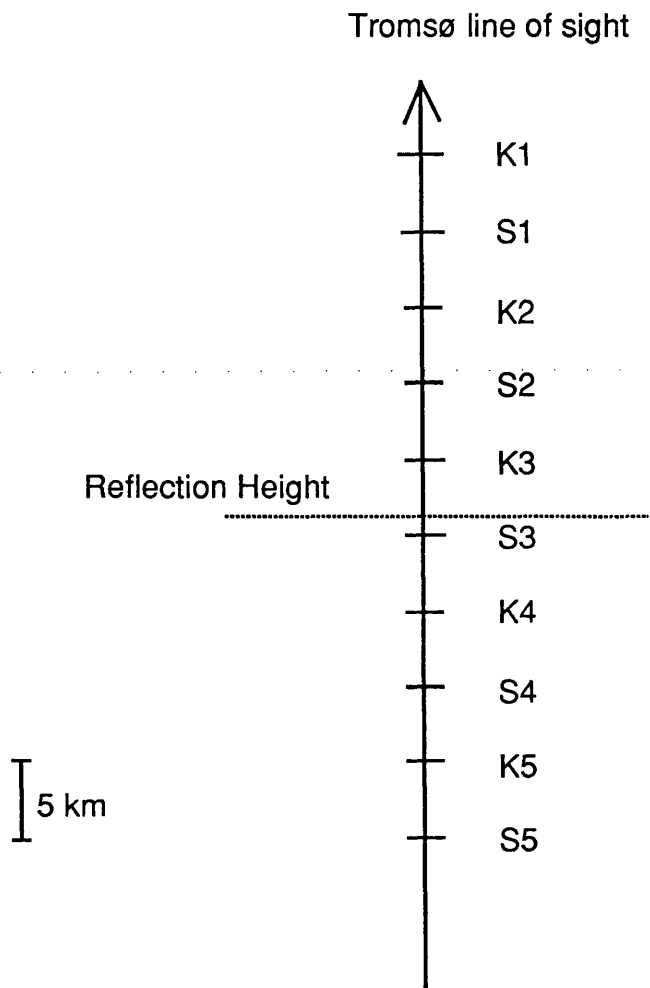


Figure 4.2 Schematic of the EISCAT remote site pointing directions during 1987 heating campaign. K1, S1 etc represent the dwell positions of the Kiruna and Sodankylä beams respectively. A common dwell position was established close to the heater reflection height

Chapter 4. Equipment and Experimental Procedure

were then moved to heights K_2 and S_2 and so on. The experiment was sufficiently flexible to allow the number, length and position of the dwell times to be varied to suit the ionospheric conditions and the heater transmission scheme.

4.4 Leicester HF diagnostics

A low power radio signal passing through a volume of ionosphere illuminated by a high power radio wave may undergo many effects, for example the formation of density irregularities in the plasma may lead to a reduction in the received signal strength (Stubbe *et al* 1982b; Jones *et al* 1984; Robinson 1989), a change in the electron density may lead to a phase change (eg Jones *et al* 1982) and if the heater signal is modulated then cross-modulation may occur (Stubbe *et al* 1982a; Robinson 1989). During the 1985 and 1987 heating campaigns a number of low power HF diagnostics were deployed, the transmitters at a site 53 km to the north of the heater, and the receivers 44 km to the south of the heater (Figure 4.3). The beam geometry resulting from this deployment allowed the diagnostic signals to traverse the ionosphere illuminated by the heater at F-region heights, but not that at D-region heights. This constraint ensured that the heater-induced effects measured by the diagnostics were due solely to phenomena occurring in the F-region. The HF diagnostic system has also been deployed at Arecibo (see Section 4.8) and observations from this site are presented in Chapter 7. Interpretation of HF data may be complicated by ionospheric tilts or multimode propagation via the D- or E- regions. During the 1987 campaign there is evidence to suggest that the diagnostics may have penetrated the F-region at times resulting in a loss of signal and during the 1989 campaign at Arecibo there is evidence for strong D-region effects. Some of the problems in interpreting the experimental data which can arise because of these features will be addressed in Chapters 6 and 7.

The diagnostic equipment comprised transmitters, receivers and data logging apparatus and these were constructed by the Ionospheric Physics Group, University of Leicester. The

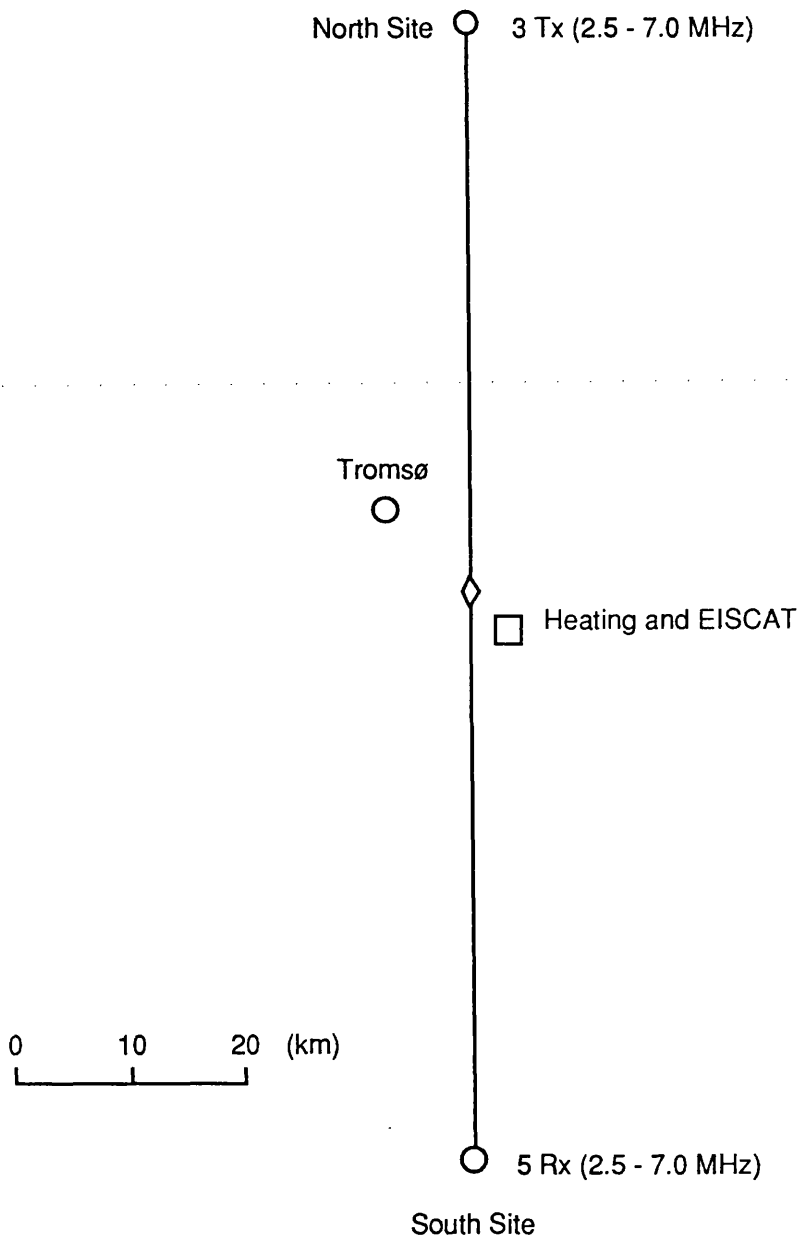


Figure 4.3 Map showing the location of the heater site at Ramfjordmoen, Tromsø and the relative positions of the diagnostic transmitter and receiver sites.

Chapter 4. Equipment and Experimental Procedure

three 30 W transmitters generate a continuous unmodulated carrier signal within a frequency range of 2.5 to 7 MHz (increased to 9 MHz for the Arecibo experiment) radiated from inverted-V dipole antennas. These antennas transmit linearly polarised signals which, at high magnetic latitudes, results in characteristic polarisations which are circular and in the opposite sense (eg Budden 1985). Therefore, the O- and X- mode polarisations are excited with equal strength.

During all of the experiments described in this thesis, five “narrow band” receivers each with a bandwidth of about 300 Hz and a “wideband” receiver (see below) were employed. Crossed active dipole antennas were connected to four of the receivers which enabled either of the two magnetoionic waves to be recorded. The polarisation being recorded is established by transmitting signals at frequencies of a few MHz (ie close to the electron gyrofrequency) where the difference in D-region absorption between O- and X-modes is most pronounced. The mode which results in the stronger signal being observed over a period of time is then assumed to be the O-mode. During the campaigns at Tromsø three of the antennas were arranged in a triangular formation to facilitate ionospheric drift measurements. The fifth receiver employed a wire dipole antenna and was tuned to the heater frequency and therefore acted as a continuous monitor of the heater status.

The transmitter and receiver frequencies were selected manually but the data logging, polarisation, and automatic gain control (AGC) were controlled by a mini-computer. The software for the diagnostic system was developed in house at Leicester and employed the FORTH computer language. Two configurations of the receiver frequencies were employed, the generalised allocation for anomalous absorption is given in Table 4.3, and that for drift velocity measurements in Table 4.4. In general for anomalous absorption measurements the frequencies are chosen such that $f_1 \approx f_H - 0.5$ MHz, $f_2 \approx f_H \pm 0.2$ MHz and $f_3 \approx f_H + 0.5$ MHz. Drift velocity measurements are not reported in this Thesis, but examples of the results obtained during heating at Tromsø may be found in Wilkinson (1988).

Receiver channel	Diagnostic frequency	Polarization
1	f_1	O-mode
2	f_2	
3	f_3	
4	f_3	X-mode
5	f_H	Heater

Table 4.3 Configuration of receiver channels for anomalous absorption measurements.

Receiver Channel	Diagnostic frequency	Polarization
1	f_1	X-mode
2	f_1	
3	f_1	
4	f_1	O-mode
5	f_H	Heater

Table 4.4 Configuration of receiver channels for plasma drift measurements.

Chapter 4. Equipment and Experimental Procedure

The real and imaginary components from the five receivers were sampled simultaneously with 8 bit precision and a logging rate of 32 Hz. These data were then stored on magnetic tape for later retrieval and analysis. Hard copy output of the diagnostic amplitudes are obtained in "real-time" by chart recorders. This output is useful in determining the effect of heating (if any) and enables judgement as to the utility of the chosen diagnostic frequencies to be exercised by the experimenter.

The diagnostic system is calibrated by recording the amplitude response of each receiver to a known signal. This calibration signal is gradually attenuated from 0 to 127 dB in steps of 1 dB for each level of the receiver attenuators (0 to 90 dB). The results are then stored digitally on magnetic tape.

During the 1987 campaign a wide band (~ tens kHz) system was deployed to observe the heater self-action effects at a high logging rate of 256 Hz. The output from the synthesizer tuned to the heater frequency was split into both the fifth "heater monitor" narrow band receiver and the wide band receiver. In operation the wide band system is very similar to the "Five-receiver" system except that data is only captured for the 8 seconds prior to and the 16 seconds after a heater switch on. Only amplitude information is stored on magnetic tape for this mode of operation. Both systems (ie wideband and five-receiver) may be employed simultaneously.

4.5 Ionosonde and Dynasonde

A vertical incidence radio sounder or ionosonde (eg Eccles and King 1970) is operated by the Auroral Observatory in Tromsø. This provides ionograms at least once per hour and at times at more frequent intervals. The F-region critical frequency and hence the electron density at the F-region peak and, by an inversion technique (eg Jackson 1971), the electron density profile may be derived from ionosonde measurements. The F-region peak density can

Chapter 4. Equipment and Experimental Procedure

be useful in “scaling” the EISCAT electron density profiles (see Section 4.7). During the 1987 campaign an additional ionosonde was deployed at the South site (Figure 4.3) to provide ionogram information for real time control of the diagnostic frequencies.

The dynasonde (Wright *et al* 1988a) is an advanced digital ionosonde which may be operated in modes additional to those of a conventional ionosonde. However, only conventional sounder data from this instrument will be utilised in the current study. Data from the dynasonde is available for only part of the March 1985 campaign where ionograms were produced at very frequent intervals.

4.6 Derivation of Temperatures from EISCAT Observations

The detailed theory pertaining to the incoherent scatter technique is extensively covered in the literature (eg Evans 1969; Beynon and Williams 1978; Rishbeth and Williams 1985). Here it is intended only to explain how, in principle, electron temperature (T_e) and ion temperature (T_i) values are derived from EISCAT observations.

During the March 1985 and February 1987 heating campaigns the temperatures were derived from the ion-line spectra obtained from long-pulse measurements. A typical ion-line spectrum is reproduced in Figure 4.4a. In the F-region and under quiet conditions, the experimental spectrum resembles the theoretical spectrum quite closely therefore the spectral characteristics may be related to ionospheric parameters. The width of the spectrum is related to the quantity T_i/m_i (where m_i is the ion mass), and the ratio T_e/T_i is a function of the ratio of the peaks to the trough in the spectrum. The electron density is a function of the total scattered power, ie the area under the curve.

In practice the parameters are not derived directly from the observed spectrum, but rather from a comparison of the experimental autocorrelation function (ACF, see Figure 4.4b) with a

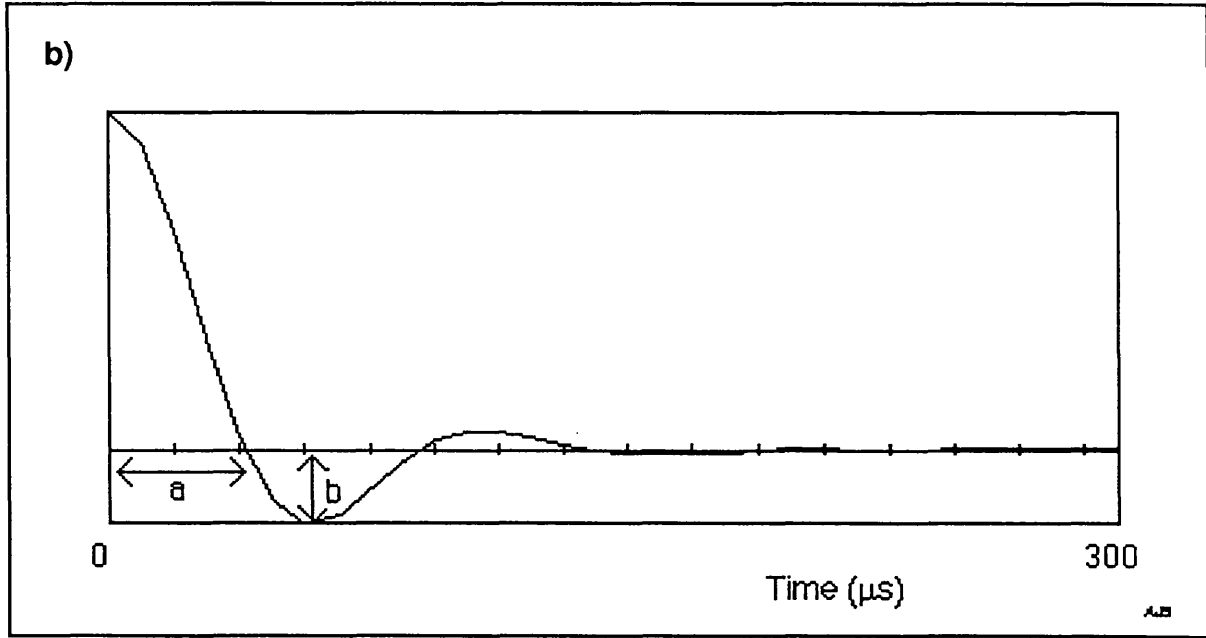
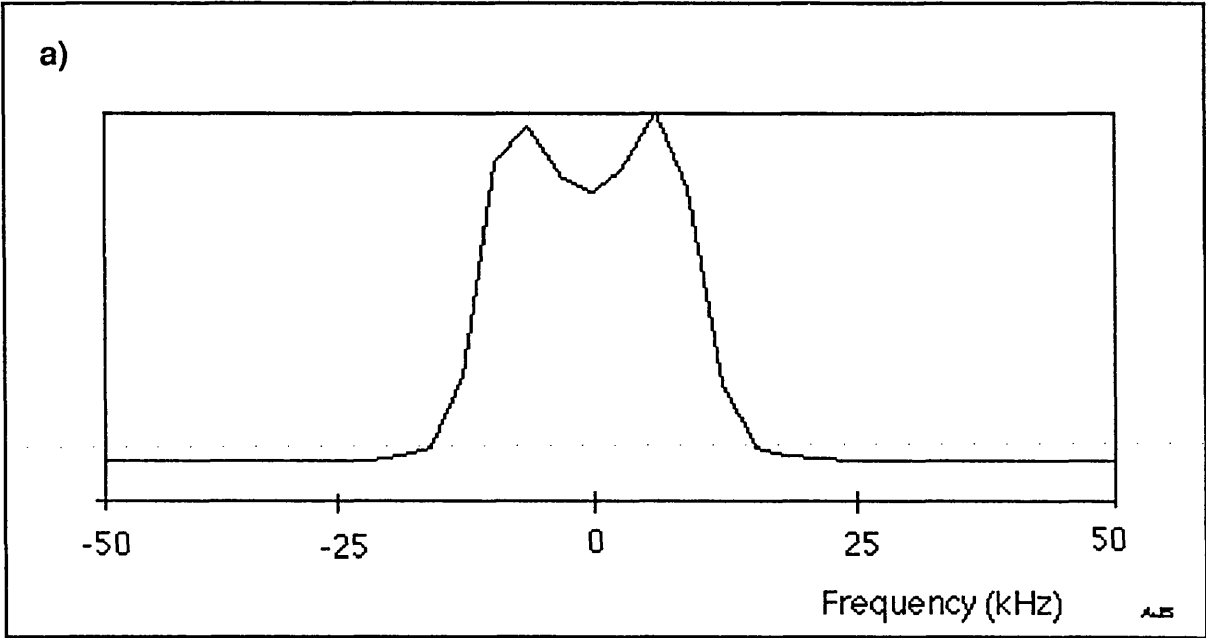


Figure 4.4 Typical EISCAT F-region observations of a) the ion-line spectrum, and b) the auto-correlation function (ACF).

series of theoretically derived ACFs. A flow-chart of the complete analysis procedure is presented in Figure 4.5. The salient aspects of the procedure will be discussed below.

After system corrections have been applied to the long-pulse data the raw density may be calculated from (eg Evans 1969),

$$N_e = \frac{C_s R^2 P_r (1 + \alpha^2 + T_r) (1 + \alpha^2)}{P_t \tau} \quad (4.2)$$

where, C_s is the system constant, R is the range, P_r is the received power, P_t the transmitted power, τ the pulse length, α the ratio of the Debye length to the radar wavelength, and $T_r = T_e/T_i$. The “quick-fit” process begins by making a crude estimate of T_e/T_i from $a \propto 1/T_i$ and $b \propto T_e/T_i$ (see Figure 4.4b) and then correcting the raw density for temperature. A theoretical ACF may then be derived from these values and then compared with the experimental ACF. The parameters are then incremented until the difference between the two ACFs is minimised. The variance in the fit provides a measure of the error in the fitted parameters. However, this procedure does not take account of the errors which are due to the signal-to-noise ratio.

There are many potential pitfalls during this analysis procedure. The ratios T_e/T_i and T_i/m_i are obtained from the ACF and therefore in order to calculate T_e and T_i , m_i must be known. During the standard analysis procedure model values of m_i , derived from a composition model, are utilised. This modelling can lead to inaccuracies especially in the transition regime between about 150 km and 200 km where the composition changes rapidly with increasing altitude. During heating experiments it is conceivable that the ion composition may be altered at heights close to the heater reflection height and this would lead to further distortions of the measured ionospheric plasma parameters. More importantly, the heater-induced excitation of the so-called ion-line overshoot (Figure 4.6) can result in serious errors in the parameters derived from

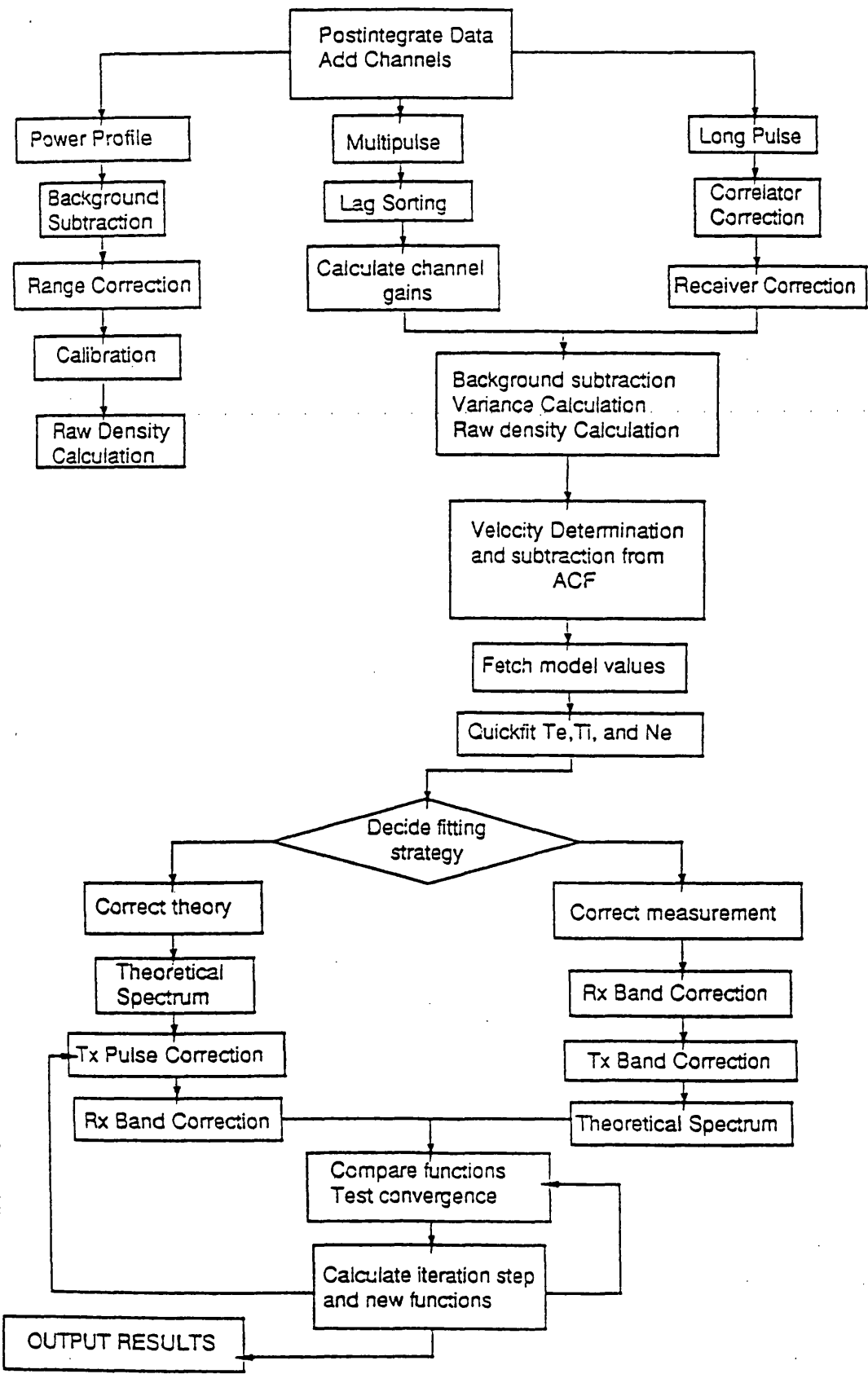


Figure 4.5 Block diagram illustrating the principal features of the UK incoherent scatter analysis program (after McCrea 1989).

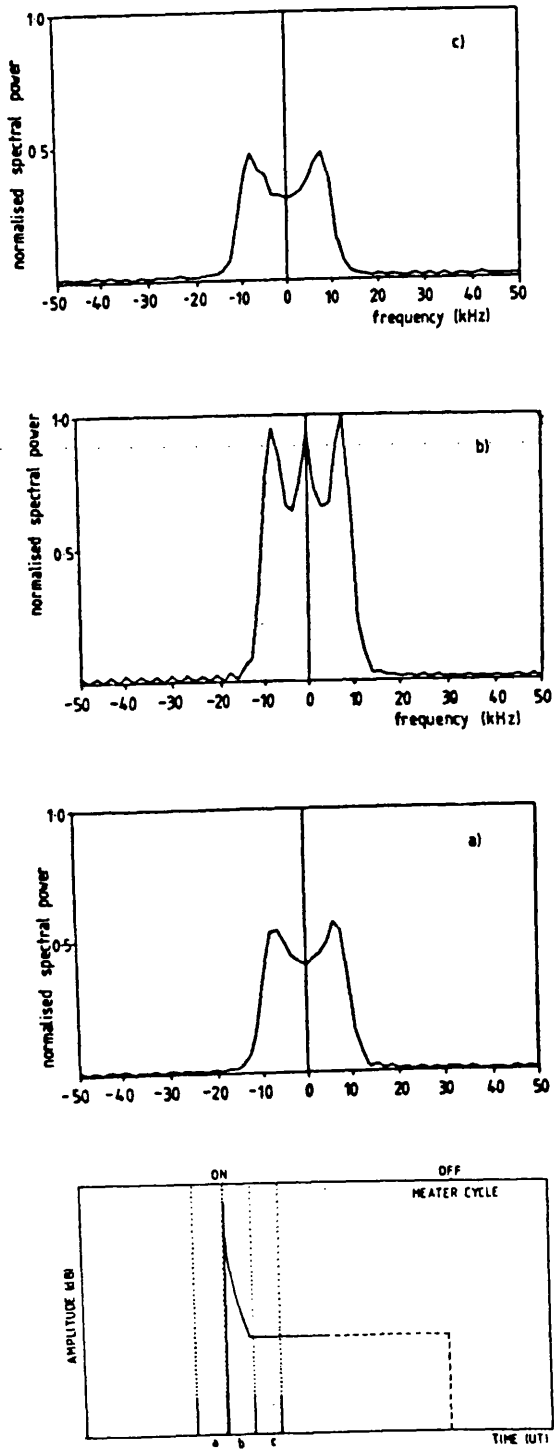


Figure 4.6 Changes in the EISCAT ion-line spectrum produced by heating. The presence of a third spectral peak at zero Doppler shift is a characteristic of these changes (after Jones *et al* 1986).

Chapter 4. Equipment and Experimental Procedure

affected spectra and therefore care must be exercised to exclude such data from analysis. Finally it may be possible that some of the received backscattered power arises from coherent rather than incoherent scatter due to small scale irregularities excited by the heater. If this is the case, then the electron density would be overestimated by Equation 4.2.

The parameter values derived from the long-pulse measurements also suffer from altitude and temporal smearing, ie the the measured values are a convolution of the actual ionospheric values from a wide range of heights and times. In order to minimise the variance of a spectrum a high signal-to-noise ratio is required. Given a fixed transmitted power and collecting area this may be achieved either by long integration times or by long-pulses. However, the longer the pulse the worse the altitude resolution, and the longer the integration period the poorer the time resolution. During many "geophysics" experiments conducted by EISCAT these constraints are of minimal importance, but during modification experiments, where the radio wave energy of the heater is being transferred to the ionospheric plasma in a height range rather less than 10 km in extent, then they can severely limit the usefulness of the data. During the experiments discussed in Chapter 5 the EISCAT temperature data had a height resolution of 30 km or 50 km and a post-integration period of either 5 or 10 seconds. Therefore, any structures in T_e or T_i on smaller altitude or shorter time scales will not be detected by the Tromsø radar.

The spectra recorded at the two remote site are obtained and analysed by a similar procedure to the one outlined above. The scattered signals detected by the remote site receivers come from an ionospheric volume which is defined by the region where the remote site beam intersects with the Tromsø beam. At an altitude of 200 km above Tromsø the intersection volume is relatively small, approximating to a cube with edges of about 5 km in extent. For the experiments discussed in this thesis, the range from the remote sites to the intersecting volume is longer than the equivalent range from Tromsø which results in a lower

Chapter 4. Equipment and Experimental Procedure

signal-to-noise ratio at the remote sites and therefore noisier spectra. By changing the location of the intersection volume at regular intervals during periods when the heater is switched on, a high resolution altitude scan of the heated volume may be obtained, but with a concomitant loss in temporal resolution (Section 4.3). A "scanning" experiment of this type was attempted during the 1987 campaign and some of the results are presented in Chapter 5.

4.7 Derivation of electron density from power profile observations

It has already been discussed in the previous section how an estimate of the electron density may be obtained from the total power contained in the ion-line spectrum (or in practice from the zero-lag of the ACF). This method of determining the electron density suffers from the same drawback as all the other long-pulse measurements, namely poor spatial resolution. However, the electron density may be determined by two alternative procedures, Faraday rotation or short pulse (or "power profile") measurements. The determination of density by the Faraday rotation technique relies on the dependence of the angle between the polarisation vectors of the transmitted and received signal on the electron density (eg Garriott *et al* 1970). The apparatus which enabled measurements of this nature to be performed was removed from the EISCAT UHF system as it introduced additional noise into the receivers. The "power profile" method of determining the electron density relies on the relationship between the received power and the density (Equation 4.2). The technique involves transmitting pulses of short duration (typically 30 μ s) and then gating the receiver to obtain a series of returns from a range of heights. Only the returned power and not the backscatter spectrum is measured during experiments of this type.

Examination of Equation 4.2 reveals that there are a number of potential pitfalls which are associated with the derivation of the electron density profile from the raw power profile. The correction of the raw power profile for the range and transmitted power are relatively straightforward, although the measurement of the transmitted power suffered from an

Chapter 4. Equipment and Experimental Procedure

intermittent fault during the 1987 campaign. This fault has resulted in an average value of the transmitted power being employed in the analysis. The EISCAT transmitted power becomes important during heating experiments because EISCAT and the heater share a common power source. Therefore, when the heater is switched on the EISCAT transmitted power can be reduced by up to 10% of the value prior to heater on.

The raw power profile also needs correcting for the temperature ratio T_e/T_i . These values may be obtained from an examination of the ion-line spectrum (see Section 4.6) which is obtained with poorer height resolution than the power profile measurements (typically about 50 km compared to 4 km). A procedure of linear interpolation between the ion-line gates has been adopted in order to calculate the temperatures at the altitude corresponding to each power profile gate. For F-region measurements the ratio of the Debye length to the radar wavelength (ie α) is small and so can be ignored.

Once the above corrections have been applied to the raw power profile, the result is proportional to the electron density. The absolute electron density is obtained by scaling the corrected power profile via the system constant. When the heater is not operated, the peak in the F-region electron density may be obtained from the critical frequency of the O-mode trace on an ionogram and then this may be assumed to be equivalent to the F-region peak density observed by EISCAT. This operation is regularly conducted at EISCAT and an average value of the system constant has been derived. During heating experiments the corrected profile may also be scaled from a knowledge of the location of the ion-line overshoot and the heater frequency. If the ion-line overshoot is assumed to occur close to the heater reflection height then the electron density at that height may be derived from the heater frequency.

4.8 The Arecibo Experiment

Arecibo is located on the island of Puerto Rico in the Caribbean. The Arecibo Observatory (18.35° north, 66.75° west geographic, magnetic dip $\sim 50^\circ$) operates a 430 MHz incoherent scatter radar with a 305 m diameter spherical dish antenna and lies approximately 17 km southwest of the heater site (18.48° north, 66.67° west) at Islote (see Figure 4.7). The HF diagnostic transmitters, described in Section 4.4, were located at the Ramey Solar Observatory (~ 60 km west of Islote) and the receivers at the Sabana Seca naval station (~ 60 km east of Islote, see Figure 4.7).

The heating facility at Arecibo which is described below has been in operation since the early 1980's. Prior to this time heating experiments were performed by mounting a powerful HF transmitter above the 305 m dish at the Arecibo Observatory. The heating facility at Islote consists of four high power transmitters each capable of a peak power of approximately 200 kW. However, the maximum continuous power is closer to 100 kW per transmitter. The transmitters feed a 4 x 8 log periodic antenna array which has a gain of approximately 23 dB. This results in a maximum continuous effective radiated power (ERP) of around 80 MW. Therefore, the ERP available at Arecibo is considerably smaller than the maximum ERP obtained by the Tromsø heater (360 MW). Because of limitations in the size of the Islote site the antennas are offset slightly from the true rows and columns which results in mode coupling, ie when the array is transmitting waves which are nominally polarised in the O- mode then there may be some contamination by X-mode signals. In addition, there is further contamination because the ionospheric characteristic polarisations are elliptical rather than circular (see explanation, p 53). Unfortunately, the total extent of the mode contamination is not known. The antenna radiation pattern is an ellipse aligned in the north-south direction. The heater may transmit waves at frequencies in specified bands between about 3 and 12 MHz. The heater lacks the sophisticated computer control available at Tromsø which means that the heater

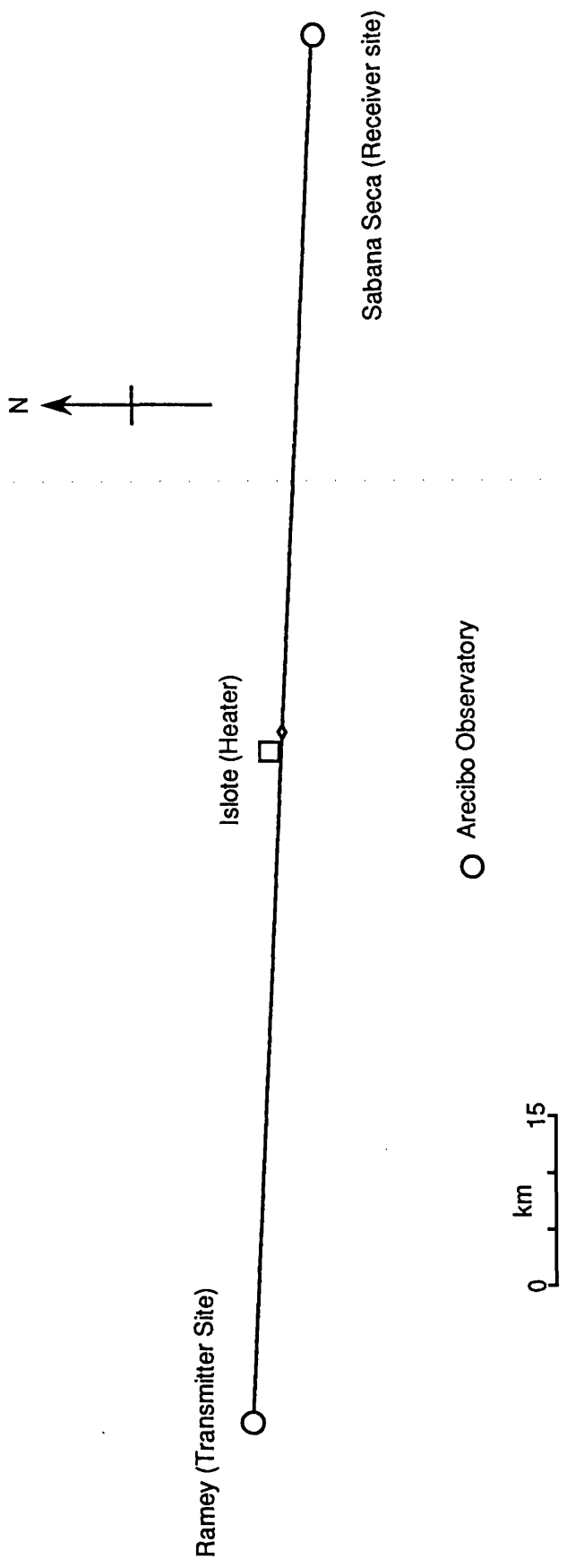


Figure 4.7 Map showing the relative positions of the Arecibo observatory, the heater site and the diagnostic transmitter and receiver sites.

Chapter 4. Equipment and Experimental Procedure

cycles employed are necessarily much simpler. A change in the transmitted frequency can take as long as 20 minutes (although 5 minutes is typical) due to the extensive manual iterative processes involved. Although changes in the power or polarisation can be achieved relatively quickly (a minute or so) they cannot be performed repeatedly due to the operator fatigue resulting from the manual adjustment required. The transmitters proved to be rather unreliable during the campaign described below with full power (ie 80 MW ERP) not being achieved during many experiments (ie one or more transmitters being 'down'). The power is supplied to the transmitters by four diesel generators which are also prone to break down.

The height profiles of the electron density and temperature and the ion temperature were measured by the 430 MHz incoherent scatter radar located at the Arecibo observatory. The large collecting area afforded by the 305 m diameter dish enables extremely weak signals to be detected. This results in a height resolution as low as 600 m being obtainable with a good signal-to-noise ratio. The beam is steerable from elevation angles within a degree of vertical to tens of degrees at all azimuth angles. The plasma parameters are derived by similar methods to those adopted by EISCAT (see previous sections) although at Arecibo the long-pulse data are also fitted for ion composition (Burnside 1988) rather than employing a model. During the experiments described here the radar operated a general purpose program which at 30 second intervals alternately collected ion-line spectral data (and hence T_e, T_i and N_e) with a height resolution of 38 km and "Barker" (or power profile and hence N_e) data with a height resolution of 0.6 km. The radar beam was directed along a single pointing direction (33° azimuth, 86.5° elevation) which intersected close to the center of the heated volume at a height of approximately 280 km in the F-region.

The electron density profiles obtained by the radar were calibrated through measurements of the F-region critical frequency made by the ionosonde located at the Arecibo Observatory (see Section 4.7). The critical density measured by the ionosonde is assumed to be equal the density at the F-region peak observed by the radar, the densities at other heights are then

Chapter 4. Equipment and Experimental Procedure

scaled accordingly. During most of the experiments ionograms were obtained at 15 minute intervals. It should be noted that the ionograms were recorded on paper and were of very poor quality (eg the frequency tick-marks were not spaced correctly).

The HF diagnostics employed during the experiments at Arecibo were essentially the same as those previously deployed at Tromsø. The diagnostic equipment has been described in detail in Section 4.4. The diagnostic ray paths and the 3 dB contour of the heater at Arecibo are illustrated to scale in Figure 4.8. The diagnostic signals do not traverse the heated D-region and therefore only the effects of F-region heating should be observed. The heated volume lies close to the mid-point of the diagnostic path (assuming no significant refraction, which should be the case provided the diagnostic and heater frequencies are more than a few MHz below the ionospheric critical frequency) and close to a line joining the transmitter and receiver sites (Figure 4.7). The reflection points of the diagnostics should occur well within the boundary of the 3 dB contour of the heater provided that the frequencies are chosen such that reflection occurs in the F-region.

At the magnetic dip angle corresponding to Arecibo the diagnostic wave energy is no longer split equally between the O- and X- mode components and the characteristic waves are no longer circular (eg Davies 1969). The crossed-dipole antennas at the receiver site deconvolve the received signal into two oppositely polarised circular components. These components are then *interpreted* as corresponding to the O- and X- modes. Therefore, at Arecibo, it is likely that the nominally O-mode channel is contaminated with X-mode signal and *vice versa*. In addition, due to the exceptionally strong D-region absorption encountered during the 1989 campaign it was not possible to adopt the usual procedures (Section 4.4) for determining whether the O- or the X- polarisation mode was being recorded. Under these conditions, it is likely that the X-mode was absorbed more than the O-mode. Therefore, the nominally O-mode channels were probably not seriously affected by X-mode contamination.

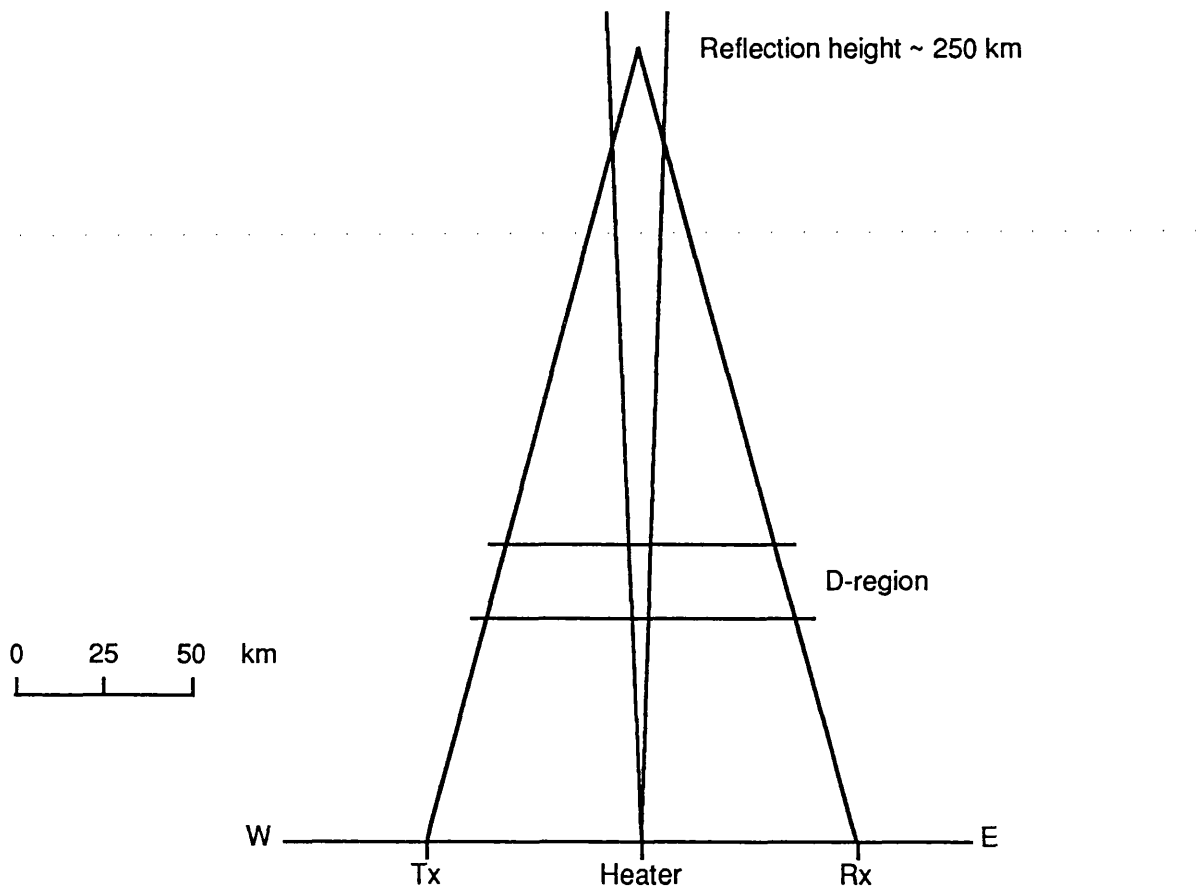


Figure 4.8 Schematic of diagnostic ray-paths through the heated ionosphere above Arcibo.

Chapter 4. Equipment and Experimental Procedure

The experiments reported in this Thesis were conducted during a single campaign of 11 days duration between 14 May 1989 and 26 May 1989. Typically, heating started at 1100 AST (Atlantic Standard Time, AST = UT -4) and finished at 1900 AST. On many days during the campaign very high electron densities were observed, with the F-region O-mode critical frequency as high as 14 MHz and D- and E- region peak frequencies of up to 7 MHz. The diagnostic transmitters were unable to radiate at frequencies higher than about 9 MHz and therefore the frequencies employed (4 - 8 MHz) were often either reflected or absorbed by the E- or D- regions. With high levels of ionisation in the D-region, the heater non-deviative absorption was large which could result in the heater power in the F-region being reduced to levels below the thresholds required for instability formation. This in turn would lead to very low levels of anomalous absorption and F-region heating. This is consistent with the lack of F-region electron heating observed during much of the campaign (see Chapters 5 and 7).

4.9 Concluding remarks

During recent ionospheric modification experiments conducted at Tromsø in northern Norway it has proved possible to study the effect of high power radio wave radiation on the bulk plasma parameters, T_e , T_i , and N_e . These measurements have been facilitated by some of the first co-ordinated heater-EISCAT experiments.

Continued deployment and use of the Leicester HF diagnostics at Tromsø has enabled a brief comparison to be made with the results previously obtained with this system (eg Robinson 1983, 1989; Jones *et al* 1982, 1984; Wilkinson 1988). The deployment of the diagnostics at Arecibo has enabled heater induced anomalous absorption of low power test waves to be studied directly at low-latitudes for the first time.

Chapter 4. Equipment and Experimental Procedure

In the following chapters the results of these experiments are discussed in detail with regard to previous results at low- and high- latitudes and also with the relevant theories pertaining to ionospheric modification. The problems which can arise in the interpretation of data obtained by the various techniques will also be addressed where appropriate.

Chapter 5 Electron and Ion temperature effects

5.1 Introduction

High power radio waves which are incident on the ionosphere can, via the action of anomalous and deviative heating, raise the plasma electron and ion temperatures (see Chapters 2 and 3) from their ambient levels. The enhancement of the temperatures in turn leads to a change in the chemical balance and diffusion processes which can result in a change in the electron density (see Chapter 6).

In this Chapter observations of the changes in T_e and T_i caused by the action of high power radio waves are presented from two sites, Tromsø in northern Norway (high latitude) and Arecibo, Puerto Rico (low latitude). At both sites the temperatures have been measured by the incoherent scatter technique (Chapter 4), by the EISCAT UHF system in the case of Tromsø and by the 430 MHz radar at Arecibo. In the following sections the spatial and temporal characteristics of the heater induced temperature changes at Tromsø are derived from the observations and the experimental data compared with the results of theoretical modelling (Chapter 3). In addition, evidence is presented which suggests that field-aligned electron temperature striations are formed within the heater beam.

5.2 General Characteristics of temperature observations

The method by which the electron and ion temperatures are derived from the ion-line spectra measured by the radars at Tromsø and Arecibo has been outlined in Chapter 4. The errors associated with the derived parameters which ensue from this analysis are functions of the signal-to-noise ratio (SNR) at the receiver (eg McCrea 1989). For the EISCAT system if the SNR is typically greater than 10 % then the resultant errors are less than 5 %.

Chapter 5 Electron and ion temperature effects

There have been two heating campaigns at Tromsø which have involved the simultaneous probing of the heated volume by EISCAT and the Leicester HF diagnostics (Chapters 4). These campaigns took place during March 1985 and February 1987. The Leicester group has also participated in a single heating campaign at Arecibo during May 1989 in which measurements were obtained by the 430 MHz incoherent scatter radar and the Leicester HF diagnostics. The deployment of the HF diagnostics enabled the level of the heater induced anomalous absorption (Chapters 2, 3 and 7) to be determined.

Schematics of the three beam geometries adopted during the two heating campaigns are depicted in Figure 5.1 and are described below.

(i) The beam geometry employed for most of the experiments during the 1985 campaign is illustrated in Figure 5.1a. In this case, both the heater and EISCAT beams are projected vertically, an arrangement which results in EISCAT measurements being made well within the 3 dB contour of the heater (neglecting the effects of refraction). A disadvantage of this geometry is that the EISCAT beam cuts several field lines which can lead to problems in the observation of field-aligned phenomena.

(ii) This problem can be overcome by adopting the geometry illustrated in Figure 5.1b, where both the heater and EISCAT beams are directed along the local field-line (approximately, azimuth 180° , elevation $76-78^\circ$). This arrangement has the drawback that the heater power flux is lower for a given height due to beam spreading and refraction. Another disadvantage with this geometry, is that the HF diagnostic signals are reflected outside of the 3 dB contour of the heater. This means that the estimates of anomalous absorption will not be obtained from the ionospheric volume with the highest level of heater power flux.

(iii) The third geometry entails the heater beam pointing vertically while EISCAT points along the field line. This has the advantages that EISCAT measures along the field line and that the HF diagnostics reflect within the 3 dB contour of the heater. The obvious disadvantage is that EISCAT makes measurements outside of the heater 3 dB contour and

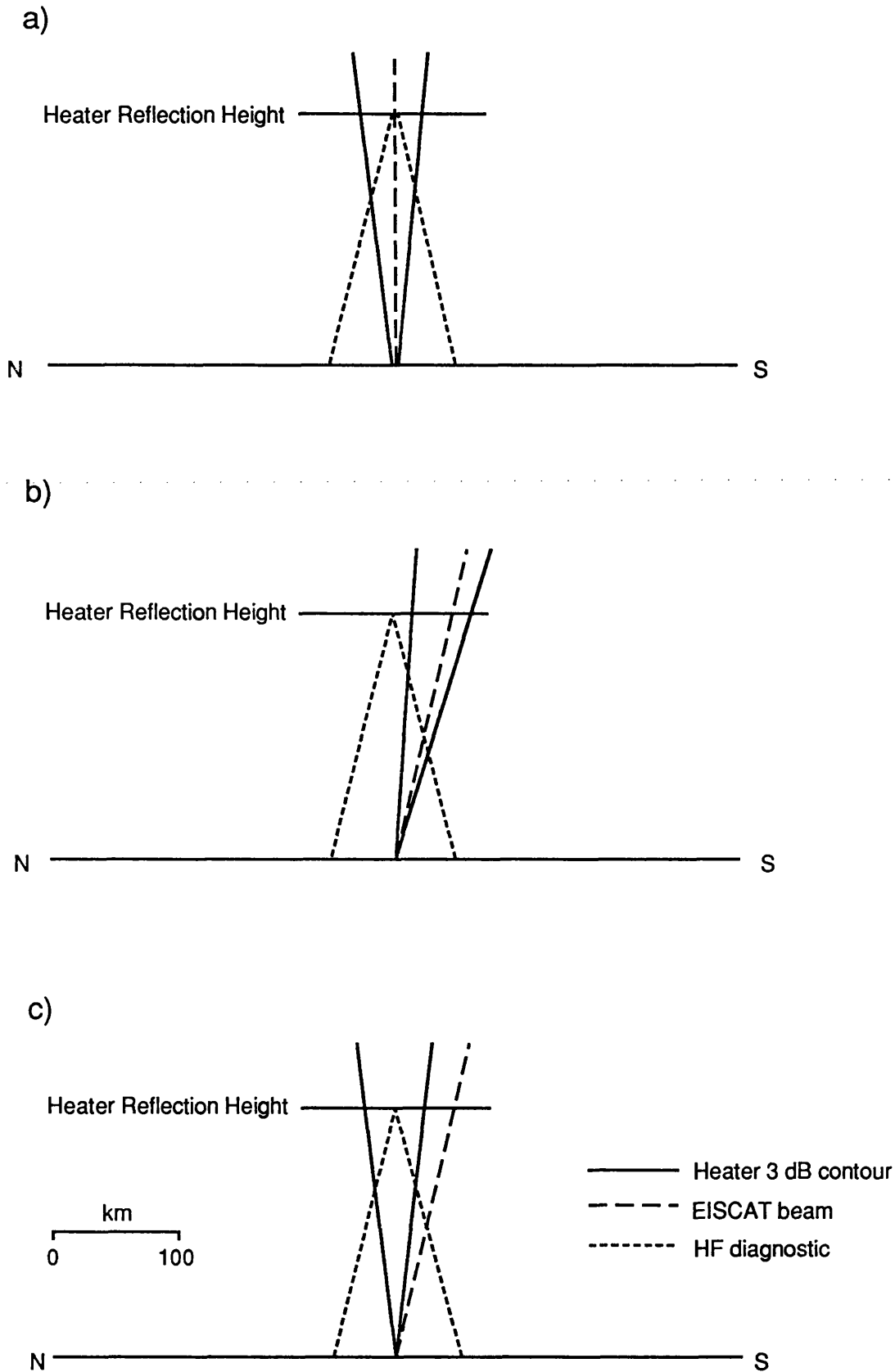


Figure 5.1. Schematic of heater, EISCAT and HF diagnostic beam geometries employed during the 1985 and 1987 heating campaigns at Tromsø. The effects of refraction have been neglected.

Chapter 5 Electron and ion temperature effects

therefore, with negligible cross-field diffusion, the observed heater-induced changes in the plasma parameters will be reduced.

During the 1985 campaign at Tromsø, EISCAT measured the electron and ion temperatures at three ranges, 148 km, 202 km and 256 km. A typical interval of data obtained during the course of this campaign, on 17 March 1985, is reproduced in Figure 5.2. These data have been post-integrated for 60 s in order to increase the SNR and thereby reduce the errors. Starting at 1202 UT, and continuing until 1258 UT, the heater was switched on for two minutes and then turned off for two minutes. The heater transmitted at a frequency of 4.544 MHz (foF2 ~ 4.8 MHz), with an effective radiated power (ERP) of approximately 240 MW and with ordinary polarisation. During this interval both the heater and EISCAT beams were directed vertically with the heater reflecting at an altitude of approximately 205 km (see Chapter 6). The EISCAT range gate (202 km) which lies closest to the heater reflection height exhibits an increase in the temperature of several hundred Kelvin upon heater switch on. A smaller increase of about 100 K is observed at 256 km, while at 148 km there is a very small, but systematically observable, increase in the electron temperature. These observations are consistent with the notion of a maximum increase in the electron temperature occurring close to the heater reflection height with some thermal diffusion to heights above and below this. However, care should be exercised when interpreting these data as they are not independent due to range sampling overlap (see Chapter 4).

Throughout the 1985 campaign, each time the heater was switched on an enhancement of the electron temperature was observed by EISCAT. An enhanced electron temperature was always observed in the gate closest to the heater reflection height, and often in the gates on either side of this gate. This may be contrasted with the behaviour in the 1987 campaign when the observed temperature was rarely enhanced. However, during the 1987 campaign on the relatively few occasions when the electron temperature was increased by the heater, the increases tended to be larger than in 1985. The difference in the behaviour of the electron

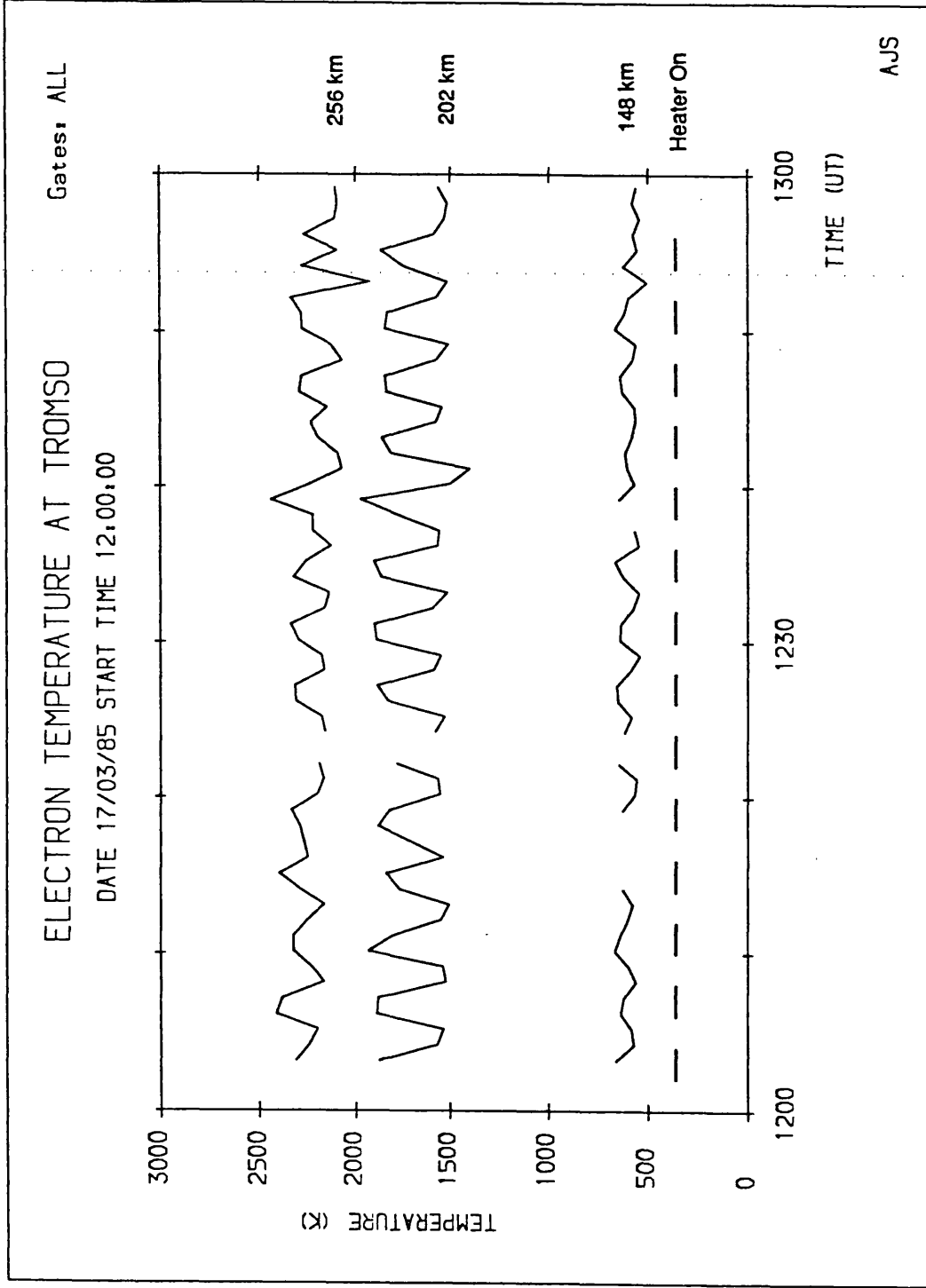


Figure 5.2 Electron temperature enhancements measured by EISCAT, at three different altitudes, on 17 March 1985, during heating at 4.544 MHz.

temperature enhancement between the two campaigns may be explained either by a difference in the ambient ionospheric conditions or by the experimental geometry. During many of the experiments in 1987 the beam geometry discussed in (iii) was adopted, and therefore EISCAT made measurements in a region of comparatively low heater power. In addition to the geometrical considerations, many of the experiments conducted during the 1987 campaign involved transmitting several heater powers (approximately 260 MW, 130 MW and 65 MW). The majority of the temperature enhancements were observed when the heater transmitted at the highest power. There are some instances where the temperature enhancement displays a clear dependence upon the heater power (see Section 5.7).

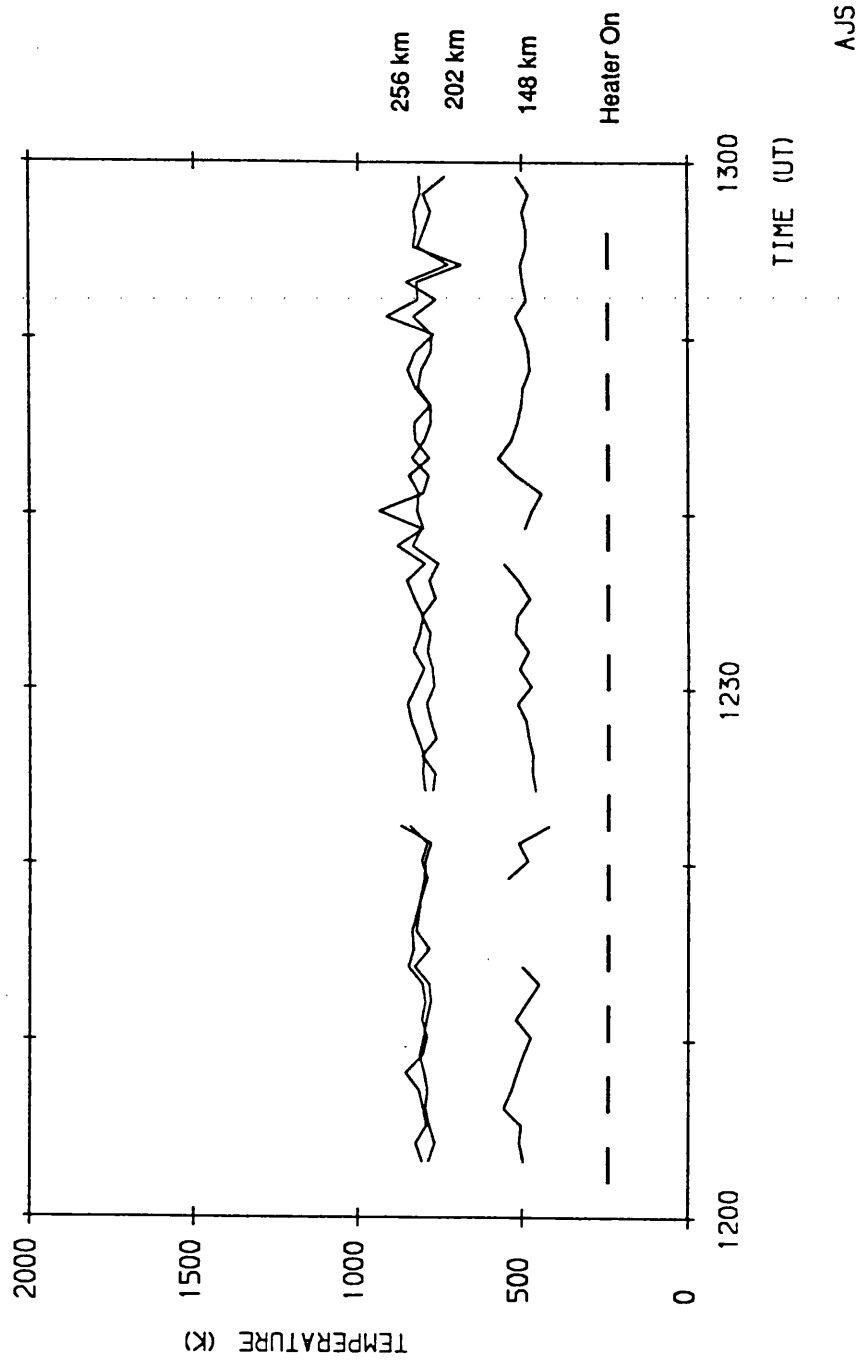
The ion temperatures corresponding to the interval in Figure 5.2 are reproduced in Figure 5.3. Examination of these data reveals that no systematic heater induced changes in the ion temperature were observable at any of the three heights. From the results of heating experiments conducted at Arecibo the expected change in the ion temperature is less than 50 K (eg Gordon and Carlson 1974). This is smaller than the errors associated with the EISCAT measurements, and therefore while no clearly defined systematic heater-induced changes in the ion temperature have been recorded during either of the campaigns held at Tromsø, the observations do not entirely preclude their existence.

In the following sections we will concentrate primarily on two intervals which have exhibited a strong response to heating in both the changes to the electron temperature and the electron density (Chapter 6). These two periods are from 0945 to 1030 UT on 23 March 1985 and 1135 to 1230 UT on 26 February 1987. The experiments which were conducted during these intervals will be described in the next section.

ION TEMPERATURE AT TROMSO

Gates: ALL

DATE 17/03/85 START TIME 12.00.00



AJS

Figure 5.3 Ion temperature measurements for the same interval as Figure 5.2

5.3 The experiments of 23 March 1985 and 26 February 1987 at Tromsø

Between 0946 and 1030 UT on 23 March 1985 the heater switching cycle consisted of 4 minutes heater on, followed by 4 minutes heater off. Throughout this period the heater employed an ERP of 240 MW, a transmitted frequency of 4.04 MHz and O-mode polarisation. From the height of the ion-line overshoot observed in the EISCAT power profile the heater reflection height was deduced to be close to 192 km (see Chapter 6). The experimental geometry (ii) described in the previous section was employed during this experiment. For this geometry the EISCAT measurements are close to the centre of the heater beam if the effects of refraction are neglected. The electron and ion temperatures were measured at heights centred on 144 km, 197 km and 249 km and were acquired with a time resolution of 10 s. The electron temperatures observed during this interval are illustrated in Figure 5.4. These data exhibit a marked increase in the electron temperature at all three heights upon each heater switch on. The largest electron temperature enhancement was observed in the EISCAT height gate which lay closest to the heater reflection height (ie 197 km), with an increase of close to 500 K. The temperature increases in the remaining two height gates are each about 100 K. It should be noted that the temperature reached equilibrium within one or two integration periods after the heater had been switched on or off. The ambient (ie unheated) temperature and the equilibrium level of the enhanced temperature remain at, essentially, constant levels throughout this period. This means that the temperatures are suitable for averaging via superposition. This process involves the averaging of data from equivalent times within the heater cycle (eg the temperature observed in the first 10 s of each heater on is averaged together, then the temperature between 10 and 20 s after heater switch on, and so on). The results of the superposition are presented in the next section where the temporal evolution of the temperature enhancement is discussed.

During the period from 1135 UT to 1230 UT on 26 February 1987 the heater was only switched on twice. Firstly, between 1141 UT and 1157 UT with an ERP of 260 MW, and

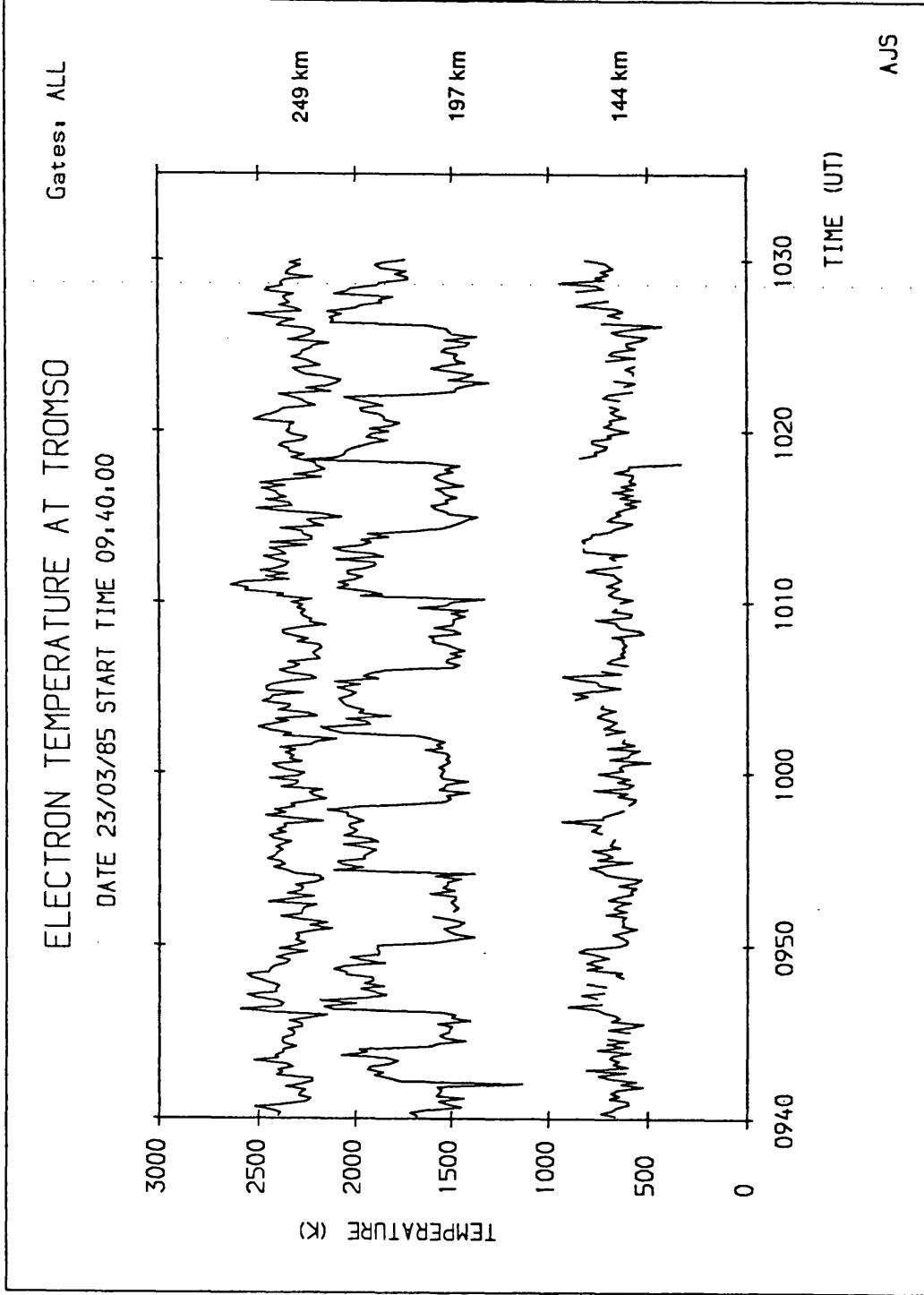


Figure 5.4 Electron temperature enhancements measured by EISCAT, at three different altitudes, on 23 March 1985, during heating at 4.04 MHz.

Chapter 5 Electron and ion temperature effects

secondly, between 1203 UT and 1219 UT with an ERP of 130 MW. A frequency of 4.04 MHz and O-mode polarisation were employed during both heater cycles. The heater beam was reflected at a height of just below 200 km. The experiment employed beam geometry (ii), yielding measurements from near the centre of the heater beam, ie where the heater power was greatest. Temperatures were recorded at six height gates centred on 163, 194, 225, 256, 286 and 317 km. The remote site beams were scanned in elevation such that the intersection volume ranged from roughly 20 km above the heater reflection height to about 20 km below (Chapter 4). At each dwell position the intersection heights of the two remote site beams were separated by about 5 km (corresponding to the width of the remote site beams at F-region heights). The electron temperature measured with a time resolution of 5 s, from all of the Tromsø height gates is illustrated in Figure 5.5. Examination of this figure reveals that the temperature is increased by up to 500 K upon heater switch on in the gate closest to the heater reflection height. An increase in the electron temperature is readily observable in all six height gates. As the heater was only switched on twice during this interval, and at a different power in each case, the technique of superposition employed in averaging the 1985 data was unsuitable. Instead, the data were smoothed by the application of a running mean. The temporal evolution of the temperature enhancement observed during this period is discussed in the next section, the occurrence of temporal fluctuations in Section 5.5 and the spatial structure in Section 5.6.

5.4 Temporal evolution of the enhancement in electron temperature

The electron temperature measured by EISCAT between 0946 UT and 1030 UT on 23 March 1985 from equivalent parts of the heater cycle have been superimposed in order to reduce the variance of the data. Temperatures which have been derived from ion-line spectra which exhibit the ion-line overshoot (Chapter 2) have not been included in the averaging process. The averaged data observed at a height of 197 km shortly after heater switch on and heater switch off are illustrated in Figures 5.6 and 5.7, respectively. In Figure 5.6 the electron

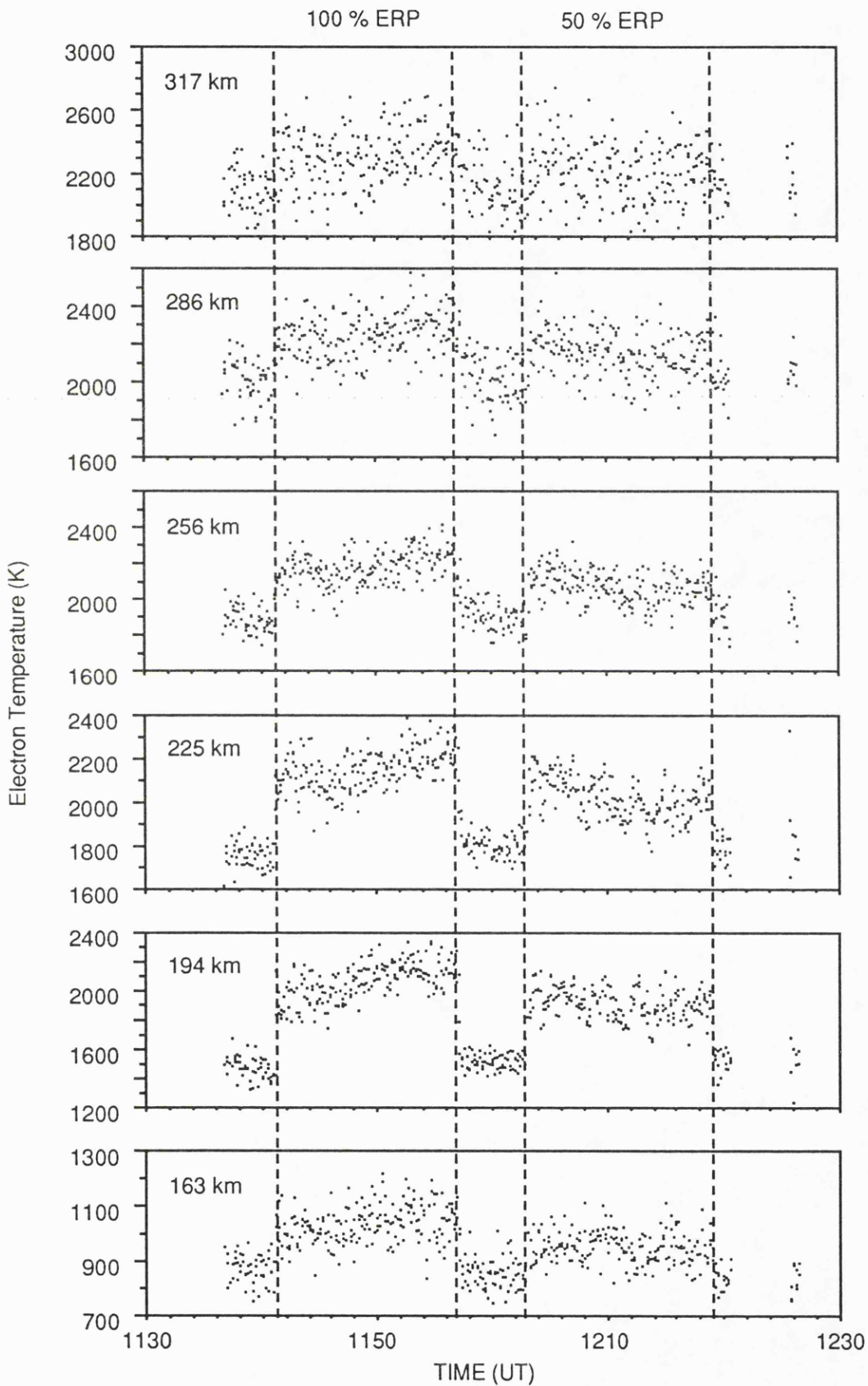


Figure 5.5 Electron temperature enhancements measured by EISCAT, at six different altitudes, on 26 February 1987, during heating at 4.04 MHz.

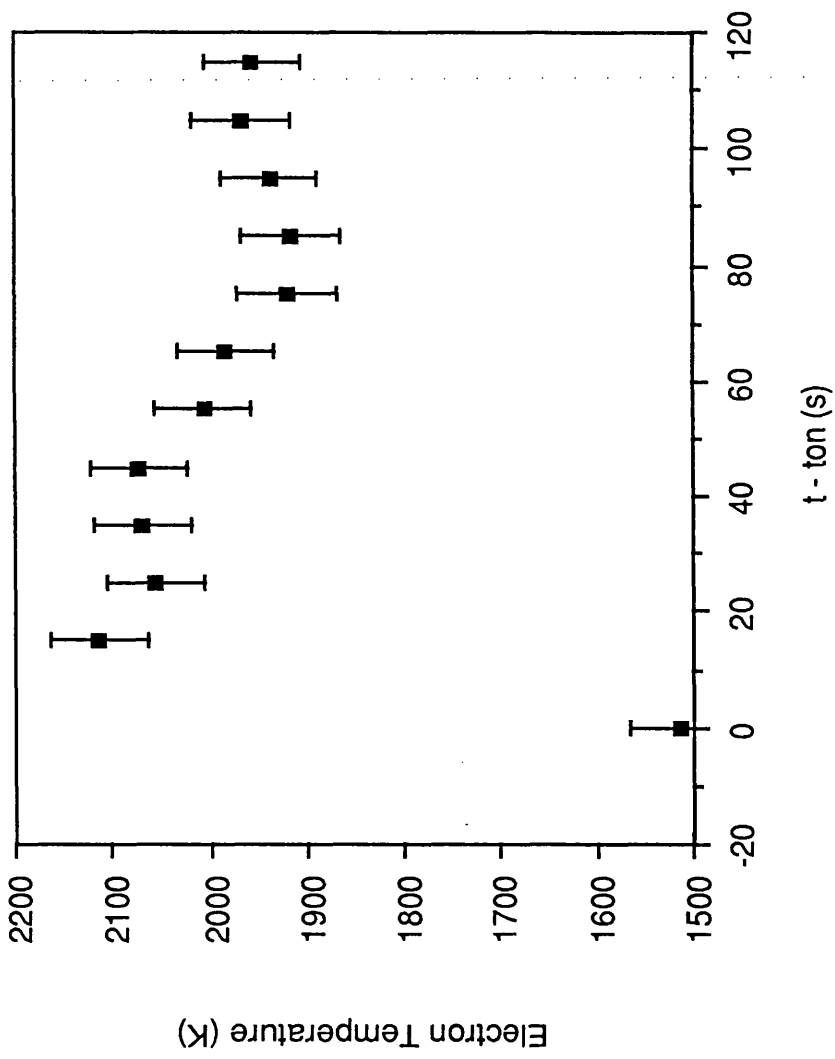


Figure 5.6 Average electron temperature enhancement measured by EISCAT at 197 km, on 23 March 1985.

Te recovery from heating (Tromso, 23/03/85 0946-1030 UT, 197 km)

A = 449.00 Constant = 3.8000

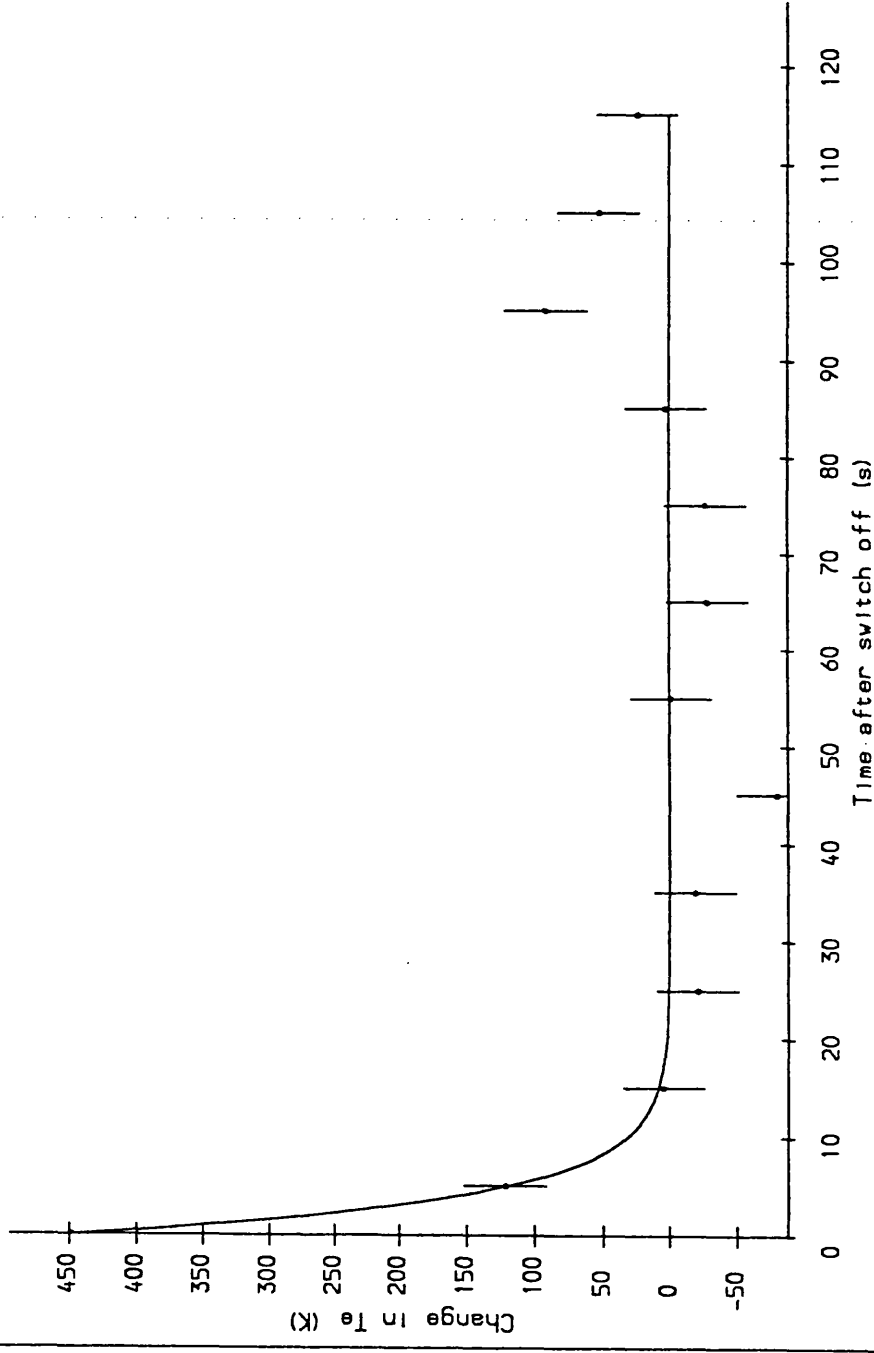


Figure 5.7 Graph showing the relaxation of the electron temperature enhancement after heater switch off at an altitude close to the heater reflection height. The solid line is a best-fit exponential.

temperature is enhanced from just over 1500 K to 2100 K in a matter of 15 s. This rapid rise time is followed by a gentle decay to a quasi-stationary equilibrium temperature of about 1950 K. It has not been possible to determine the growth time of the enhancement as this is faster than the time resolution of the data. The electron temperatures observed at heights of 144 km and 256 km also exhibit a rapid rise upon heater switch on.

When the heater is switched off, the temperature falls to the levels observed prior to heating in about 15 s (Figure 5.7). There is some evidence to suggest that the temperature fluctuates about the zero level. The implications of this are discussed in more detail in Section 5.5. The solid line depicted in Figure 5.7 is a "best-fit" function of the form,

$$\Delta T(t) = \Delta T_0 \exp(-t / \tau_D) \quad (5.1)$$

where, ΔT_0 is the difference between the average temperature during heater on and the averaged temperature during heater off, t is the time since the heater was switched off, and τ_D is the decay time constant. The time constants for the three EISCAT height gates are presented in Table 5.1. The values of τ_D , at under 4 s for 144 and 197 km and 9 s at 256 km, are less than those derived by Wilkinson (1988) from data obtained during the same campaign. The difference in the decay constant may possibly be explained either by a change in the cooling rate or, more speculatively, by the occurrence of anomalous collisions, ie where the electrons collide with the electrostatic waves generated by the heater. However, why these mechanisms should have a greater effect during this interval remains unclear.

The change in the electron temperature during the first four minutes after the heater was switched on at 1141 UT on 26 February 1987 at heights of 256, 286, and 317 km is depicted in Figure 5.8. A running mean with a 30 s window has been applied to these data. The temperatures measured shortly after heater turn on for the other three EISCAT gates are

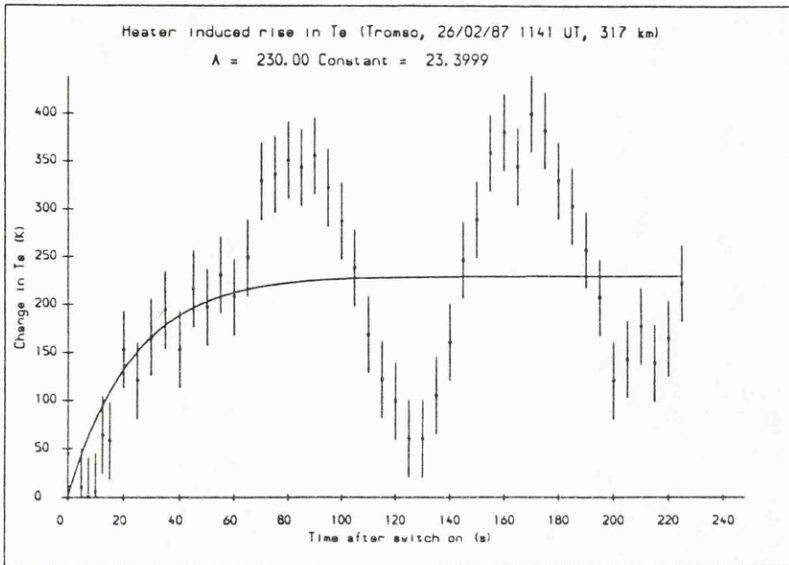
HEIGHT (KM)	τ_D (s)
144	3.6
197	3.8
249	9.0

Table 5.1 Electron temperature recovery time during a heating experiment on 23 March 1985, 0946 - 1030 UT.

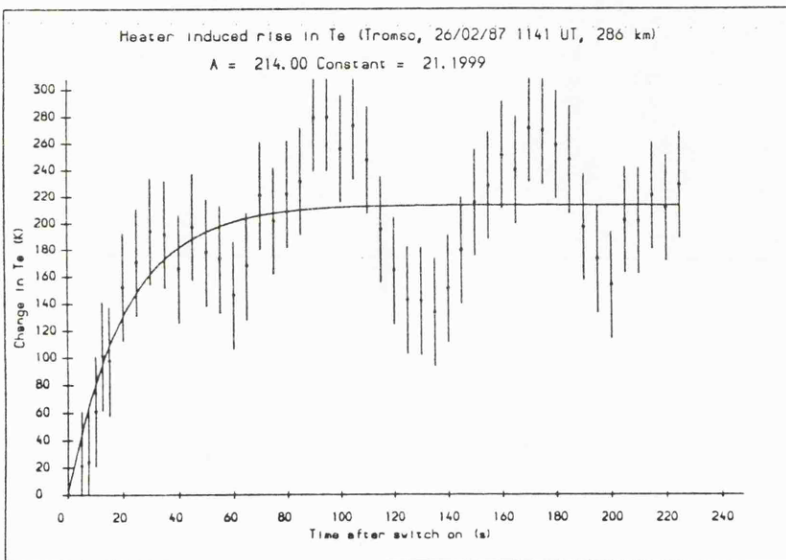
HEIGHT (km)	τ_R (s)	τ_D (s)
163	-	8.0
194	-	3.7
225	-	11.7
256	17.4	21.5
286	21.2	42.7
317	23.4	70.6

Table 5.2 Electron temperature rise and recovery times during a heating experiment on 26 February 1987, 1141 - 1203 UT.

a)



b)



c)

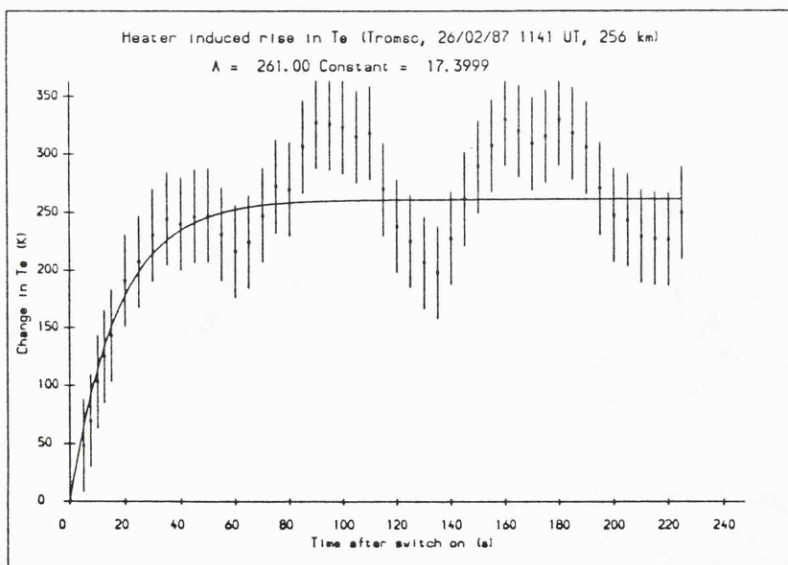


Figure 5.8 Electron temperature measured shortly after heater switch on at 1141 UT, 26 February 1987 for three heights, a) 317 km, b) 286 km, c) 256 km. Solid curves are best-fit exponentials.

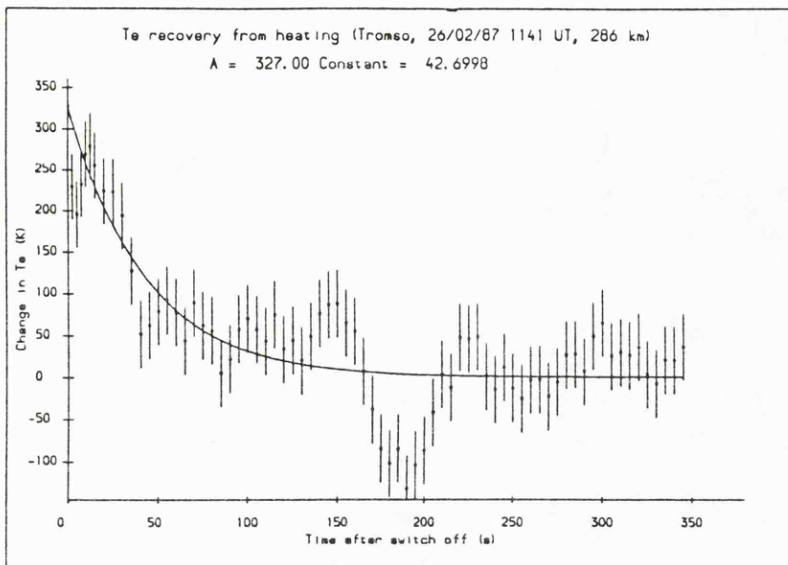
seriously affected by the presence of the ion-line overshoot and are not presented. At each of the heights in Figure 5.8, the electron temperature eventually rises to a value about 200 K above the mean ambient level observed during heater off. The wave-like activity which commences about 60 s after heater switch on is investigated in more detail in the next section. The solid line in each of the figures represents a least-squares fit to the data of the form,

$$\Delta T(t) = \Delta T_0 (1 - \exp (t / \tau_R)) \quad (5.2)$$

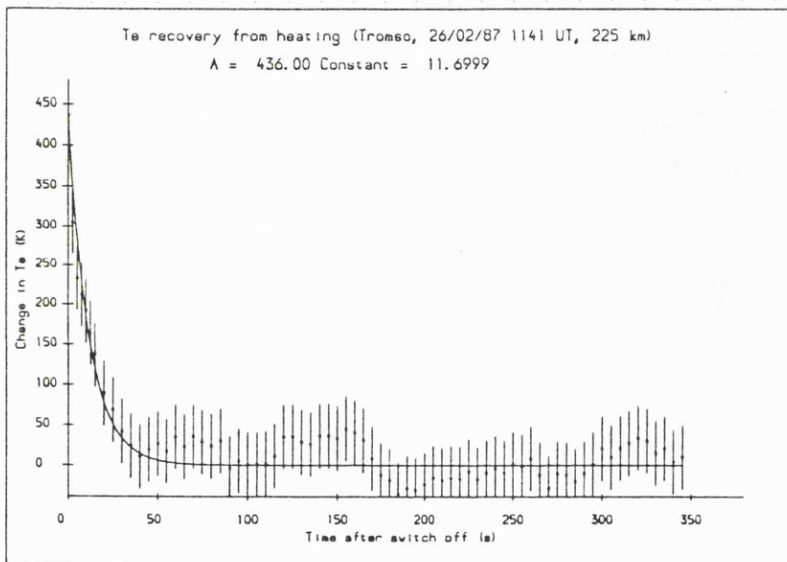
where ΔT_0 is the difference between the mean temperature levels during heater on and heater off, t is the time since the heater was switched off and τ_R is the rise time constant. The rise time constants which have been derived at the three heights illustrated in Figure 5.8 are presented in Table 5.2. Similar rise times were observed during 50 % power heating at 1203 UT. These values are also similar to those found at Arecibo (Mantas *et al* 1981) and close to those for large scale density changes inferred from HF phase measurements made at Tromsø (Jones *et al* 1982; Robinson 1989). The rise time seems to be essentially unchanged with altitude at a value of close to 20 s and there is some evidence (Figure 5.8a) to suggest that a delay exists in the time between heater switch on and when the temperature starts to rise.

The temperatures measured by EISCAT from 1157 UT, where the heater is switched off, through 1203 UT, where the heater is once more switched on, for three altitudes (194, 225 and 286 km) are illustrated in Figure 5.9. A running mean with a 30 s window has been applied to the 5 s resolution raw data. The temperatures exhibit less fluctuation during the off phase than during heater on, although there is some evidence to suggest that the wave-like activity observed during heater on (Section 5.5) also occurs after the heater has been switched off. The solid lines depicted in Figure 5.9 represent the best-fit curves of the form of Equation 5.1. The decay time constants which have been derived for all six EISCAT height gates are presented in Table 5.2. The electron temperature perturbation after 50 % heating at 1203-1219 UT exhibits similar decay rates. These values for full power heating have then been

a)



b)



c)

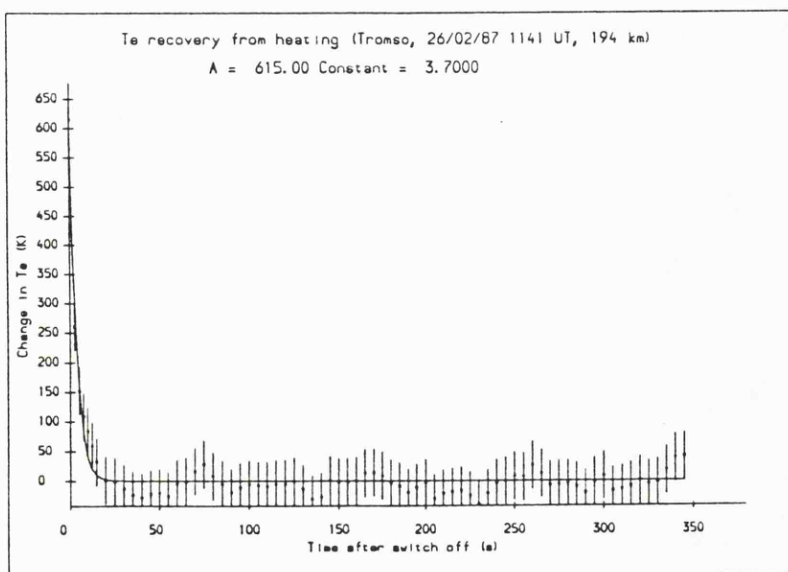


Figure 5.9 Electron temperature measured shortly after heater switch off at 1157 UT, 26 February 1987 for three heights, a) 286 km, b) 225 km, c) 194 km. Solid curves are best-fit exponentials.

Chapter 5 Electron and ion temperature effects

plotted against the absolute separation of the height gate from the heater reflection height (Figure 5.10). It has been assumed that the heater reflection height lies close to the 194 km height gate (see Chapter 6). Examination of Figure 5.10 reveals that the decay time increases as the separation from the heater reflection height increases. This behaviour is similar to that observed at Arecibo (Mantas *et al* 1981) where the smallest decay time was found just above the heater reflection height. However, it must be stressed that the Arecibo measurements were obtained over a much smaller altitude extent. The overall electron cooling rate at a given height depends upon the relative contributions of a number of different electron energy loss processes (eg Banks and Kockarts 1973; Schunk and Nagy 1978; Gurevich 1978). These include collisions (with ion and neutrals), rotational and vibrational excitation of neutral molecules, electronic excitation of the O(³P) state (Carlson and Mantas 1982) and thermal conductivity. In the F-region it is believed that the cooling rate due to the electronic excitation of O(³P) dominates, although this has been questioned on the basis of experimental evidence at Arecibo by Carlson and Mantas (1982). It is expected that the cooling rate should decrease with increasing height (Schunk and Nagy 1978) which explains the observations above the heater reflection height, but not the decay constant observed below this height. The decay time at the gate closest to the reflection height is significantly smaller than those observed by Wilkinson (1988) and, possibly, this may be explained either by an exceptionally high cooling rate or by anomalous collision processes. The effect of anomalous collisions would be expected to be strongest close to the heater reflection height. Although it was not possible to measure accurately the level of anomalous absorption during this interval as the low power HF diagnostic signals were reflected outside of the 3 dB contour of the heater, estimates of the anomalous absorption are presented in Table 5.3 (located after p71).

The growth of the electron temperature due to heating has been modelled by the theory described in Chapter 3. The background (ie unheated) electron density and temperature and ion temperature obtained by EISCAT, the neutral atmospheric parameters from MSIS 1986 (Hedin 1983), ion composition (Quegan *private communication*) and the electron loss rates

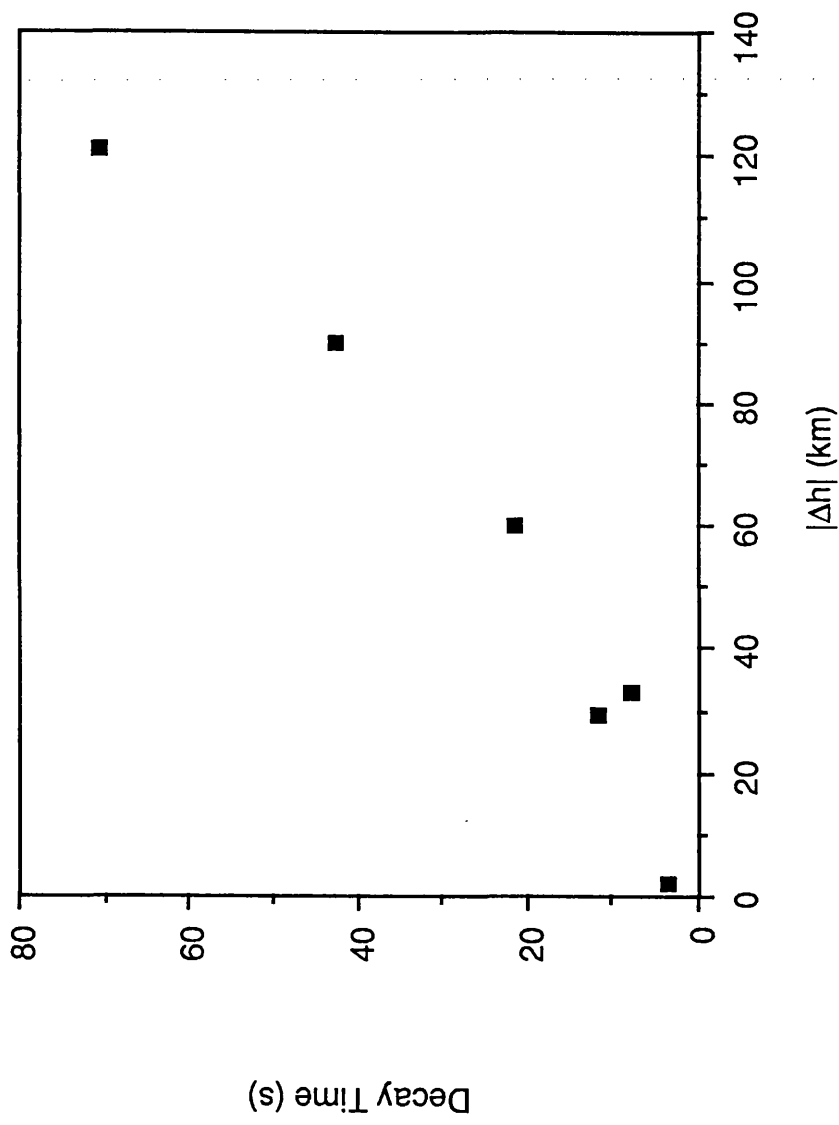


Figure 5.10 The decay time of the electron temperature enhancement after heater switch off as a function of separation from the heater reflection height for EISCAT measurements between 1157 and 1203 UT on 26 February 1987.

Chapter 5 Electron and ion temperature effects

(Schunk and Nagy 1978) have been employed as the starting conditions for the model (see Table 3.1). Two different thermal conductivity models (Schunk and Nagy 1978; Gurevich 1978) have been considered, although both give similar results at heights above about 200 km (see Chapter 3). The thermal conductivity of Schunk and Nagy (1978) has been employed in modelling the temporal response of electron temperature to heating. The heat input, Q_0 has been chosen such that an asymptotic temperature peak of 50 % relative to the ambient temperature occurs at heights close to the heater reflection height.

Experimental observations of the relative change in electron temperature obtained on the 26 February 1987 starting at 1141 UT are depicted in Figure 5.11. At each height, data derived from the numerical model have also been plotted. At altitudes far from the interaction region the model underestimates the observed value of $\Delta T_e/T_e$ (see Section 5.6 for further discussion). As it is only the growth times that are of interest here, the theoretical values of $\Delta T_e/T_e$ at each height have been multiplied by a factor (0.9 at 225 km, 1.2 at 256 km, 2.0 at 286 km and 3.8 at 317 km) such that the modelled equilibrium level roughly corresponds to that of experiment. Examination of Figure 5.11 reveals that there is a reasonable agreement between the model and experiment as to the time taken for $\Delta T_e/T_e$ to saturate.

The experimental data depicted in Figure 5.11d exhibits a delay of 10-20 s after heater switch on before any appreciable value of $\Delta T_e/T_e$ is obtained. This delay probably arises from the finite time required before the temperature is sufficiently enhanced in the source region to affect the heat flow away from that region and hence, change the temperature. The modelled curve exhibits a much shorter delay. The discrepancy between model and experiment may be a result of random fluctuations (or striations, see next section) in the observed temperature. Alternatively, it may be that the background ionospheric parameters (eg thermal conductivity) assumed by the model are significantly different from the values prevailing during the experiment. After the first 20-30 s the growth time of the temperature enhancement is similar

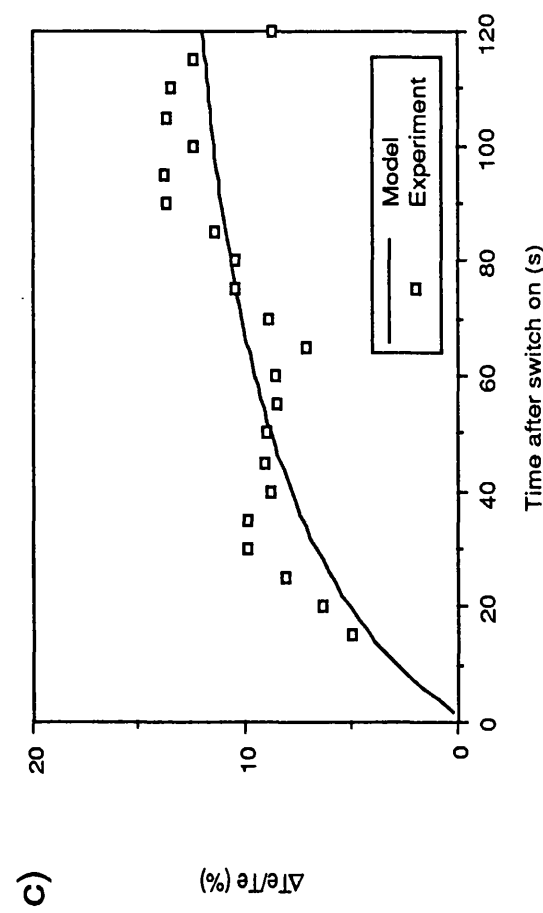
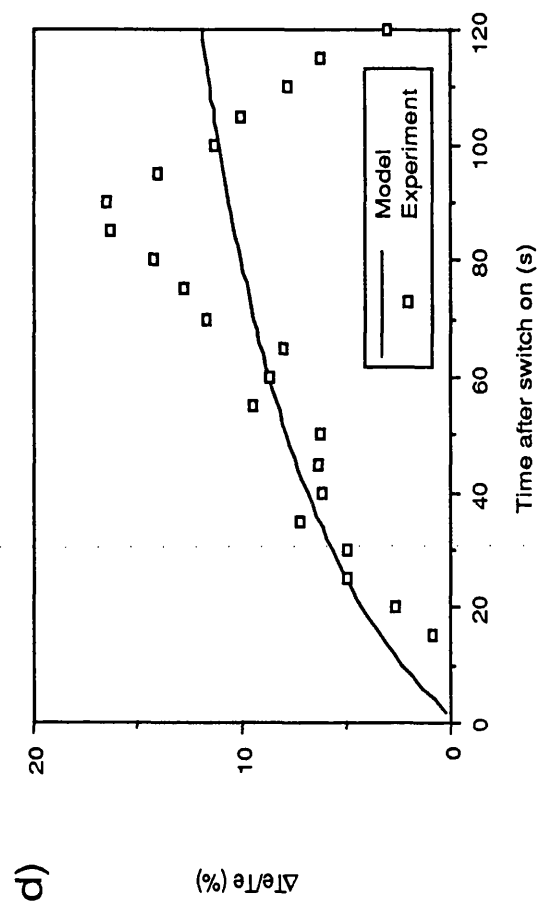
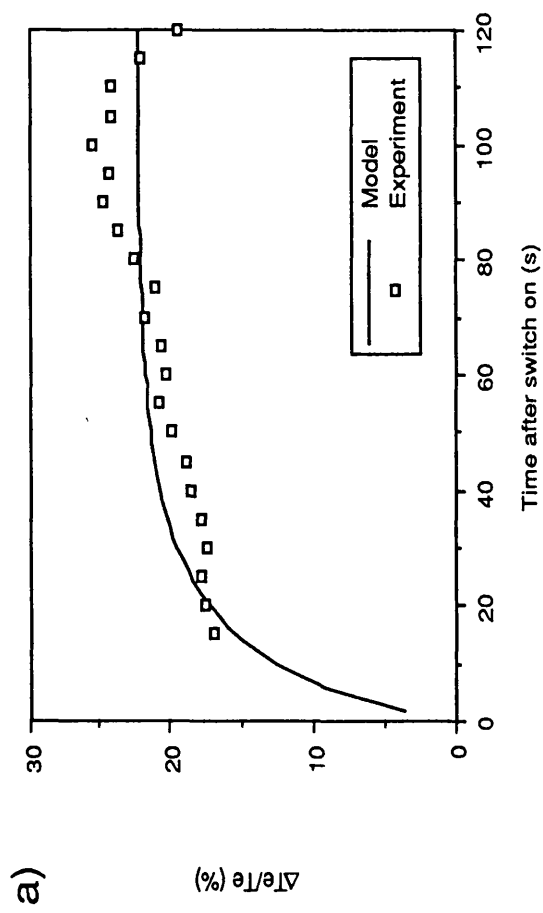
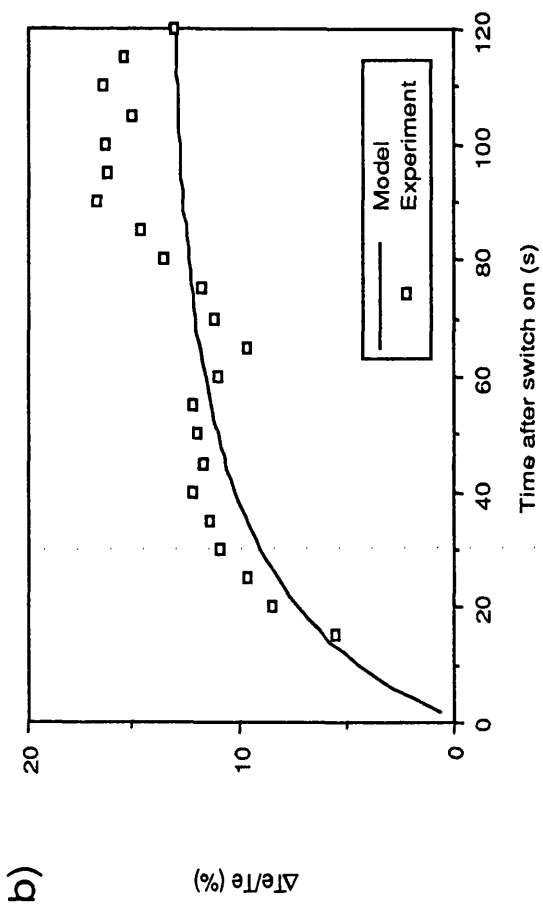


Figure 5.11. Change in electron temperature versus time after heater switch on at heights of a) 225 km, b) 256 km, c) 286 km, d) 317 km

for model and experiment (allowing for the fluctuations in the observations).

5.5 Thermal Striations

It was observed in the previous section that the electron temperature measured after heater switch on exhibited strong periodic fluctuations. Smaller, irregular fluctuations were also observed during the intervals when the heater was switched off (Figure 5.9). This behaviour is reminiscent of that reported by Carlson and Mantas (1982) during similar experiments at Arecibo. Carlson and Mantas attributed these observations to the formation of heater-induced thermal striations through the action of the thermal self-focussing instability (eg Perkins and Valeo 1974; Cragin and Fejer 1974; Cragin *et al* 1977; Perkins and Goldman 1981). In this section we have considered the possibility that the electron temperature oscillations observed at Tromsø may also have been caused by thermal self-focussing.

The electron temperature measured by EISCAT for the entire duration of the heater on between 1141 and 1157 UT is presented for three heights in Figure 5.12. A running mean with a 25 s window has been applied to these data. The two large oscillations in the electron temperature which occur about 60 s after heater turn on are observed at all three heights. The depth of the modulation is 100 K at the two lower heights and about 200 K at 317 km. There are also other features in the temperature which are common to each of the three heights. It is also evident that the period of the temperature oscillations does not remain constant throughout this interval. The data obtained at 286 km and 317 km from the entire interval have been cross-correlated with those obtained at a height of 256 km (Figure 5.13). Data from times where the temperature had not yet reached quasi-equilibrium have been omitted. Where data gaps exist the values have been set to the mean level of the entire data set. The mean of the time series has been subtracted from each of the data points and the time series has been linearly detrended prior to cross-correlation. Both the correlation functions reproduced in Figure 5.13 exhibit a peak close to the zero lag with a fluctuation about zero at other lags. The

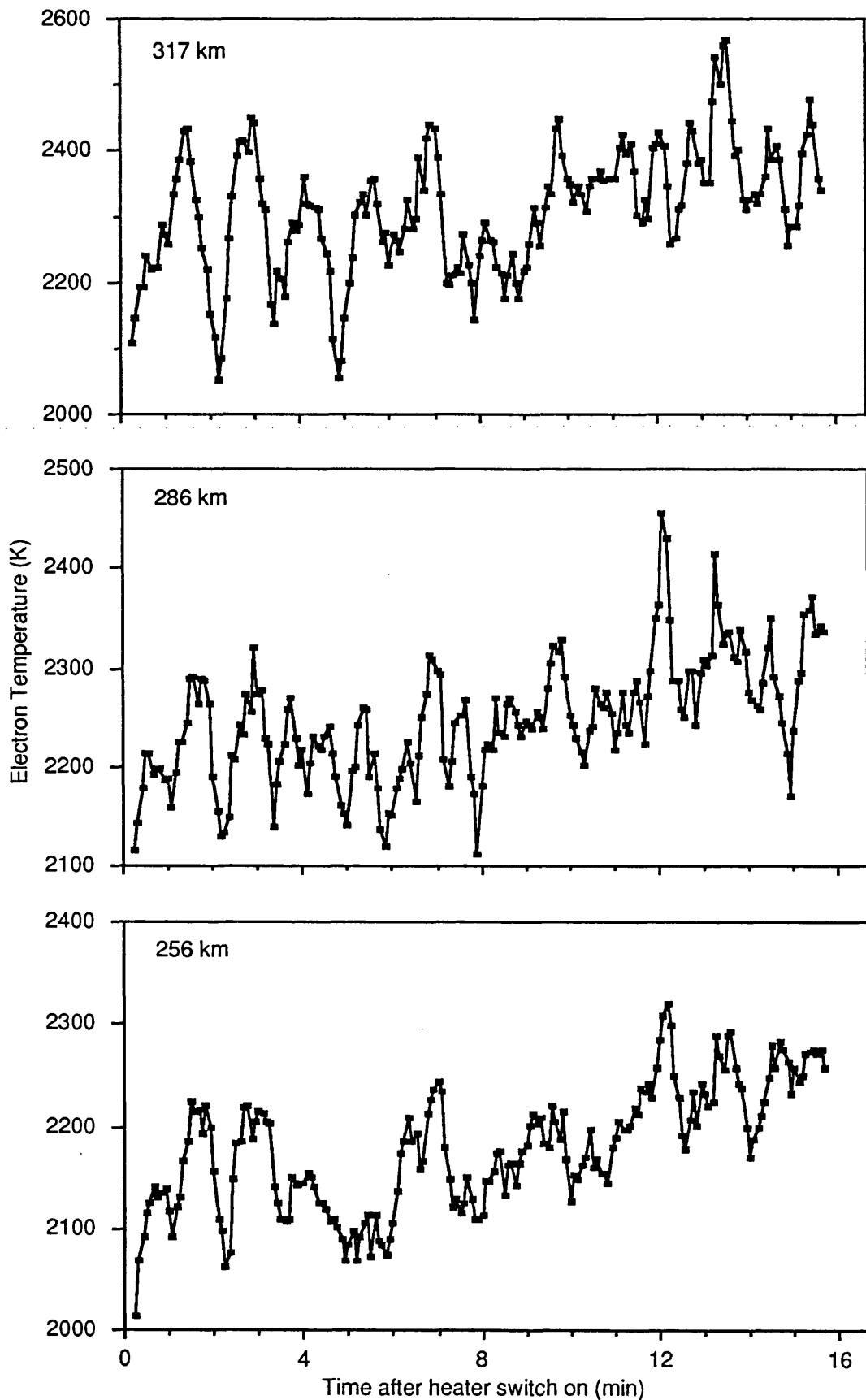
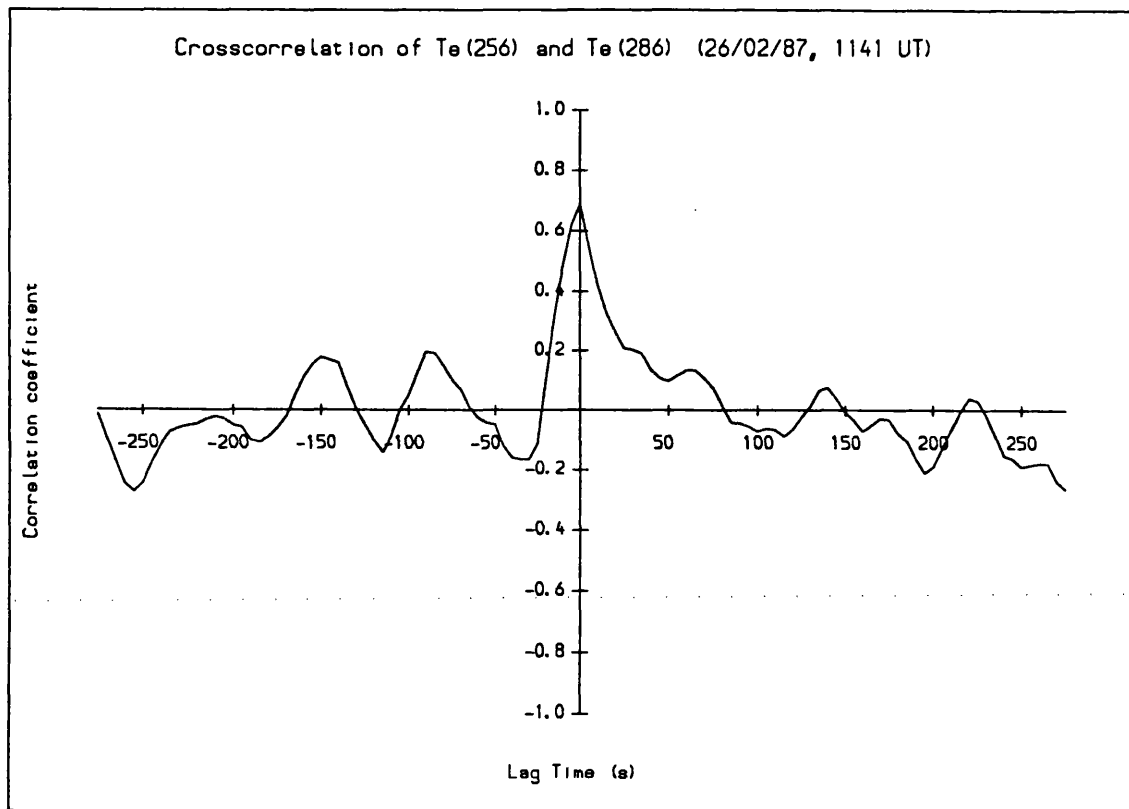


Figure 5.12 Electron temperature measured by EISCAT, 26 February 1987. A 25 s running mean has been applied to the data.

a)



b)

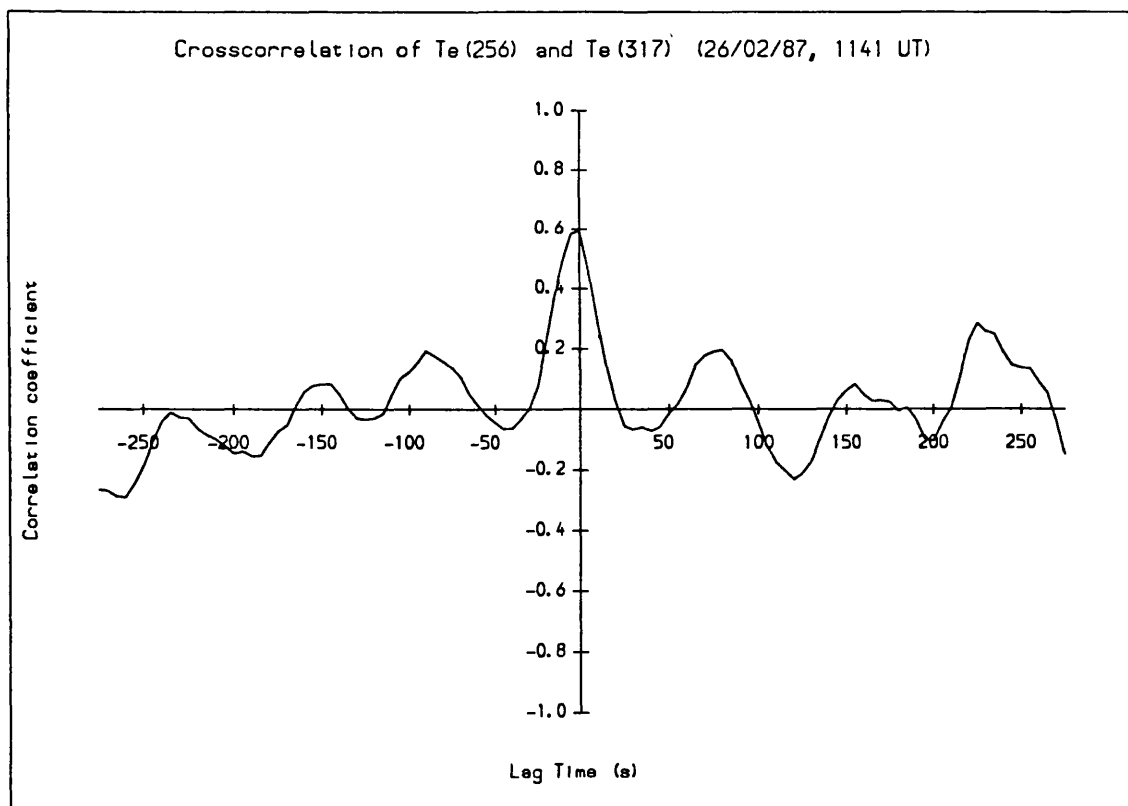


Figure 5.13 Cross-correlograms of electron temperature observed from 1141 and 1157 UT on 26 February 1987 at heights of a) 256 and 286 km, b) 256 and 317 km.

Chapter 5 Electron and ion temperature effects

location of the peak at the zero lag suggests that there is no phase shift in the temperature oscillations with height. The correlation coefficient, ie the peak value, is approximately 0.6-0.7 which indicates that the time series are similar at each of the three heights. The smaller peaks at non-zero lags indicate that there is a common sinusoidal component at the three heights with a period of approximately 70-80 s.

The period of the electron temperature oscillations which commence at about 60 s after the heater switch on at 1141 UT is close to 70-80 s. The ion drift velocity during this interval has been ascertained from EISCAT tristatic measurements to lie between 20 ms^{-1} and 50 ms^{-1} . The statistical errors associated with these measurements are about 20 ms^{-1} . In addition, further errors may be introduced if the ion velocity was not uniform over the region probed by the remote sites as these did not point at the same ionospheric volume at this time. If, on the basis of the EISCAT observations, a mean velocity of $35 \pm 20 \text{ ms}^{-1}$ is assumed, a period of 70 s implies a temperature striation with field perpendicular scale-size of approximately $2.0 \pm 1.5 \text{ km}$. This is similar to the scale sizes observed during plasma line experiments (Duncan and Gordon 1982) and those derived for oscillations in T_e/T_i (Robinson 1985) at Arecibo.

5.6 Spatial structure of the electron temperature enhancement

The height profile of the relative change in the electron temperature observed by the EISCAT receiver at Tromsø three minutes after heater switch on during 26 February 1987 at 1141 UT is presented in Figure 5.14. At heights above the interaction region ($\sim 200 \text{ km}$) $\Delta T_e/T_e$ falls with scale lengths of several tens of kilometers. Below the interaction height the scale lengths are much shorter than this. The solid curve in Figure 5.14 has been derived from the non-stationary model described in Chapter 3 utilising the standard ambient parameters and the Schunk and Nagy (1978) thermal conductivity model. The modelled values have been calculated with a height resolution of 5 km and a peak equilibrium value of $\Delta T_e/T_e$ of 40 %, which closely matches that observed by Tromsø. The initial heater interaction height has been

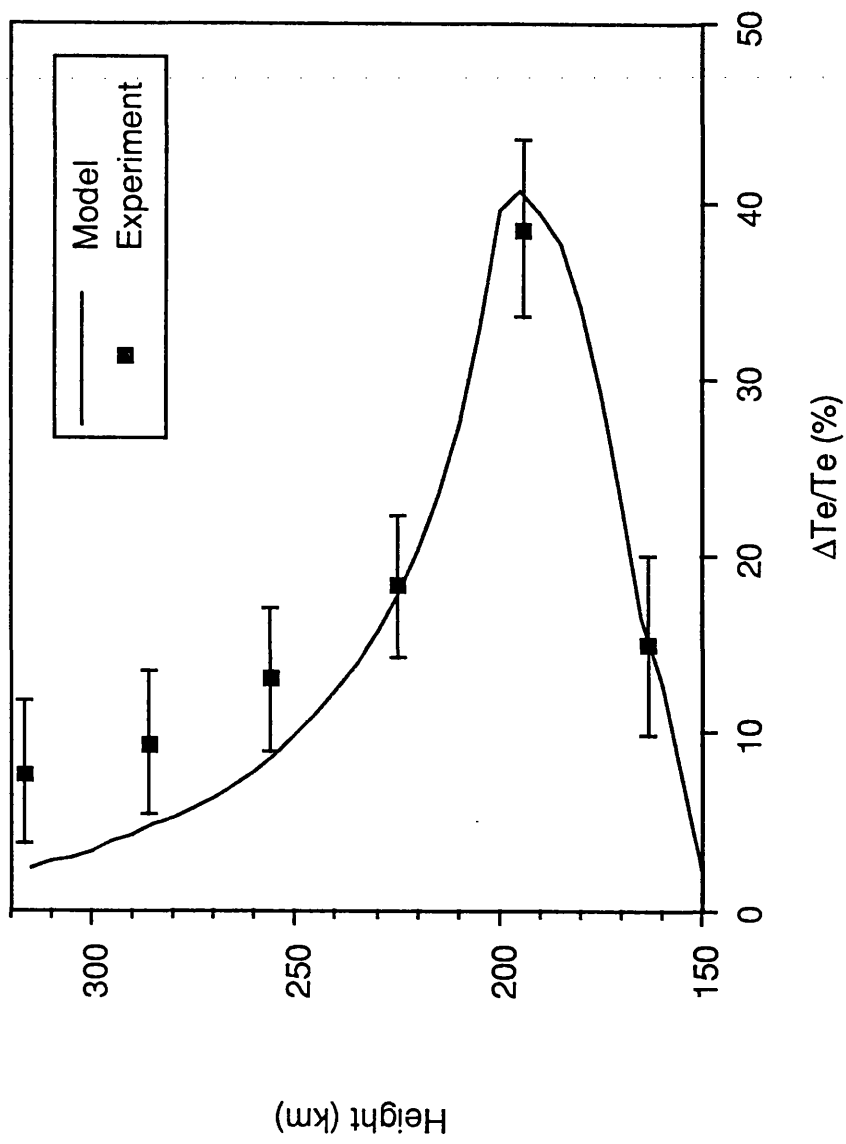


Figure 5.14. $\Delta T_e/T_e$ against height obtained from EISCAT observations together with a theoretical curve.

Chapter 5 Electron and ion temperature effects

assumed to lie at about 200 km (see Chapter 6). The experimental data points below a height of 230 km lie close to the theoretical curve. However, at heights above this altitude the theory seriously underestimates the observations. This discrepancy between the model and the experimental values may be caused by, 1) deficiencies in the ambient ionospheric parameters which are employed as starting values in the model, 2) altitude smearing of the EISCAT Tromsø data and 3) non-negligible collisional heating at altitudes below the heater reflection height. The first two of these possible causes are addressed in more detail below. The occurrence of significant collisional absorption below the heater reflection height would invalidate the assumption made by the model that the heat source is located in a narrow region in the ionosphere.

The background ionospheric parameters and expressions governing the cooling rates which have been employed in the modelling were derived from a number of sources, principally, MSIS 86, the Sheffield-UCL coupled model (Quegan *et al* 1982) and Schunk and Nagy (1978). It was reported in Chapter 3 how the model results were dependent on at least some of the input parameters, eg the density of molecular nitrogen, $[N_2]$ and the thermal conductivity.

The electron temperature derived from the ion-line spectrum obtained by the long-pulse technique is a convolution of the temperatures which occur over the width of the height gate (eg Lejeune and Lathuillere 1986), which is about 30 km during the 1987 experiment. This means that if the variations in the electron temperature are smaller than the width of the long-pulse gate then this detailed structure will be lost. At heights close to the heater interaction height the model predicts that the electron temperature will change rapidly with height (Figure 5.14) and therefore EISCAT long-pulse measurements may underestimate the temperature in this region. Evidence is presented below which suggests that this is indeed the case, and that the peak value of $\Delta T_e/T_e$ employed in the model should be higher than 40 %.

Chapter 5 Electron and ion temperature effects

During the 1987 campaign, the enhanced electron temperature was measured with an improved height resolution over that obtainable by the Tromsø site alone by employing the remote sites in an altitude scanning mode (see Section 5.3). The effective height resolution of the temperature obtained at the remote sites depends upon two criteria, 1) the accuracy of the pointing direction and 2) the size of the common volume of the remote site and Tromsø beams, a quantity which is a function of the antenna beamwidths. The pointing direction of the EISCAT remote site antenna may be determined to less than 0.02° (Rishbeth and Williams 1985) which results in a height accuracy of better than 0.5 km for F-region altitudes. The beamwidth of the remote sites in the F-region over Tromsø is approximately 5 km, therefore, it is this second factor which determines the overall height resolution. During the interval of interest (ie 1141 - 1203 UT on 26 February 1987) the scanning mode did not function entirely as planned and hence the data which were obtained were of only limited value. It should also be noted that the scanning of the remote site beams takes a finite time to scan from the highest altitude to the lowest (about 10 minutes during this experiment). Therefore, if the ambient ionospheric conditions change during this interval then this will reduce the reliability of the estimate of $\Delta T_e/T_e$ at the remote sites. There is some evidence (Figure 5.12a) to suggest that a slow change in the ambient T_e does occur during this interval, as the quasi-steady state temperature observed towards the end of the heater on period is about 100 K higher than that observed shortly after heater switch on.

The change in the electron temperature measured at both Tromsø and the remote sites is plotted in Figure 5.15, along with the best-fit theoretical curve derived below. The peak value of ΔT_e exhibited by the remote site data is close to 55 % of the ambient value, although this occurs at an altitude about 10 km below the initial heater reflection height (see Chapter 6). It is clear that the heater reflection height will change if the plasma electron density is changed. Observations of changes in the electron density are presented in Chapter 6 along with measurements of the change in reflection height of low power HF waves reflected in the modified region. The larger peak value of $\Delta T_e/T_e$ observed at the remote sites, compared to

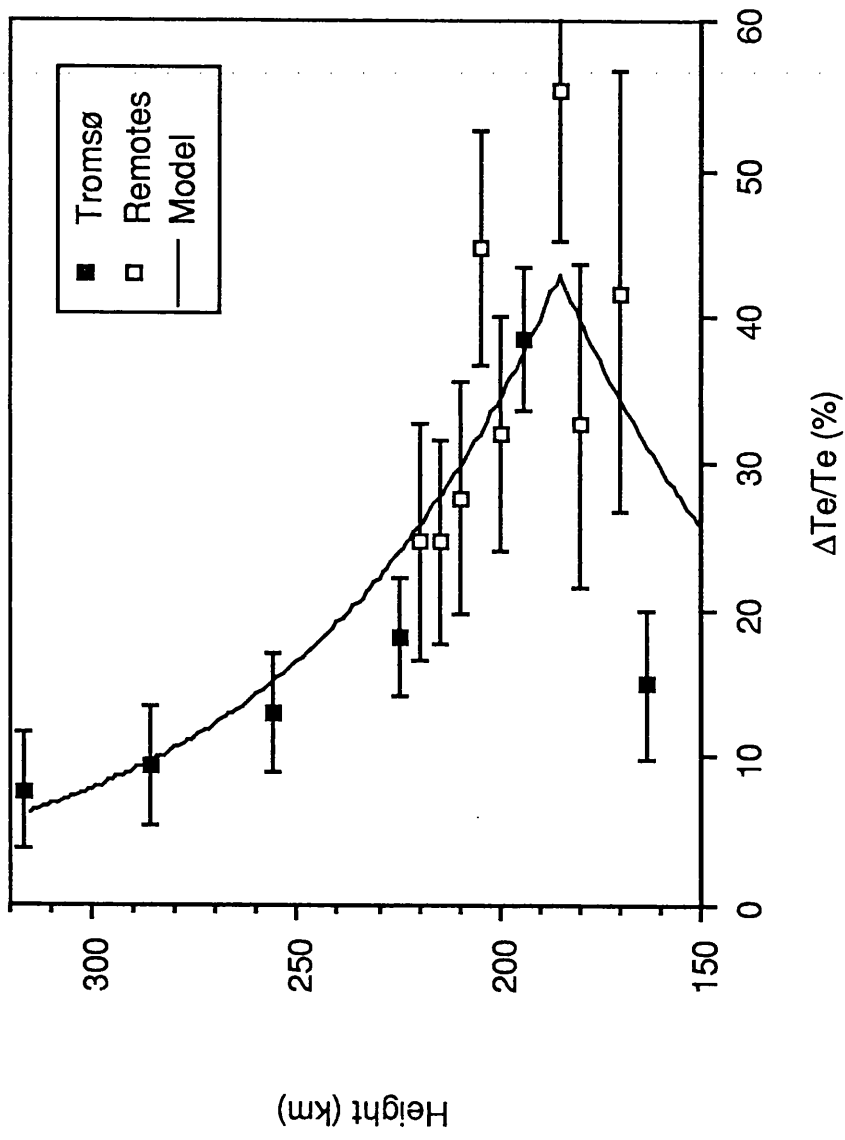


Figure 5.15. $\Delta Te/Te$ against height obtained from EISCAT measurements. The solid curve is the exponential of the form of Equation 3.7 which best fits the EISCAT data.

Tromsø, lends some credence to the notion that Tromsø underestimates the electron temperature change at heights close to the interaction region due to averaging within the long-pulse.

If the stationary model discussed in Chapter 3 is adopted, then the data may be fitted by a single exponential of the form of Equation 3.7. This is a reasonable model, provided that the displacement of the heater reflection height during heating is less than the temperature scale length, L_T . During this experiment, the value of L_T at 185 km lies between 24 km (model 1, Gurevich 1978) and 34 km (model 2, Schunk and Nagy 1978) prior to heating and between 23 km (model 1) and 31 km (model 2) after heating. The displacement of the heater reflection height is less than 10 km (Chapter 6) and therefore the use of the stationary model is satisfactory. If $\log_e(\Delta T_e/T_e)$ versus altitude separation from the peak in $\Delta T_e/T_e$ is plotted, then the least-squares best-fit straight line in Figure 5.16 is obtained. The best fit is obtained when the peak in $\Delta T_e/T_e$ lies at about 185 km. The value of L_T , derived from $(-1/\text{gradient})$, is 68 ± 10 km. This value is considerably higher than that calculated by either thermal conductivity model. $L_T = (K_e / \delta \nu)^{1/2}$, where K_e is the thermal conductivity, δ is the fractional energy loss per collision and ν is the collision frequency. Of these parameters, K_e is known to about 20 % (Schunk and Nagy 1978), and ν reasonably well. The value of δ is not well known, and the discrepancy between the modelled and experimental values of L_T could be explained by reducing δ by 50 %. The peak value of ΔT_e , calculated from the intercept of the straight line, is approximately 43 % of the ambient electron temperature.

5.7 Power dependence of $\Delta T_e/T_e$

During the 1987 campaign a number of heater power stepping experiments were conducted. The results of the experiments where a significant value of $\Delta T_e/T_e$ ($> 10\%$) was observed with full power heating are presented in Figure 5.17. Examination of this figure reveals that the change in electron temperature is very clearly dependent upon the heater

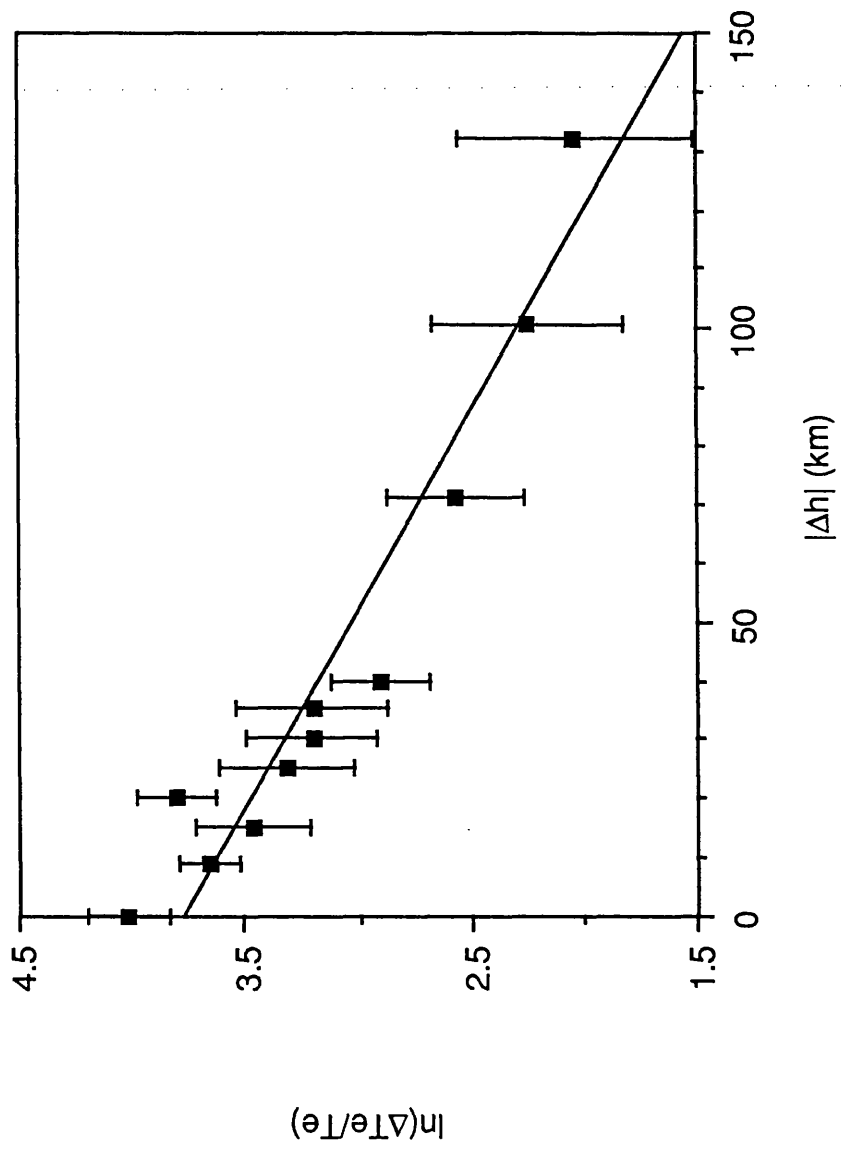


Figure 5.16. A graph of $\ln(\Delta T_e/T_e)$ against the separation from the heater reflection height at 1141 UT on 26 February 1987

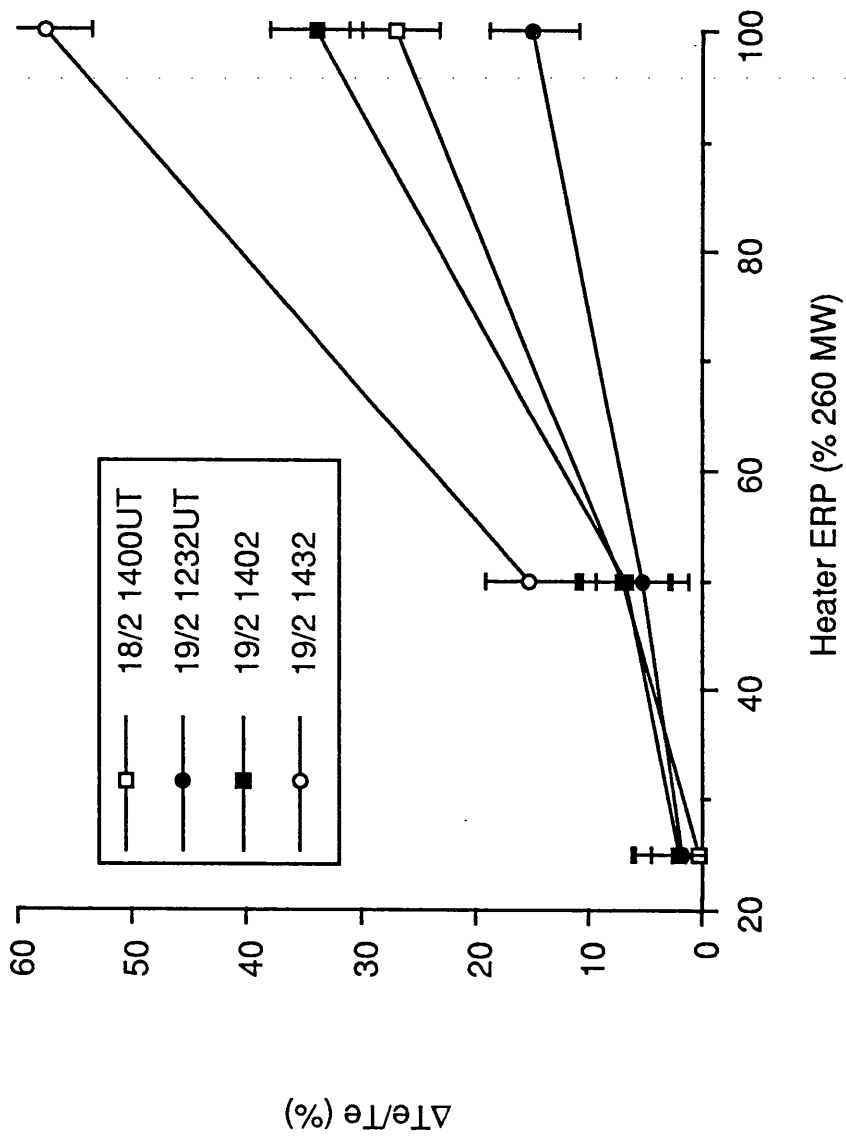


Figure 5.17 Graph showing the relationship between electron temperature enhancement and heater ERP for four experiments

power employed. If we assume that $\Delta T_e/T_e \propto (\text{ERP})^n$ then by plotting the natural log of $\Delta T_e/T_e$ against the heater ERP (in dB) we would expect the data to lie on a straight line. The data from the various experiments have been averaged and the straight line of Figure 5.18 obtained. The gradient of this line is ~ 0.53 , which after conversion from dB to nepers (ie multiplying by a factor of $10 / 2.3$) implies that for these periods the value of $\Delta T_e/T_e$ depends very nearly upon the $(\text{ERP})^2$. This result may be contrasted with the behaviour during the experiment on 26 February described Section 5.3 where the peak value of $\Delta T_e/T_e$ during 50 % ERP is slightly greater than half that of $\Delta T_e/T_e$ during the full power heater on (ie $n \sim 1$).

From Equation 3.3 we have that $\Delta T_e/T_e \propto Q$, the heat input per unit volume from the EM wave. Q is composed of a contribution due to deviative absorption, Q_d , and a contribution due to anomalous absorption, Q_a . Q_d is proportional to the heater ERP (Chapter 2). The dependence of Q_a on heater power is more complicated due to the existence of electric field thresholds and the nonlinear growth and stabilisation of the FAIs which cause the anomalous absorption of the heater wave (Robinson 1989; see Chapters 3 and 7). However, an approximate value for Q_a (Perkins *et al* 1974) is that it is proportional to $(E_0/E_t)^4$, where $E_0^2 \propto$ heater ERP, and E_t is the threshold electric field required to excite a parametric instability. In experiments at Tromsø, Stubbe *et al* (1982a) have reported that the ERP dependence of anomalous absorption suffered by the heater wave is highly dependent upon the ionospheric variability. Only during periods of fast ionospheric fading, ie when changes on the scale of the order of one diagnostic wavelength occur on a shorter time scale than the resonance instability (Chapter 3) growth time, is there a positive correlation between anomalous absorption and heater ERP.

If we interpret the experimental results in terms of the ERP dependencies, then it is probable that during the intervals on the 18 and 19 February 1987 that the total heat input to the ionosphere from the heater wave was dominated by anomalous processes. On 26

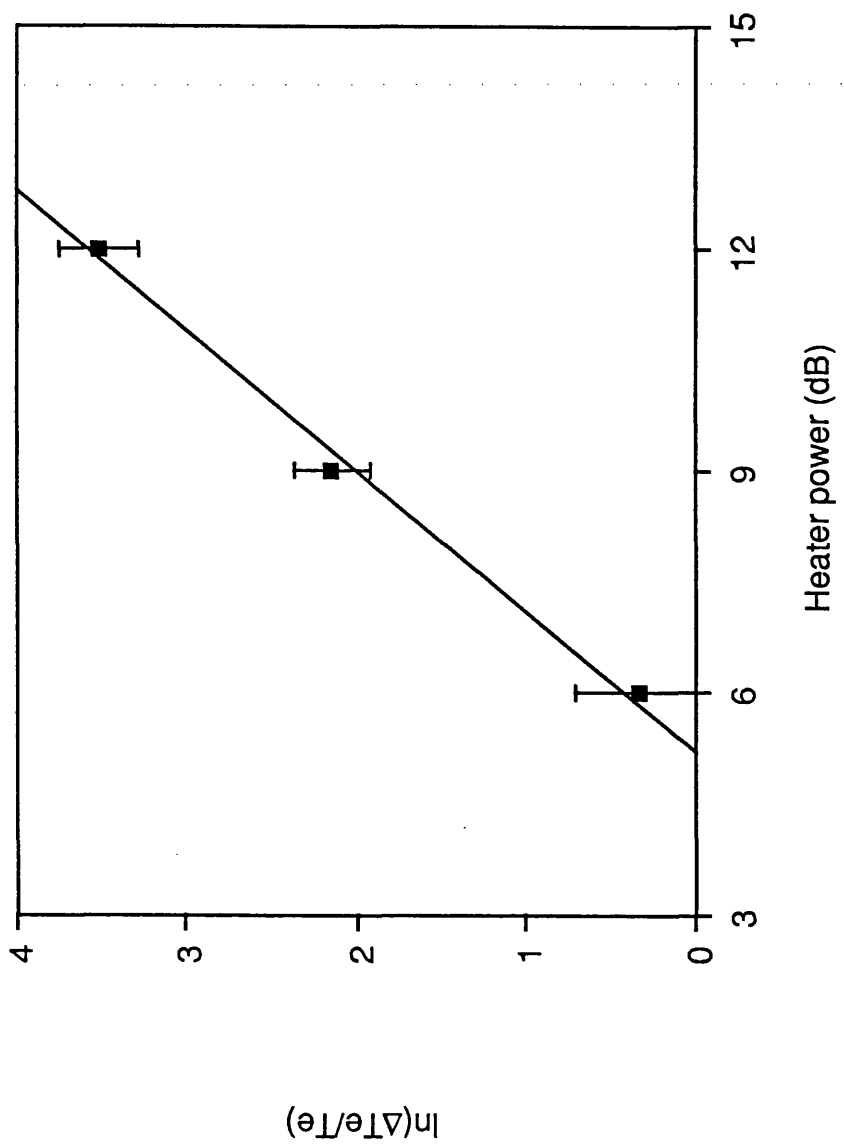


Figure 5.18 Graph showing the relationship between $\ln(\Delta T_e/T_e)$ and heater ERP (in dB).

February, the heating appears to be dominated by collisional absorption. Measurements of the anomalous absorption by means of low power HF diagnostics was made difficult during the interval on 26 February due to the of the alignment of the heater beam. The mid-point of the diagnostic propagation path lies outside of the 3 dB contour of the heater which may make comparison with the other periods difficult. However, the values of diagnostic absorption measured during the intervals are given in Table 5.3. It is clear from the table that the level of anomalous absorption during the intervals on the 18 and 19 February is higher than that observed on the 26 February. The lower level of anomalous absorption supports the interpretation of the ERP dependency of $\Delta T_e/T_e$, although it may be a consequence of the beam geometry.

5.8 Electron temperature measurements at Arecibo

In this section observations of the electron temperatures obtained during a heating campaign held at Arecibo during May 1989 are reported. These measurements are also of particular relevance to the HF propagation experiment described in Chapter 7.

The experiment reported here commenced on 16 May 1989 at 1630 Atlantic Standard Time (AST = UT - 4) and finished at 1900 AST. It is discussed in detail in Chapter 7, so only a brief description is included here. From 1700 AST onwards, the heater switching cycle consisted of 5 minutes heater on at full power (ERP = 80 MW), followed by 10 minutes off. During this interval, the heater wave was reflected in the F-region at an altitude of, typically, 260 km (Chapter 7), although the exact height varied with time. The 430 MHz incoherent scatter radar recorded ion-line spectra from heights of 146 km through to 682 km with a height resolution of 38 km. An integration time of about 15 s was employed but the resultant time resolution was about 30 s, because in addition to the ion-line spectra, the radar also made power profile measurements (see Chapter 7).

Date	Time (UT)	Diagnostic Frequency (MHz)	
		3.65	4.2
18/02/87	1400	3.6 dB	- dB
19/02/87	1232	5.6	13.6
	1402	5.7	6.3
	1432	2.9	5.7
26/02/87	1141	2.0	2.3

Table 5.3 Anomalous absorption measured on two HF diagnostic frequencies during several heating experiments. No value was obtained for the 4.2 MHz diagnostic on the 18 February 1987 as the wave had penetrated the F-region peak.

Chapter 5 Electron and ion temperature effects

The electron temperatures derived from the ion-line spectra have been averaged during the periods when the heater was on, and those when the heater was off for heights close to the heater reflection height. It should be noted that at least some of the ion-line spectra are likely to have been contaminated by the ion-line overshoot as this was observed in the power profile measurements. Unfortunately, the raw spectra are not available for examination, and therefore it is assumed that the derived temperatures have not been significantly distorted by the presence of the ion-line overshoot. The change in the electron temperature due to heating, normalised to the ambient temperature, has then been calculated for each heater switch on (Table 5.4). The background temperature has been derived from a linear interpolation of the temperatures observed before and after heater on. The electron temperature was not enhanced each time that the heater was switched on. However, on a few occasions during this period the electron temperature has been enhanced by as much as 600 K although, typically, the increase is much less than this. Enhancements of a similar size have been reported previously for *nighttime* experiments at Arecibo (eg Mantas *et al* 1981; Djuth *et al* 1987b) and have also been observed at Tromsø (see above). The relatively low amount of F-region heating during most of this period is probably due to the high D-region absorption which was prevalent at this time (Chapter 7). The large increases in the electron temperature may be explained either as a deformation due to the occurrence of the ion-line overshoot, or by a temporary lowering in the D-region absorption, and hence to higher HF energy flux in the F-region. However, there is little evidence for the latter effect in the diagnostic data presented in Chapter 7, so that it is likely that the temperatures suffer some distortion due to the presence of the ion-line overshoot. The extent of the unreliability of the temperatures cannot be assessed.

The value of $\Delta T_e/T_e$ has been plotted as a height profile for some of the intervals where a strong heating effect has been observed (see Figure 5.19). The altitude extent of the enhanced region is much less than that observed at Tromsø. It has been suggested (eg Bernhardt and Duncan 1982) that the temperature is enhanced along the magnetic field line.

TIME (AST)	HEIGHT (km)								
	146	184	222	261	299	337	376	414	452
1700	-1.0	0.2	29.4	12.2	2.0	-0.6	-0.4	0.2	0.1
1715	2.7	9.9	22.0	9.6	-1.4	-0.6	0.1	-0.2	1.3
1730	1.8	5.1	1.7	-1.2	0.1	-0.5	-0.8	0.1	0.2
1745	-6.9	-11.3	0.5	10.2	2.8	1.6	0.5	0.4	0.6
1800	-0.1	-1.0	9.0	12.8	5.6	0.6	-0.2	0.2	-0.6
1815	0.1	-3.0	-0.4	0.1	1.0	-0.3	0.2	-0.2	0.5
1830	1.3	2.8	0.9	-0.9	-0.6	-0.2	0.8	1.3	0.1
1845	0.4	3.0	2.8	11.9	5.6	1.1	0.5	0.7	-0.5

Table 5.4 Values of $\Delta T_e/T_e$ (in %) during the heating on 16 May 1989. The errors are about 1 % except at 184, 222 and 261 km where the errors are as high as 11 %.

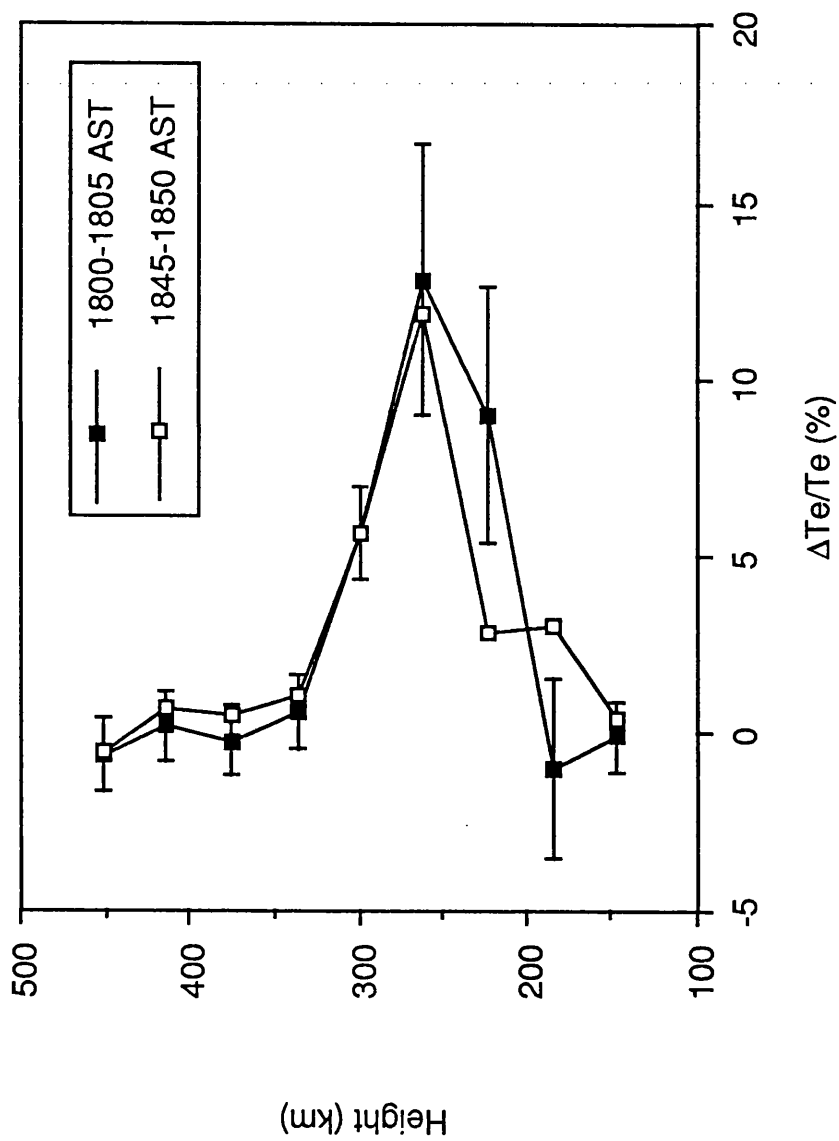


Figure 5.19 $\Delta T_e / T_e$ against height, obtained from 430 MHz radar observations at Arecibo, 16 May 1989.

The different height extent might then be explained in terms of the different magnetic field geometries at Arecibo and Tromsø. At Tromsø, the EISCAT beam is directed along the magnetic field, whereas at Arecibo the 430 MHz radar beam cuts several different field lines. The scale length of the enhanced region in the direction parallel to the field may be given by,

$$L_{T\parallel} = L_{T(\text{radar})} / \cos \theta \quad (5.3)$$

where $L_{T(\text{radar})}$ is the scale length measured by the radar, and θ is the angle between the geomagnetic field line and the radar beam. This results in an $L_{T\parallel}$ at Arecibo of about 62 km, which compares favourably with the value of 68 km observed at Tromsø (see Section 5.6).

5.9 Chapter Summary

In this chapter observations of the electron temperature indicate enhancements over a wide range of heights when the ionosphere is illuminated by high power radio waves. A peak enhancement of some 50 % of the ambient value has been measured in the electron temperature during daytime experiments at Tromsø. The temporal evolution and spatial structure of the modified electron temperature has been compared with the results of a theoretical model of the heating process. Good agreement between theory and experiment is noted for the temporal development of the temperature enhancement. While there is good agreement between the non-stationary model and experiment for the spatial structure of the temperature enhancement at heights below about 230 km, above this the model consistently underestimates the value of $\Delta T_e/T_e$. Possible explanations for this discrepancy have been discussed. The value of L_T , estimated from fitting EISCAT data to the stationary model, has been found to be about double that predicted by theory. This has been explained by a low electron fractional energy loss per collision with the neutral particles.

Chapter 5 Electron and ion temperature effects

The observation of electron temperature oscillations have been explained in terms of the formation of thermal striations as a consequence of the excitation of the thermal self-focussing instability.

No evidence of significant heater-induced changes in the ion temperature was found. However, EISCAT is unable to measure the ion temperature to better than about 50 K so any smaller changes would remain undetected.

Chapter 6 Electron density effects

6.1 Introduction

Observations of the enhanced electron temperatures resulting from the action of high power radio waves on the ionosphere have been presented in Chapters 2 and 5. This enhancement of the electron temperature results in a change in the chemical balance and diffusion properties of the ionosphere in the vicinity of the temperature enhancement. This in turn leads to a change in the electron density.

In this chapter the observed changes in the electron density due to the interaction of high power radio waves with the ionospheric plasma are presented for experiments performed at Tromsø. The heater induced changes in the electron density have been observed by the EISCAT radar and by measuring the change in the phase path of HF test waves propagating through the modified region. The observations obtained by these two experimental methods are compared with the ionospheric response predicted by the theoretical model described in Chapter 3.

6.2 General characteristics of incoherent scatter measurements

The returned signal power, P_s measured by an incoherent scatter radar is related to the local plasma electron density, N by the radar equation (eg Evans 1969),

$$P_s = \frac{C_{sys} (P_t \tau)}{R^2} \frac{N \sigma_e}{(1 + \alpha^2 + T_e/T_i) (1 + \alpha^2)} \approx \frac{C_{sys} (P_t \tau)}{R^2} \frac{N \sigma_e}{(1 + T_e/T_i)} \quad (6.1a, b)$$

where, T_e is electron temperature, T_i is ion temperature, $\alpha = 4\pi \lambda_d / \lambda$, C_{sys} is a constant related to the radar system, P_t is the transmitted power, τ is the transmitted pulse width, σ_e is

the electron cross-section, R is the range from the radar to the scattering volume, λ_d is the Debye length and λ the radar wavelength. For the EISCAT UHF radar during typical daytime conditions in the F-region above Tromsø (and therefore for the heating experiments reported in this Chapter), $\alpha \ll 1$ and, therefore, the approximation, Equation 6.1b is valid. It is possible that, due to the heater-induced excitation of field aligned irregularities, a proportion of the received power is a result of coherent rather than incoherent scatter. If this is the case, then the electron density estimated from Equation 6.1 may be in error, especially at altitudes close to the heater reflection height.

In order to determine the electron density as a function of height, the range corrected EISCAT power profile must be corrected for the ratio T_e/T_i (Equation 6.1b), the value of which can be derived from long-pulse (ie spectral) data (see Chapters 4 and 5). However, in general for F-region studies, the long-pulse data are obtained at a much poorer height resolution than the power profile data. This means that the temperature data must be interpolated in order to correct the power profile at heights between the long-pulse gates. In addition, the range of heights over which the power profile and long-pulse measurements are measured are not necessarily the same. Therefore, on occasions, either the temperature or power profile data may need to be extrapolated to obtain density values at altitudes outside these ranges. In the case of times of heater off during the 1985 campaign and for the entire 1987 campaign, the temperature data have been linearly interpolated when correcting the power profile for temperature. For the periods of heater on during the 1985 campaign the value of $\Delta T_e/T_e$ is assumed to fall off exponentially from a peak value (see Chapter 5) and interpolation is based on this exponential fall. The values of electron temperature and ion temperature are interpolated separately and then combined to produce the ratio, T_e/T_i .

In practice, the value of C_{sys} is difficult to obtain directly so the EISCAT power profile measurements are usually scaled by equating the peak power in the F-region with the

Chapter 6. Electron density effects

maximum density derived from the value of foF2 either measured by an ionosonde, or by observations of the frequency offset of the EISCAT plasma-line (Kirkwood *et al* 1986). During heating experiments, where the ion-line overshoot (Chapter 2; see Figure 6.1) is observed an alternative method of scaling the power profile exists. The ion-line overshoot occurs close to the heater reflection height, so that the ambient power (ie without the overshoot) at that height corresponds to the electron density, and therefore the plasma frequency, which matches the heater frequency. Comparison of electron density measurements obtained during heater on with those obtained during heater off is complicated further by a reduction in the EISCAT transmitted power when the heater is turned on. For example, during the 1987 campaign a heater effective radiated power (ERP) of 240 MW resulted in a reduction of the EISCAT transmitted power by approximately 8 % of the ambient value.

A power profile obtained immediately after heater switch on on 17 March 1985 at Tromsø is illustrated in Figure 6.1. This profile has been integrated for a period of 10 s and has a height resolution of approximately 4.5 km. The large peak in power at 205 km is the heater induced ion-line overshoot. The magnitude of this peak often exceeds the power observed at adjacent heights by an order of magnitude or more. During the 1985 campaign the ion-line overshoot was only observed during the 10 s integration period immediately after heater switch on. However, during the 1987 campaign the ion-line overshoot often occurred at other times when the heater was switched on. It should also be noted that the data in Figure 6.1 are not corrected for temperature and exhibit a high level of fluctuation with height. In order to improve the signal to noise ratio the data have been further averaged by one of several methods, these being similar to those described in Chapter 5 for the temperature measurements. It should be noted that care must be exercised to ensure that power profile data containing the ion-line overshoot are excluded from the averaging process.

A typical heating experiment was performed at Tromsø on 17 March 1985 between 1200 and 1234 UT. After this interval an error occurred in the power profile program and therefore

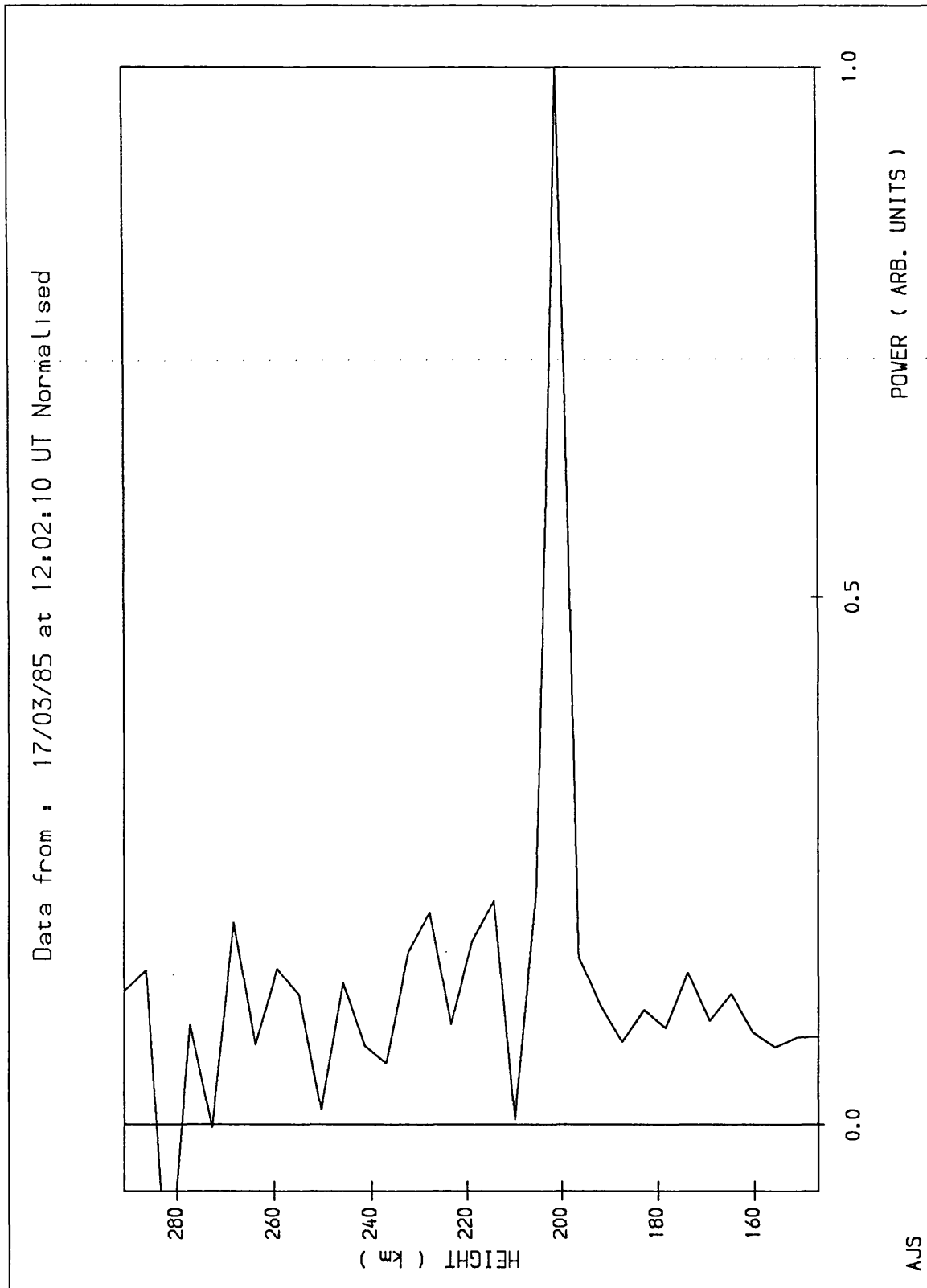


Figure 6.1 EISCAT power profile illustrating the ion-line 'overshoot'.

Chapter 6. Electron density effects

the electron density could not be determined. During this period the heater transmitted vertically with an ERP of 240 MW, at a frequency of 4.544 MHz and with O-mode polarisation. A switching cycle of 2 minutes on followed by 2 minutes off was adopted. The electron and ion temperature data recorded during this interval were presented in Chapter 5. The time variation of the range corrected backscatter power at several heights during this period is depicted in Figure 6.2. The data have been smoothed by the application of a 30 s running mean. The general level of signal variation associated with the power profile measurements even with a 30 s running mean is clearly evident in this figure. The drop in received power at around 1222 UT is due to a problem with the EISCAT receiver and is not caused by heating effects in the ionosphere.

The electron density height profiles averaged over the last minute of each heater off and the first and second minutes of each heater on period during this interval, except data from around 1222 UT have not been included, are reproduced in Figure 6.3. The error bar depicted in this figure was derived from the statistical errors arising from the averaging process, but does not include the errors due to the temperature correction. The errors tend to increase with increasing altitude. No ionograms were available during this period so the value of C_{sys} has been derived, and the power profile scaled, from the electron density at the heater reflection height, which is assumed to be located at the same height as the ion-line overshoot. Observations of the ion-line overshoot performed during this period indicate that the heater wave was reflected at an average height of close to 205 km, well below the F-region peak. It is evident from Figure 6.3 that during the first minute after heater switch on, the electron density was depleted by some 10 % of the ambient (ie unheated) value in the vicinity of the heater reflection height, although the magnitude of this depletion is comparable with the errors. By the second minute after heater switch on, the electron density has partially recovered to the ambient value. These results are discussed in more detail in Section 6.4.2.

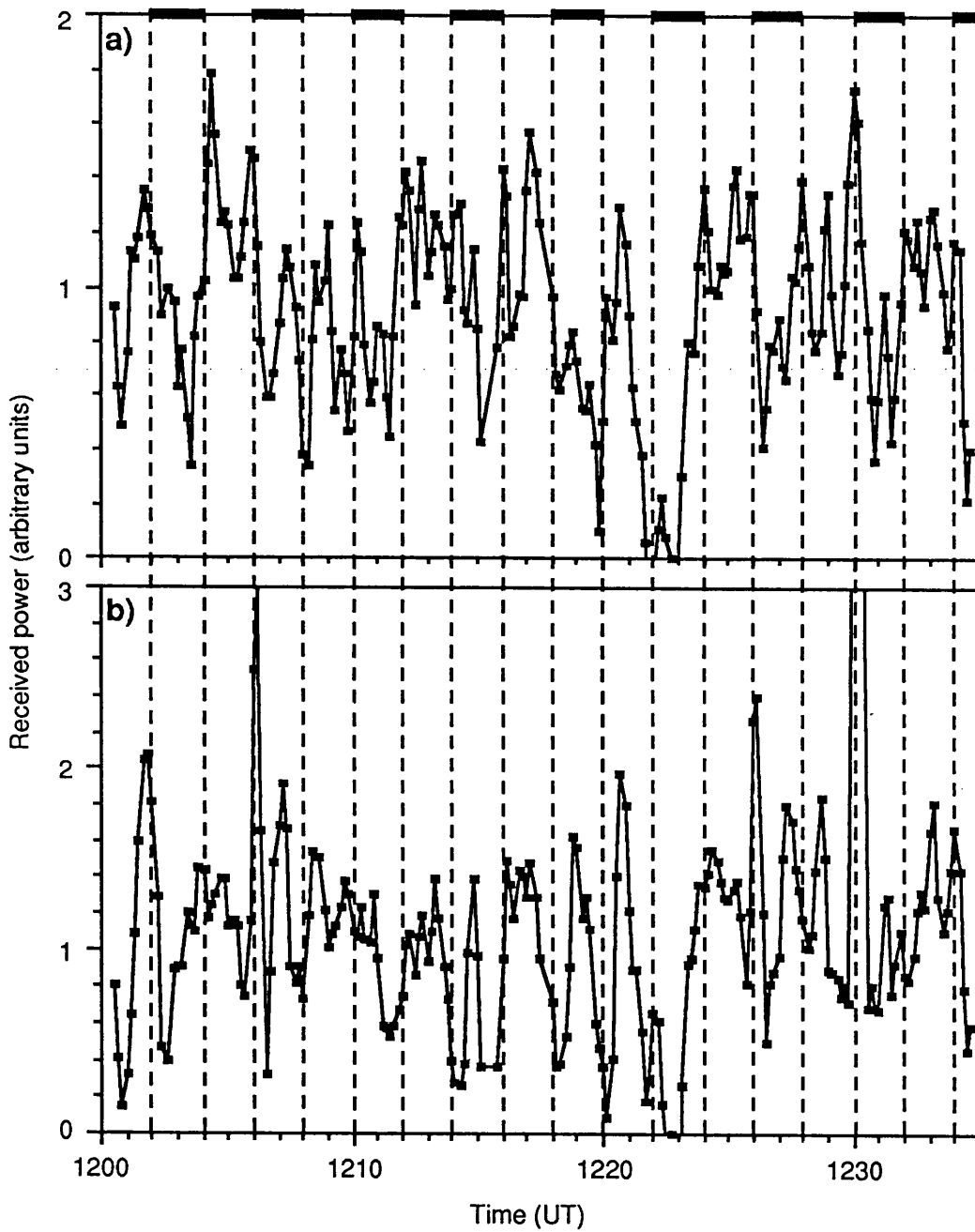


Figure 6.2 EISCAT backscattered power measured at altitudes of a) 196 km and b) 205 km on 17 March 1985. The bars indicate heater on periods.

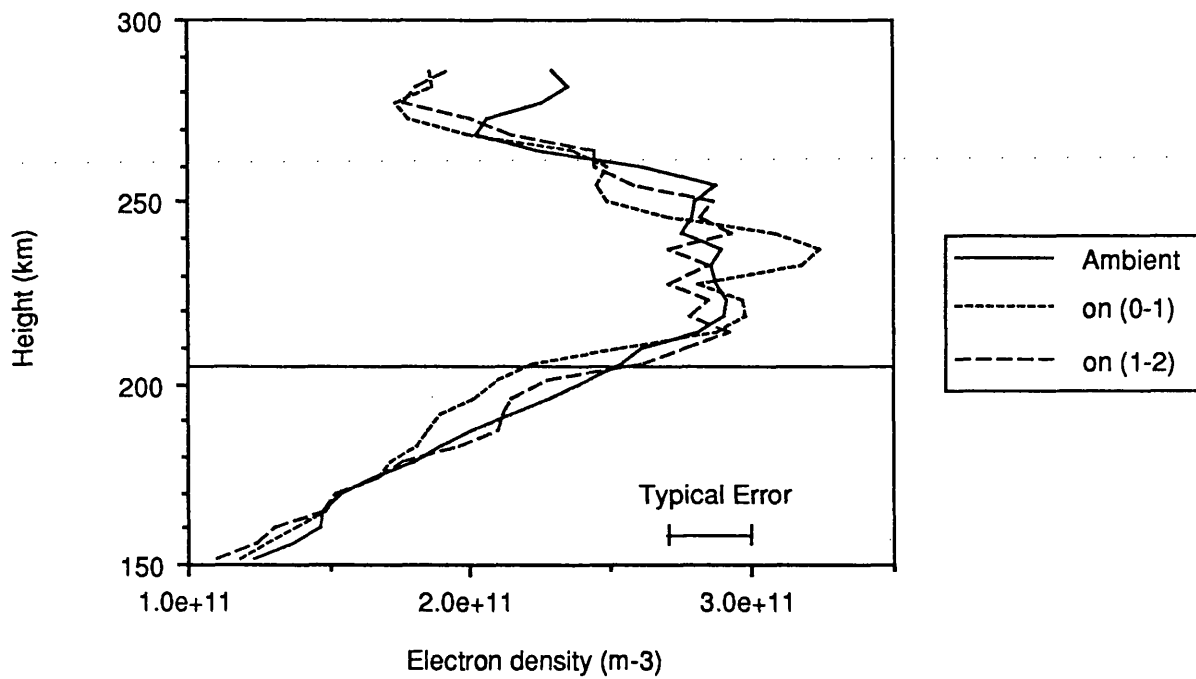


Figure 6.3 Electron density profiles measured by EISCAT on 17 March 1985, between 1200 and 1234 UT. The data have been averaged over 7 heater cycles. The solid line represents the initial heater reflection height derived from the ion-line overshoot.

6.3 General characteristics of test-wave phase and Doppler measurements

The HF diagnostic system employed during the campaigns at Tromsø has been described in detail in Chapter 4, and previous observations of the phase changes measured during heating at Tromsø have been discussed in Chapter 2. Observations of heater-induced Doppler shifts of test waves during similar experiments in the Soviet Union have also been presented in Chapter 2.

The phase path of an HF wave propagating via the ionosphere is dependent upon the refractive index of the ionospheric plasma. The refractive index, which can be expressed in terms of the Appleton-Hartree equation (Appleton 1932; Equation 3.15) is a function of the electron density. Therefore, a change in the electron density will modify the phase path of an HF diagnostic wave. The change in phase measured on a 4.7 MHz X-mode test wave during the experiment on the 17 March 1985, described in the previous section, is depicted in Figure 6.4. Any background trends in the phase have been removed by a) setting the phase to zero at the instant of each heater switch on, and b) subtracting the linear change in ambient phase between successive switch on times from the measured phase values. Given the stability of the oscillators in the diagnostic transmitters and receivers and assuming no aliasing occurs then the resulting error in the measured phase is only a few multiples of 2π radians. However, ionospheric phenomena such as gravity waves can lead to a variation in the phase considerably more than this.

The rate of change of phase is related to the Doppler shift in the wave frequency, Δf by the following expression (eg Davies 1969),

$$\Delta f = - \frac{1}{\lambda} \frac{dP}{dt} \quad (6.2)$$

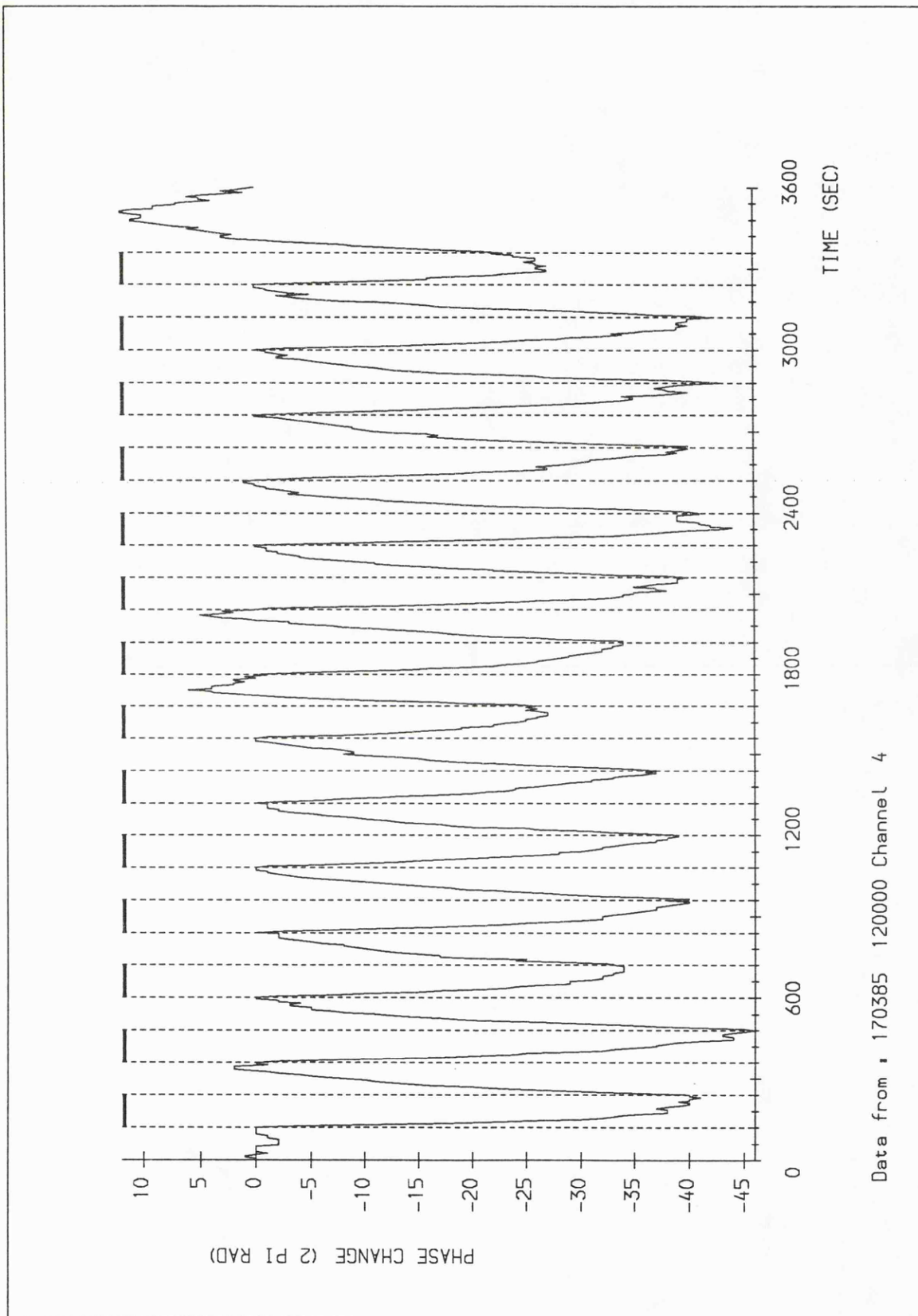


Figure 6.4 Phase changes of 4.7 MHz X-mode diagnostic signal during heating (ERP=260 MW, $f = 4.544$ MHz) on 17 March 1985, 1200-1300 UT. The bars indicate heater on periods.

Chapter 6. Electron density effects

where, λ is the wavelength of the radio wave, $P = \lambda \phi / 2\pi$, and ϕ is the measured phase.

From Equation 6.2 it is evident that the change in phase may also be represented by plotting a time series of the frequency spectrum of the diagnostic signal (ie a spectrogram). The spectrogram obtained for the 4.7 MHz X-mode test wave discussed above is illustrated in Figure 6.5. An FFT has been applied to the diagnostic data at successive intervals of 20 s, which leads to a frequency resolution of 0.05 Hz. Only frequency components which exhibit more than 50 % of the peak power in any one integration period have been plotted.

Examination of Figure 6.5 reveals that when the heater is switched on the diagnostic wave undergoes a sudden reduction in frequency. The frequency gradually returns to close to the ambient value after about 40-60 s. When the heater is switched off, the frequency suddenly increases, and then slowly returns to the ambient value. This behaviour can be interpreted in terms of a electron density depletion (eg Vas'kov *et al* 1981; Jones *et al* 1982; Gurevich and Migulin 1982; Migulin and Gurevich 1985). These authors reasoned that the initial reduction in frequency is symptomatic of an increase in the reflection height of the test-wave (although see below). As the transmitted frequency of the wave has not changed then the wave frequency matching condition must remain the same (ie the wave reflects where $N_e = f^2 / 81$, where f is the wave frequency), and therefore the electron density must be changing. In order for the wave reflection height to go upwards the density must have been reduced. Qualitatively, this result is broadly consistent with the EISCAT observations presented in Section 6.2. A comparison of the change in electron density deduced from the EISCAT and diagnostic phase measurements is presented in the following section.

It is useful to note that a change in the phase path (or alternatively a Doppler frequency shift) can be caused by either a change of real distance and/or a change in refractive index. For linear electron density profiles, Davies (1969) has $\Delta\phi \propto f$ for the case of a change in real distance, while for small changes in the refractive index, $\Delta\phi \propto f^{-1}$. Where $\Delta\phi$ is the change in

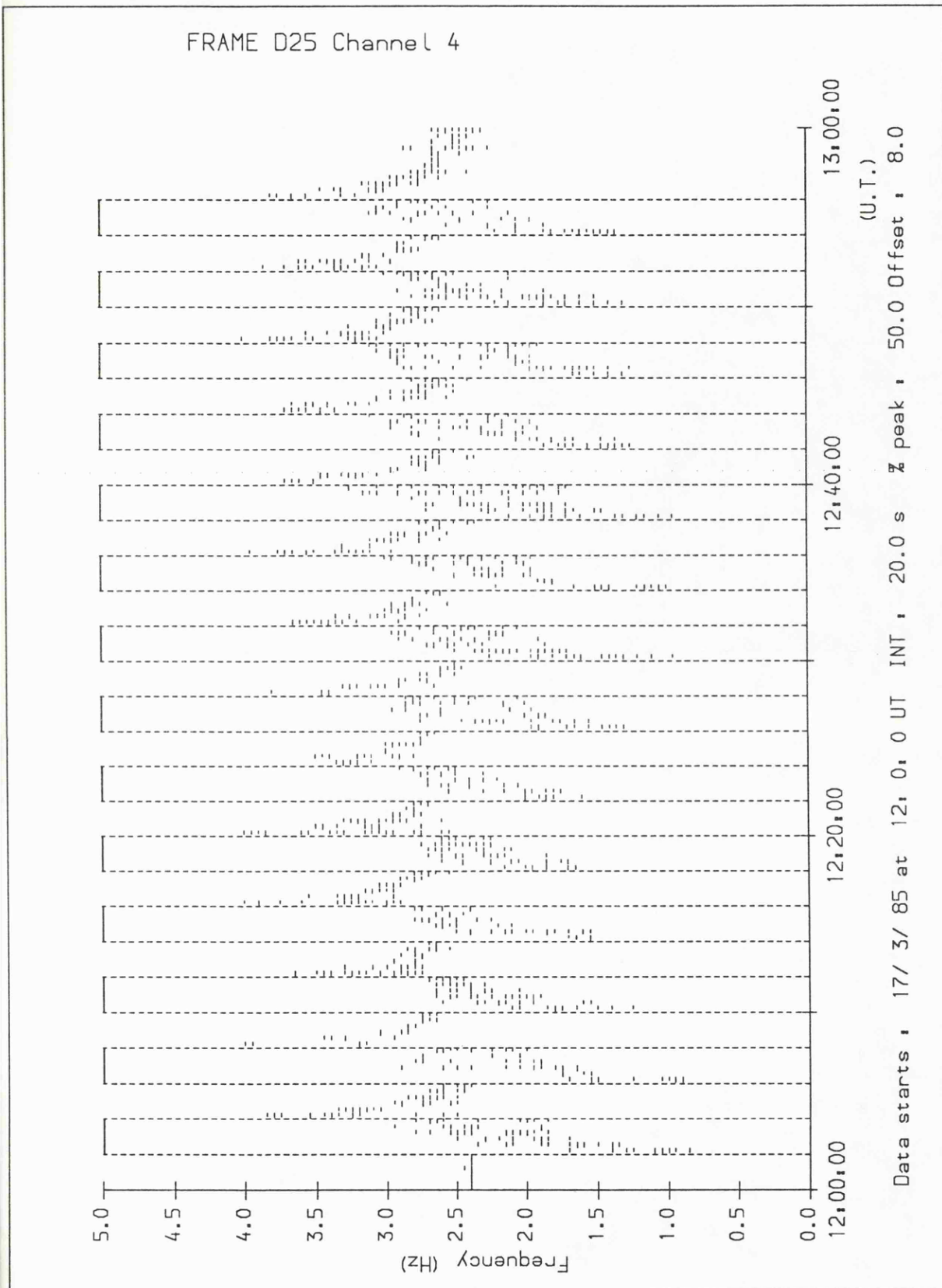


Figure 6.5 Spectrogram for same diagnostic frequency and interval as Figure 6.4. The bars indicate heater on periods.

phase and f is the wave frequency. Therefore, by making measurements on several neighbouring frequencies it may be possible to deduce which mechanism is the primary cause of the observed change in phase.

6.4 Spatial structure of the heater-induced change in the electron density

6.4.1 Experiment of 23 March 1985

The heater cycle employed during the experiment performed between 0946 and 1030 UT on 23 March 1985 has been described in detail in Section 5.3. To summarise, a switching cycle of 4 minutes on, 4 minutes off was adopted, with an ERP of 260 MW and O-mode polarisation. The electron density profile measured by EISCAT representing conditions between 2 and 4 minutes after the heater was switched off is illustrated in Figure 6.6. This profile has been obtained by superposing the data observed during each heater off during the experimental period and then averaging. It has been assumed (with some justification - see Table 6.4 and Figure 6.13) that the electron density has completely recovered from heating two minutes after heater switch off. The data have been smoothed in height by a 13 km (ie 3 height gate) running mean. The error bars depicted in Figure 6.6 have been derived from the statistical errors associated with averaging the data. No ionograms were available during this experiment and therefore the profile has been scaled by assuming that the heater reflection height coincided with the ion-line overshoot (Section 6.2). As might be expected during a pre-noon interval where the ambient electron density was increasing, the heater reflection height decreased slightly during this period with an average height of 192 ± 2 km. The F-region peak lay at around 250 km, so that the heater interaction height was well below this.

The averaged electron density profiles observed during heater on (0-2 minutes and 2-4 minutes after switch on) are plotted together with the ambient profile in Figure 6.7a. The error

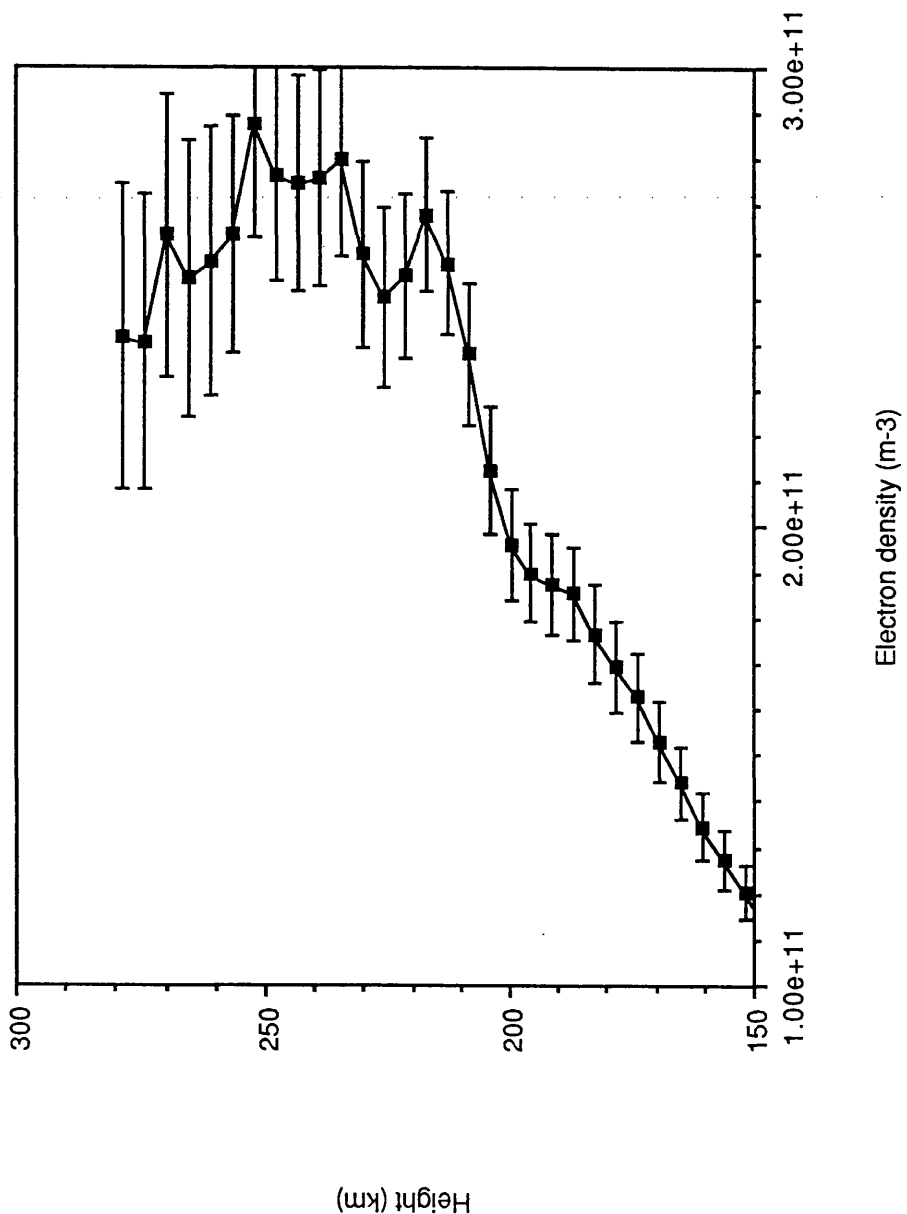


Figure 6.6 Ambient electron density measured by EISCAT on 23 March 1985 between 0946 - 1030 UT (averaged over six heater cycles)

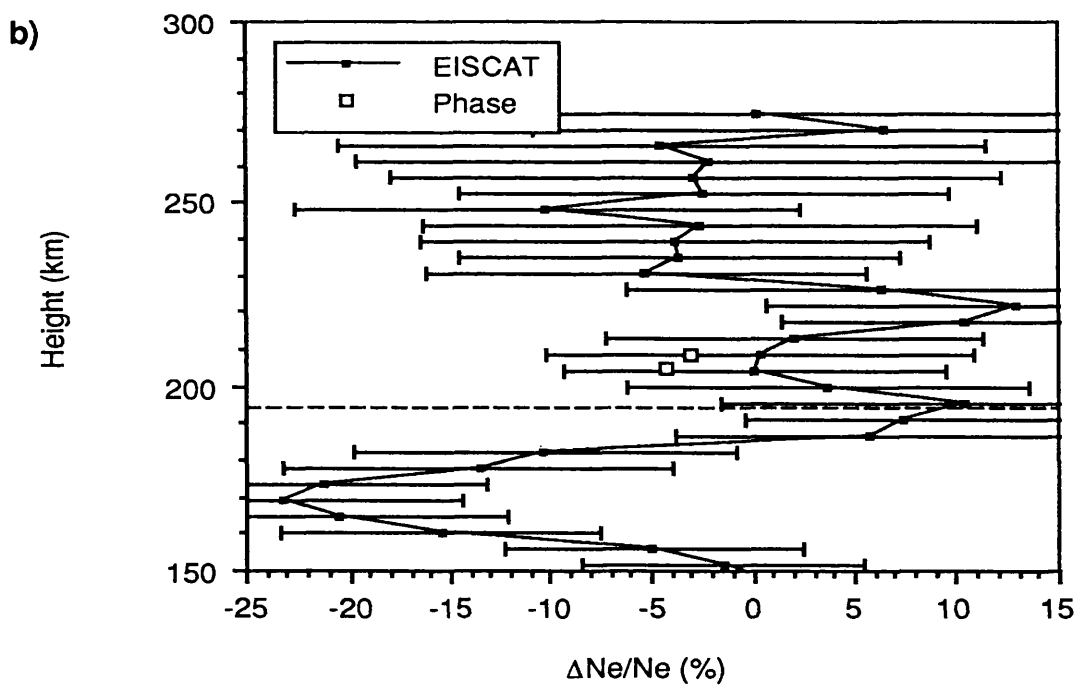
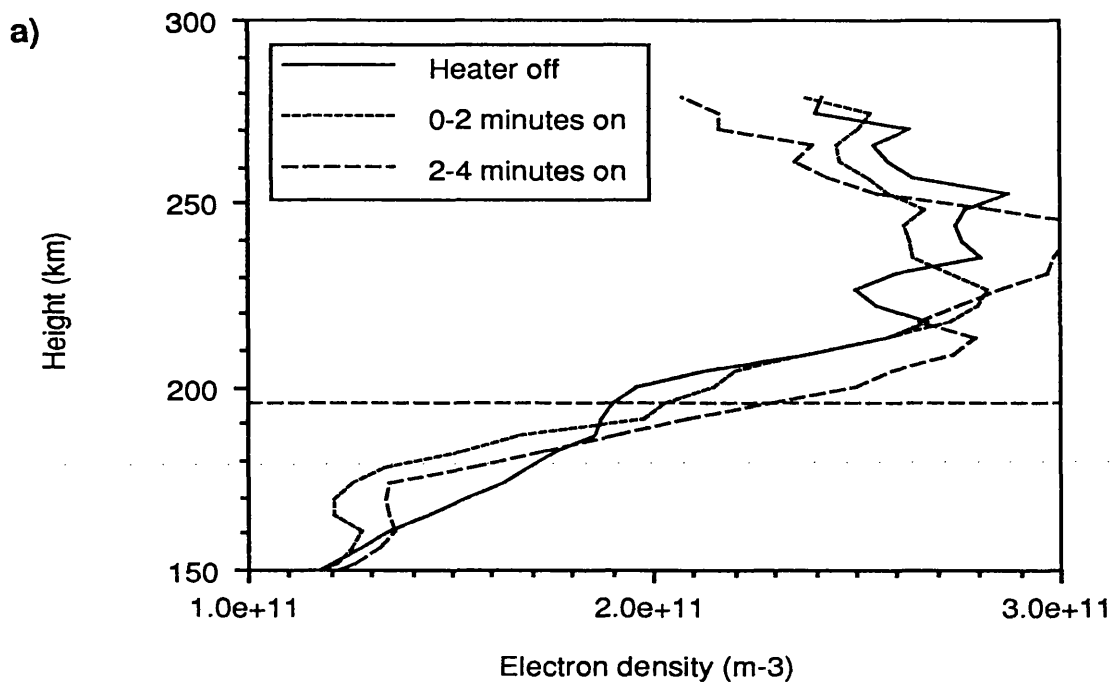


Figure 6.7 a) Electron density profiles measured by EISCAT on 23 March 1985, 0940-1030 UT.

b) Change in electron density due to heating (0-2 minutes after switch on).

The dashed lines indicate the ambient heater reflection height deduced from the ion-line overshoot height.

Chapter 6. Electron density effects

bars observed during heater on were similar in magnitude to those found during heater off (Figure 6.6) and therefore they have been omitted from this figure for clarity. The profiles have been smoothed in height by a 13 km running mean. In Figure 6.7b the observed change in the electron density due to heating divided by the ambient density ($\Delta N_e/N_e$) during the period 0-2 minutes after heater switch on has been plotted against height. The change in electron density derived from the measurements of the diagnostic phase which are also depicted in this figure are discussed below. It is evident from Figure 6.7b, that the electron density is depleted at heights about 20-30 km below the initial heater interaction region by close to 25% of the ambient value. This may be compared with nighttime observations at Arecibo where the observed density depletions exceeded 50 % (Duncan *et al* 1988). The discrepancy between the EISCAT profiles observed during heater on and heater off at heights above about 250 km is due to the extrapolation of the heater-enhanced electron temperature above the topmost (250 km) long-pulse gate (Chapter 5). The density profile observed 2-4 minutes after heater switch on is noticeably noisier above 250 km than either of the other two profiles. However, at such a large separation from the heater interaction height it seems unlikely, that this is caused by the heater. An interesting feature to note is that the depletion in the electron density established in the first two minutes after heater switch on at heights around 180 km appears to be reduced in size 2 to 4 minutes after heater switch on. This is consistent with the results of modelling reported by Robinson (1989). The phase measurements (Figure 6.8) also suggest that the density recovers towards its ambient value after several minutes of heating. It is also clear that the electron density above the initial heater reflection height increases after 2-4 minutes after heater switch on.

The change in phase observed on the 4.7 MHz test wave during heating between 0940 and 1040 UT on 23 March 1985 is illustrated in Figure 6.8. During this period the HF diagnostics were configured for drift velocity measurements (see Chapter 4) and hence only one diagnostic frequency was employed (with one O-mode and three X-mode receivers). Therefore, it was not possible to determine whether the change in phase was due to changes

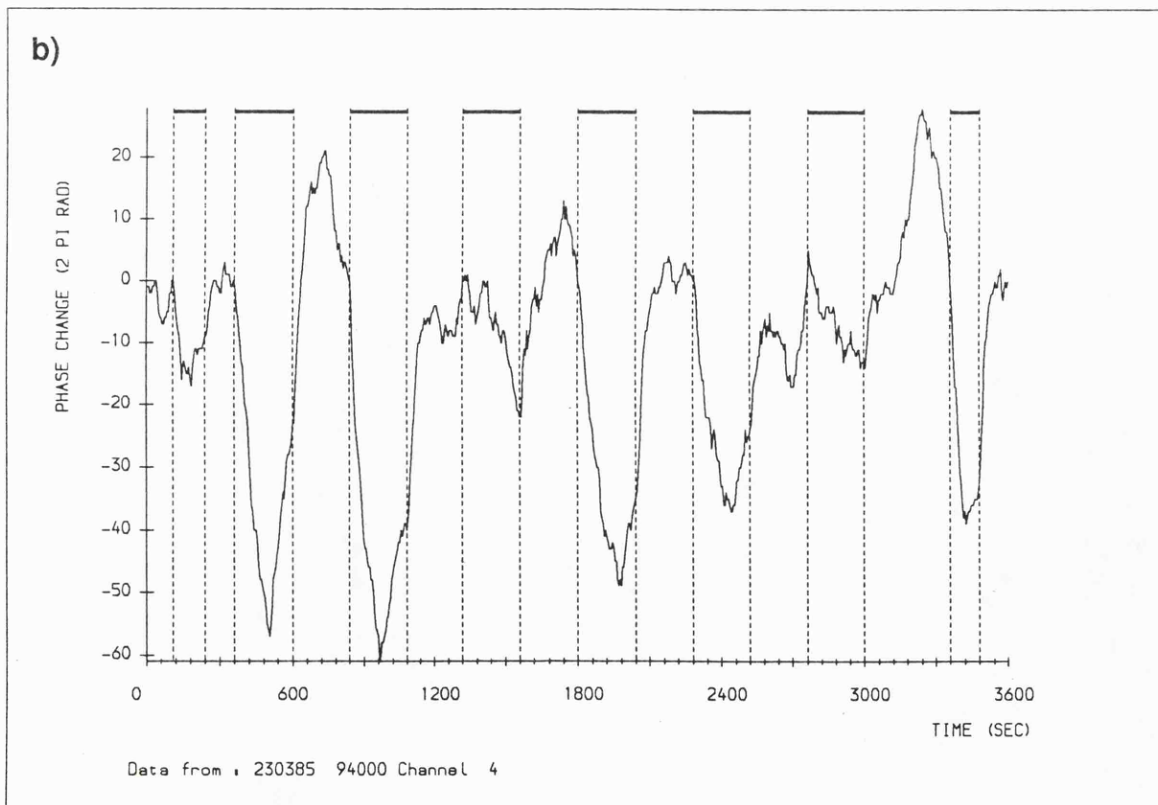
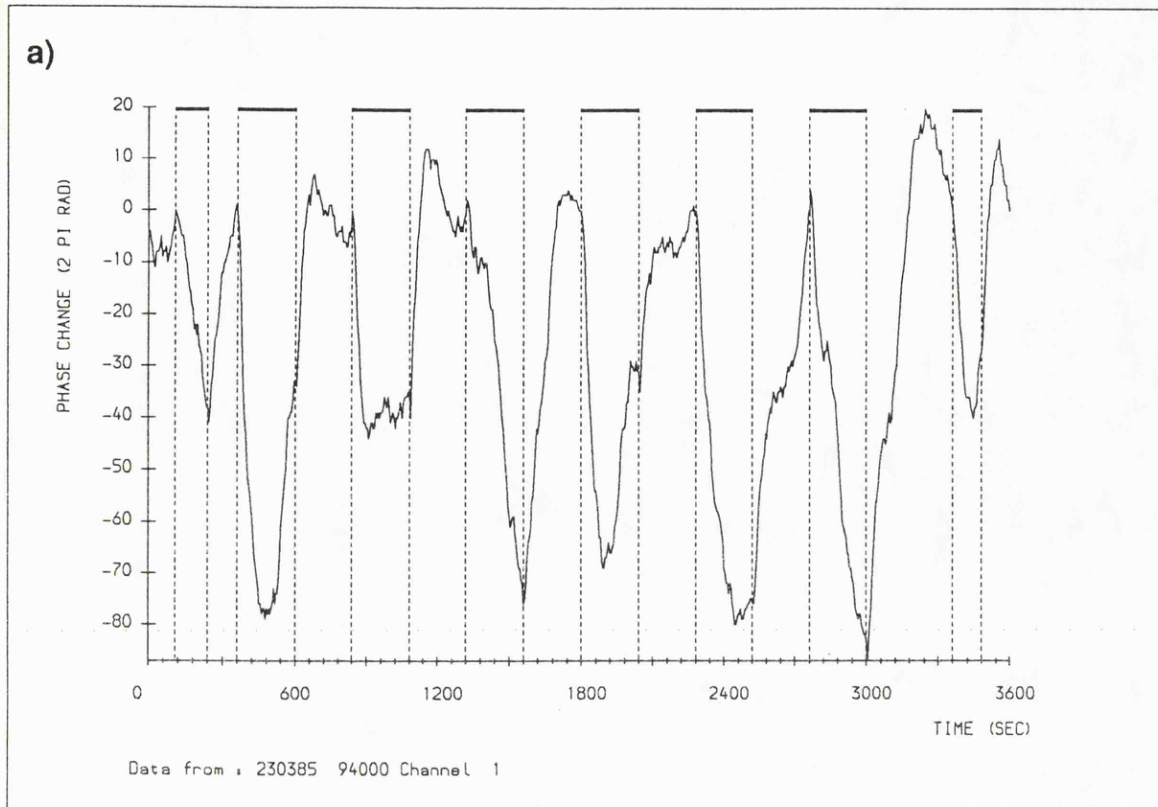


Figure 6.8 Phase changes of 4.7 MHz diagnostic signal during periods of heating on 23 March 1985, 0940-1040 UT. a) X-mode, b) O-mode.

of the reflection height or in the refractive index. The phase changes measured by the three X-mode receivers were averaged in order to reduce the random errors. The average saturated reduction in phase due to heating, $\Delta\phi$ for both of the polarisation modes is presented in Table 6.1. A reduction in the phase can be interpreted in terms of an increase in the reflection height of the diagnostic wave. If it is assumed that the observed phase change is due entirely to a change in reflection height Δh , caused by the density perturbation then,

$$\Delta h \approx - 0.5 \Delta\phi \lambda \quad (6.3)$$

where $\Delta\phi$ is the change in phase in units of 2π radians and λ is the wavelength of the diagnostic signal. Equation 6.3 assumes that the ionosphere is horizontally stratified, vertical incidence and ignores the effects of refraction. The following calculation of $\Delta N_e/N_e$ also ignores the effects of changes in the electron density gradient during heating.

The values of Δh which have been calculated from the saturated phase changes are given in Table 6.1, for both diagnostic polarisations. The frequency matching condition for reflection of the test wave (ie $\omega = \omega_p \sin \theta$, for O-mode waves, where θ is the elevation angle of the test-wave) must now be met at $h_1 + \Delta h$, where h_1 is the reflection height of the test wave prior to heating. Therefore, the electron density at $h_1 + \Delta h$ is known, and this may be compared with the ambient value observed by EISCAT at that height, and from this $\Delta N_e/N_e$ can be derived (Table 6.1). If the diagnostic waves are assumed to reflect specularly, then the experimental geometry (Chapter 4) yields $\theta \sim 76^\circ$. In deriving the reflection height for the X-mode test-wave the electron gyrofrequency, f_G has been taken to be 1.4 MHz. The calculated values of $\Delta N_e/N_e$ have been plotted with the EISCAT observations in Figure 6.7b. The value of $\Delta N_e/N_e$ derived from the phase measurements are within the errors of the EISCAT observations. However, because of the drift mode configuration employed by the diagnostics during this period, $\Delta N_e/N_e$ was only obtained at two heights and therefore a more extensive comparison with the EISCAT results was not possible.

	4.44 MHz O-mode	4.44 MHz X-mode
$\Delta\phi$ (2π rad)	-36.3	-64.4
Δh (km)	1.2	2.2
Ne_{eff} ($\times 10^{11} \text{ m}^{-3}$)	2.291	2.064
$h_1 + \Delta h$ (km)	208.2	204.6
$Ne_{\text{off}}(h_1 + \Delta h)$	2.364	2.156
$\Delta Ne/Ne$ (%)	-3.1	-4.3

Table 6.1 Measured and derived parameters employed in calculating the change in electron density with heating on 23/3/85, 0940-1030 UT. Ne_{eff} is the diagnostic reflection electron density and $Ne_{\text{off}}(h_1 + \Delta h)$ is the *ambient* electron density at the diagnostic reflection height after heating. Other notation is explained in the text.

6.4.2 Experiment of 17 March 1985

The magnitude of the electron density perturbation has also been derived from diagnostic phase data obtained on 17 March 1985 (1200 - 1300 UT, see Figure 6.4). During this period the diagnostics were configured in the anomalous absorption mode (Chapter 4), and therefore values of $\Delta N_e/N_e$ were obtained at five heights (Table 6.2). It should be noted that the phase change, $|\Delta\phi| \propto -f$ for these data. This frequency dependence of $\Delta\phi$ does not indicate whether the phase change is primarily due to changes in the path length or to small changes in the refractive index (Davies 1969). However, in the following calculation of $\Delta N_e/N_e$, it has been assumed that $\Delta\phi$ is due entirely to a change in path length.

The values of $\Delta N_e/N_e$ deduced from the phase measurements are compared with those derived from EISCAT observations (0-1 minutes after heater switch on) in Figure 6.9a. Two sets of phase measurements are presented in order to take account of the change in electron density gradient; (i) employed the density profile observed during heater off, and (ii) that measured during heater on. Both the diagnostic phase and EISCAT measurements agree that the electron density has been reduced by heating in the vicinity of the heater reflection height. However, the observations yield different magnitudes of the density perturbation, with EISCAT measuring a depletion of close to 10 % and the diagnostic phase a maximum depletion of about 4 %, although this discrepancy is within the errors of the EISCAT observations. It is interesting to note that utilising the higher density gradient (ii) leads to greater magnitudes of $\Delta N_e/N_e$ in the interaction region. Some comments on the advantages and weaknesses associated with each of the measurement techniques are given in Section 6.4.4.

The change in phase path has also been calculated by tracing the diagnostic ray paths (Jones and Stephenson 1975) through the electron density profiles measured by EISCAT during heater off and heater on. This method does take account of variation in the refractive

	Diagnostic frequency (MHz) and mode				
	3.8 O	4.286 O	4.7 O	4.7 X	Heater
$\Delta\phi$ (2π rad)	-38	-26	-14	-38	+31
Δh (km)	1.5	0.9	0.4	1.2	-1.0
$N_{e_{\text{eff}}}$ ($\times 10^{11} \text{ m}^{-3}$)	1.678	2.135	2.568	2.326	2.549
$h_1 + \Delta h$ (km)	176.4	192.8	207.6	198.6	205
$N_{e_{\text{off}}}(h_1 + \Delta h)$	1.730	2.168	2.576	2.365	2.531
$\Delta N_e/N_e$ (%)	-3.0	-1.5	-0.3	-1.6	+0.7

Table 6.2 Measured and derived parameters employed in calculating the change in electron density from diagnostic phase observations on 17/3/85, 1200 - 1300 UT. Notation as for Table 6.1.

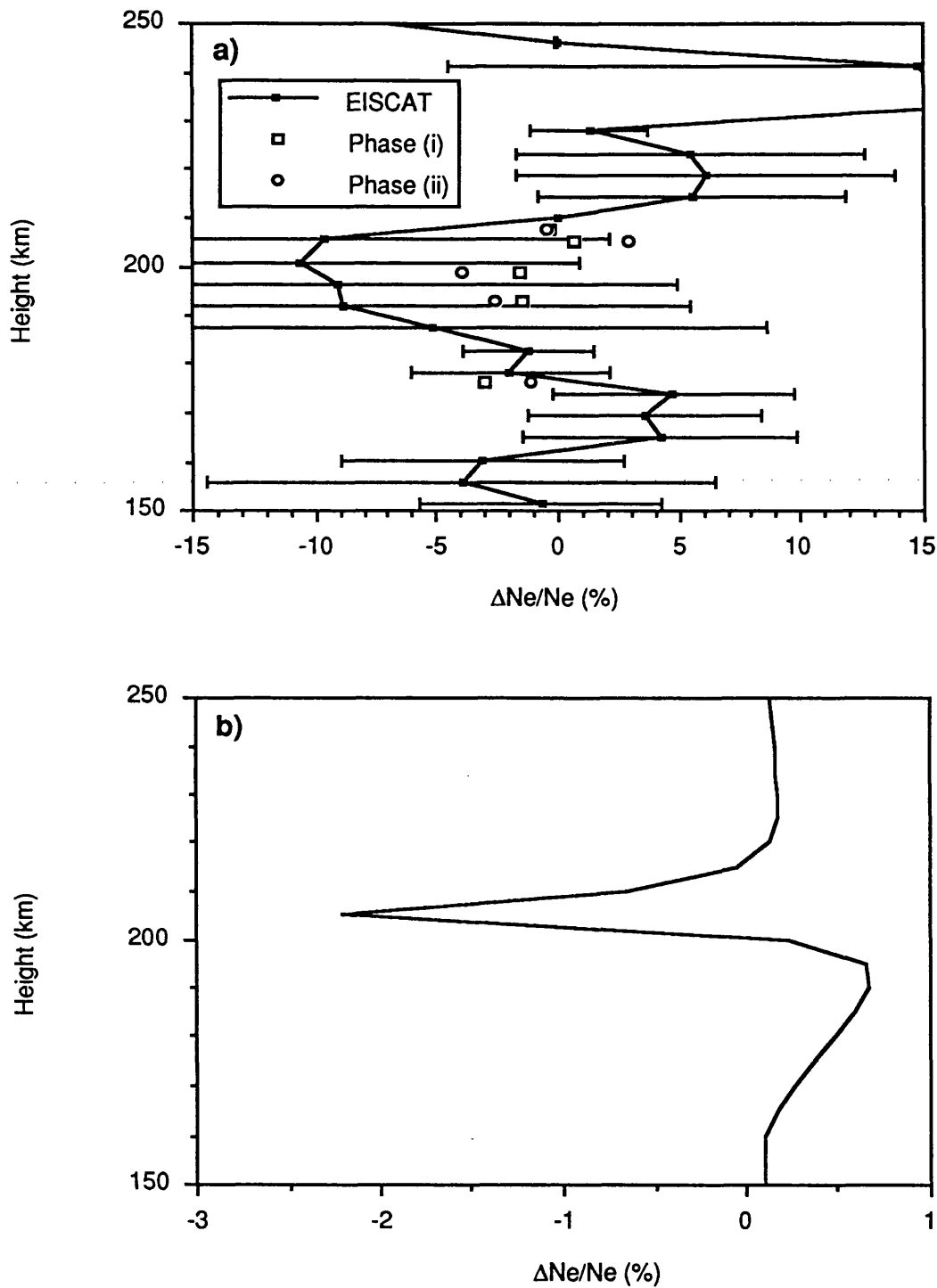


Figure 6.9 Change in electron density due to heating on 17 March 1985, 1200-1234 UT. a) Measurements by EISCAT (0-1 minutes after switch on) and diagnostic phase (assuming different density gradients), b) theoretical prediction. The heater reflection height, derived from ion-line overshoot measurements ~ 205 km.

index, but relies on the EISCAT observations and a number of modelled parameters (eg the electron-neutral collision frequency). The values of $\Delta\phi$ derived by this method exceed those measured by the diagnostics by a factor of about 2 to 3.

A theoretical model which describes the growth of the heater-induced electron density perturbation has been discussed in Chapter 3. The results of this modelling together with the observed values of $\Delta N_e/N_e$ on 17 March 1985 are presented in Figure 6.9b. The ambient conditions pertaining to the experiment have been employed by the model. Several features of this figure are worthy of note.

i) The magnitude of the electron density depletion observed by EISCAT is about an order of magnitude larger than that predicted by theory. However, the depletion deduced from the diagnostic phase measurements is similar in magnitude to the theoretical value. Previous theoretical and experimental results (see Chapter 2) have, in general, found depletions of a few percent.

ii) The general shape of the EISCAT and theoretical $\Delta N_e/N_e$ profiles are similar, ie the density is enhanced below the reflection height, depleted close to the reflection height and again enhanced above this height. However, the depletion region observed by both EISCAT and the phase measurements is considerably broader in height than that predicted by the theoretical model. The broadening of the electron density depletion observed experimentally could be explained by a change in the heater reflection height over the period of averaging.

6.4.3 Experiment of 26 February 1987

The experiment conducted on 26 February 1987 has been described in detail in Chapter 5. During the period from 1141-1157 UT, the heater transmitted with an ERP of 260 MW and with O-mode polarisation. The height profile of $\Delta N_e/N_e$ averaged between 1 and 3 minutes after heater switch on at 1141 UT is presented in Figure 6.10. At this time it is found that the electron density is enhanced by about 15 % of the ambient level in the vicinity of the heater

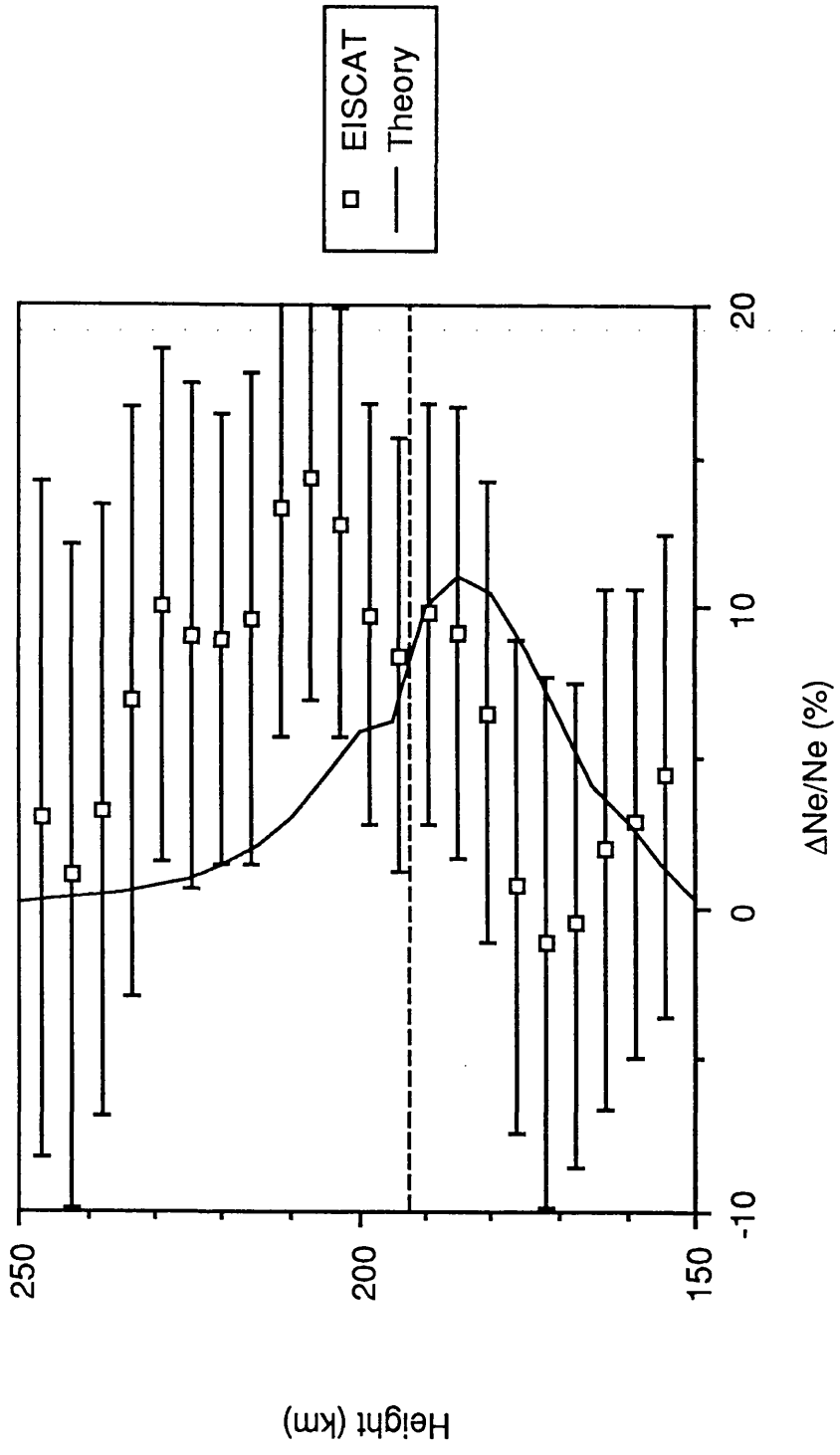


Figure 6.10 $\Delta\text{Ne}/\text{Ne}$ against height after 2 minutes of heating, 26 February 1987, 1141 UT. The initial heater reflection height is indicated by the dotted line.

Chapter 6. Electron density effects

reflection height, a result different from those previously discussed. In this instance the ambient density has been taken to be equivalent to that measured prior to the heater switch on at 1141 UT. Unfortunately, EISCAT only collected data from about 1139 UT onwards which means that there is a degree of uncertainty associated with the resulting density profile. In addition, there is evidence (Section 6.5) to suggest that the ambient density increased during the period of heater on. If this background change is assumed to be linear, then the “ambient” density a few minutes after heater switch on should not be significantly different from that observed before heating. The value of $\Delta N_e/N_e$ as a function of height obtained from the theoretical model described in Chapter 3 for conditions pertaining to the experiment on 26 February 1987 is also illustrated in Figure 6.10. The EISCAT observations and theory are in reasonable agreement as to the magnitude of the enhancement close to and below the initial heater reflection height. However, above this height the theory predicts a smaller enhancement of the density than is observed by EISCAT. This may be due to deficiencies in the ionospheric parameters employed as starting values in the model. The dependence of the model results on some of the input parameters (eg thermal conductivity) was reported in Chapter 3.

Measurements of the diagnostic phase made during this period do not exhibit any systematic change with the heater switching cycle. This was probably due to the experimental geometry employed at this time which was designed to investigate the effect of heating along the geomagnetic field. Hence, the heater beam was directed along the local field line (at an elevation of approximately 75°, South). With this geometry the mid-point of the diagnostic ray-path lay about 60 km to the north of the centre of the heater beam. Ray-tracing (Jones and Stephenson 1975) the path of the diagnostic waves through the ambient electron density profile measured by EISCAT reveals that they were reflected close to the 9 dB contour of the heater. This implies that the heater power in the vicinity of the diagnostic reflection region was relatively low, and explains why the diagnostics observed no modification effects.

6.4.4 Comments on the accuracy of the measurement techniques

In principle, EISCAT is capable of measuring the electron density in the F-region to an accuracy of about 10 % (Rishbeth and Williams 1985). However, this level of precision is usually obtained only if the data are integrated over a period of more than a few minutes. During heating experiments large integration times are not possible for a number of reasons, these including the rapidly changing density during the first few minutes of heating, and furthermore that after this time the ambient conditions may have changed. These problems may, to a certain extent, be offset by superposing the data from several heater cycles. The observed saturated value of $|\Delta N_e/N_e| < 15\%$, ie the heater induced change in density is of the same order as the errors in the EISCAT measurement (see Figure 6.9a). This implies that the heater induced density change is on the limits of detection by observing the change in the EISCAT power profile. In addition, it is assumed that the ion composition (which is employed in determining the electron and ion temperatures) remains constant during heating. If this is not the case, given that ion composition is likely to change with the increase in electron temperature, then further errors are introduced into the estimate of the electron density. Finally, it is possible that the received power is comprised of both incoherent and coherent backscatter (Chapter 4). If coherent backscatter is present then the relationship between the received power and electron density given by Equation 6.1 is no longer valid.

The random fluctuation of the diagnostic phase is, in general, less than about ten 2π radians. In principle, this results in a more accurate determination of the heater induced density change than the EISCAT power profile observations, especially when the ambient ionosphere is relatively quiet. However, the interpretation of the phase change in terms of a modification of the electron density is not so straightforward. In deriving $\Delta N/N$ from Equation 6.3, in addition to the assumptions already highlighted, it is also assumed that all of the change in phase path occurs close to the diagnostic reflection height. Since the density can be modified over a

Chapter 6. Electron density effects

broad range of heights (eg Figure 6.10) then this will not necessarily be the case. The validity of this assumption can be tested by examining the frequency dependence of $\Delta\phi$ (Section 6.3; 6.4.2). Furthermore, if a tilt in the ionosphere is introduced during heating then this will have a significant effect on the phase path (lengthening or shortening it depending on the direction of the tilt). In addition, the effect of heating on the electron density will not be uniform across the width of the heater beam. This large-scale inhomogeneity may lead to more than one propagation path linking the diagnostic transmitters and receivers. This multi-path propagation could result in a distortion of the phase measurements. It should also be noted that in deducing $\Delta N/N$ from the phase measurements a knowledge of the ambient electron density profile is required. For the experiments reported here this was obtained from EISCAT power profile measurements which have a height resolution of about 4 km, while the change in diagnostic reflection height was, in general, less than 2 km. This means that changes in the electron density gradient on smaller scales than 4 km are not accounted for, which could result in the value of $\Delta N_e/N_e$ being underestimated.

6.4.5 Comparison of 1985 and 1987 results

In the collision and recombination dominated lower F-region, an increase in the electron temperature leads to an increase in the electron density. Where diffusion processes dominate (eg the upper F-region), the opposite is true. Gurevich (1978) notes that the boundary between these two regimes is located typically at heights of between 180 and 200 km.

The observations presented for two days in 1985 indicate that the electron density was depleted in the region of the heater reflection height (205 km for 17 March; 192 km for 23 March). For 26 February 1987, an enhancement in the electron density was observed at, and above, the initial heater interaction height of 195 km. These results suggest that the location of the boundary between the collision and diffusion dominated regimes is extremely variable.

6.5 Temporal development of the heater-induced change in electron density

In order to ascertain the time constants associated with the growth and recovery of the heater induced perturbation in electron density, exponential curves of the form,

$$\Delta N = \Delta N_{\max} (1 - \exp(-t/\tau_G)); \quad \Delta N = \Delta N_{\max} \exp(-t/\tau_D) \quad (6.4a, b)$$

have been fitted to the EISCAT, phase and theoretical data for the intervals shortly after heater switch on and heater switch off, respectively. $\Delta N = N(t) - N(\text{ambient})$, where $N(t)$ is the electron density at time t after heater switch on or off, $N(\text{ambient})$ is the density observed during heater off, and τ_G and τ_D are, respectively, the characteristic growth and decay times of the electron density perturbation. ΔN_{\max} is the average value of ΔN observed once the heater-induced change has saturated. The best-fit values of τ_G and τ_D are obtained by minimising the sum of the residuals (differences squared) between the observations and the exponential curve.

The electron density as a function of time measured for several heights near to the peak of the electron density perturbation observed on 26 February 1987 (Figure 6.10) between 1138 and 1203 UT is presented in Figure 6.11. These data have been derived from EISCAT power profile measurements, corrected for range and T_e/T_i following Equation 6.1b. Only the relative value of the density variation is required so the system constant, C_{sys} has not been employed to scale the data. It is evident from Figure 6.11 that the random variation in the observed electron density is similar in magnitude to the enhancement in density caused by the heater. A trend in the ambient density also seems to exist as the density observed after the period of heater on is significantly higher than that observed beforehand. It is not possible to ascertain whether this trend is due to a natural change in the ambient conditions or whether the ionospheric recovery time after an extended period (16 minutes) of heating is longer than about six minutes.

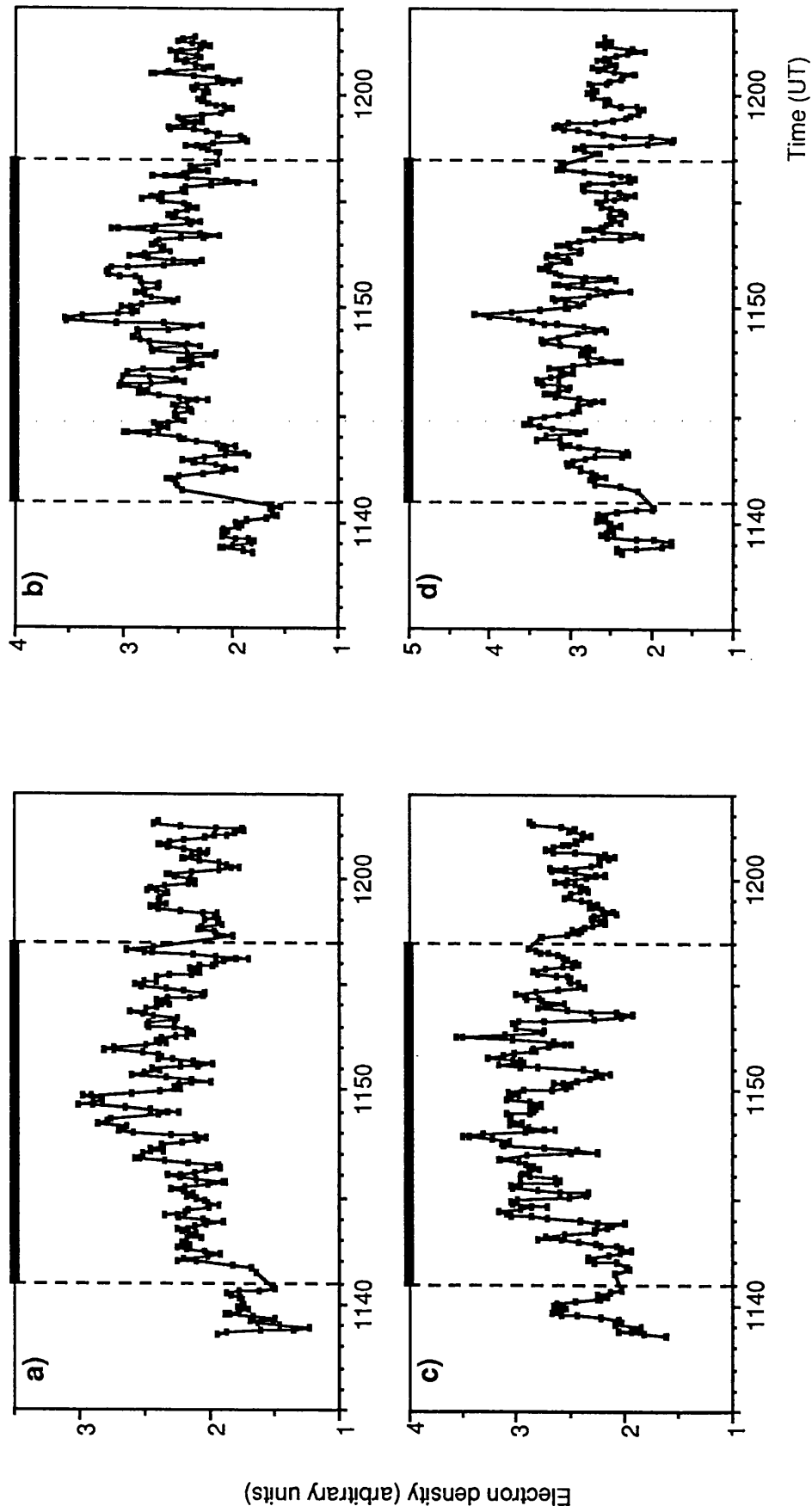


Figure 6.11 Electron density on 26 February 1987 as a function of time at heights close to the heater reflection height a)190 km, b) 194 km, c) 198 km and d) 203 km. Heater on time marked by dashed lines

Chapter 6. Electron density effects

The growth of the electron density perturbation predicted by the theoretical model described in Chapter 3 for several heights is illustrated in Figure 6.12. Currently, this model cannot be applied to conditions where the heater has been switched off, and therefore, no decay times have been obtained. The best-fit characteristic times observed by EISCAT and obtained from the model for a number of altitudes on 26 February 1987 at 1141 UT are presented in Table 6.3. The growth and decay times of the diagnostic phase changes for this interval cannot be estimated for reasons outlined in Section 6.4.3. It has previously been observed that the random fluctuations in the EISCAT power profile data are similar in magnitude to the heater-induced density change. This renders fitting the exponential curves to the data difficult, which is reflected in the low confidence levels obtained by the χ -squared test. The confidence levels obtained for the fit to the EISCAT data during the growth period are between 50 % and 80 %, and for the decay phase are between 20 % and 40 %. The errors in the value of τ_D are then around 50 % and the errors for τ_G are similar. The fit to the theoretical data has a confidence level of better than 99 %. From Table 6.3 it is clear that the growth time estimated from the EISCAT data is significantly higher than that obtained from theory. Given the low confidence in the fit, and the large error in τ_G it is likely that the experimental values overestimate the true value. The values of τ_D are very much smaller than τ_G , a result different from those previously obtained at Tromsø where $\tau_D \sim \tau_G$ (eg Jones *et al* 1982).

The ambient electron density observed by EISCAT at heights around 160-200 km during the heating experiment on 23 March 1985 between 0940 and 1030 UT was relatively constant. This means that the electron densities obtained during this period are suitable for averaging by superposition, eg the data from 0 to 10 s after heater switch on during each heater cycle have been averaged, then the data from 10 to 20 s and so on. This process has the effect of reducing the variance of the data. The change in phase of the HF diagnostics observed during this period has also been averaged in a like manner. Examples of both EISCAT and phase data

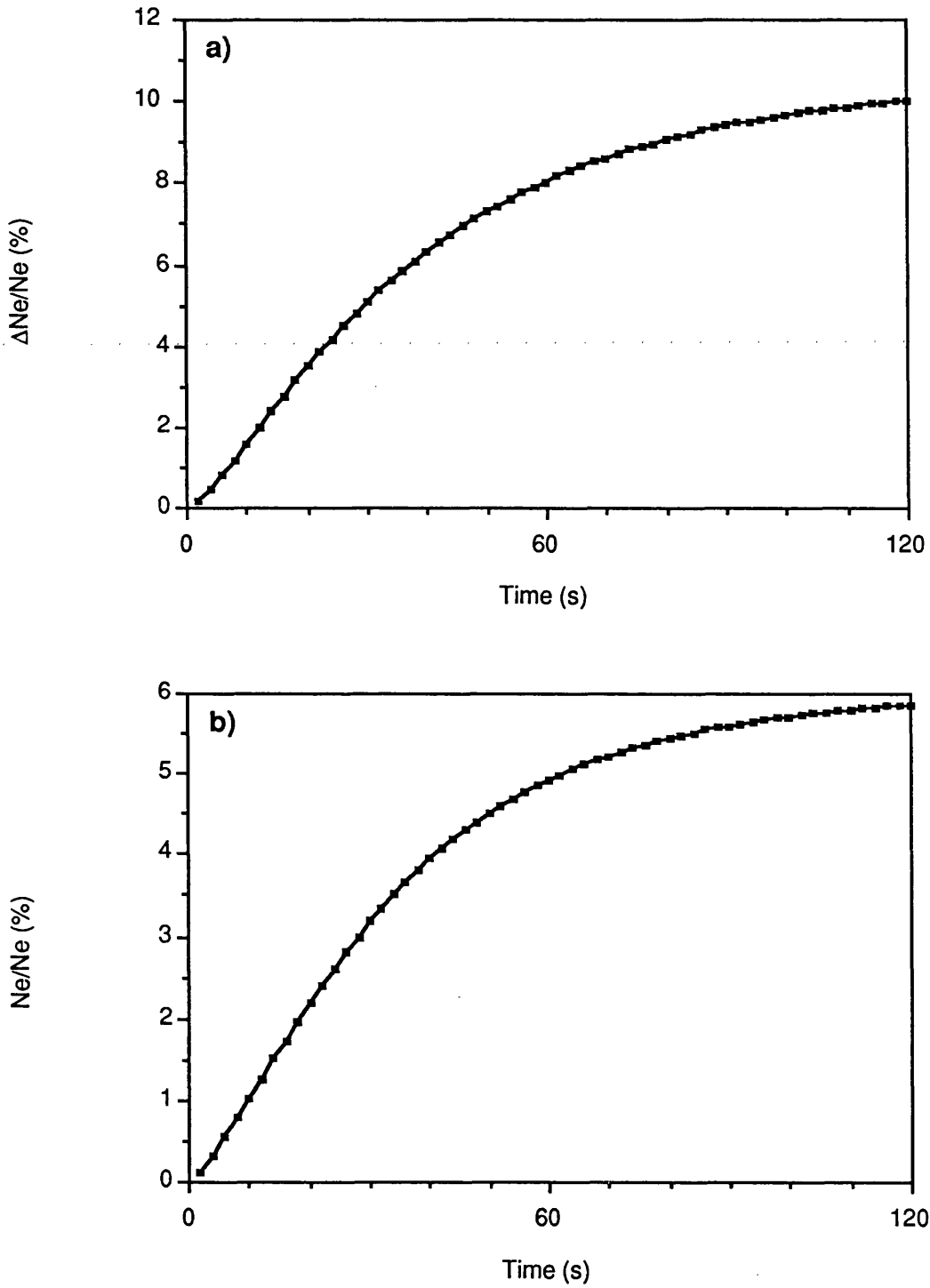


Figure 6.12 Growth of the heater-induced electron density enhancement, modelled for conditions on 26 February 1987, 1141-1143 UT, at a height of a) 190 km, b) 200 km.

SOURCE	HEIGHT (km)	τ_g (s)	τ_D (s)
EISCAT Power Profile	189	151	(¹)
	194	108	(¹)
	198	150	13
	203	79	25
Theory	190	38	-
	195	45	-
	200	36	-
	205	36	-

(¹) No sensible value of τ could be fitted to these data.

Table 6.3. Characteristic growth and decay times of the heater-induced electron density enhancement observed at Tromsø on 26 February 1987, 1141 UT.

from this interval are illustrated in Figure 6.13. Examination of this figure reveals that the fluctuations in the density measured by EISCAT are similar in magnitude to the reduction in the electron density caused by the heater. It is interesting to note that the density measured by EISCAT, although still reduced from the ambient value, increases during the period of the heating. A small increase can be also discerned in the phase observations after 150 s of heating, although this is not so pronounced. A gradual "filling in" of the electron density depletion caused by heating has been predicted theoretically by Robinson (1989).

The best-fit characteristic growth and decay times derived from the observations in Figure 6.13 along with theoretical values are presented in Table 6.4. The two different heights for the diagnostic phase measurements are the reflection heights prior to heating of the 4.44 MHz X and O-mode signals. The confidence levels of the fit for the phase measurements and the theoretical model are better than 99 %. However, those for EISCAT vary between 60 % and 80 %, which suggests that the growth and recovery of the electron density perturbation measured by EISCAT is not exponential in form. The EISCAT growth time is in reasonable agreement with that for the theory, but these are both less than the value determined from the phase data. However, it must be remembered that the change in phase depends on the change of the refractive index (ie electron density) along the entire diagnostic ray-path and not only at heights close to the reflection height. The EISCAT decay times are similar to those determined from the phase measurements. The values of τ_G are not significantly different from τ_D , which is in agreement with the results of earlier experiments (Jones *et al* 1982), but not with those of 26 February 1987. It should be noted that, in general, the characteristic response times of the density perturbation are longer than the equivalent times observed for the change in electron temperature (Chapter 5).

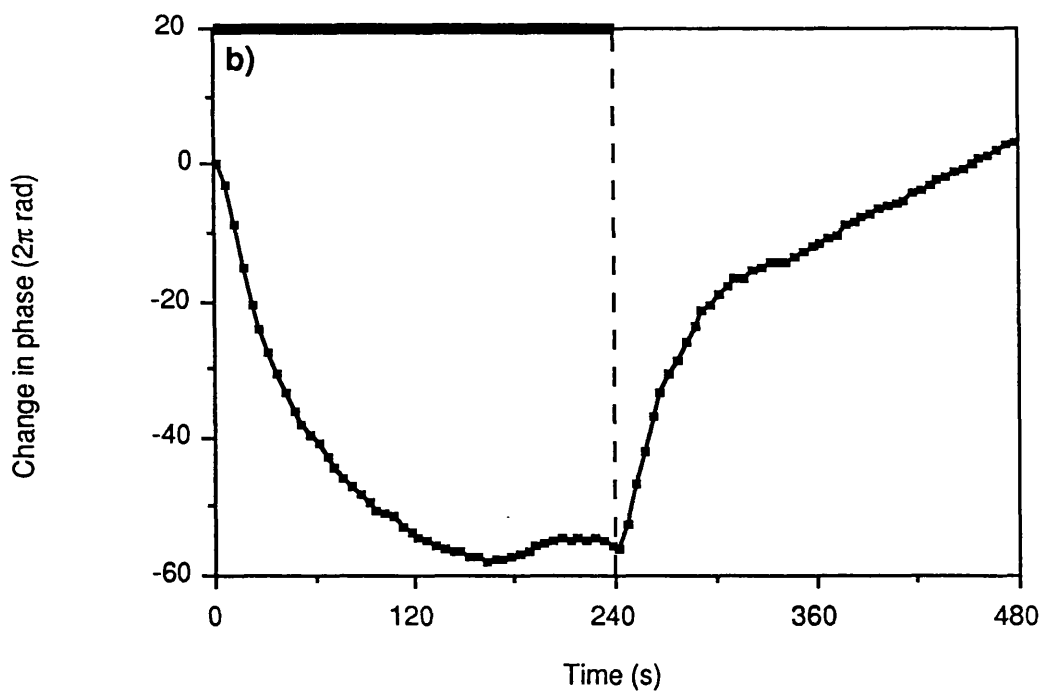
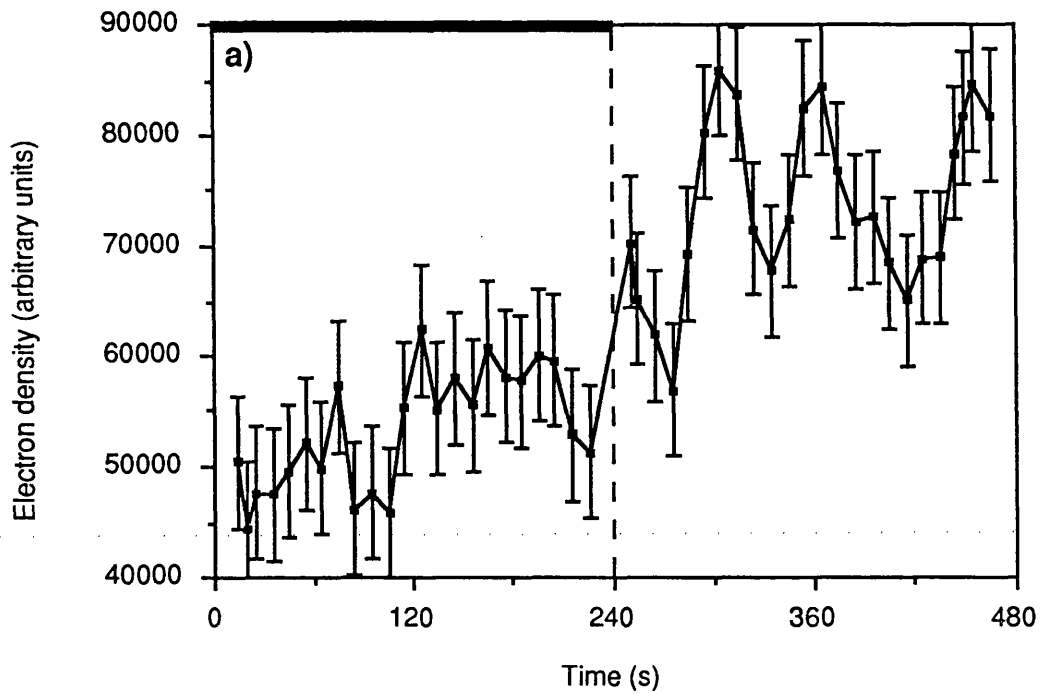


Figure 6.13 Time development of a) Electron density measured by EISCAT, and b) phase changes of 4.44 MHz X-mode diagnostic due to heating on 23 March 1985, 0946-1030 UT. Data have been averaged over 6 heater cycles. The bars indicate the heater on time.

SOURCE	HEIGHT (km)	τ_g (s)	τ_D (s)
EISCAT Power Profile	169	(¹)	25
	178	17	54
Diagnostic Phase	202	47	63
	207	60	25
Theory	190	21	-
	195	7	-

(¹) No sensible value of τ could be fitted to these data.

Table 6.4. Characteristic growth and decay times of the heater-induced electron density perturbation observed at Tromsø on 23 March 1985, 0940 - 1030 UT.

6.6 Dependence of phase change on $\Delta T_e/T_e$

The effect of changing the heater ERP on the observed change in phase has been discussed for earlier experiments at Tromsø by Jones *et al* (1982) (see also Chapter 2). These authors concluded that the change in phase was only well correlated with ERP when the wide band absorption was also well correlated with ERP. With the advent of EISCAT measurements of the heater-induced electron temperature enhancements (Chapter 5), it has become possible to attempt to determine the relationship between the electron temperature and electron density perturbations.

The absolute value of the maximum height change, $|\Delta h|$ as a function of $\Delta T_e/T_e$ for all diagnostic frequencies is illustrated in Figure 6.14. $|\Delta h|$ has been calculated from the changes in the phase (Equation 6.3) observed during experiments on 18 and 19 February 1987. Assuming that the density gradient is both linear and unchanging and that the change in refractive index on the diagnostic ray-path occurs only in the vicinity of the diagnostic reflection height then $|\Delta h| \propto |\Delta N|$. The theoretical model (Chapter 3) predicts that $\Delta N_e/N_e$ increases linearly with increasing $\Delta T_e/T_e$, however, the data presented in Figure 6.14 indicate that $|\Delta h|$ saturates as $\Delta T_e/T_e$ is increased. The solid line in Figure 6.14 represents the exponential curve which best-fits the data. The fit has a confidence level (from χ -squared test) of better than 99 %. This saturation of Δh with increasing $\Delta T_e/T_e$ probably arises because the assumptions made above are liable to be invalid for high values of $\Delta T_e/T_e$ (ie for stronger heating). It has been established earlier in this chapter that, for a given phase change, an increase in the density gradient leads to an increase in the deduced density change. During strong heating, the density gradients close to the heater interaction region are likely to be highly modified from the ambient values.

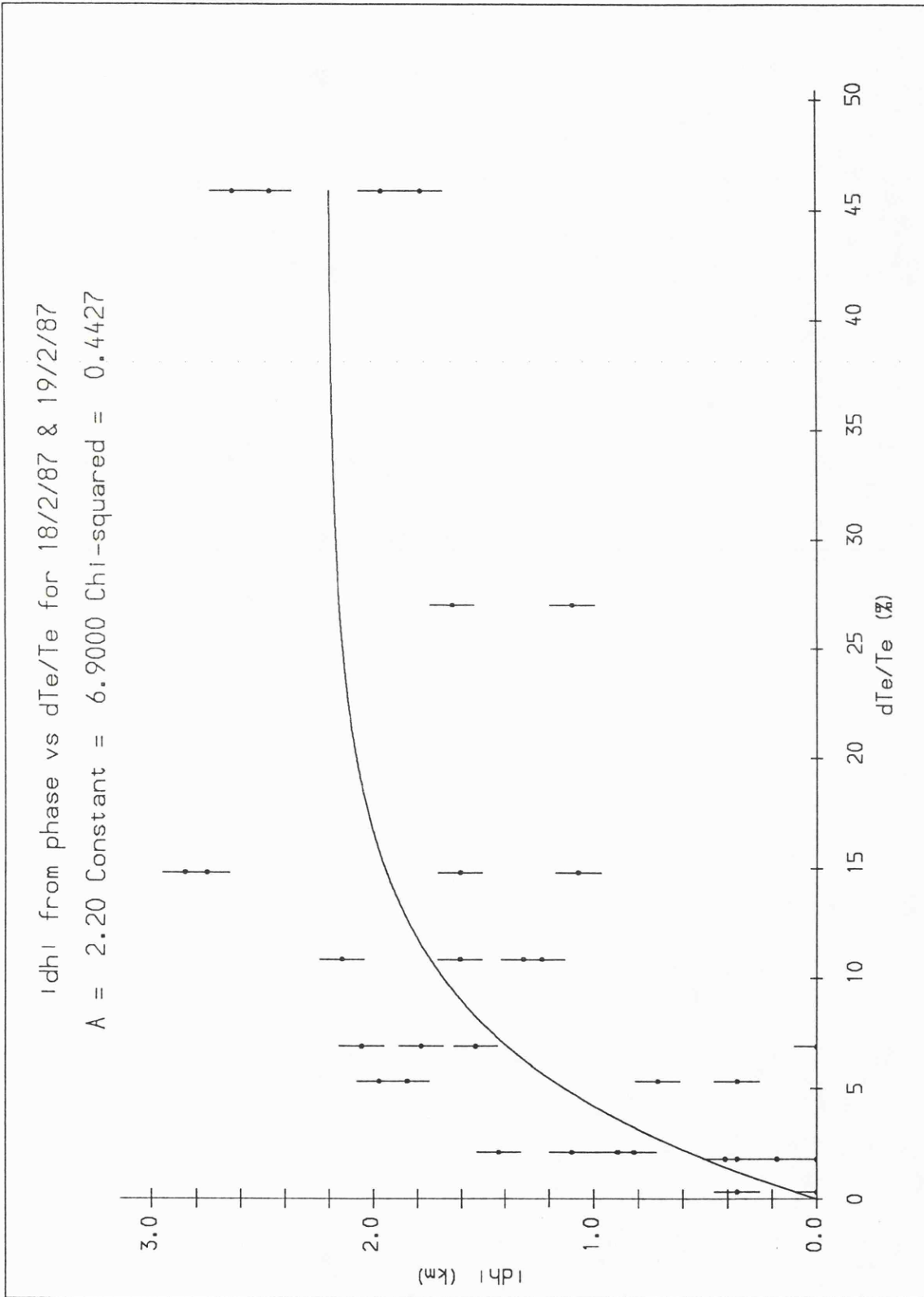


Figure 6.14 Heater-induced diagnostic reflection height changes deduced from phase measurements on 18 and 19 March 1985 as a function of the change in electron temperature observed by EISCAT.

6.7 Concluding remarks

In this chapter evidence has been presented which suggests that the plasma electron density is modified in the vicinity of the reflection region of high power radio waves. Two observational techniques (incoherent scatter and phase changes of HF test waves) have been employed in an attempt to measure this change in electron density. There is some agreement between the results obtained by each method, although not at all times. In some cases, the value of $\Delta N/N$ measured by EISCAT exceeded that deduced from the phase observations by a factor of between 3 and 4. It is possible that, in the presence of more than one propagation path due to heater-induced ionospheric tilts or large-scale inhomogeneities, the measured phase cannot be interpreted in terms of a change in electron density. Alternatively, in the presence of coherent backscatter, the EISCAT power observations can longer be interpreted in terms of electron density. The problems and advantages associated with each of the techniques have been assessed. EISCAT proves to be only just capable of determining the effect of the heater on the electron density.

While the ionospheric electron temperature is always enhanced by the action of high power radio waves, it appears that the electron density can be either enhanced or depleted. In the experiments reported here, both responses have been observed. Qualitatively, it seems likely that the background ionospheric conditions and the regime (ie whether collision or diffusion dominated) in which the heater is initially reflected play an important role in determining the electron density response to heating.

Chapter 7 HF Diagnostic Observations at Arecibo

7.1 Introduction

The observation of the change in amplitude, phase and frequency of low power HF radio waves which have passed through the heated volume has proved to be a powerful diagnostic technique during modification experiments at Tromsø (Stubbe *et al* 1982a, b; Jones *et al* 1982, 1983, 1984, 1986; Robinson 1989; Chapters 5 and 6). From measurements of the signal strength and the phase of these low power diagnostic signals it has been possible to determine the scale sizes (see Section 7.5) of the field aligned irregularities (FAI) which are generated during heating and are responsible for anomalous absorption (Chapters 2 and 3) and large scale plasma perturbations (Chapter 6), respectively. Measurement of the reflected heater signal strength has indicated the presence of heater self-absorption and a hysteresis effect which together provide information on the FAI generation mechanisms (Kopka *et al* 1982; Jones *et al* 1983, 1986; Robinson 1983, 1985, 1988, 1989; Wilkinson 1988; Fejer *et al* 1989).

It has been demonstrated (Robinson 1983, 1989; see Chapter 2) how the magnitude of anomalous absorption is dependent upon the magnetic field geometry. In order to test the relationship between anomalous absorption and geomagnetic latitude, the experiments performed at Tromsø (dip angle 78°) have recently been repeated at Arecibo, Puerto Rico (dip angle 50°). In this chapter the first direct observations of anomalous absorption during heating experiments at low-latitudes are reported. The scale sizes of the FAIs and the time constants associated with the anomalous absorption growth and decay are deduced from the observations and compared with results obtained during similar experiments at Tromsø (eg Robinson 1989). The general characteristics of the low power HF diagnostic signals and the sources of error which affect them are discussed in the next section.

7.2 General Characteristics of the diagnostic signals

The operation and deployment of the low power HF diagnostic equipment employed during the experiments reported in this chapter has been described in Chapter 4. Both the real and imaginary components of the signal are recorded which means that amplitude and phase information is obtained. In general, the amplitude measurements reveal changes in the reflectivity (or absorption) characteristics of the ionosphere and the phase measurements are sensitive to changes in the refractive index caused by heater-induced perturbations of the plasma electron density.

The measurement of the HF diagnostic signal amplitude is subject to two principal sources of error, a) system errors which may be revealed by calibration measurements and b) random errors due to natural signal fading. The procedure adopted for calibrating the diagnostic receiver attenuators has been described in detail in Chapter 4. Typical calibration curves for all ten receiver attenuator levels which were recorded during the experimental campaign held at Arecibo in May 1989 are illustrated in Figure 7.1. The calibration data from only one channel are illustrated since those obtained for the remaining channels are similar. The attenuator levels, which are monitored in real time by the data control computer, are nominally incremented in steps of 10 dB. The calibration curves indicate an error of approximately ± 0.2 dB in each of the nominal levels. The "spike" observed at a receiver attenuation of 0 dB and a programmable attenuation of around 105 dB is not present on each occasion that the receivers are calibrated. This behaviour suggests that the spike is probably due to noise present during the calibration procedure rather than a problem with the attenuator. The errors which are due to the natural fading and the methods by which they can be minimised are discussed below.

A typical interval of HF diagnostic amplitude data recorded during the 1989 heating campaign held at Arecibo is presented in Figure 7.2. The period illustrated is from 21 May

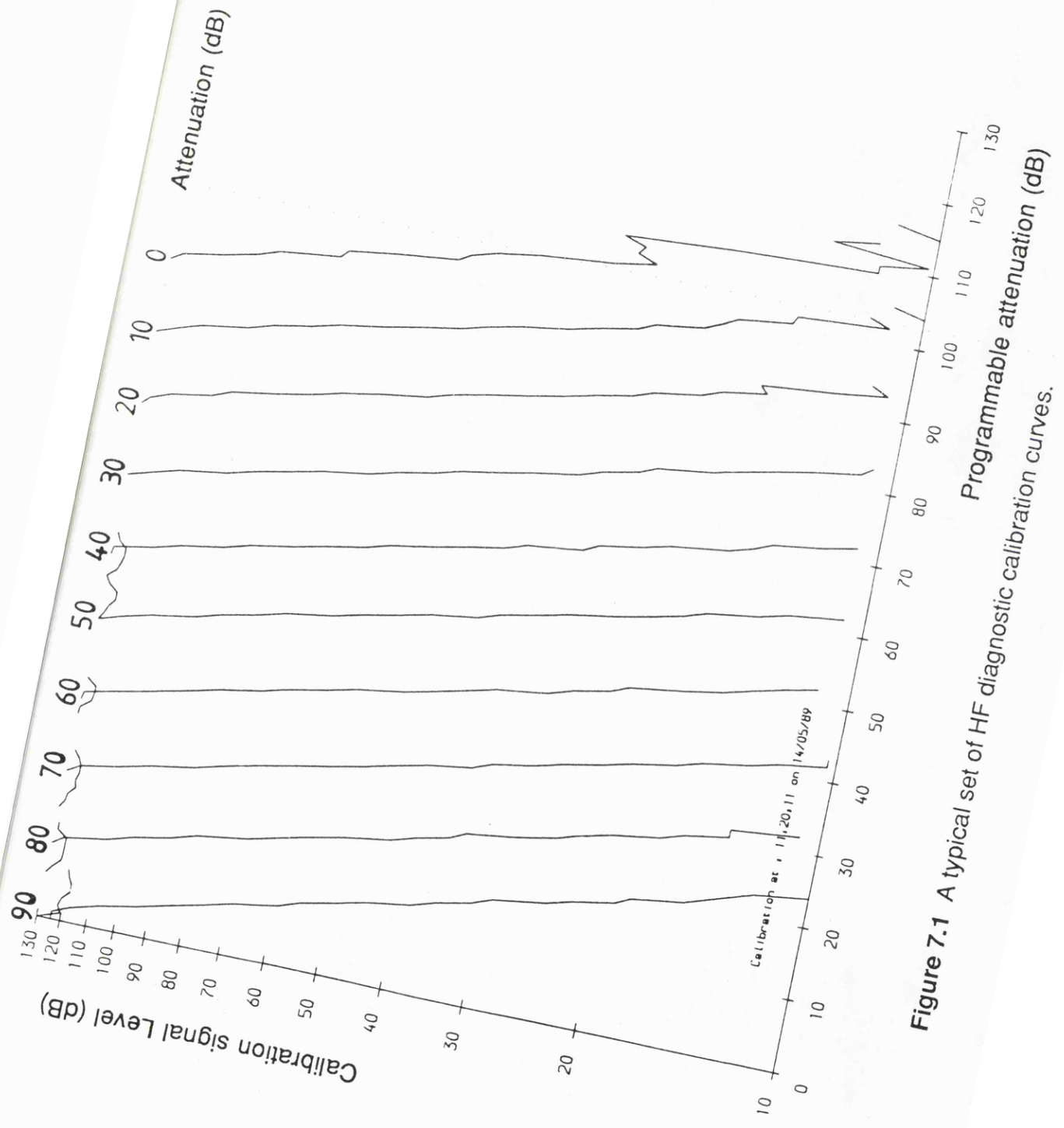
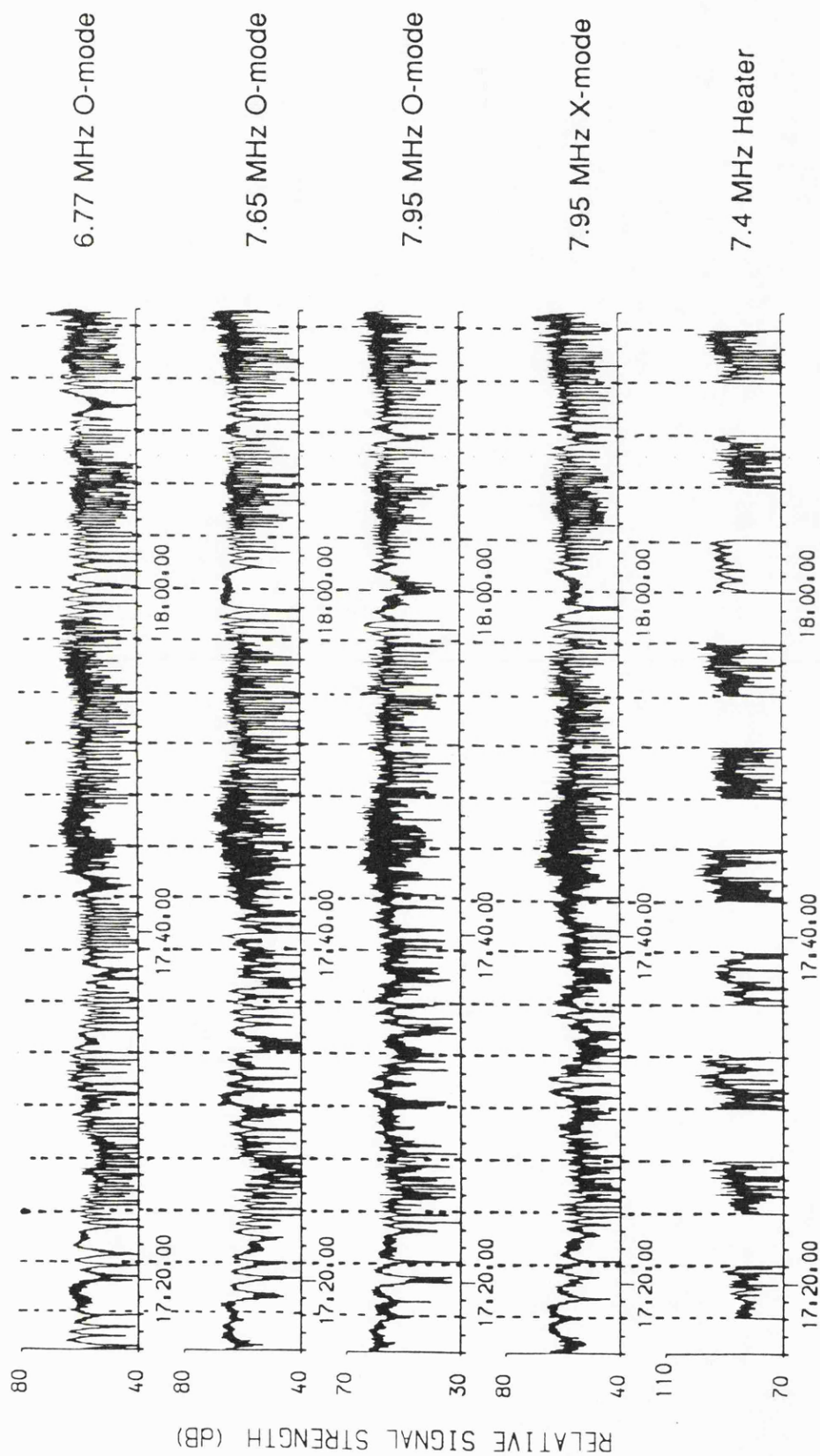


Figure 7.1 A typical set of HF diagnostic calibration curves.



(A. S. T.)

Figure 7.2 Amplitude variation for four different HF diagnostic signals during heating on 21 May 1989, 1816-1916 AST. The bottom panel is the reflected heater signal.

Chapter 7. HF observations at Arecibo

1989 and starts at 1716 AST (Atlantic Standard Time, $AST = UT - 4$) and ends at 1816 AST. During this interval the heater transmitted at full power ($ERP = 80$ MW) with a frequency of 7.4 MHz. Prior to 1800 AST the heater wave was polarised in the ordinary mode and after 1800 AST in the extraordinary mode. The heater cycle consisted of a 3 minute period of heater on followed by 3 minutes of heater off. A feature to note in the diagnostic signals is the highly variable signal strength due to natural fading effects. The fading amplitude is at times as much as 20 dB from peak to peak and therefore any heater induced reduction in the signal strength (eg possibly 1724 - 1727 AST) is not readily discernible. As the natural signal fading is random and the heater-induced change in diagnostic amplitude is systematic then suitable averaging of the the diagnostic signal levels could reveal the heater-induced effects. In order to smooth the signal amplitudes and reveal any systematic changes in the diagnostic signal level caused by the heater two methods are employed,

- i) The signal data may be averaged over a fixed time interval
- ii) The signal data from several identical heater cycles may be superposed.

Method (i) is suitable if no temporal information is required and if care is taken to ensure that the signal levels are in quasi-stationary equilibrium (QSE) over the entire averaging interval. QSE implies that there are no trends in the signal strength during the period covered by the average. It should also be ensured that the averaging interval is considerably longer than the fading period. Given that, typically (eg Figure 7.2), the fading period is much shorter than the duration of the heater on or off times then this criterion should be readily achieved. In cases where heater-induced anomalous absorption is observed there is a finite transition time after heater switch on or switch off before QSE is attained at the new signal level (Section 7.6). This means that care must be taken to ensure that data from the transition period are not included in the average. The response time observed during experiments at Tromsø was, in general, less than 5 s (Robinson 1989) which is a small fraction of the heater on (or off) periods typically employed. Observations at Arecibo reveal response times considerably longer than this (see Section 7.6) but which still comprise a small fraction of the heater on and off periods. The

criteria described above have been employed in establishing whether the data are suitable for averaging. If the data prove to be suitable then they are converted from logarithmic units (ie dBs) to linear units and then averaged. The averaged values are then converted back to logarithmic units. During the 1989 campaign at Arecibo the diagnostic signal amplitudes were sampled at a frequency of 32 Hz. Given a typical averaging interval of over a minute, then several thousand samples are included in the average. This means that the statistical error associated with the mean is a reasonable estimate of the error on the QSE signal level.

The second averaging method is employed to smooth the data if temporal information is required. Signal level data from equivalent intervals in relation to the heater cycle are averaged, eg the signal strength observed during the first 10 s after heater switch on from several heater cycles could be averaged, then data from 10 - 20 s after heater switch on, and so on. Care must be exercised during this procedure to ensure that each of the heater cycles are identical (ie same heater power, polarization and frequency) and that the levels of anomalous absorption observed during each heater cycle are comparable. The signal levels are converted to linear units before averaging and then converted back to logarithmic units. By superposing data from several heater cycles in this way, a shorter integration time may be employed while the random errors are kept at similar levels to the non-superposed case (method i). Alternatively, if the same integration time is employed then the random errors due to fading will be reduced by superposing the data in this manner. The integration times which can be attained by superposing the data in this way, while maintaining moderate errors, are smaller than the time required for the diagnostic signal level to respond to heating. This means that these response times may then be deduced (Section 7.6). However, despite the superposition of data from several heater cycles the shorter integration times employed in method (ii), in general, result in larger errors in the averaged signal levels than those obtained by method (i).

7.3 Measurement of Diagnostic Signal Absorption

The heater-induced absorption, Γ of a diagnostic signal may be defined by the following expression,

$$\Gamma = A_{\text{off}} - A_{\text{on}} \quad (\text{dB}) \quad (7.1)$$

where, A_{off} and A_{on} are the quasi-stationary equilibrium signal levels during heater off and on respectively. In the case of signal levels which have been averaged according to method (i) described in the previous section, then A_{off} is determined by,

$$A_{\text{off}} = A_1 + \frac{(A_2 - A_1)(t_h - t_1)}{(t_2 - t_1)} \quad (7.2)$$

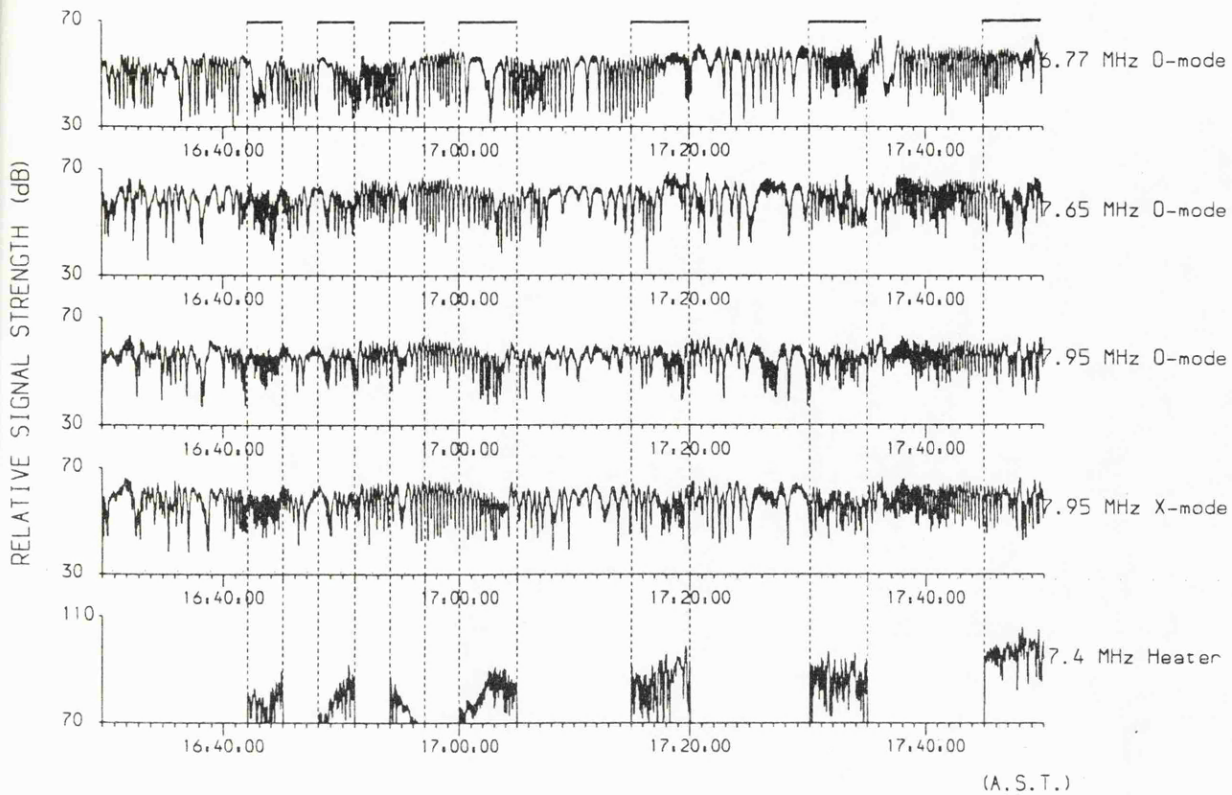
where, A_1 and A_2 are the diagnostic signal amplitudes averaged during the intervals of heater off before and after heater on, respectively and t_1 , t_2 and t_h are the mean times of the averaging intervals before, after and during heater on. Equation 7.2 can account for a linear change in the ambient signal level between times t_1 and t_2 , provided that $t_2 - t_1$ is greater than the fading time.

It has been previously discussed (Robinson 1989; Chapter 3) how the expected level of anomalous absorption at Arecibo should be small compared to that observed at Tromsø for the same ionospheric conditions. In addition, it has been suggested that the highly ionised D/E - regions encountered during the May 1989 campaign at Arecibo (Section 7.6) may have reduced the heater power in the F-region to below the threshold of the instability which is responsible for the growth of the field aligned irregularities which in turn lead to anomalous absorption (Chapters 2 and 3). These considerations may explain why only one interval during the campaign has yielded clear examples of heater induced diagnostic signal absorption. The

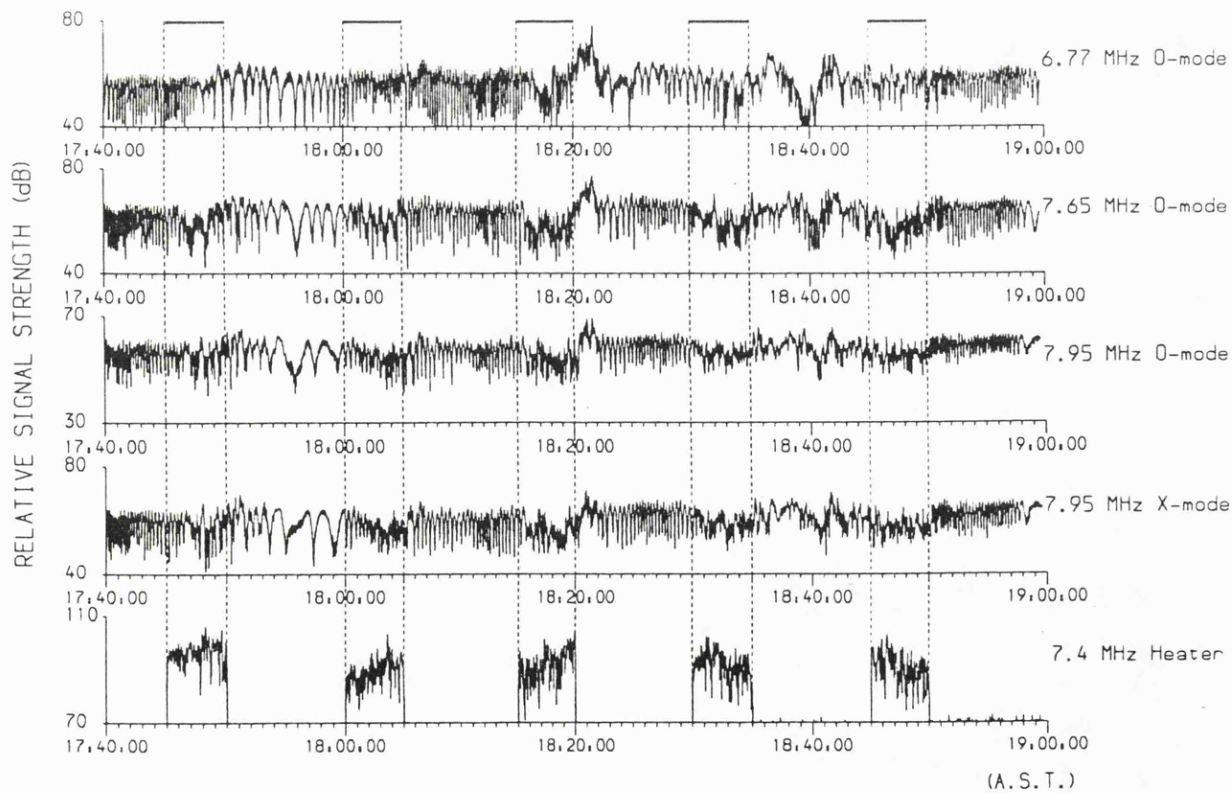
Chapter 7. HF observations at Arecibo

diagnostic signal amplitudes for this interval, which occurred on 16 May 1989 between 1630 and 1900 AST, are presented in Figure 7.3. During this period the heater transmitted a frequency of 7.4 MHz and with O-mode polarization. Two separate heater cycles were employed during this interval, the first between 1642 and 1657 AST (Figure 7.4a) and the second from 1700 AST onwards (Figure 7.4b). It is evident from Figure 7.3 that the natural signal fading has an amplitude of close to 10 dB peak-to-peak, but there are several examples of a well defined heater-induced reduction in the diagnostic signal level (especially 1815 AST onwards). However, the reduction in the signal level is comparable in size with that of fading which means that the data must be averaged in order to obtain a reliable estimate of the absorption. Another interesting feature of the data illustrated in Figure 7.3b is the increase in the fading rate during heating and the very regular, but slower fading which occurs immediately after heater switch off (except after the 1830-1835 AST heater on). The former observation has been attributed to the generation of FAIs during heating (eg Wilkinson 1988) while the latter response has not been previously observed at Tromsø. The diagnostic signal which is nominally polarised in the X-mode also exhibits a level of heater-induced absorption comparable in size with that of the O-mode diagnostic of the same frequency. Previous experiments at Boulder and Tromsø have revealed that only O-mode diagnostic signals should undergo anomalous absorption. However, the mode contamination which arises from the non-circularly polarised characteristic waves at low-latitudes (Davies 1969; Chapter 4) may explain the attenuation of the X-mode diagnostic wave.

An ionogram recorded by the Arecibo observatory ionosonde at 1629 AST (Figure 7.5) indicates a minimum frequency in the F-region of around 5 MHz and an O-mode peak frequency of between 11 and 12 MHz. Ionisation at lower altitudes (ie D/E region) has a critical frequency of close to 5 MHz and a minimum frequency of about 4 MHz. The existence of an D/E-region valley or whether the lack of a reflected signal below 4 MHz indicates absorption or no ionisation below this frequency cannot be deduced from this ionogram. During the experiments reported here, diagnostic frequencies in the range 6.7 to 8 MHz were employed.



(A. S. T.)



(A. S. T.)

Figure 7.3 Diagnostic signal strength versus time on 16 May 1989, 1630-1900 AST. The dotted lines indicate periods when the heater was switched on.

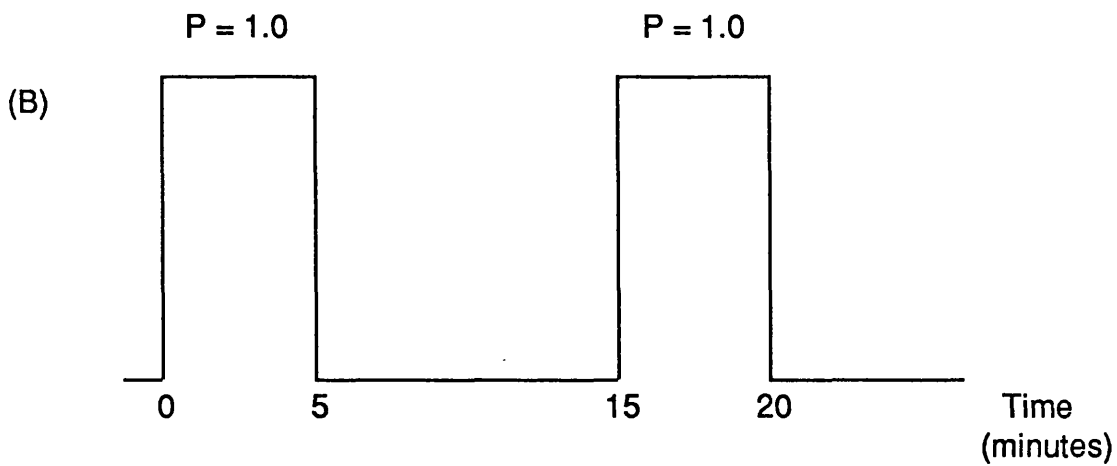
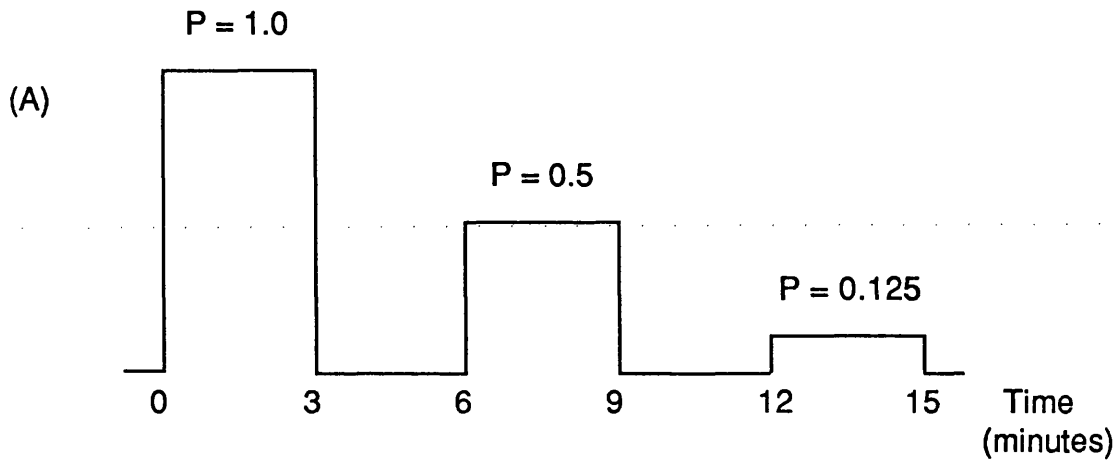


Figure 7.4 Schematic of heater cycles employed at Arecibo on 16/05/89. P(1.0) = 80 MW ERP. a) 1642 - 1657 AST, b) 1700 - 1900 AST.

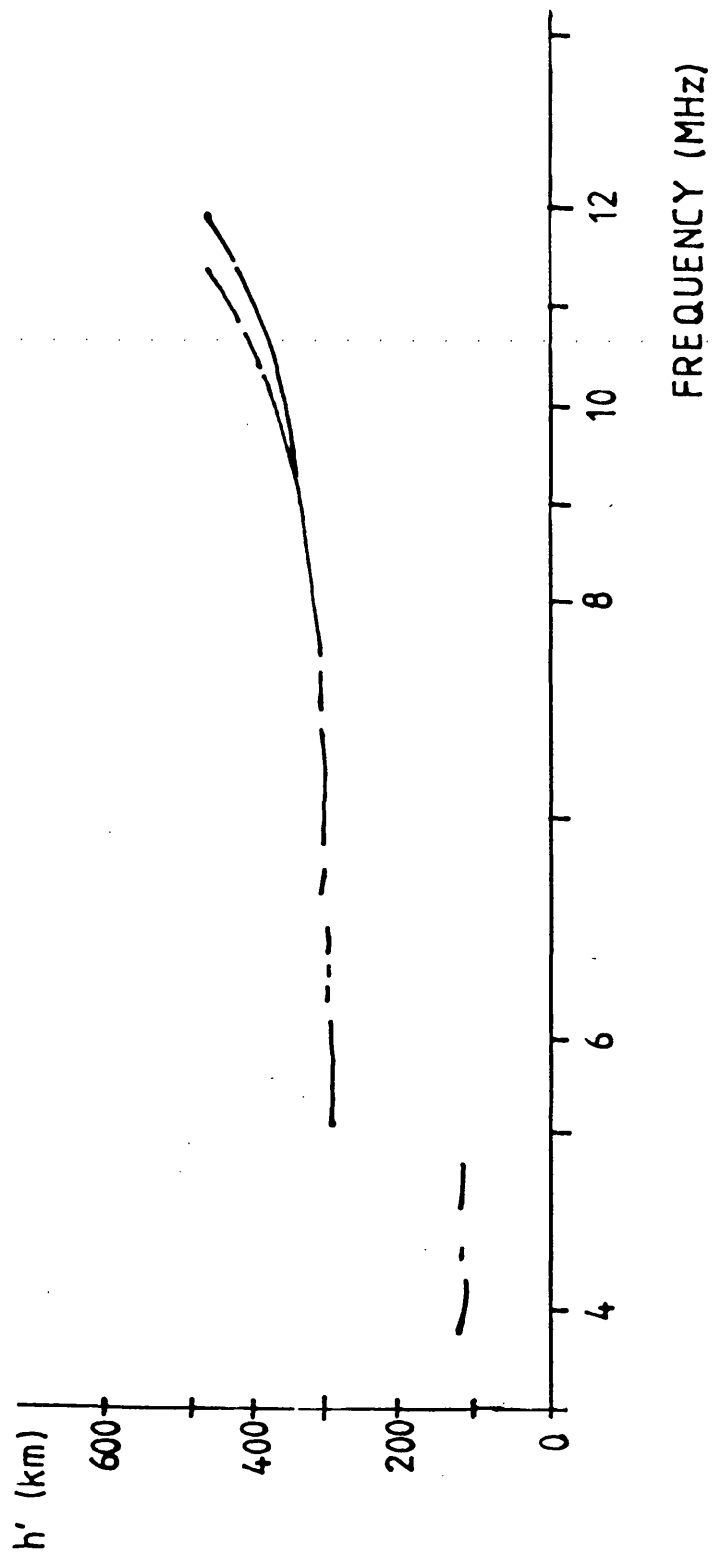


Figure 7.5 Ionogram obtained during heater off on 16 May 1989, at 1629 AST.

Chapter 7. HF observations at Arecibo

This implies that all of the diagnostic signals were reflected in the F-region at altitudes well below the peak. While a problem with the ionosonde meant that no ionograms were obtained after 1629 AST, electron density profiles obtained by the 430 MHz radar suggest that although the height of the F-region peak remained fairly constant during the entire interval between 1630 and 1900 AST the bottomside electron density fell (Figure 7.6). The radar did not measure electron density below a height of about 100 - 150 km and therefore any changes in the peak D-region electron density were not detected.

The signal amplitudes of the three O-mode diagnostics have been averaged by employing the method (i) described in the previous section. Averaged signal levels from each heater on and off period during the interval of interest are reproduced in Table 7.1. Data from times up to about 60 s after a heater turn on or turn off have not been included in the averaging. Examination of Table 7.1 reveals that the amplitude of the diagnostic signals tends to increase with time which suggests that the level of diagnostic D-region absorption decreases with the onset of local sunset. The value of Γ for each heater on has been derived from the data contained in Table 7.1 via Equations 7.1 and 7.2 (Table 7.2). Examination of Table 7.2 suggests that the heater-induced reduction in the diagnostic signal levels can be divided into three periods, before 1700 AST where a power stepping heater cycle was employed (Figure 7.4a), 1715 through 1800 AST where the peak absorption is around 3 dB and 1815 AST and after where the maximum absorption is over 5 dB. The higher levels of heater induced absorption generally observed after 1815 AST may be due to the expected post-sunset reduction in the D-region absorption, and hence greater heater power levels in the F-region.

7.4 Possible Causes of the reduction in Diagnostic signal level

Robinson (1989) has discussed three possible mechanisms which could lead to a reduction of the diagnostic signal amplitude during the heating of the ionosphere by intense radio waves,

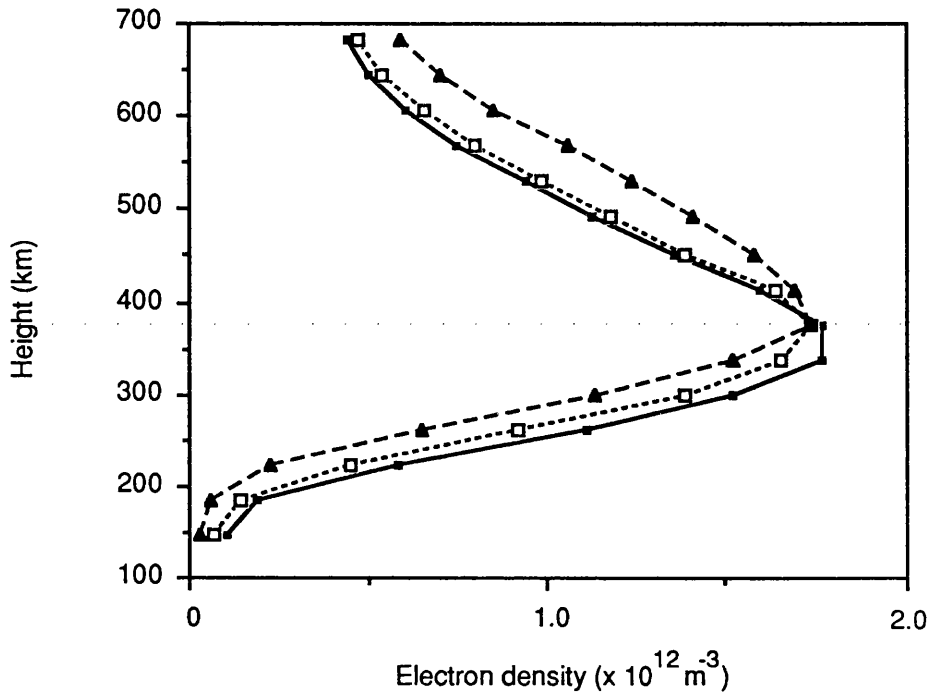


Figure 7.6 Ambient electron density measured by the Arecibo 430 MHz radar on 16 May 1989, —●— 1628-1640 AST, - - - □ - - - 1739-1744 AST and - - - ▲ - - - 1839-1844 AST.

TIME (AST)	HEATER STATUS	FREQUENCY (MHZ)		
		6.77	7.65	7.95
163500 - 164100	OFF	52.1	59.3	55.9
164230 - 164430	100 %	47.9	56.5	54.1
164600 - 164730	OFF	48.6	58.2	54.3
164830 - 165030	50 %	51.2	56.8	54.3
165200 - 165330	OFF	49.1	61.0	56.2
165430 - 165630	12.5 %	50.4	60.8	56.0
165800 - 165930	OFF	54.4	62.4	57.6
170100 - 170300	100 %	51.9	59.6	54.0
171000 - 171400	OFF	52.9	60.3	55.9
171600 - 171800	100 %	52.7	59.1	55.6
172500 - 172900	OFF	54.6	61.5	55.2
173200 - 173400	100 %	54.6	59.4	54.6
174000 - 174400	OFF	54.9	61.4	56.4
174700 - 174900	100 %	55.6	58.5	55.1
175500 - 175900	OFF	56.5	62.5	55.6
180200 - 180400	100 %	56.8	60.4	54.4
181000 - 181400	OFF	56.5	62.6	56.8
181700 - 181900	100 %	54.5	57.3	53.1
182500 - 182900	OFF	59.7	65.2	59.2
183200 - 183400	100 %	56.1	59.8	56.0
184000 - 184400	OFF	58.6	64.1	57.7
184700 - 184900	100 %	57.6	57.7	55.7
185300 - 185700	OFF	57.7	64.2	59.6

Table 7.1 Averaged diagnostic signal strength (in dB) for intervals of heater switch on and off on 16 May 1989. The error in the signal strength ~ 0.2 dB. 100 % power is equivalent to an ERP of 80 MW.

TIME (AST)	POWER (%)	FREQUENCY (MHz)		
		6.77	7.65	7.95
1642	100	2.0	2.1	0.8
1648	50	-2.4	2.7	0.9
1654	12.5	1.1	0.8	0.8
1700	100	1.9	2.1	3.1
1715	100	0.8	1.6	0.1
1730	100	0.1	2.1	1.1
1745	100	-0.1	3.3	1.0
1800	100	-0.3	2.1	1.7
1815	100	3.3	6.3	4.7
1830	100	3.2	5.0	2.6
1845	100	0.6	6.4	2.8

Table 7.2 Difference in signal level (in dB) between periods of heater off and heater on (16 May 1989). The errors ~ 0.4 dB. A power of 100 % \equiv 80 MW ERP.

Chapter 7. HF observations at Arecibo

- i) Enhanced D-region absorption
- ii) F-region defocussing due to large scale changes in the plasma density
- iii) F-region scattering of EM waves into Langmuir waves by small scale FAI, ie anomalous absorption.

For the 1989 campaign at Arecibo and the earlier experiments at Tromsø the separation of the transmitter and receiver stations (see Chapter 4) were sufficient to ensure that the diagnostic waves did not propagate through the heated D-region. In addition, heater-induced D-region absorption has a much faster onset time than that exhibited by the Arecibo data (Section 7.6). Therefore, we may conclude that it was unlikely that the attenuation of the diagnostic signal was due to D-region effects.

For a reduction in the diagnostic signal amplitude to be caused by mechanism (ii) there must be large scale changes in the plasma electron density. During the period under discussion there is some evidence to suggest that such changes have occurred as a heater-induced increase in electron temperature of close to 200 K has been measured by the 430 MHz radar (Chapter 5). However, no clearly defined heater induced Doppler shifts or phase changes have been observed in the diagnostic signals, a result which is consistent with zero or very small changes in electron density (Jones *et al* 1982; Gurevich and Migulin 1982; Chapter 6). Defocussing may still occur even if the changes in the electron density are small as it is the geometry of the density structure that is important (eg consider the effects of a curved mirror) rather than its magnitude.

Robinson (1989) eliminated defocussing as an amplitude reduction mechanism for the Tromsø experiment on the grounds that the absorption time constants were much less than the times measured for large scale changes in the electron density to occur. For the experiments reported here there was no measurable systematic change in the electron density

Chapter 7. HF observations at Arecibo

measured by the 430 MHz radar or deduced from the HF diagnostic phase and therefore it was not possible to deduce the relevant time constant. However, Mantas *et al* (1981; see also Chapter 2) report large scale electron temperature growth and decay times of between 17 and 35 s during heating above Arecibo, although response times considerably shorter than this have been recorded at Tromsø (Wilkinson 1988; Chapter 5). However, the electron density is slower to respond to heating than the electron temperature (eg Chapters 3, 5 and 6) and therefore we may assume that the electron density time constant is at least 30 s. The time constants for large-scale modification are greater than the absorption recovery time, but similar to the absorption onset time (Section 7.6). In view of this, while it has not been possible to eliminate defocussing entirely as a potential source of the observed amplitude reduction, it seems unlikely that it plays a significant role.

The attenuation of the X-mode signal cannot be explained in terms of current anomalous absorption theory (mechanism iii). However, it is likely that as a result of the elliptically polarised characteristic modes present at low latitudes (Davies 1969) that the nominally X-mode diagnostic is contaminated by the O-mode signal (Chapter 4) which does exhibit a heater-induced attenuation. Alternatively, the heater induced excitation of Bernstein waves (Fejer and Leer 1972) might explain the attenuation of the X-mode signal, although no evidence for X-mode anomalous absorption has been reported for experiments at Tromsø.

7.5 Calculation of FAI scale lengths

Typical unheated electron density height profiles measured on the 16 May 1989 between 1628 and 1640 AST by the Arecibo Observatory 430 MHz radar are presented in Figure 7.7. The power profile has a height resolution of 600 m, but unfortunately was unavailable after about 1730 AST. The "long-pulse" profile has a much poorer height resolution of 38 km but is available throughout the experiment. The peak electron density of these profiles has been inferred from the value of foF2 deduced from the ionogram illustrated in Figure 7.5.

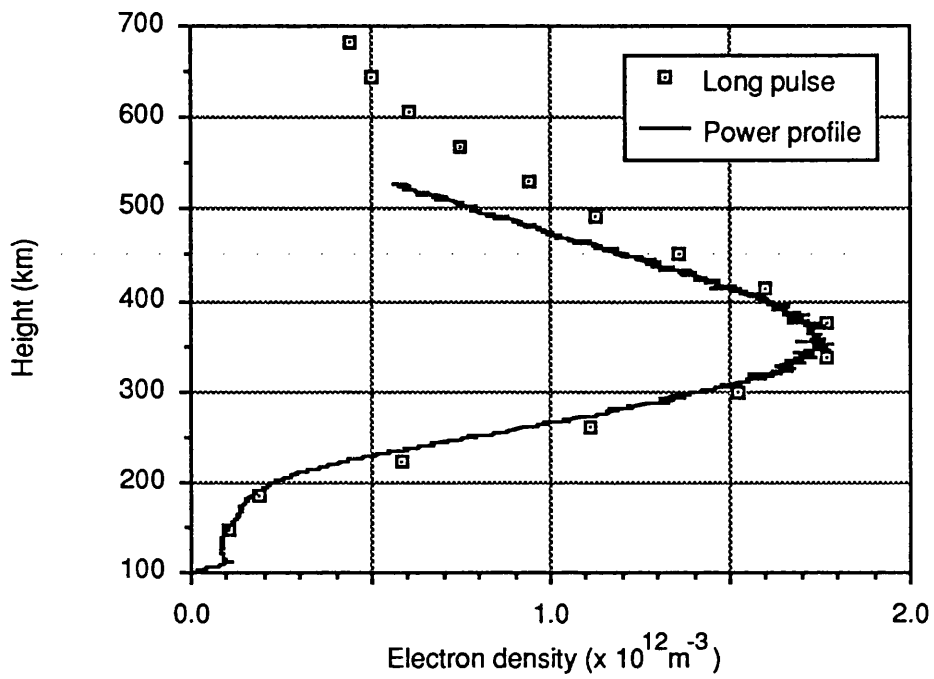


Figure 7.7 A comparison of the electron density measured on 16 May 1989, 1628-1640 AST by the long-pulse and barker coded (power profile) techniques.

Chapter 7. HF observations at Arecibo

Examination of Figure 7.7 indicates that at heights below the F-region peak the two profiles are in quite close agreement. In the topside ionosphere the agreement is less good, although this is not important in the experiments reported here where the heater and diagnostics are reflected below the F-region peak. The close agreement between the profiles in the vicinity of the heater and diagnostic reflection heights implies that, despite their poor height resolution, the long-pulse profiles illustrated in Figure 7.6 provide a reasonable estimate of the density profile. Ray-tracing (Jones and Stephenson 1975) of the diagnostic waves through the ambient density profiles integrated between 1739 - 1744 AST and 1839 - 1844 AST has enabled the reflection height and the upper-hybrid resonance height for the heater and each of the diagnostics to be determined (Table 7.3). It should be noted that the diagnostic waves detected at the receiver site were transmitted at an elevation angle of about 78° , while the heater was propagated vertically.

The anomalous absorption expressed as a function of diagnostic frequency and striation amplitude, δ_0 is given by Equations (3.9) and (3.11). Contours of constant δ_0 derived from these equations and employing parameters appropriate for the conditions prevailing at Arecibo ($\theta = 40^\circ$) during the experiment reported in the previous section have been plotted in Figure 7.8. An arbitrary reference frequency of 7.5 MHz has been employed which corresponds to a reference density, $N_0 = 6.9 \times 10^{11} \text{ m}^{-3}$, the scale height (also referenced to 7.5 MHz) is roughly constant over the region where the heater and diagnostics are reflected (see Figure 7.6 and Table 7.3) at a value of about 59 km. The experimental values of the anomalous absorption (Table 7.2) averaged over the heater ons between 1715 and 1805 AST (period I) and between 1815 and 1850 (period II) are also depicted in Figure 7.8. The errors have been calculated from the errors associated with the tabulated data. The peak experimental values of $\delta_0 = 0.8\%$ and 1.3% for periods I and II, respectively, each correspond to the diagnostic closest to the heater frequency. These striation amplitudes are below the peak value observed during experiments at Tromsø (Jones *et al* 1984; Robinson 1989), but are similar to the value obtained at Boulder by Minkoff *et al* (1974).

(A) 1739 - 1744 AST

FREQUENCY (MHz)	REFLECTION HEIGHT (km)	UPPER-HYBRID HEIGHT (km)
6.77	230.6	229.0
7.65	243.3	241.9
7.95	247.9	246.4
HEATER (7.4)	241.7	240.2

(B) 1839 - 1844 AST

FREQUENCY (MHz)	REFLECTION HEIGHT (km)	UPPER-HYBRID HEIGHT (km)
6.77	252.4	250.8
7.65	265.3	263.7
7.95	269.9	268.3
HEATER (7.4)	263.5	261.9

Table 7.3 Diagnostic reflection and upper-hybrid resonance heights on 16 May 1989. The heater ray was propagated vertically and the diagnostics at an elevation of about 78°.

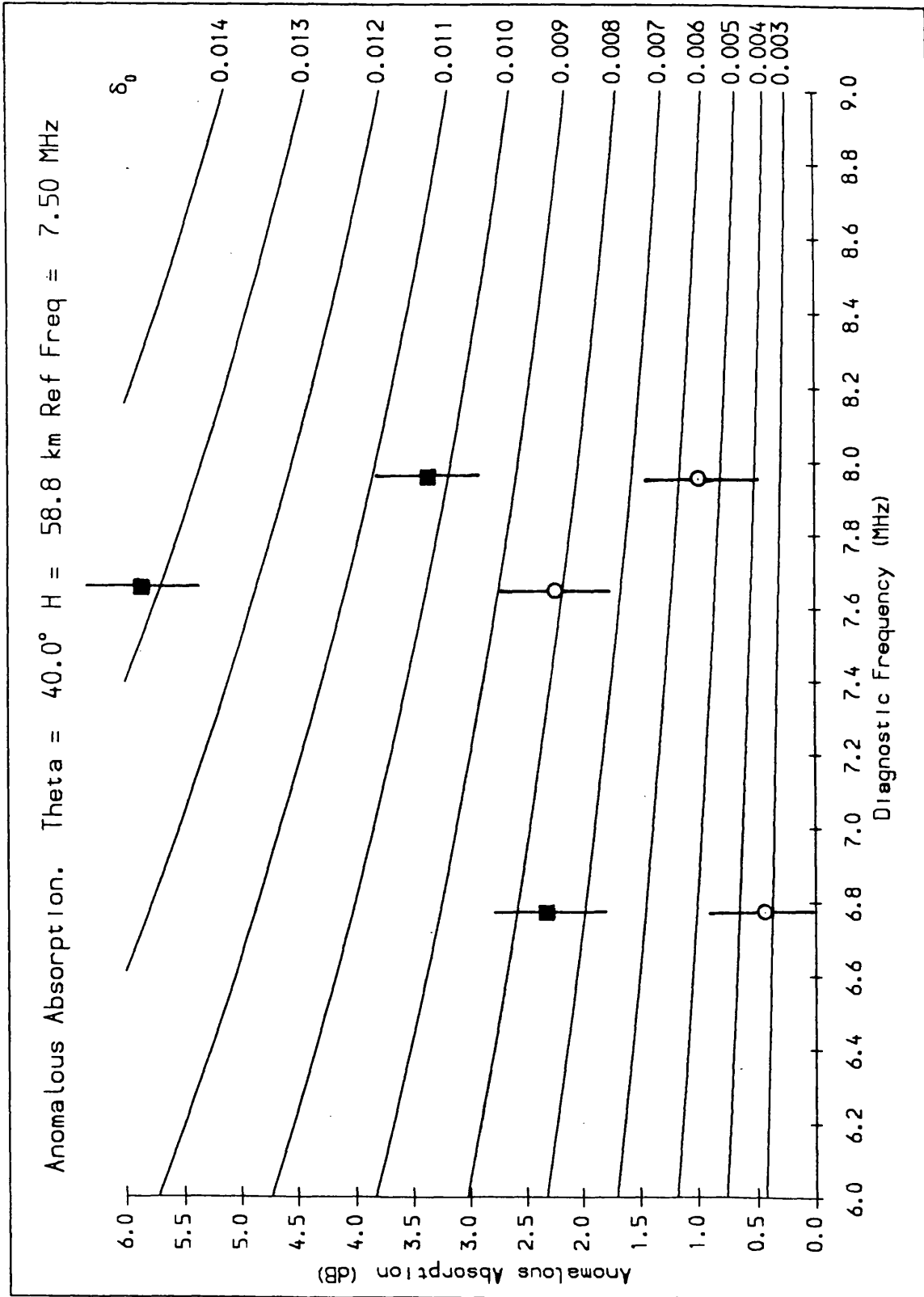


Figure 7.8 Experimental data from 16 May 1989 (○ 1715-1800 AST, ■ 1815-1900 AST) plotted together with theoretical contours of constant δ_0 for anomalous absorption as a function of ω_0 .

From Figure 7.8 it is evident that the maximum value of Γ is observed for the diagnostic frequency closest to the heater frequency. It is assumed that the maximum value of Γ occurs at the heater upper-hybrid resonance height, h_1 and that the striations are symmetrical about a plane perpendicular to the field through an axial point at h_1 . Furthermore, we also assume that $\langle |\Delta n|^2 \rangle$ and hence δ_0^2 varies as $\exp(-2|\Delta h|/L_{||} \cos \theta)$, where $|\Delta h|$ is the separation between the upper-hybrid resonance heights of the diagnostic and heater and $L_{||}$ is the field-aligned scale length. This expression implicitly assumes that the scale size is the same both above and below the heater interaction region.

The natural logarithm of the values of δ_0 determined from the experimental values in Figure 7.8 have been plotted against the altitude separation of the diagnostic and pump upper-hybrid resonance heights (Table 7.3) for periods I and II and the results displayed in Figure 7.9. The errors have been derived from the errors in δ_0 illustrated in Figure 7.8. At dip-angles corresponding to Arecibo the anomalous absorption for a given δ_0 is not independent of diagnostic frequency (Figure 7.8), therefore $\ln \delta_0$ has been plotted instead of Γ (Jones *et al* 1984; Robinson 1989) in Figure 7.9. A best fit straight line has been drawn through the experimental data and from the gradient values of $L_{||} \sim 25$ km in the case of period II and $L_{||} \sim 13$ km for period I have been deduced. These are similar in size to the value of $L_{||}$ reported by Jones *et al* (1984) for heating experiments at Tromsø although smaller than those presented by Robinson (1989).

7.6 Response Times

It has been established (Section 7.3) that the natural amplitude fading observed on 16 May 1989 at Arecibo is comparable in size with the heater induced attenuation of the diagnostic signals. Therefore, the diagnostic signal amplitudes have been averaged in order to reduce

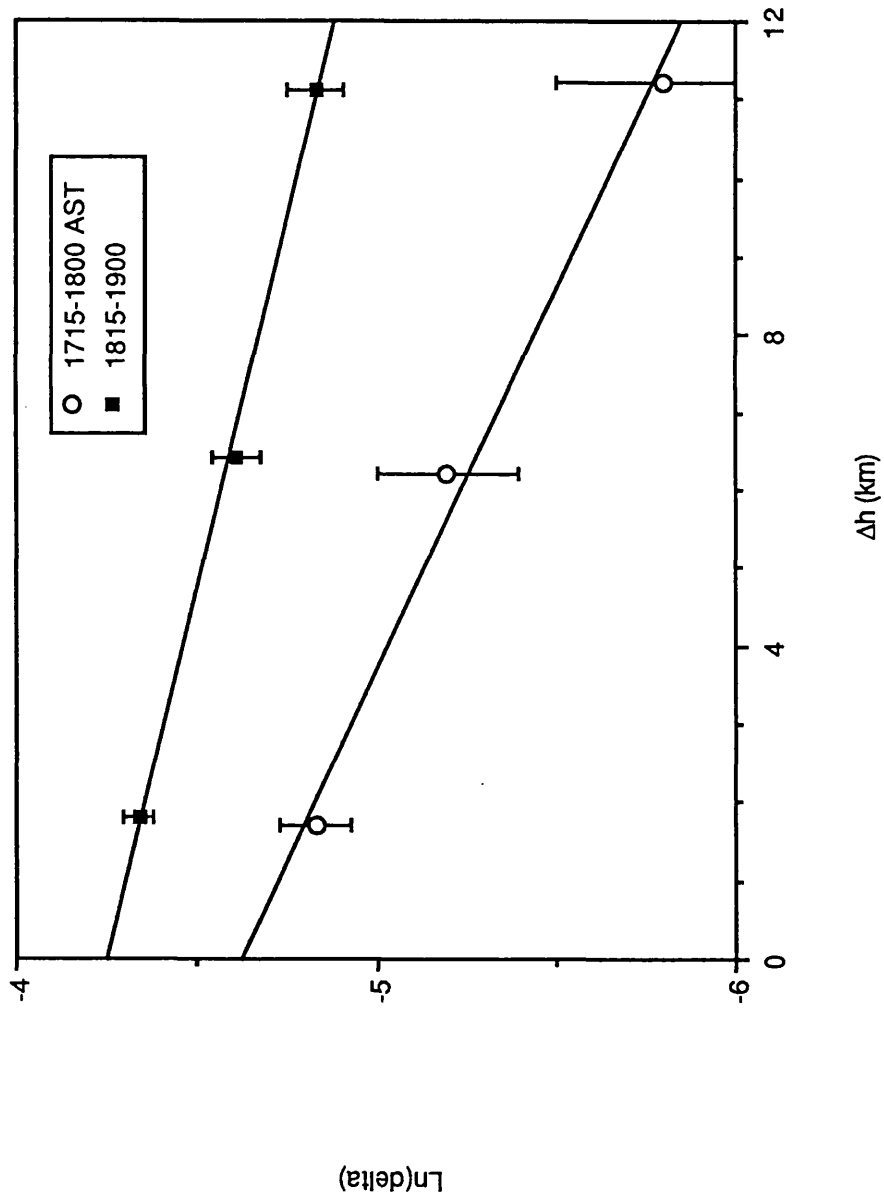


Figure 7.9 Measured values of $\ln(\delta)$ as a function of $|\Delta h|$ deduced from I/S radar electron density profiles.

the errors. In order to retain temporal information this smoothing has been performed by following method (ii) described in Section 7.3. The averaged signal amplitudes of the three O-mode diagnostics for the heater cycles between 1815 and 1900 AST are depicted in Figure 7.10. The error bars, which are typically between 1 and 2 dB, have been omitted from the figure for clarity. The diagnostic amplitude response to heating before this interval is not strong enough to obtain well defined time constants. The signal amplitudes have been averaged with a time resolution of 1 s. It is clear from Figure 7.10 that there is a measurable attenuation of the test-wave at each frequency.

The time constants for the absorption onset and recovery phases have been derived from the signal amplitude data which were presented in Figure 7.10. After the data have been averaged, the 0 dB level has been adjusted so that it corresponds to the quasi-stationary signal level observed during periods when the heater was switched on. The quasi-stationary signal amplitude when the heater was switched off then corresponds to the level of the anomalous absorption, Γ . The signal amplitude of the 7.65 MHz diagnostic as a function of time after heater switch on is illustrated in Figure 7.11. A function which has the form,

$$S_o(t_1) = \Gamma \exp(-t_1 / \tau_o) \quad (7.3)$$

has then been fitted to these data, where, t_1 is the time after the heater switch on, and τ_o is the absorption onset time constant.

For the recovery phase after heater switch off, a function has been fitted to the data of the form,

$$S_r(t_2) = \Gamma (1 - \exp(-t_2 / \tau_r)) \quad (7.4)$$

where, t_2 is the time after heater switch off, and τ_r is the absorption recovery time constant.

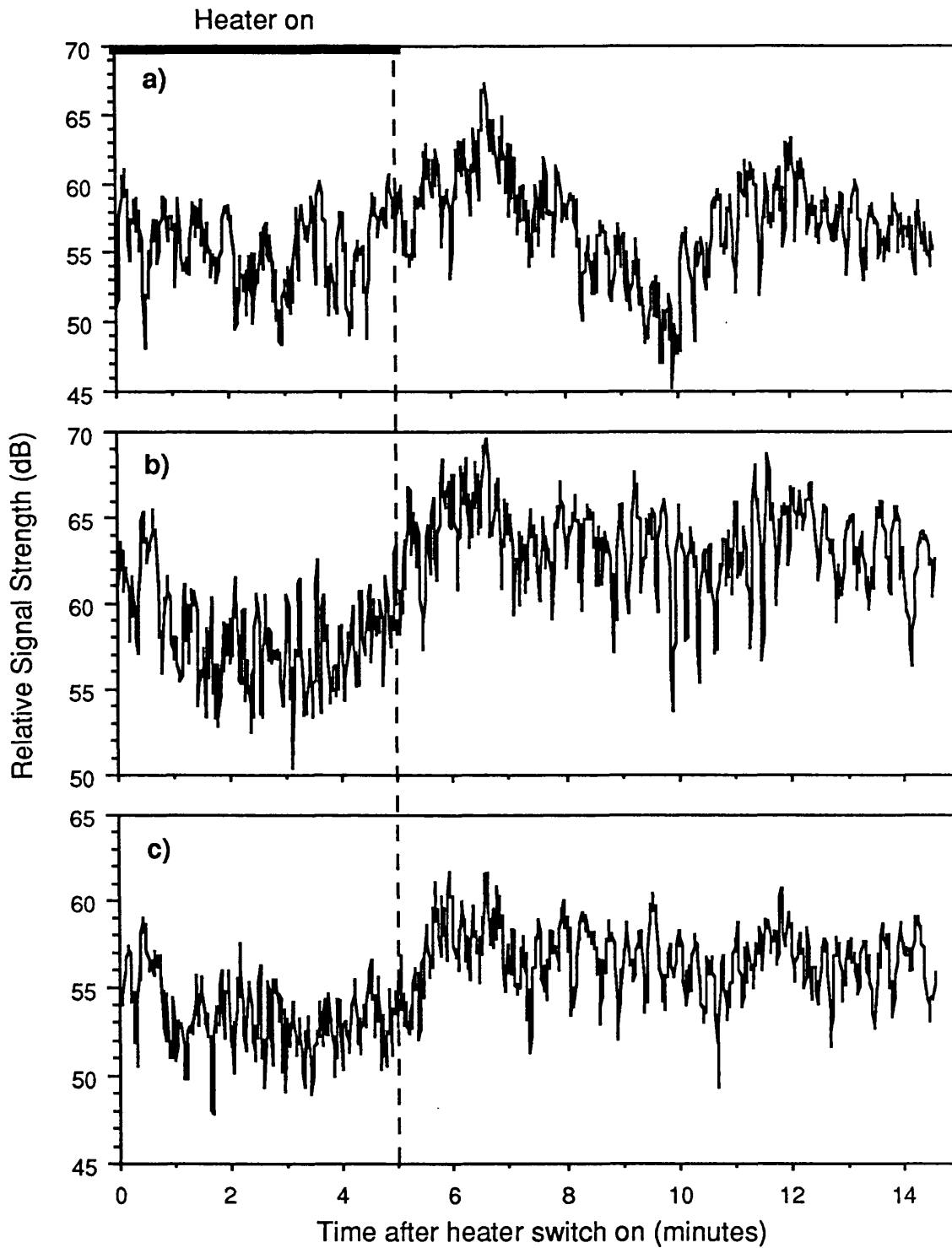


Figure 7.10 Superposed diagnostic signal strength, 16 May 1989, 1815-1900 AST
a) 6.77 MHz, b) 7.65 MHz, c) 7.95 MHz (O-mode). Heater frequency was 7.4 MHz.

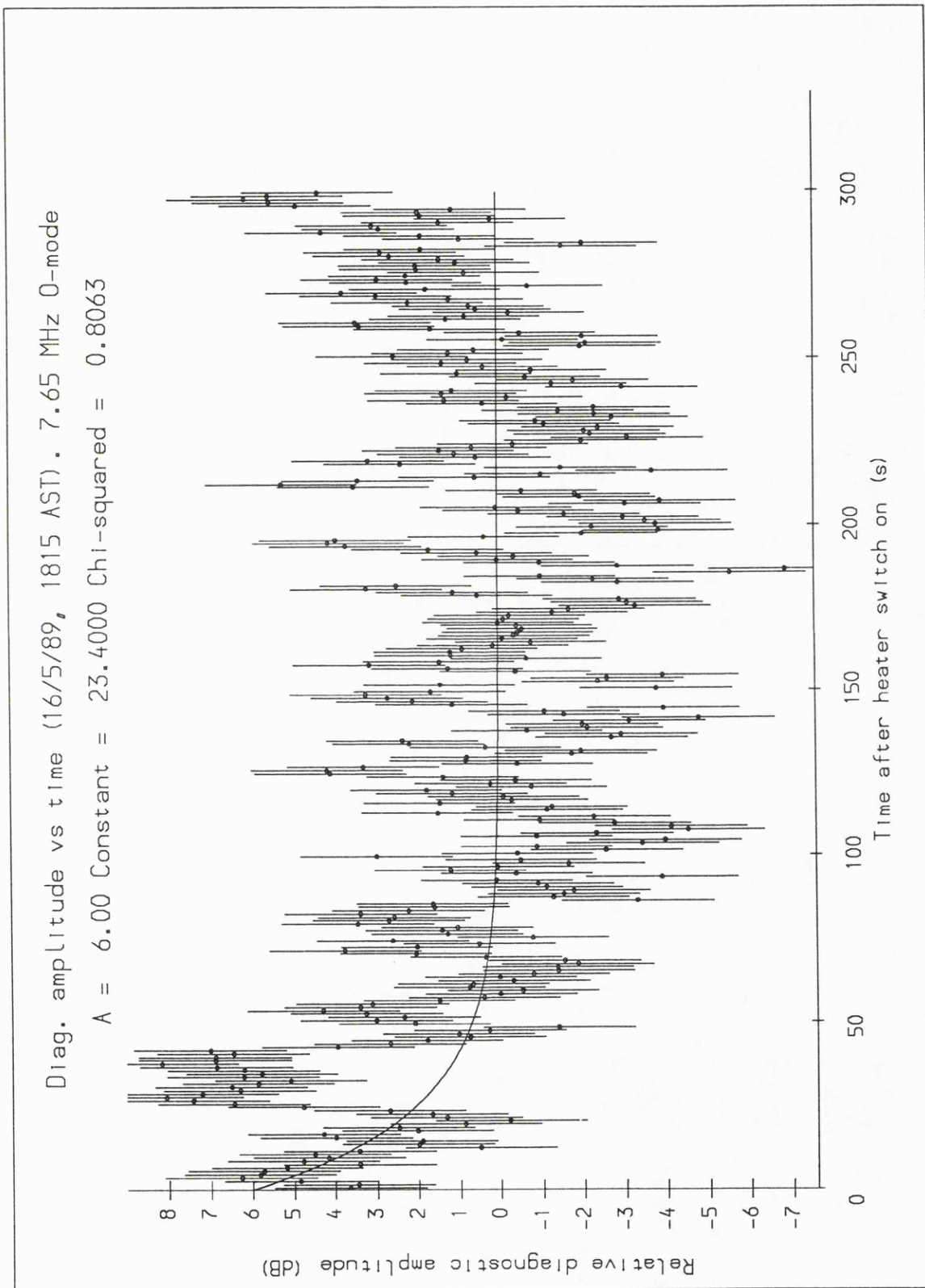


Figure 7.11 Amplitude of 7.65 MHz diagnostic versus time after heater switch on. Data have been averaged over 3 heater cycles on 16 May 1989, 1815-1900 AST. The solid line represents the least-squares fit to the data.

Amplitude data for the 7.65 MHz diagnostic from only the first few minutes after heater switch off are illustrated in Figure 7.12. However, the best-fit exponential included on this graph has been fitted to the entire 10 minute duration of the heater off period.

During the curve fitting of the 7.65 MHz diagnostic amplitude data, the level of Γ has been fixed at a value of 6 dB for both the onset and recovery periods. This corresponds closely to the signal amplitudes observed while the heater was switched off (Figure 7.12). The “best” value of τ is then defined by that value of τ which minimises Δ , where

$$\Delta = \sum_{n=1}^N (S(t_n, \tau) - D(t_n))^2 \quad (7.5)$$

$D(t_n)$ is the diagnostic signal strength of the n th datum at time t_n after heater switch on (or heater switch off, in the case of recovery), and N is the total number of data points.

It should be emphasised that the data which comprise the amplitude spike around 30-40 s after heater switch on (Figure 7.11) have been ignored for the purposes of curve fitting. Similar curve fitting has been performed for the remaining diagnostics, and the results are presented in Table 7.4. The values of χ^2 associated with the fit are also included in the table. For the 7.65 and 7.95 MHz diagnostics the confidence levels are better than about 70 %. In the case of the 6.77 MHz diagnostic the heater induced attenuation is similar in magnitude to the errors, and therefore the confidence of the fit is very low (less than 20 %). The recovery times are similar to the values reported by Robinson (1989) for experiments at Tromsø, but the onset times are nearly an order of magnitude slower.

There are several possible explanations for the relatively slow onset time of the diagnostic absorption;

- i) The slow onset time of the anomalous absorption is consistent with a low incident power in

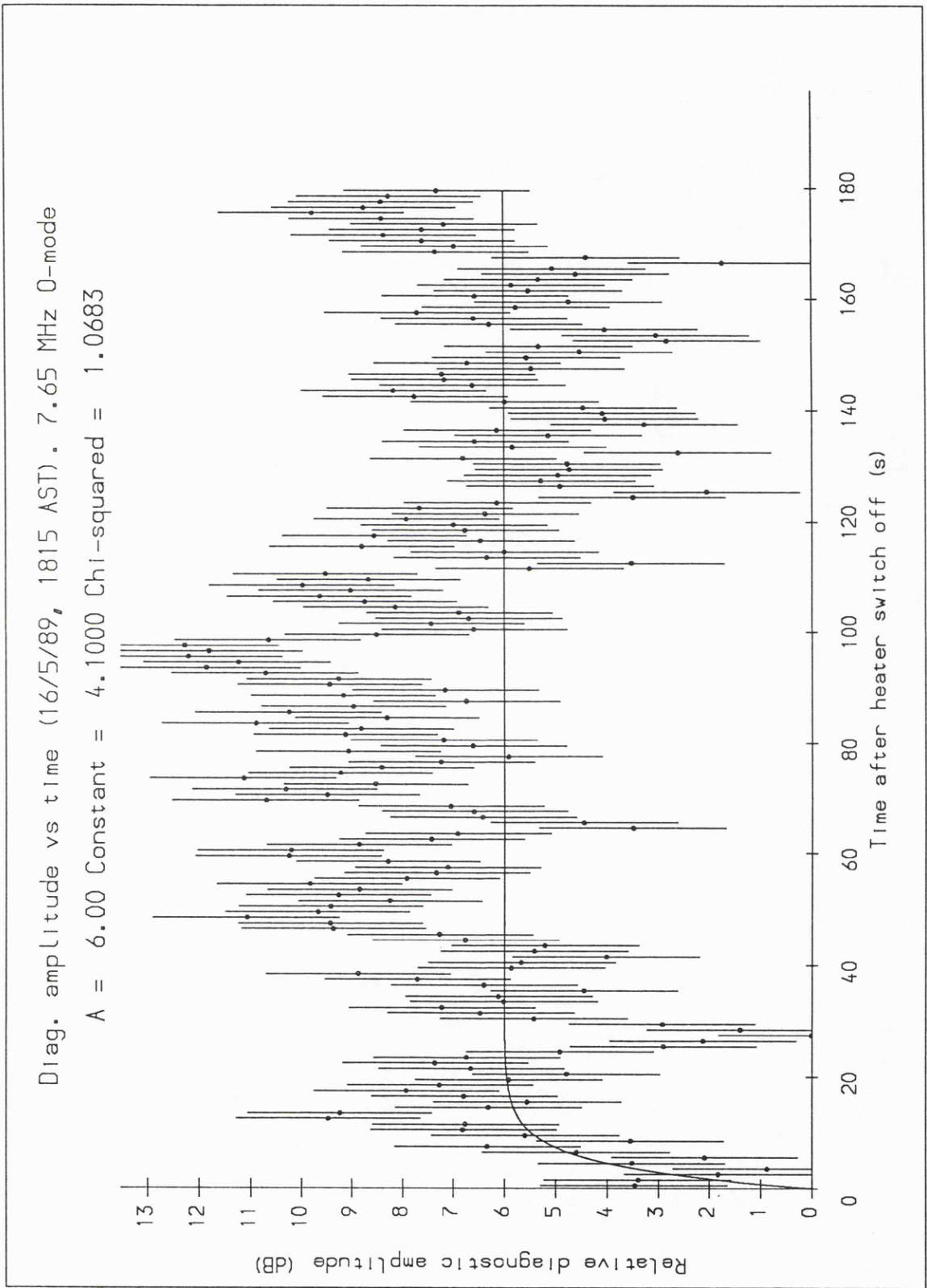


Figure 7.12 As for Figure 11, except data is from period after heater switch off. For clarity, only the first three minutes after switch off are shown.

Frequency (MHz)	τ_o	χ^2	τ_r	χ^2
6.77	11.3	1.08	11.6	1.14
7.65	23.4	0.806	4.1	0.987
7.95	31.5	0.849	14.6	0.948

Table 7.4 Time constants for onset and recovery of diagnostic attenuation for three O-mode test waves. Data from 16 May 1989, 1815-1900 AST.

the F-region as the growth rate (γ) of the instability which leads to the absorption, $\gamma \propto E_0^4$ (Robinson 1989), where E_0 is the incident electric field-strength. The low power in the F-region is possibly a consequence of the high D-region absorption observed during this period.

(ii) Fialer (1974) reported that the growth rate of the field aligned irregularities (FAI) which are thought to be responsible for anomalous absorption was dependent on whether the ionosphere had previously been heated (pre-conditioned). It was found that for a 'cold' (ie previously unheated) ionosphere the FAIs exhibited a growth time of several minutes. However, for a preconditioned ionosphere the FAIs saturated after only a few seconds of heating. For the experiment of the 16 May 1989, the heater was turned off for ten minutes after each heater on to allow the ionosphere to return to an unperturbed (or 'cold') state. The absence of preconditioning could explain the long absorption onset times observed during this experiment.

For a quiet ionosphere (ie slow fading rate) the saturated absorption level does not depend on the incident power providing that this is greater than the instability threshold (Stubbe *et al* 1982b; Robinson 1989). If the absorption observed during this experiment is attributed to anomalous processes then the instability threshold has obviously been exceeded and given the relatively slow fading rate (Figure 7.3) this implies that the level of anomalous absorption is close to saturation. This would mean that for the ionospheric conditions which occurred during the experiments described here, the maximum level of anomalous absorption at Arecibo is about 6 dB. This may be compared to the theoretical maximum of about 18 dB at Tromsø (Stubbe and Kopka 1980). The anomalous absorption level for a diagnostic frequency of 7.65 MHz as a function of dip angle (Equations 3.9 and 3.11) has been illustrated in Figure 2.2. For an anomalous absorption level of 18 dB at Tromsø ($\theta = 12^\circ$), the corresponding level at Arecibo ($\theta = 40^\circ$) is about 4 dB. The latter level is reasonably close to the experimental value of 6 dB derived from observations at Arecibo.

7.7 Concluding Remarks

The amplitude of HF diagnostic signals propagating through the heated volume has been measured during heating experiments at Arecibo, Puerto Rico. From these observations anomalous absorption has been measured directly at a low latitude site for the first time. The magnitude of the anomalous absorption is found to be very much less at Arecibo compared to typical values at Tromsø, a result which is consistent with the theory described by Robinson (1989). The field-aligned scale size of the irregularities responsible for anomalous absorption has been deduced and found to be comparable with measurements made at Tromsø. The recovery rate of the anomalous absorption is similar to the value at Tromsø, but the onset time is longer than that observed at Tromsø. This is consistent with, either a low incident heater power in the F-region or alternatively an absence of ionospheric preconditioning due to the long periods of heater off employed during the experiments reported here.

Chapter 8 Summary and Conclusions

8.1 Introduction

In this thesis the results of a series of "heating" experiments, in which the ionosphere has been modified through the action of high power HF radio waves, have been presented. During experiments performed with the heating facility located at Tromsø, Norway, the EISCAT radar was the principal diagnostic probe of the modified ionosphere. During similar experiments at Arecibo, Puerto Rico, in addition to the diagnostics provided by the incoherent scatter radar, the reflected amplitude and phase of low power diagnostic signals propagating through the modified region have also been measured. From these experimental investigations the effect of heating on the high-latitude F-region electron temperature and density has been studied in detail for the first time and the first direct observations of the anomalous absorption of low power diagnostic signals at low-latitudes have been reported. The results of ionospheric modification theories have been compared with these experimental observations.

8.2 Summary of principal observations

The results which have been established as a consequence of the experiments reported in this thesis may be summarised as follows :

- a) The large-scale enhancement of the F-region electron temperature during heating has been measured by the EISCAT radar with a height resolution of 30 km which is much better than that previously obtained. The temporal growth and spatial structure of the electron temperature enhancement have been successfully modelled by the theory discussed in Chapter 3. In addition to the net enhancement in electron temperature, temporal fluctuations

Chapter 8 Summary and Conclusions

have also been observed. These fluctuations have been attributed to the excitation of the thermal self-focussing instability.

b) From EISCAT measurements of the change in electron density during artificial modification, evidence has been presented which illustrates a marked contrast between the result of heating at a height of about 200 km in March 1985 when the electron density was depleted, and in February 1987, when the density was enhanced. This difference in behaviour probably arises from a difference in the location of the transition region between molecular and atomic ions and hence in the position of the diffusion and chemical recombination regimes. Large-scale changes in electron density have also been inferred from observations of the phase of low power HF signals propagating through the heated volume. Although some agreement was found between the estimates of the change in electron density deduced from the EISCAT and phase observations, at other times the density perturbation measured by the phase technique was a factor of 3-4 smaller than that measured by EISCAT, although it was similar to that predicted by theory. Problems with the interpretation of the phase observations in terms of an electron density perturbation in the presence of multipath propagation, changing density gradients or ionospheric tilts or the large errors associated with the EISCAT measurements could be the cause of the discrepancy between the phase and EISCAT observations.

c) Measurements of the amplitude of a low power HF signal reflected within the region illuminated by the high power beam have been performed at both Tromsø and Arecibo. During experiments at Arecibo the first observations of wideband absorption at low-latitudes have been obtained. The measured level of the absorption is below that commonly observed during similar experiments at Tromsø, in agreement with accepted theory. Calculations of the scale size and amplitude of the field-aligned irregularities associated with the anomalous absorption at Arecibo reveal similar values to those obtained for experiments at Tromsø. However, important differences, as yet unexplained, remain between the observations of

anomalous absorption made at Tromsø and those made at Arecibo. The foremost difference is that the X-mode diagnostic appears to be attenuated during heating at Arecibo, while this has never been observed at Tromsø. This may be a consequence of mode contamination in the receivers due to the elliptical characteristic polarisations at low latitudes.

8.3 Future Work

One of the principal problems with the use of EISCAT to measure the heater-induced large-scale changes in electron temperature and electron density is the relatively low height resolution (~ 30 km) available for temperature measurements in the F-region. This low height resolution means that any fine scale structure in the heated temperature profile will not be observed. In addition, in the determination of the electron density, the high resolution (~ 4 km) power profile measurements were corrected for the ratio of electron to ion temperature. This correction process entails the temperatures being interpolated between the heights at which they are measured, and then being applied to the high resolution power profile.

The height resolution of the temperature observations may be improved to a certain extent by transmitting coded pulses, eg alternating codes, from EISCAT. The transmission of alternating codes enables spectra, and hence the electron and ion temperatures to be measured with a height resolution of approximately 8 km at altitudes below about 250 km, although with a concomitant loss in time resolution. A heating experiment in which EISCAT employs alternating codes in measuring the large-scale changes electron temperature and density at high altitude resolution is planned for the near future.

Currently, the heater-induced electron temperature and density perturbations have only been observed along a single pointing direction (either vertically or along the local magnetic field-line). In order to measure the cross-field diffusion, the spatial structure of the thermally self-focussed heater beam and also the extent of the heated volume, the EISCAT beam

Chapter 8 Summary and Conclusions

should be scanned laterally through the heated region. As the temperature perturbation saturates soon after heater switch on, a five position scan could be employed within a reasonable time scale. However, the density perturbation takes longer to be established and hence in order to determine the cross-field structure, excessively long heater on times may be required, during the course of which the ambient ionosphere may change.

To date, the Tromsø transmitter remains the most powerful heater outside of the Soviet Union. In a recent refurbishment, which is now nearing completion, the number of dipole elements of one of the antenna arrays at the Ramfjordmoen site has been increased. This increase in the size of the array will have the effect of reducing the beamwidth, increasing the gain and thereby leads to an increase in the effective radiated power. It is estimated that the ERP from the extended antenna array will exceed 1000 MW. With this increase in power it should be possible for the heater to excite a whole range of new plasma instabilities. In addition, the heater will be able to generate more intense perturbations of the electron temperature and density.

Although the attenuation of low power diagnostic signals propagating through the heated volume has been observed at Arecibo, these effects only occurred during one interval of the campaign described in this thesis. Recently, preliminary analysis of the data obtained during a second campaign (March 1990) has revealed observations of anomalous absorption at far more regular intervals. Further study of these data should help to explain the apparent discrepancies in the behaviour of anomalous absorption at Tromsø and Arecibo.

The comparative study of low and high latitude heating effects and their interpretation in terms of non-linear instability theory, has added greatly to our knowledge of the growth of plasma irregularities and the associated changes in electron density and temperature produced in the ionosphere during heating.

References

References

Appleton E.V., 1932, J. Inst. Electr. Eng., **71**, 647.

Bailey V.A. , and Martyn D.F., 1934, Nature, **133**, 218.

Bailey V.A. , and Martyn D.F., 1934, Phil. Mag., **18**, 369.

Banks P.M. , and Kockharts G., *Aeronomy*, Academic Press, New York, 1973.

Barr R. , Rietveld M.T. , Kopka H. , Stubbe P. and Nielsen E., 1985, Nature, **317**, 155.

Barr R. , Stubbe P. , Rietveld M.T. , and Kopka H., 1986, JGR, **91**, 4451.

Barry G.H. , Griffiths L.J. , and Taenzer J.C., 1966, JGR, **71**, 4173.

Belikov V.V., Benediktov E.A., Zyuzin V.A., and Komrakov G.P., 1989, Geomag. and Aeron., **29**, 135.

Bernhardt P.A., and Duncan L.M., 1982, JATP, **44**, 1061.

Bernhardt P.A., Duncan L.M., and Tepley C.A., 1989, JGR, **94**, 7003.

Beynon W.J.G., and Williams P.J.S., 1978, Rep. Prog. Phys., **41**, 909.

Biondi A.A. , Sipler D.P. , and Hake Jr R.D., 1970, JGR, **75**, 6421.

Birkmayer W. , Hagfors T. , and Kofman W., 1986, PRL, **57**, 1008.

Brandt R.G., 1990, AGARD EPP-symposium, Bergen, Preprint.

Budden K.G., *Radio waves in the ionosphere*, Cambridge University press, London, 1961.

References

Budden K.G., *The propagation of radio waves*, Cambridge University press, London, 1985.

Burnside R.G., 1988, *Arecibo Observatory Report*, March.

Cannon P.S., 1982, *JATP*, **44**, 819.

Cannon P.S. , Turenen T. , and Rycroft M.J., 1982, *JATP*, **44**, 831.

Carlson H.C. , Gordon W.E., and Showen R.L., 1972, *JGR*, **77**, 1242.

Carlson H.C. , and Duncan L.M., 1977, *RS*, **12**, 1001.

Carlson H.C., and Mantas G.P., 1982, *JGR*, **87**, 4515.

Carlson H.C. , Wickwar V.B. , and Mantas G.P., 1982, *JATP*, **44**, 1089.

Caroll J.C., Violette E.J., and Utlaut W.F., 1974, *RS*, **9**, 895.

Clavier P.A., 1961, *J. Appl. Phys.*, **32**, 570.

Cohen R. , and Whitehead J.D., 1970, *JGR*, **75**, 6439.

Coster A.J., Djuth F.T., Jost R.J., and Gordon W.E., 1985, *JGR*, **90**, 2807.

Cragin B.L., and Fejer J.A., 1974, *RS*, **9**, 1071.

Cragin B.L., Fejer J.A., and Leer E., 1977, *RS*, **12**, 273.

Das A.C., and Fejer J.A., 1979, *JGR*, **84**, 6701.

Davies K., *Ionospheric radio waves*, Ginn-Blaisdell, Waltham, 1969.

Dawson J. , and Oberman C., 1963, *Phys. Fluids*, **6**, 394.

References

Derblom H., Thidé B., Leyser T.B., Nordling J.A., Hedberg Å, Stubbe P., and Kopka H., 1989, JGR, **94**, 10111.

Djuth F.T., 1984, RS, **19**, 383.

Djuth F.T. , Gonzales C.A. , and Ierkic H.M., 1986, JGR, **91**, 12089.

Djuth F.T., Jost R.J., Ierkic H.M., Sulzer M.P., and Noble S.T., 1987a, GRL, **14**, 194.

Djuth F.T. , Thidé B. , Ierkic H.M. , and Sulzer M.P., 1987b, GRL, **14**, 953.

Duncan L.M., and Gordon W.E., 1982, JATP, **44**, 1009.

Duncan L.M. and Sheerin J.P., 1985, JGR, **90**, 8371.

Duncan L.M., 1985, JATP, **47**, 1267.

Duncan L.M., Sheerin J.P., Behnke R.A., 1988, PRL, **61**, 239.

Duncan L.M., 1990, AGARD EPP-symposium, Bergen, Preprint.

Dysthe K.B., Mjølhus E., Pécseli H., and Rydpal K., 1983, Phys. Fluids, **26**, 146.

Eccles D. , and King J.W., 1970, JATP, **32**, 517.

Evans J.V., 1969, Proc IEEE, **57**, 496.

Farley D.T. Jr, 1963, JGR, **68**, 401.

Fejer J.A., 1955, JATP, **7**, 322.

Fejer J.A., 1970, JATP, **32**, 597.

References

Fejer J.A., and Leer E., 1972, JGR, **77**, 700.

Fejer J.A., 1979, RGSP, **17**, 135.

Fejer J.A. , Gonzales C.A. , Ierkic H.M. , Sulzer M.P., Tepley C.A., Duncan L.M. , Djuth F.T. ,
Ganguly S. , and Gordon W.E., 1985, JATP, **47**, 1165.

Fejer J.A. , and Sulzer M.P., 1987, JGR, **92**, 3441.

Fejer J.A., Djuth F.T., Ierkic H.M., and Sulzer M.P., 1989, JATP, **51**, 721.

Ferraro A.J. , Lee H.S. , Allshouse R., Carroll K. , Tomko A.A., Kelly F.J. , and Joiner R.G.,
1982, JATP, **44**, 1113.

Fialer P.A., 1974, RS, **9**, 923.

Garriot O.K. , DaRosa A.V. , and Ross W.J., 1970, JATP, **32**, 705.

Ginzburg V.L., and Gurevich A.V., 1960, Sov. Phys. -Uspekhi, **3**, 115.

Gordon W.E. , Carlson H.C. , and Showen R.L., 1971, JGR, **76**, 7808.

Gordon W.E. , and Carlson H.C., 1974, RS, **9**, 1041.

Grach S.M., Karashtin A.N., Mityakov N.A., Rapoport V.O., and Trakhtengerts V.Yu., 1977,
Radio Phys. Quantum Electron., **20**, 1254.

Grach S.M., Karashtin A.N., Mityakov N.A., Rapoport V.O., and Trakhtengerts V.Yu., 1979,
Sov. J. Plasma Phys., **4**, 742.

Graham K.N. , and Fejer J.A., 1976, RS, **11**, 1057.

Gurevich A.V., *Non-linear Phenomena in the Ionosphere*, Springer-Verlag, New York, 1978.

References

- Gurevich A.V., and Migulin V.V., 1982, JATP, **44**, 1019.
- Gurevich A.V. , Dimant Ya. S. , Milikh G.M. , and Vas'kov V.V., 1985, JATP, **47**, 1057.
- Hagfors T. , Kofman W. , Kopka H. , Stubbe P. , and Äijanen T., 1983, RS, **18**, 861.
- Hansen J.D., Morales G.J., Duncan L.M., Maggs J.E., and Dimante G., 1990, UCLA report PPG-1309 (submitted to PRL).
- Haslett J.C. , and Megill L.R., 1974, RS, **9**, 1005.
- Hedin A.E., 1983, JGR, **88**, 10170.
- Helliwell R.A. , and Carpenter D.L., 1963, JGR, **68**, 4409.
- Ho T., 1981, EISCAT technical reports, 81/24-28.
- Holt O., 1985, JATP, **47**, 537.
- Holway L.H. and Meltz G., 1973, JGR, **78**, 8402.
- Inhester B., Das A.C., and Fejer J.A., 1981, JGR, **86**, 9101.
- Jackson J.E., 1971, *The $p'(f)$ to $N(h)$ inversion problem in ionospheric soundings*, GFSC report, X-625-71-186, Greenbolt, Maryland.
- Jones T.B. , Davies K. , and Wieder B., 1972, Nature, **238**, 33.
- Jones T.B. , Robinson T. , Kopka H. , and Stubbe P., 1982, JGR, **87**, 1557.
- Jones T.B. , Robinson T. , Stubbe P. , and Kopka H., 1983, RS, **18**, 835.
- Jones T.B. , Robinson T. , Stubbe P. , and Kopka H., 1984, JATP, **46**, 147.

References

- Jones T.B. , Robinson T. , Stubbe P. , and Kopka H., 1986, JATP, **48**, 1027.
- Jones T.B., Stocker A.J., and Robinson T.R., 1988, University of Leicester, Ionospheric physics report for Royal Aerospace Establishment, Farnborough.
- Jones R.M., and Stephenson J.J., 1975, *A versatile 3D raytracing computer program for radio waves in the ionosphere*, OT-Rep-75-76, US. Gov. Print., Washington D.C.
- Kirkwood S., Collis P.N., and Schmidt W., 1986, JATP, **48**, 773.
- Kohl H. , LaHoz C. , Folkestad K. , Hansen T. , Kopka H. , Rose G. , and Stubbe P., *Active Experiments in space symposium*, Alpbach, ESA-SP-195, pp 91, 1983.
- Kopka H., Stubbe P., Jones T.B., and Robinson T., 1982, Nature, **295**, 680.
- Kuo S.P., and Lee M.C., 1982, Phys. Lett., **91A**, 444.
- Landau L.D., and Lifshitz E.M., *Electrodynamics of continuous media*, Pergammon, Oxford, 1960.
- Lejeune G., and Lathuillere C., 1986, JATP, **48**, 849.
- Lundborg B. , and Thidé B., 1985, RS, **20**, 947.
- Lundborg B. , and Thidé B., 1986, RS, **21**, 486.
- Mantas G.P. , Carlson H.C. , and LaHoz C.H. , 1981, JGR, **86**, 561.
- Mayr H.G., and Harris I., *Exploration of the polar upper atmosphere* (ed C.S. Deedt and J.A. Holtet), p31, D. Rheidel, Dordrecht, Holland, 1980.
- McCrea I.W., 1989, Ph. D. Thesis, University of Leicester.

References

- Meltz G. , and LeLevier R.E., 1970, JGR, 75, 6406.
- Meltz G. , Holway L.H. , and Tomljonovich N.M., 1974, RS, 9, 1049.
- Mendillo M., 1981, ASR, 1, 275.
- Migulin V.V. , and Gurevich A.V., 1985, JATP, 47, 1181.
- Minkoff J., 1974, RS, 9, 997.
- Minkoff J., Kugelmann P., and Weissman I., 1974, RS, 9, 941.
- Mjølhus E., 1985, JGR, 90, 4269.
- Newman A.L., Carlson H.C. Jr, Mantas G.P., and Djuth F.T., 1988, GRL, 15, 311.
- Perkins F.W., and Valeo E.J., 1974, PRL, 32, 1234.
- Perkins F.W. , Oberman C. , and Valeo E.J., 1974, JGR, 79, 1478.
- Perkins F.W. , and Roble R.G., 1978, JGR, 83, 1611.
- Perkins F.W., and Goldman M.V., 1981, JGR, 86, 600.
- Quegan S., Bailey G.J., Moffett R.J., and Spiro R.W., 1982, JATP, 44, 619.
- Rietveld M.T., Stubbe P., and Kopka H., 1989, RS, 24, 270.
- Rishbeth H., and Garriott O.K., *Introduction to ionospheric physics*, Academic press, New York, 1969.
- Rishbeth H., and Williams P.J.S., 1985, Q. Jl. R. astr. Soc., 26, 478.

References

- Robinson T.R., 1983, Ph.D. Thesis, University of Leicester.
- Robinson T.R., 1985, JATP, **47**, 1245.
- Robinson T.R., 1988, Plasma Phys. Controlled Fusion, **30**, 45.
- Robinson T.R., Honary F.A., and Stocker A.J., 1988, University of Leicester Ionospheric physics report, No. 44.
- Robinson T.R., 1989, Phys. Reports, **179**, 81.
- Roble R.G., 1975, Planet. Space Sci., **23**, 1017.
- Rose G. , Grondal B. , Neshe E. , Ott W. , Spenner K. , Holtet J., Måseide K. , and Trøim J., 1985, JGR, **90**, 2851.
- Schunk R.W., and Nagy A.F., 1978, RGSP, **16**, 355.
- Schunk R.W., *Solar-Terrestrial physics* (ed R.L. Carovillano and J.M. Forbes), p609, D. Rheidel, Dordrecht, Holland, 1983.
- Shoucri M.M. , Morales G.J., and Maggs J.E., 1984, JGR, **89**, 2907.
- Showen R.L., and Behnke R.A., 1978, JGR, **83**, 207.
- Showen R.L., and Kim D.M., 1978, JGR, **83**, 623.
- Stocker A.J., Robinson T.R., and Jones T.B., 1990, AGARD EPP-symposium, Bergen, AGARD-CP-485, 7-1.
- Stubbe P. , and Kopka H., 1977, JGR, **82**, 2319.
- Stubbe P. , and Kopka H., 1979, MPI report-W-02-79-04.

References

- Stubbe P. , and Kopka H., *Exploration of the Polar Upper Atmosphere* (ed C.S. Deehr and J.A. Holtet), p83, D Rheidel, Dordrecht, Holland, 1980.
- Stubbe P. , Kopka H. , Lauche H. , Rietveld M.T. , Brekke A., Holt O. , Jones T.B. , Robinson T. Hedberg Å. , Thidé B., Crochet M. , and Lotz H.J., 1982a, JATP, **44**, 1025.
- Stubbe P. , Kopka H. , Jones T.B. , and Robinson T., 1982b, JGR, **87**, 1551.
- Stubbe P. , Kopka H. , Rietveld M.T. , and Dowden R.L., 1982c, JATP, **44**, 1123.
- Stubbe P. , Kopka H. , Thidé B. , and Hedberg Å., 1984, JGR, **89**, 7523.
- Stubbe P. , Kopka H. , Rietveld M.T. , Frey A. , Høeg P., Kohl H. , Nielsen E. , Rose R. , LaHoz C. , Barr R. , Derblom H., Hedberg Å , Thidé B. , Jones T.B. , Robinson T. , Brekke A. , Hansen T. , and Holt O., 1985, JATP, **47**, 1151.
- Sulzer M.P., Ierkic H.M., and Fejer J.A., 1989, JGR, **94**, 6841.
- Tellegen B.D.H., 1933, Nature, **131**, 840.
- Thidé B., Derblom H., Hedberg Å., Kopka H., and Stubbe P., 1983, RS, **18**, 851.
- Thome G.D., and Blood D.W., 1974, RS, **9**, 917.
- Thomson J.A., 1970, JGR, **75**, 6446.
- Turenen T., 1986, JATP, **48**, 777.
- Utlaut W.F. , and Cohen R., 1971, Science, **174**, 245.
- Utlaut W.F. , and Violette E.J., 1972, JGR, **77**, 6804.
- Utlaut W.F. , and Violette E.J., 1974, RS, **9**, 895.

References

Utlaut W.F., 1975, Proc. IEEE, **63**, 1022.

Vas'kov V.V., and Gurevich A.V., 1975, Sov. Phys. JETP, **42**, 91.

Vas'kov V.V., and Gurevich A.V., 1977, Sov. Phys. JETP, **46**, 487.

Vas'kov V.V. , Golyan S.F. , Gruzdev Yu.V., Gurevich A.V. , Dimant Ya.S. , Kim V.Yu. ,
Lobachevskii L.A., Migulin V.V. , Panchenko V.A. , Petrov M.S. , Polimatidi V.P. , Sitnikov
V.I., Shoya L.D. , Shlyuger I.S., and Yurin K.I., 1981, JETP Lett, **34**, 558.

Walker J.C.G., 1979, RGSP, **17**, 534.

Wilkinson A.J., 1988, Ph.D. Thesis, University of Leicester.

Willis J.W., and Davis J.R., 1973, JGR, **78**, 5710.

Wong A.Y. , Santoru J. , Darrow C. , Wang L. , and Roederer J.G., 1983, RS, **18**, 815.

Wong A.Y. , Tanikawa T. , and Kuthi A., 1987, PRL, **58**, 1375.

Wright J.W. , Kressman R.I. , Viridi T.S. , and Collis P.N., 1988a, JATP, **50**, 405.

Wright J.W. , Kopka H. , and Stubbe P., 1988b, GRL, **15**, 1531.

Zinn J. , Sutherland C.D. , Stone S.N. , and Duncan L.M., 1982, JATP, **44**, 1143.

Zyuzin V.A., Kim V.Yu., Komrakov G.P., Panchenko V.A., and Polomatidi V.P., 1989,
Geomag. and Aeron., **29**, 137.

References

Abbreviations

ASR	Advances in Space Research
GRL	Geophysics Research Letters
JATP	Journal of Atmospheric and Terrestrial Physics
JGR	Journal of Geophysical Research
PRL	Physical Review Letters
RS	Radio Science
RGSP	Reviews of geophysics and space physics